:44813

National Library of Canada
Canadian Theses Division
Ottawa, Canada
K1A 0N4

Bibliothèque nationale du Canada
Division des thèses canadiennes

PERMISSION TO MICROFILM — AUTORISATION DE MICROFILMER

• Please print or type — Écrire en lettres moulées ou dactylographier

Full Name of Author — Nom complet de l'auteur

V. DAVID ... STEC

Date of Birth — Date de naissance

... 11 ... 7

Country of Birth — Lieu de naissance

...

Permanent Address — Résidence fixe

...

Title of Thesis — Titre de la thèse

...

University — Université

... University of ...

Degree for which thesis was presented — Grade pour lequel cette thèse fut présentée

... Ph.D

Year this degree conferred — Année d'obtention de ce grade

... 1980

Name of Supervisor — Nom du directeur de thèse

... K. P. Pearson

Permission is hereby granted to the NATIONAL LIBRARY OF CANADA to microfilm this thesis and to lend or sell copies of the film.

The author reserves other publication rights, and neither the thesis nor extensive extracts from it may be printed or otherwise reproduced without the author's written permission.

L'autorisation est, par la présente, accordée à la BIBLIOTHÈQUE NATIONALE DU CANADA de microfilmer cette thèse et de prêter ou de vendre des exemplaires du film.

L'auteur se réserve les autres droits de publication, ni la thèse ni de longs extraits de celle-ci ne doivent être imprimés ou autrement reproduits sans l'autorisation écrite de l'auteur.

Date

April 30, 1980

Signature

...

NL-91 (4/77)

National Library of Canada
Collections Development Branch

Canadian Theses on
Microfiche Service

Bibliothèque nationale du Canada
Direction du développement des collections

Service des thèses canadiennes
sur microfiche

NOTICE

The quality of this microfiche is heavily dependent upon the quality of the original thesis submitted for microfilming. Every effort has been made to ensure the highest quality of reproduction possible.

If pages are missing, contact the university which granted the degree.

Some pages may have indistinct print especially if the original pages were typed with a poor typewriter ribbon or if the university sent us a poor photocopy.

Previously copyrighted materials (journal articles, published tests, etc.) are not filmed.

Reproduction in full or in part of this film is governed by the Canadian Copyright Act, R.S.C. 1970, c. C-30. Please read the authorization forms which accompany this thesis.

THIS DISSERTATION
HAS BEEN MICROFILMED
EXACTLY AS RECEIVED

AVIS

La qualité de cette microfiche dépend grandement de la qualité de la thèse soumise au microfilmage. Nous avons tout fait pour assurer une qualité supérieure de reproduction.

S'il manque des pages, veuillez communiquer avec l'université qui a conféré le grade.

La qualité d'impression de certaines pages peut laisser à désirer, surtout si les pages originales ont été dactylographiées à l'aide d'un ruban usé ou si l'université nous a fait parvenir une photocopie de mauvaise qualité.

Les documents qui font déjà l'objet d'un droit d'auteur (articles de revue, examens publiés, etc.) ne sont pas microfilmés.

La reproduction, même partielle, de ce microfilm est soumise à la Loi canadienne sur le droit d'auteur, SRC 1970, c. C-30. Veuillez prendre connaissance des formules d'autorisation qui accompagnent cette thèse.

LA THÈSE A ÉTÉ
MICROFILMÉE TELLE QUE
NOUS L'AVONS REÇUE

Ottawa, Canada
K1A 0N4

NL-339 (Rev. 8/80)

THE UNIVERSITY OF ALBERTA

DEFORMATION OF ICE UNDER LOW STRESSES

by

(C) DAVID CHARLES CLEJUS SEGO

A THESIS

SUBMITTED TO THE FACULTY OF GRADUATE STUDIES AND RESEARCH

IN PARTIAL FULFILMENT OF THE REQUIREMENTS FOR THE DEGREE

OF DOCTOR OF PHILOSOPHY

IN

CIVIL ENGINEERING

DEPARTMENT OF CIVIL ENGINEERING

EDMONTON, ALBERTA

SPRING 1980

THE UNIVERSITY OF ALBERTA

FACULTY OF GRADUATE STUDIES AND RESEARCH

The undersigned certify that they have read, and recommend to the Faculty of Graduate Studies and Research, for acceptance, a thesis entitled DEFORMATION OF ICE UNDER LOW STRESSES submitted by DAVID CHARLES CLETUS SEGO in partial fulfilment of the requirements for the degree of DOCTOR OF PHILOSOPHY in GEOTECHNICAL ENGINEERING.

.....

Supervisor

.....

.....

.....

.....

External Examiner

Date..March 28, 1980.....

University of Alberta

TO MOM AND IN MEMORY OF DAD

University of Alberta

ABSTRACT

This thesis contains the results of a laboratory study conducted on samples of equaxial polycrystalline ice. These samples were prepared in the laboratory to reproduce ice similar to that used during previous studies reported in the literature. The ice was tested at temperatures warmer than -2.0°C to establish the flow law which governs the creep behaviour of this ice under various loading conditions.

Uniaxial compression experiments were conducted under a constant stress and the results suggest that a Cottrell-Aytekin type relationship reproduces the strain-time data. This relationship reproduced the experimental results provided the exponent on the time was expressed as a function of the axial stress. The measured strain-time curves suggest that at strains less than the onset of tertiary strain no prolonged steady state creep was observed.

Comparison of the minimum strain rate data at each stress with the results of constant strain rate experiments revealed a size effect influence on the data. When this size effect influence was accounted for, the laboratory data and the comparison of this data with previous results suggest the flow law of ice is best represented by a simple power law with an exponent on the stress of 3.0. Experiments conducted under complex stress conditions revealed that this flow law is a function only of the second stress invariant.

Punch penetration experiments were also conducted on this ice. Analysis of this data determined that cavity expansion would model the punch penetration. This model allowed the laboratory data to be predicted using the flow law established from the uniaxial experiments. The depth of embedment of the punch beneath the surface had no influence on the punch resistance during a constant penetration rate.

The finite element method was used to analyse the uniaxial compression and the punch experiments. The results of the analysis compared closely with the laboratory measured data. The analysis of a punch embedded beneath the surface confirmed the lack of influence of the embedment on the deformation results.

ACKNOWLEDGEMENTS

The research undertaking reported in this thesis was carried out under the supervision of Professor N.R. Morgenstern at the University of Alberta. The author is greatly indebted to Professor Morgenstern for his suggestion of this topic, his continued encouragement, and guidance throughout this program. Professor D.W. Murray also provided valuable advice and assistance during the modification of the finite element programs.

The author wishes to acknowledge with gratitude the continued support, love, and understanding of Karen. These have made the past 6 years easier and the last 6 months possible.

The financial assistance provide to the author from the National Research Council, the Transportation Development Agency, and the University of Alberta are gratefully acknowledged. This research work was also supported by a grant from Imperial Oil University Research Fund.

The author would also like to thank the many colleagues at the University of Alberta. The discussions of various aspects of Geotechnical Engineering have enhanced the author's knowledge and benefitted this research work. Special thanks are extended to W.D. Roggensack and K.W. Savigny for their assistance in the laboratory.

A. Muir was responsible for the fabrication and machining of the laboratory equipment. R. Gitzel provided assistance with the electronic measuring equipment and

remote recorders. O. Wood provided valuable assistance, along with D. Fushtey and H. Soderberg in the laboratory.

A special thanks to M.B. Dusseault would consented to review the manuscript and made helpful corrections.

Finally the author would like to acknowledge the following who helped in getting the text ready; G. Cyre, K. Sego, A. Thurton, and B. Waldie.

Table of Contents

Chapter — Page

CHAPTER 1
Introduction 1

1.1 General 1

1.2 Scope of Research 2

1.3 Outline and Summary of Thesis 4

CHAPTER 2
Literature Review 7

2.1 Introduction 7

2.2 Single Crystal of Ice 8

2.2.1 Elastic Behaviour 8

2.2.2 Plastic Deformation 10

2.3 Columnar Grain Ice 20

2.3.1 Elastic Behaviour 22

2.3.2 Plastic Deformation 25

2.4 Equiaxial Polycrystalline Ice 29

2.4.1 Elastic deformation 32

2.4.2 Plastic Deformation 34

2.4.2.1 Strain-time law 36

2.4.2.2 Flow law resulting from short-term loading 39

2.4.2.3 Flow law resulting from long-term loading 50

2.4.3 Factors affecting the flow law of ice 54

2.4.3.1 Reanalysis of creep data 64

CHAPTER 3
Test Equipment and Test Procedure 91

3.1 Ice Sample Preparation 91

3.1.1 Introduction 91

3.1.2 Equipment Used in Ice Making 95
3.1.3 Ice Making Procedure 98
3.1.4 Sample Storage 104
3.2 Ice Thin Section 105
3.2.1 Ice Thin Section Equipment 106
3.2.2 Procedure Used in Preparing Thin Sections 108
3.3 Constant Displacement Rate Loading Test 108
3.3.1 Introduction 108
3.3.2 Equipment 108
3.3.3 Sample Preparation 110
3.3.4 Test Procedure 115
3.4 Constant Displacement Rate Punching Test 118
3.4.1 Introduction 118
3.4.2 Equipment 118
3.4.3 Sample Preparation 119
3.4.4 Test procedure 121
3.5 Constant Stress Loading Test 123
3.5.1 Introduction 123
3.5.2 Equipment 124
3.5.3 Sample Preparation 126
3.5.4 Test Procedure 127
3.6 Simple Shear Loading Test 131
3.6.1 Introduction 131
3.6.2 Equipment 131
3.6.3 Sample preparation 133
3.6.4 Test procedure 134
CHAPTER 4

Analysis of Laboratory Creep Data 152

4.1 Introduction 152

4.2 Experimental results of constant stress tests 152

4.3 Data reduction 154

4.4 Strain-time relationships 157

4.4.1 Determination of parameters for strain-time relationship 161

4.5 Flow law determination 167

4.5.1 Introduction 167

4.5.2 Correspondence of constant-stress and constant strain-rate experimental data 168

4.5.3 Flow law determined from constant stress experiments 170

4.5.4 Flow law determined from constant strain-rate experiments 171

4.6 Flow law determined from combined data of constant strain-rate and constant stress tests 173

4.6.1 Factors influencing the flow law of ice 173

4.6.2 Grain size ratio 174

4.6.3 Influence of grain size ratio on minimum strain-rate 177

4.6.3.1 Comparison of laboratory data and data from literature 183

4.6.3.2 Temperature influence on minimum creep rate 186

4.7 Method to predict length of experiment 189

4.7.0.1 Prediction of time to achieve minimum strain-rate during testing 192

4.7.0.2 Time to failure 197

4.7.1 Comparison of laboratory and field flow laws 200

4.8 Conclusion 207

CHAPTER 5

Analysis of Data under Complex Stress States 251

5.1 Introduction 251

5.2 Theory of expansion of a spherical cavity 253

5.3 Material properties required to predict punch data 259

5.4 Laboratory punch data 261

5.5 Analysis of punch data using laboratory determined flow law 263

5.5.1 Temperature influence on laboratory punch data 269

5.5.2 Analysis of asymptotic punch resistance 270

5.5.3 Influence of depth of embedment on punch resistance 273

5.6 Analysis of multiaxial state of stress in creep studies 279

5.7 Multiaxial state of stress 280

5.7.1 Influence of hydrostatic stress state on flow law 282

5.7.2 Influence of simple shear stress state on creep deformation. 283

5.8 Conclusion 287

Chapter 6
Finite Element Analysis of Laboratory Data 305

6.1 Introduction 305

6.2 Finite element method 306

6.3 Finite element programs 311

6.3.1 Modifications to constant strain triangle 312

6.3.2 Check on solutions of programs 314

6.4 Use of finite element to predict behaviour of experiments 320

6.5 Conclusion 325

CHAPTER 7
Concluding Remarks 345

7.1 Strain time behaviour 345

7.2 Flow law of polycrystalline ice 346

7.3 Complex loading conditions 347

7.4 Further research 348

APPENDIX A
Laboratory Experiment Data 369

APPENDIX B
Finte Element Programs and Modification to model steady state creep 399

List of Figures

Figure		Page
2.1	Dynamic stiffness constants of aged single crystals of ice versus temperature at frequency of 30 Mhz	79
2.2	Schematic diagrams representing types of bending of single crystals of ice under load	79
2.3	Creep of single crystal of ice at -2.3°C under constant applied stress on basal plane	80
2.4	Typical creep curves of polycrystalline material at a constant temperature and applied stress	80
2.5	Frequency dependence of Effective Young's Modulus for polycrystalline ice at -10°C	81
2.6	Young's Modulus as function of brine volume or porosity	81
2.7	Typical creep curve of columnar grained ice with comparison to polycrystalline ice	82
2.8	Longitudinal-wave velocity and damping ratio of ice versus temperature	83
2.9	Longitudinal-wave velocity and damping ratio of ice versus frequency	83
2.10	Longitudinal-wave velocity of ice versus confining pressure	84
2.11	Longitudinal-wave velocity of ice versus ice density	84
2.12	Constant stress creep of polycrystalline ice	85
2.13	Steady-state strain-rate versus stress of polycrystalline ice	85
2.14	Steady-state strain-rate versus stress of polycrystalline ice during tertiary creep	86
2.15	Normalized secondary-creep rate versus average grain diameter for both inclusion-free and inclusion-bearing polycrystalline ice	86
2.16	Compiled strain-rate versus stress creep data of field and selected laboratory data	87
2.17	Strain-rate versus density for snow and ice samples	88
2.18	Normalized strain-rate versus axial stress of	

polycrystalline ice at different densities.....89

2.19 Normalized strain-rate versus axial stress of polycrystalline ice at -2.0°C.....90

3.1 Dissolved oxygen versus time required to deair 6 liters of water.....137

3.2 Moulds used for making ice samples.....138

3.3 Average crystal diameter (d) versus distance from datum of thin section.....139

3.4 Typical plot of data from the constant displacement rate experiment (Sample UC43).....140

3.5 Typical plot of data from the constant displacement rate penetration experiment (Sample Pen36).....141

3.6 Temperature records of constant stress loading cells...142

3.7 Typical plot of data from the constant stress loading experiment (Sample CSA34).....143

3.8 Simple shear loading system.....144

3.9 Detail of loading system in simple shear experiment....145

3.10 Typical plot of data from the constant stress simple shear loading experiment (Sample SS32).....146

4.1 Compiled plot of strain-time curves of constant stress experiments.....222

4.2 Data plot of constant stress sample CSC37.....223

4.3 Data plot of constant stress sample CSB35.....224

4.4 Comparison of parabolic strain-time relation and laboratory measured data.....225

4.5 Comparison of Andrade one-third relation and laboratory measured data.....226

4.6 Comparison of logarithm strain-time relation and laboratory measured data.....227

4.7 Comparison of hyperbolic sine relation and laboratory measured data.....228

4.8 Logarithm strain-rate versus logarithm (t+1) of sample CSA34.....229

4.9 Applied stress versus m parameter of constant stress

experiments.....230

4.10 Applied stress versus A parameter of constant stress experiment.....230

4.11 Normalized minimum strain-rate versus applied stress of constant stress experiments.....231

4.12 Normalized minimum strain-rate versus peak stress of constant strain-rate experiments.....231

4.13 Comparison of Equation 4.10 and the strain-time data measured at a constant stress of 100 kPa.....232

4.14 Comparison of Equation 4.10 and the strain-time data measured at a constant stress of 150 kPa.....233

4.15 Comparison of Equation 4.10 and the strain-time data measured at a constant stress of 200 kPa.....234

4.16 Comparison of Equation 4.10 and strain-time data measured at a constant stress of 300 kPa.....235

4.17 Axial stress versus axial strain-rate for ice illustrating data in the ductile, transition and brittle zone from Mellor (1979).....236

4.18 Data plot of constant strain-rate experiment (Sample UC48).....237

4.19 Normalized strain-rate versus axial stress of combined constant stress and constant strain-rate data.238

4.20 Normalized strain-rate versus GSR.....239

4.21 Proof stress versus GSR.....239

4.22 Normalized strain-rate versus axial stress showing comparison of laboratory data corrected to GSR=0.015 and data not corrected.....240

4.23 Normalized strain-rate versus axial stress of laboratory data and data available from the ice literature.....241

4.24 Normalized strain-rate versus axial stress of laboratory data corrected to GSR=0.03 and data available from ice literature.....242

4.25 Normalized strain-rate versus [1/1+T] at a constant stress of 300 kPa.....243

4.26 Normalized strain-rate versus axial stress of laboratory data corrected to a GSR=0.03 and

temperature equal to -2.0°C. and the data available from the ice literature....244

4.27 Normalized strain-rate versus axial stress showing influence of temperature on the flow law of ice close to 0.0°C....245

4.28 Time to minimum strain-rate versus axial stress....246

4.29 Axial strain at the onset of tertiary creep versus applied stress of laboratory data....247

4.30 Normalized strain-rate versus axial strain at the onset of tertiary creep of the laboratory data....248

4.31 Measured time to failure versus axial stress for experimental laboratory data....249

4.32 Normalized strain-rate versus axial strain of laboratory data for both the peak strain and at a total strain of 10%....249

4.33 Normalized strain-rate versus axial stress of laboratory data illustrating comparison of flow law with exponent equal to 3.0 and Equation 4.32....250

5.1 Regions of operation of different wedge indentation mechanism....290

5.2 Schema for transformation of a cavity expansion to a deep circular punch problem....290

5.3 Typical plot of punch resistance versus time during a constant displacement rate experiment. (Sample Pen48)..291

5.4 Normalized settlement rate versus punch resistance....292

5.5 Normalized settlement rate versus punch resistance using an exponent equal to 3.0....293

5.6 Bearing capacity versus depth of embedment in a cohesive material....294

5.7 Temperature versus asymptotic punch resistance....295

5.8 Normalized settlement rate versus peak punch resistance corrected to -2.0°C....296

5.9 Normalized settlement rate versus asymptotic punch resistance corrected to -2.0°C....297

5.10 Asymptotic punch resistance versus the depth to the diameter ratio (D/B)....298

5.11 Parameters governing punch resistance versus depth to diameter ratio (D/B) for frozen sand from Ladanyi and Paquin (1978). 298

5.12 Punch resistance versus normalized settlement rate of punch experiments on polycrystalline ice..... 299

5.13 Plot of stress versus time of Sample UC44 which illustrates influence of confining pressure on experiment. 300

5.14 Idealized stress distribution in simple shear experiment. 301

5.15 Normalized strain-rate versus effective shear stress comparison between simple shear data and Equation 4.19. 302

6.1 Approximation of smooth stress time curve..... 329

6.2 Simplified flow chart for incremental analysis of creep.... 330

6.3 Boundary conditions and material properties of thick-walled cylinder problem..... 331

6.4 Finite element grid used to evaluate axi-symmetric program..... 332

6.5 Elastic stress distribution versus r/B for thick-walled cylinder problem..... 333

6.6 Elastic radial displacement versus r/B for thick-walled cylinder problem..... 334

6.7 Comparison of stress distribution of axi-symmetric finite element results to closed-form solution during steady-state creep..... 335

6.8 Comparison of displacement and displacement rate of the internal radius of thick-walled cylinder problem during steady-state creep..... 336

6.9 Finite element grid used to evaluate the plane strain program..... 337

6.10 Comparison of stress distribution of plane strain finite element results to closed-form solution during steady-state creep..... 338

6.11 Finite element grid used to study unconfined compression test..... 339

6.12 Normalized strain-rate versus axial stress comparison of finite element results and laboratory measured data. 340

6.13 Finite element grid used to study penetration test....341

6.14 Normalized settlement rate versus punch resistance comparison of finite element and laboratory measured data....342

6.15 Finite element grid used to study influence of depth of embedment of punch penetration results....343

6.16 Plot of displacement field surrounding the punch for D/B=5....344

A.1 Data plot of constant stress sample CSA34....370

A.2 Data plot of constant stress sample CSB35....371

A.3 Data plot of constant stress sample CSGR38....372

A.4 Data plot of constant stress sample CSC37....373

A.5 Data plot of constant stress sample CSD39....374

A.6 Data plot of constant stress sample CSE42....375

A.7 Data plot of constant strain-rate sample UC15....376

A.8 Data plot of constant strain-rate sample UC19....377

A.9 Data plot of constant strain-rate sample UC20....378

A.10 Data plot of constant strain-rate sample UC29....379

A.11 Data plot of constant strain-rate sample UC33....380

A.12 Data plot of constant strain-rate sample UC43....381

A.13 Data plot of constant strain-rate sample UC44....382

A.14 Data plot of constant strain-rate sample UC46....383

A.15 Data plot of constant strain-rate sample UC48....384

A.16 Data plot of constant strain-rate sample UC50....385

A.17 Data plot of constant displacement rate punch sample Pen16....386

A.18 Data plot of constant displacement rate punch sample Pen25....387

A.19 Data plot of constant displacement rate punch sample Pen29....388

A.20 Data plot of constant displacement rate punch sample Pen32 389

A.21 Data plot of constant displacement rate punch sample Pen36 390

A.22 Data plot of constant displacement rate punch sample Pen41 391

A.23 Data plot of constant displacement rate punch sample Pen48 392

A.24 Data plot of constant stress simple shear sample SS32 .. 393

A.25 Logarithm strain rate versus logarithm (t+1) of sample CSB35 394

A.26 Logarithm strain rate versus logarithm (t+1) of sample CSGR38 395

A.27 Logarithm strain rate versus logarithm (t+1) of sample CSC37 396

A.28 Logarithm strain rate versus logarithm (t+1) of sample CSD39 397

A.29 Logarithm strain rate versus logarithm (t+1) of sample CSE42 398

List of Plates

Plate		Page
3.1	Ice making equipment	147
3.2	Thin section of ice sample region affected during freezing	147
3.3	Thin section equipment	148
3.4	Constant displacement rate triaxial cell	148
3.5	Constant displacement rate loading system	149
3.6	Milling machine used to trim samples	149
3.7	Shell mill cutter used to trim ice	150
3.8	Constant stress cell	150
3.9	Constant stress loading system	151
3.10	Constant stress loading system with cell and sample	151
5.1	Thin section showing highly disturbed zone of ice crystals beneath punch	303
5.2	Thin section showing undisturbed zone of ice crystals at a distance from the punch	303
5.3	Photo of simple shear experiment illustrating uniform deformation of ice sample	304

List of Tables

Table		Page
2.1	Author's and experimental conditions used to determine the elastic properties of ice	70
2.2	Dynamic elastic constants of single crystals of ice at -16°C	71
2.3	Relationships used to fit strain-time data of single crystals of ice in easy glide	72
2.4	Parameters used to relate shear strain-rate to shear stress in single crystal studies	73
2.5	Summary of data of authors from literature	74
2.6	Data summary of creep results in tertiary creep region from Steinemman (1958)	76
2.7	Data summary showing influence of density of ice sample on strain-rate	77
3.1	Summary of bulk density and average grain size data	136
4.1	Summary of strain-time parameters at various stress levels	210
4.2	Summary of strain-time parameters at various temperature and a constant axial stress of 300 kPa	210
4.3	Summary of constant stress data	211
4.4	Summary of constant strain-rate data	211
4.5	Summary of data used to study influence of grain size ratio	212
4.6	Summary of data corrected for grain size ratio	213
4.7	Summary of data of proof stress and exponent related to grain size ratio	214
4.8	Data summary of authors from literature	215
4.9	Summary of data showing temperature influence	217
4.10	Summary of temperature corrected data from this research	218
4.11	Summary of time to the minimum strain-rate	219

4.12 Summary of data related to failure of each sample.....220

4.13 Summary of constant strain-rate data at 10% strain....221

5.1 Summary of punch experiment data.....288

5.2 Summary of punch resistance corrected to -2.0°C.....289

6.1 Summary of elastic results of thick-walled cylinder problem presented in Figure 6.3.....326

6.2 Summary of steady-state creep results of the thick-walled cylinder problem presented in Figure 6.3..327

6.3 Summary of punch data and predicted results using cavity expansion model and finite element program.....328

CHAPTER 1

Introduction

1.1 General

The recent world situation in the world related to petroleum reserves and availability of oil has required that the energy potential of the North be ascertained. Exploration work in the Arctic has discovered that oil and gas reserves are such that it is economically attractive to transport this resource southward. The Alyeska Oil Pipeline which is now completed represents the first of the major transportation projects to bring this energy to market. Within Canada, the Foothills and the Polar Gas pipelines are now in the advanced planning stage with completion dates expected within the decade.

These major projects, along with the requirements for exploration within the North, have required that engineers design and construct facilities within a permafrost region. To design and construct these facilities, an understanding of permafrost is required by the designer. The permafrost region in Canada and many of the Engineering characteristics of it have been described by Brown (1970). He points out that much of the frozen soil has a large quantity of ice contained within it. It is this characteristic of frozen soil which has caused many Engineering problems in the North. The ice within the soil influences the load carrying capacity and the deformation characteristics of the frozen

soil.

Mackay (1972) describes and classifies the various types of ice contained within the permafrost. This ice causes the strength and the deformation behaviour of the frozen soil to differ from that of thawed soil (Vialov (1965a)). The character of the deformation behaviour of ice rich frozen soil has been studied and the similarity to that of polycrystalline ice noted by Vialov (1965a), Ladanyi (1972a), McRoberts (1973), and Roggensack (1977).

The deformation behaviour of ice rich frozen soil is an important input parameter to the design of foundations in permafrost regions and the analysis of the stability of ice rich slopes (Ladanyi and Johnston (1974), Weaver (1979), and Savigny (1980)). The proper design of the foundation to carry a load requires that the time-dependent deformation of the frozen soil be understood. This requirement and the similarity between the deformation of frozen soil and that of ice has necessitated that a complete understanding of ice behaviour under stress be achieved. For the design of foundations the factors influencing the creep deformation of polycrystalline ice must be understood.

1.2 Scope of Research

For foundations design on ice rich frozen soil, Nixon (1978) recommends the frozen soil be considered as ice. Then using the deformation behaviour of ice and the loading conditions of the structure the foundation is designed. He

uses the ice deformation behaviour ascertained from searching the literature. The work in this thesis has been undertaken to improve the data base on ice behaviour for the design of foundations in ice rich frozen soil.

The results of this thesis are applicable to understanding the deformation behaviour of ice-rich frozen soil. Ice-rich frozen soil consists of a mixture of ice and mineral soil in which the ice is in excess of that required to fill the pore space (Brown and Kupsch (1974)). The experimental findings are not applicable to analysing the behaviour of dry permafrost or ice-poor permafrost. In these frozen soils the ice does not exceed the volume of the pore space in the soil.

Creep studies of ice were undertaken to evaluate its strain-time behaviour and the flow law of ice at -1.5°C. The influence on this flow law of varying the stress state from the uniaxial condition was studied. The use of the punch experiment was evaluated to see if it could be used to measure the material properties. Punch experiments were undertaken in the laboratory to establish how well the theory of Ladanyi and Johnston (1974) modelled the deformation behaviour beneath a punch and if the theory could be used to develop a flow law.

Finite element programs were developed to account for steady state creep in plane strain and axi-symmetric configurations. The steady-state creep behaviour was used because a study of the literature suggested this behaviour

controlled the creep deformation within ice and frozen soil.

1.3 Outline and Summary of Thesis

Chapter 2 contains a review of the information available in the literature on how ice behaves under various loading conditions. It is pointed out that three types of ice have been studied and that the behaviour of each is different. The major portion of the review centres on the behaviour of polycrystalline ice, because it is the deformation behaviour of this ice to which frozen soil has been compared. The discussion centers on establishing the appropriate flow law and the deformation behaviour which is pertinent to design of foundations. The Chapter concludes with establishing a flow law of polycrystalline ice based on literature data. This provides a datumn for the research discussed in the following chapters.

In Chapter 3 the laboratory method for preparing the ice used in the experiments is described. The equipment used during the experiment and the procedures followed in carrying out the experiments are outlined. A brief discussion as to why each type of experiment was conducted is also given.

Chapter 4 is a presentation of the analysis of the time-dependent deformation of ice under uniaxial compression. The behaviour of the ice is outlined and the various factors which influence this behaviour are presented. The results obtained suggest a method for

extending the range of applicability of the flow law and dispute the finding of a bi-linear flow law at low stresses. When the laboratory data are corrected for all the factors which influence it, the data compares closely with the data from the literature.

The use of a new method of testing ice is examined in Chapter 5. An experiment was conducted in which a punch was penetrated into an ice sample, and the results used to establish the applicability of this experiment for measuring the properties of the ice. The theory for the expansion of a spherical cavity and the experimental data from Chapter 4 were combined to predict the experimental punch data. These results support the use of a penetration experiment to evaluate the material properties of ice. Visual evidence in support of the spherical cavity model is provided using photographs of thin sections taken of the ice beneath the punch. The lack of influence of complex stress states on the flow law of ice is supported by analysing the experimental results of a triaxial and of a simple shear experiment.

Chapter 6 discusses the use of two finite element computer programs developed during this research work for use in analysing the steady state deformation of frozen soil and ice. These programs have also been used to predict the results of the compression experiment and of punch experiment using the flow law evaluated for this ice. The deformation field from the finite element analysis is presented and supports the use of the cavity expansion

analysis for modelling the punch experiments.

The final Chapter contains the conclusions of this research work and suggestions of future work which will advance the field.

CHAPTER 2

Literature Review

2.1 Introduction

In this chapter the literature on the deformation of ice is reviewed. The review is presented in four categories. The separation of the literature into these categories reflects the three types of laboratory ice which have been used in laboratory deformation studies and the field deformation studies reported on natural ice bodies. Each category is reviewed under the topics of elastic deformation behaviour, and plastic deformation behaviour. Material deformation is examined to establish the factors which influence the behaviour, and how the behaviour of each ice type is interrelated. The processes which control the deformation are pointed out as well as the differences in the processes of deformation.

This review does not cover of all aspects of ice behaviour. The physical model used to explain each process will not be discussed in detail. Hobbs (1974) has presented an exhaustive review of the physical behaviour of ice. This work plus the shorter compilations by Glen (1975) and Michel (1979a) will be used as the primary authoritative references for the following review. The original references referred to in the following have been examined in most instances to extend the review.

2.2 Single Crystal of Ice

The single crystal of 1H ice has a hexagonal crystal structure, which imparts to the crystal an anisotropic physical behaviour. Complete details of the crystal structure of ice are discussed by Glen (1974) and Hobbs (1974). These authors also discuss the physical properties of 1H ice and how its physical properties are influenced by this crystal structure. Only the elastic and plastic deformation behaviour of ice single crystals will be reviewed in this section.

2.2.1 Elastic Behaviour

The purely elastic behaviour of a single crystal of ice is due primarily to changes in spacing between molecules within the ice crystal under an applied stress. During loading of a single crystal of ice, dislocations within the crystal also occur under the applied stress. This dislocation motion causes a permanent rearrangement within the crystal which results in plastic or non-recoverable deformation within the crystal lattice. The dislocation motion causes a single ice crystal to act in a non-elastic manner, since some deformation will remain on unloading. The permanent change in position of dislocations within an ice crystal under load distinguishes plastic behaviour from elastic behaviour. To separate the two behaviours the elastic properties of an single ice crystal must be measured using short-term loading techniques. These techniques apply

a load to the sample for short time periods to ensure little plastic deformation occurs within the ice during the loading interval. The ice, therefore, only undergoes pure elastic deformation under this load.

The measurement of the elastic properties of a single ice crystal is further complicated because of the crystal structure. This structure requires that independent elastic constants be measured in five directions. Hobbs (1974) explains the physical basis of this requirement. The determination of the five elastic constants was first made by Jona and Scherrer (1952).

The elastic constants of a single crystal have now been determined by many authors. Table 2.1 gives a list of the authors, the ultrasonic technique used in the measurement, and the experimental conditions used by each author. Table 2.2 gives the elastic stiffness constant determined by each author in Table 2.1. Dantl (1968) attributes differences in the results of Table 2.2 to conditions of growth and age of each ice specimen used in the experiments. The variation of these constants with temperature has also been examined. Figure 2.1 shows the variation of the stiffness coefficient with temperature. The relationship with temperature for each constant is given by Hobbs (1974). These laboratory determined elastic constants have been used by Michel (1978) to establish the elastic constants of polycrystalline ice which is composed of a large number of individual crystals (Section 2.3.1).

Single crystals of ice are not completely elastic even under the most rapidly applied loading. As stress waves travel through the ice crystals, the strain associated with this stress will not be in phase with the applied stress. This behaviour is known as anelasticity. As a consequence of this phase lag energy is lost but no permanent deformation occurs within the ice crystal. This energy loss has important consequences related to seismic studies on glaciers and ice shelves. Glen (1975) gives a detailed discussion of the theory and the results of laboratory studies related to anelasticity.

2.2.2 Plastic Deformation

Plastic deformation may occur immediately or may take extended periods of time to occur. The deformation behaviour of single crystals both under a constant applied stress and under a constant strain-rate loading condition will be considered. The time dependent plastic deformation is called creep if it occurs under a constant applied load or stress. Creep experiments are the usual test method employed to examine the plastic deformation of single crystals of ice and metal. The constant strain-rate experiment can also be used to examine the time dependent behaviour of ice. In recent years this testing method has been used extensively (Jones and Burnet (1978)).

Glen (1974), in his discussion on the crystal structure of ice, points out that a basal plane exists which is normal

to the optical c-axis of the crystal. The bonding across the basal plane is the weakest bond within the ice crystal. This plane is also the source and path of least resistance for movement of dislocations within the ice crystal. The movement of dislocations within the crystal causes the plastic deformation observed when the crystal is loaded. Glen (1975) states,

> *"An ice crystal can slip readily on the basal plane, i.e., the planes perpendicular to the c-axis, and so provided there is a component of shear stress acting on these planes plastic deformation can occur".*

To have slip on the basal plane the load applied to the ice sample must produce a resolved shear stress on the basal plane. If no shear stress exists on the basal plane, it is very difficult for plastic deformation to take place within the crystal. McConnel (1891) initially showed that plastic deformation occurs if an ice crystal has a resolved shear stress on the basal plane. Figure 2.2 illustrates the direction of load application relative to the c-axis orientation in experiments conducted by Nakaya (1958). The diagrams on the left show the loading direction and c-axis orientation in the undeformed sample. The diagrams on the right illustrate the observed deformation of each sample. Qualitatively the deformation of a single crystal can be examined by representing the structure of the crystal as a set of playing cards. The face of each card represents a basal plane within the ice crystal.

The direction of slip within the basal plane has also been studied (Mugge (1895), Glen and Perutz (1954), Steinemann (1954)). These authors did not find a preferential slip direction within a single crystal. Kamb (1961) showed that if the shear strain-rate is parallel to each slip direction in the crystal, the relationship between the strain-rate and the parallel shear stress is given by:

$$[dV/dt](i) = (\text{constant})[\delta(i)]\ \underline{n} \qquad (2.1)$$

where

$[dV/dt](i)$ ≡ shear strain-rate in glide direction (i)

$\delta(i)$ = shear stress parallel to glide direction (i)

n = exponent on stress

(*NOTE* It should be noted that through out this thesis an exponent is indicated by underlining it in the equation. The exponent n in Equation 2.1 is an example.)

Then for values of n equal to 1 and n equal to 3 no preferred glide direction within the single crystal exists. This shows that easy glide for the above two conditions would occur in the direction of the resolved maximum shear stress. The experimental evidence displays some deviation from the above, but these deviations have not been explained from a physical process point of view (Glen and Jones (1967)).

Higashi et al. (1968) caused non-basal glide to occur within a single crystal. Non-basal glide is slip which causes plastic deformation within crystals on planes other than the basal plane. These authors applied stresses such that no shear stresses would occur on the basal plane of the crystal. The deformation of the single crystal was then measured. They found that plastic deformation occurred within the single crystals, but only under applied stresses of about 10 times larger than that required to cause plastic deformation parallel to the basal plane. Non-basal glide is referred to as hard glide and basal glide as easy glide in Hobbs (1974). It should also be pointed out that glide and slip both refer to dislocation motion within the crystal. This finding demonstrates that the plastic deformation of a single ice crystal is a function primarily of the magnitude and direction of the applied load. Later in this section the influence of factors other than the load will be outlined.

Figure 2.3 presents laboratory results from Steinemann (1954) which illustrate that the strain-rate at each applied stress increases with time during the experiment. The strain-rate increases until at large strains a nearly constant strain-rate is established under a constant applied stress. The experimentally determined constant strain-rate occurs at a total strain of about 20% within the single crystals. The strain-time behaviour of the single crystals of ice differs from the behaviour of polycrystalline ice and many single crystals of metals.

Polycrystalline ice and metal single crystals deformed under a constant applied stress produce a strain-time curve shown in Figure 2.4. This Figure illustrates that the strain-rates for these materials decrease with time until a minimum or steady-state strain-rate is reached. This is in contrast to the strain-time behaviour of a single ice crystal shown in Figure 2.3.

The strain-time curves illustrated in Figure 2.4 are called the typical creep curves since they show the deformation behaviour of most polycrystalline materials and many single metal crystals (Conway (1967)). The typical strain-time curve II in Figure 2.4 is usually divided into 4 regions from the deformation or strain point of view. Region 1 is between O and A and is instantaneous elastic deformation. A-B is region 2 and is characterised by a decreasing strain rate with time. This region has been termed the primary portion of the strain-time curve. Region 3 occurs between B to C and is the deformation region over which the sample deforms at a constant or at a minimum strain-rate. It is termed the secondary portion of the strain-time curve. The time interval of this region is variable and will be discussed in detail in the section on polycrystalline ice. The 4th region between C and D is called the tertiary portion and is associated with increases in the strain-rate beyond point C. Within region IV a second constant strain-rate may occur after large strains within the sample are reached. Point C is called the inflection

point and except for samples under very low stress point B and C occur at the same location (Mellor (1979)). Curves of this shape have long been studied in Engineering in relation to design of machinery to resist creep.

A comparison of Figure 2.3 and Figure 2.4 shows the contrast in the shape of these curves. The strain-time behaviour of the single ice crystal curve begins at point B on the typical creep curve and then duplicates the typical creep curve. During time dependent deformation the single crystal softens with increasing strain, whereas, the polycrystalline material initially hardens then becomes [illegible] beyond point B. Glen (1975) explains single crystal [illegible]ur as follows:

> *"Initially there are a relatively small number of dislocations available for the deformation, and that their velocity is limited at the stress available. As deformation proceeds and more dislocations are produced by multiplication processes, the rate of deformation can accelerate, this effect being more important than the interaction of dislocations which causes the reverse effect in metal single crystals."*

The polycrystalline behaviour in contrast is influenced by the single crystal behaviour, but it is also affected by the behaviour of the crystal boundaries.

The shape of the strain-time curve for a single crystal illus[illegible]ated in Figure 2.3 has been approximated using a power [illegible] relation. The strain is expressed in terms of the

time of loading raised to a power m. The relationship used by various authors to represent the strain-time curves are contained in Table 2.3. These equations result from curve fits through the strain-time data of the experiments and do not represent a unique physical relationship. The power law exponent (m) used to fit the data varies between 1.5 and 2.0. Each relationship is for easy glide on the basal plane of a single ice crystal only.

In studies of the influence of temperature on plastic deformation it has been found that the deformation associated with easy glide decreases as temperature decreases (Griggs and Coles (1954) and Steinemann (1954)). The ice crystal is known to become harder with a decrease in temperature and thus has an increase in resistance to deformation. The strain-time law of Griggs and Coles (1954) contained in Table 2.3 includes the temperature as a variable.

In analysing the plastic deformation of materials, especially the results of creep experiments, it is usual to determine the constant strain-rate associated with the linear portion of the strain-time curve. This constant strain-rate is then analysed to establish the relationship between the measured strain-rate, applied stress and temperature (Glen (1955), and Hult (1966)). This method is usually adopted since the strains associated with the initial portion of the strain-time curve are small compared to the total strain the sample undergoes. The constant

strain-rate is also amenable to comparison with various factors which influence the plastic behaviour of a single crystal.

The constant resolved shear stress on the basal plane of a single crystal has been related to the constant shear strain-rate of the sample using a power law relation (Hobbs (1974), and Glen (1975)). The usual form is:

$$[dV/dt] = A[\delta]^{n} \qquad (2.2)$$

where

$[dV/dt]$ = shear strain-rate

δ = shear stress

The value of A and n in Equation 2.2 given by various authors have been tabulated in Table 2.4. The type of loading condition applied in each experiment is noted in the Table. Note that a number of the authors have conducted constant strain-rate experiments. These authors have related the peak yield stress during the constant strain-rate experiment and the constant strain-rate during the experiment using the above power law relationship. The exponents from these experiments are also contained in Table 2.4. The exponent of the power law (n) determined from the plastic deformation on single crystals of ice varies between 1.5 and 3.0 as shown in Table 2.4. The tabulated data do not suggest that a difference exists between the results of the two different loading conditions.

The influence of temperature on the flow law is given by the Arrhenius relationship (Glen (1975)). The flow law relationship given by Equation 2.2 is rewritten as:

$$[dV/dt]=K[\delta]^{n} \{\exp(-Q/KT)\} \qquad (2.3)$$

where

[dV/dt] = shear strain-rate

δ = shear stress

Q = activation energy

K = Boltzmann's constant

K = constant

T = temperature (K)

Higashi et al. (1969), Readey and Kingery (1964), Higashi et al. (1965), Glen and Jones (1967), Mellor and Testa (1969a), Muguruma (1969), and Jones and Burnet (1978) have used the Arrhenius relationship to relate the shear strain-rate with the shear stress and temperature from constant stress experiments and constant strain-rate experiments. The value of the activation energy obtained by various authors differs and Glen (1975) recommends using an average value of 0.68 eV between -10°C and -50°C.

Muguruma (1969) showed that the surface preparation of the single crystal influenced its plastic deformation behaviour. He tested samples with various surface treatments and presented evidence on how each treatment influenced the yield strength of the ice sample under constant strain-rate

experimental conditions. His data supported Higashi et al. (1965) in that the surface preparation of the crystal influences the plastic deformation behaviour of the ice crystal.

The plastic deformation of single crystals is also influenced by chemical impurities contained within the ice crystal. This occurs because the deformation of an ice crystal is controlled by the motion of dislocations on the basal planes. These dislocations are controlled by defects within the crystals which are in turn influenced by chemical impurities within the crystal. Jones (1967), Jones and Glen (1968), Jones and Glen (1969), and Nakamura and Jones (1970) have studied the influence of different chemicals contained within the ice on the plastic deformation behaviour of single ice crystals. Hobbs (1974) presents a detailed discussion of this influence on the plastic deformation of the ice crystals.

Rigbsy (1957) showed that an all-round confining pressure applied to a single ice crystal had no influence on the strain-rate of the single crystal under a constant applied shear stress. This demonstrates that confining pressure can be neglected when studying the influence of the applied stress on the plastic deformation of a single ice crystal. Rigbsy (1957), however, noted that the influence of the hydrostatic pressure could only be neglected if the influence of the temperature change due to an increase in an all round pressure was accounted for in the analysis of the

data.

Non-basal glide was shown to exist by Butkovich and Landauer (1958), and Vialov (1958). They demonstrated that the strain-rate associated with non-basal glide is about 100 times slower than the strain-rate associated with easy glide within a single crystal. Bartlett and Readings (1964) and Higashi et al. (1968) also found that non-basal glide can occur in single ice crystals. The strain-time curve for a sample deformed under non-basal glide is different from that of a single crystal deformed in easy glide. The curve for a sample undergoing hard glide has a shape similar to that of polycrystalline ice shown in Figure 2.4 and not of a single ice crystal in easy glide shown in Figure 2.3.

This brief review discussed the time dependent plastic deformation behaviour of an single ice crystal and presented evidence that this behaviour is influenced by the following:

1. Orientation of a crystal axis, i.e. resolved shear stress on basal plane;
2. Magnitude of the applied shear stress;
3. Temperature during the experiment;
4. Surface preparation of the single crystal;
5. Chemical impurities contained within the crystal.

2.3 Columnar Grain Ice

Columnar grained ice grows on lakes and rivers. It is composed of columns of ice crystals, with the long axis of the crystal column oriented parallel to the direction of heat flow during formation of the ice cover. This ice

typically has the optic c-axis randomly oriented in the plane normal to the long axis of the crystal. Michel and Ramseier (1971) have classified this as S2 ice in their ice classification system.

The deformation behaviour of columnar grained ice is important in Engineering because of loads placed on Engineering structures by river and lake ice. The deformation behaviour is also important in understanding the response of the lake and river ice to loads from construction platforms or transportation routes. S2 ice has also been studied extensively within the laboratory, because its deformation behaviour is between that of a single ice crystal and that of equiaxial polycrystalline ice aggregate. Its deformation behaviour is, therefore, important in understanding the behaviour of polycrystalline ice.

The process of the formation of S2 ice is described by Pounder (1965) and Michel (1979a). The physical properties of this ice have been reviewed in Glen (1974) and Hobbs (1974). The reader is cautioned when examining experimental results or discussion of results to ensure that the direction of each measurement relative to the column axis is given. This caution is given, because S2 ice has a random orientation of the c-axis only in the plane normal to the column axis. The ice behaves in an anisotropic manner if loaded parallel to the crystal column axis. Also one must distinguish experimental results of S2 ice from those in the literature of equiaxial polycrystalline ice which has the

c-axis of its crystals generally oriented randomly in three dimensions. Both ice types have been called polycrystalline in the ice literature. The results of each must not be grouped together, since each is a different material and behaves in a different manner.

2.3.1 Elastic Behaviour

The elastic behaviour of columnar grained ice is a function of the orientation of the crystal and of the grain boundaries of the crystal. The influence of the crystal orientation on the Young's Modulus of an ice single crystal was discussed in Section 2.2.1. The crystal boundaries must also influence the elastic behaviour because, on the crystal level, these boundaries represent non-homogeneties within the ice and points of stress concentrations. The influence of these two major factors on the elastic deformation of S2 ice will be outlined in the following paragraphs. Additional factors as presented in the literature will be discussed later in this section.

Gold (1958) conducted a detailed study of the Young's Modulus of columnar grained ice. He showed that ice obeyed Hooke's law and thus acted as an elastic material under the following conditions:

1. temperature range -3.0°C to -40.0°C;
2. applied stress less than 1000 kPa;
3. loading duration less than 10.0 seconds.

Gold demonstrated that the time dependent deformation within

the ice resulted in a decrease of the Young's Modulus from the value under instantaneous loading. This confirmed the finding for the deformation of a single ice crystal which showed that the apparent elastic behaviour is dependent on time-rate of loading.

Gold (1958) also gave the following relationship for the temperature influence on the Young's Modulus of columnar grained ice:

$$E = [5.69 - 0.0648 \bullet T] \qquad (2.4)$$

where

E = Young's Modulus (GPa)

T = Temperature in °C

This relationship was independent of the loading direction normal to the long axis of each crystal. Gold found that the value of Young's Modulus decreased with decreasing sample size for the S2 ice tested. This is an important finding as it shows a size of sample effect on the elastic deformation properties of columnar grained ice. He found that the ice sample became less rigid as the sample size decreased while maintaining the ice crystal size constant.

Recent studies of Young's Modulus of columnar grained ice have built on the early work of Gold. From these studies it becomes apparent that the rate of loading the sample was the most important factor influencing the measured Young's Modulus. Figure 2.5 shows the variation of Young's Modulus

with rate of loading the sample. It includes the results of a number of authors with the references given on the plot. The data shows that Young's Modulus is strongly dependent on the loading rate used in the experiment.

Michel (1979a) presents the following relationships for the temperature dependence of Young's Modulus of pure columnar grained ice:

$$E(\text{perpendicular}) = [9.27(1-1.36 \times 10^{-3} \bullet T)] \quad (2.5)$$

$$E(\text{parallel}) = [9.62(1-1.07 \times 10^{-3} \bullet T)] \quad (2.6)$$

where

E (perpendicular) = Young's Modulus perpendicular to long axis of S2 ice

E (parallel) = Young's Modulus parallel to long axis of S2 ice

T = temperature in °C

Equation 2.5 and 2.6 were obtained using the elastic constants measured from dynamic loading experiments of a single ice crystal and a model using a random orientation of the c-axis within the plane perpendicular to the long axis of the ice columns. These equations show a slight anisotropy of the Young's Modulus in S2 ice as would be expected from the study of orientation of the crystal within an ice specimen.

The value of Young's Modulus for columnar grained ice

is also influenced by the density of the ice. Nakaya (1959) and Pounder (1965) studied the influence of porosity of ice on its Young's Modulus value. They found that for Arctic sea ice and porous ice the Young's Modulus could be represented using a linear relation between Young's Modulus and ice porosity. Figure 2.6 shows the influence that the porosity of the ice has on the measured Young's Modulus. As the porosity of the ice increases the Young's Modulus decreases.

This brief review of the literature on the short-term deformation of S2 ice outlined the following factors influencing its elastic behaviour:

1. Rate of loading;
2. Temperature;
3. Density;
4. Direction of measurement relative to long axis of crystal.

2.3.2 Plastic Deformation

The plastic deformation of S2 ice is reviewed in this section. The studies conducted on S2 ice generally have been for a shorter loading time than S1 (single crystal ice). The shorter loading period used during the experiments reflects the type of loading that S2 is generally subjected to in the field. The deformation of S2 ice in the field usually results from a short-term loading condition during which the ice usually undergoes small strains. Gold (1965) states that natural ice covers such as rivers and lakes are subjected to creep strain of less than 1% total strain as a result of

loads applied under normal Engineering circumstances. The duration of loading on these ice covers is also of a short-term nature. Masterson et al. (1979) has described strains induced in floating ice islands used in oil exploration off-shore from a Canadian Arctic Island. The strains within the ice were also very small even under the long-term loading associated with drilling of an oil well. This shows that the loading imposed on S2 ice causes only small total strains. Therefore, experiments have not been conducted which subjected the S2 ice to large strains and long-term loading conditions.

The time dependent plasic behaviour of S2 ice has been discussed by Gold (1960, and 1965) and Michel (1978). Gold (1960) examined the crack formation associated with S2 ice subjected to a constant load. He presented a strain-time curve which showed that columnar grained ice has a period of increasing strain-rate during the primary portion of the strain-time curve. Figure 2.7 shows the strain-time behaviour of S2 ice. This finding was confirmed by Gold (1965). Columnar grained ice deforms in a similar manner to single ice crystal at very low strains. At strains above about 0.1% the strain-time curve changes and the columnar ice behaves in a manner similar to the typical creep curve shown in Figure 2.4. In Figure 2.7, note the initial portion of the strain-time curve which resembles the curve of a single crystal (Figure 2.3) but followed by a typical creep curve.

In all the constant loading experiments conducted by Gold, the load was applied normal to the long axis of the crystal, therefore, the load was applied in the plane of the ice sheet. Gold (1965) in a companion paper analysed the experimental results and presented the following relationship between the applied stress and strain-rate for columnar grained ice:

$$de/dt = A[\sigma]^{3.11} \qquad (2.7)$$

where

e = strain

σ = stress

A = constant dependent on temperature

A is a parameter which depends on time of loading and strain attained in each experiment. The exponent determined in these experiments is 3.11. Equation 2.7 suggests that the exponent in the flow law governing the creep of S2 ice is equal to approximately 3.0. Gold (1973) also recommends that a power law relationship with an exponent equal to 3.0 should be used to describe the flow law for columnar grained ice. The use of an exponent equal to 3.0 has been accepted in analysing the flow law of columnar grained ice for the stress range 1000 kPa and 10,000 kPa (Sinha (1978)).

The flow law of S2 ice has been extended to the stress region less than 1000 kPa by Sinha (1978). Sinha presents a method of analysing columnar grained ice data which, using

available laboratory data, justifies the extension of the use of the exponent equal to 3.0 to low stresses. This justification is not based on laboratory results but on the predictions determined by a rheologic model used to describe the strain-time curve of the columnar grained ice.

Sinha (1978) has also used his model to predict that much of the experimental data at low stresses is questionable. The low stress data demonstrates a decrease in the exponent of the power law from 3.0 to 1.0 as the axial stress decreases below about 200 kPa (Butkovich and Landauer (1960), Mellor and Testa (1969b), and Colbeck and Evans (1973)). According to Sinha these experiments are questionable because the load applied during each experiment was not maintained for a sufficient period of time to establish a minimum or constant strain-rate. As a result the strain-rates measured in the experiment and used to establish the flow law were all too fast for the given loading condition. This improper data results in a flow law which predicted that the exponent decreases from 3.0 to about 1.0.

Muguruma (1969), using a constant strain-rate experiment, showed that the yield stress in columnar grained ice is dependent on the ice crystal grain size. He developed the following relationship:

$$\sigma = 0.75 + 0.31\ (d)^{-0.5} \qquad (2.8)$$

where

Yield stress (Kg/cm^2)

= average grain size (mm)

This equation shows that the ice crystal size influences the plastic as well as the elastic deformation behaviour of S2 ice. Equation 2.8 is valid for crystal size greater than 2.0 mm and for the sample size used in his constant strain-rate experiment.

The influence of temperature on the flow law of columnar grained ice is predicted using the same Arrhenius relationship as for single crystals of ice. It will not be reviewed in detail in this section. It should be pointed out that few creep experiments on S2 ice have been conducted at temperatures warmer than -7.0°C.

The review of the literature on columnar grained ice shows that the plastic deformation is influenced by:

1. crystal orientation;
2. temperature;
3. density;
4. impurities;
5. crystal size and sample size.

2.4 Equiaxial Polycrystalline Ice

Equiaxial polycrystalline ice is usually found in glaciers and ice shelves. The crystals have approximately equal axial diameters (equal dimensions in each direction) as the result of their growth during compression and deformation within the natural ice body (Paterson (1969)).

The ice mass is composed of single crystals with a random orientation of the optic c-axis of each crystal. This ice type is classified as T1 using the classification system of Michel and Ramseier (1971). It has been studied extensively, and the laboratory data has been used to develop a flow law for ice which is then used in various models to predict the deformation behaviour of glaciers and other natural ice bodies.

The studies on polycrystalline ice have nearly all centered on developing a flow law to describe its plastic deformation. Until recently little interest has been directed to a study of the elastic deformations of polcrystalline ice because most of the field problems of interest involved conditions under which large deformations took place. The field problems have been related to the flow of glaciers and large ice shelves. The mass of polycrystalline ice in each of these field conditions has undergone deformations of hundred's of metres under varying stress conditions and over long periods of time.

The type of field problem for which a knowledge of the behaviour of ice is important has changed recently. During the past ten years with the rapid development in the American and Canadian far North, larger structures are being built or are being planned for construction in the permafrost region. The design of these structures requires a knowledge of the dynamic response of permafrost. The frozen soil has varying quantities of ice contained within it, and

thus the dynamic response of ice is required to understand the frozen soil behaviour.

In order to design a foundation for these structures, the time dependent deformation of frozen soils has been studied. These studies show that ice rich frozen soil behaves in a manner very similar to polycrystalline ice (Vialov (1965), Sayles (1968) and Ladanyi (1972a)). The frozen ground behaviour has required a review and evaluation of the time dependent behaviour of polycrystalline ice. This review is necessary because ice behaviour is used as an upper bound to the deformation behaviour of frozen soil.

In order to evaluate the creep characteristic of polycrystalline ice, the researchers developed an artifical model ice within the laboratory which could be used to produce small samples (Glen (1955), Steinemann (1958), Mellor and Testa (1969b) and Barnes et al. (1971). The laboratory ice produced is equiaxial, isotropic and has a random crystal c-axis orientation. The laboratory experiments performed using this ice helped establish the flow law of the ice and evaluate the influence of various factors on this flow law. Studies have also been conducted using samples of polycrystalline ice obtained from tunnels within glaciers (Colbeck (1970) and Colbeck and Evans (1973). The results of these will be compared with the results of the laboratory prepared ice and the differences between the two outlined.

The results of laboratory deformation studies of

polycrystalline ice under the topics of elastic and plastic deformation are reviewed in the following paragraphs.

2.4.1 Elastic deformation

Michel (1979a) gives the value of the Young's Modulus of polycrystalline ice as:

$$E = [8.93(1-1.28 \times 10^{-3} \bullet T)] \qquad (2.9)$$

where

E = Young's Modulus (GPa)

T° = Temperature in degrees below 0°C.

Equation 2.9 was determined using the dynamic elastic constants of a single ice crystal. The elastic constants were calculated assuming a random crystal c-axis orientation within the ice sample.

Studies of dynamic properties of polycrystalline ice have identified the following as important factors which influence the dynamic response of the ice (Vinson (1978)):

1. temperature;
2. frequency;
3. confining pressure;
4. density.

The results of laboratory studies of the dynamic response of ice are reproduced in Figure 2.8 through Figure 2.11. The plots show experimental data from various authors, who used different dynamic methods to determine the response of the

ice. The reader is referred to the summary by Vinson (1978) for a discussion on the various methods of testing and to the original author for details of each test method.

In Figures 2.8 through 2.11 the ordinate axis presents the longitudinal wave velocity and not the dynamic Young's Modulus. The Young's Modulus can be determined from the longitudinal velocity using the following relationship Vinson (1978):

$$E = [V^2 \bullet p] \qquad (2.10)$$

where

E= Young's Modulus (GPa.)

V = Longitudinal velocity (m/sec.)

p = Dynamic density ($N \bullet sec.^2/m^4$)

In Figure 2.8 the lack of influence of the temperature in the range 0°C to -20°C on the dynamic Young Modulus is illustrated. These results are based on field, as well as, laboratory experiments. Figure 2.9 shows that the frequency used in the determination of the dynamic properties has a strong influence only in the low frequency range. The response of the polycrystalline ice is analogous to the behaviour reported by Sinha (1978) for columnar grained ice and illustrated in Figure 2.5. In both Figures the Young's Modulus is influenced only in the low frequency region.

Confining pressure has an important influence on the dynamic Young's Modulus, of laboratory samples at warm

temperatures. This behaviour is shown in Figure 2.10 after Vinson and Chaichanavong (1976). In comparing laboratory and field experiments Bennett (1972) found no significant difference between the wave velocities of unconfined samples and samples subjected to confining pressure. This discrepancy in the results has not been explained by either author. The possible influence of the confining pressure must be noted and should be examined in detail, since it will have an important influence on the field behaviour of ice under dynamic loading.

Figure 2.11 illustrates that density is the most important influencing factor on the dynamic Young's Modulus of ice. Field and laboratory studies presented the same behaviour of increasing longitudinal velocity with increasing density. This behaviour is as expected and supports the finding that the Young's Modulus of ice increases with a decrease in porosity shown in Figure 2.6. This brief review suggests that ice density is the most important factor influencing the dynamic behaviour of polycrystalline ice.

2.4.2 Plastic Deformation

Glen (1975) recognized that two loading and deformation conditions could exist in ice. More importantly he recognized that two flow laws exist for ice. He states:

"there is some confusion in the literature as to which of the two is being sought in some cases."

The two flow laws he recognized are the result of:

1. Loading condition applied for a long time resulting in large deformations which are associated with recrystallization and accelerating strain-rates within the ice.
2. Loading conditions which are associated with deformation in the ice which have not produced recrystallization.

During the review of the literature the loading condition for which the data is valid will be discussed. This is required, since during recrystallization a change in crystal size and orientation of the c-axis occurs, which changes the characteristics of the ice being subjected to load (Kamb (1961) and Rigsby (1960)). During the review, the loading condition for which the results are valid will be pointed out to emphasize that few experimental laboratory programs determined the flow law valid for the first loading condition above. The experimental programs studied the deformation behaviour of ice under a short-term loading condition, and, using the results, the authors presented flow laws which are valid for the second loading condition. These flow laws have been incorrectly compared with field results which result from long-term loading conditions. This has resulted in a flow law which extends over a wide range of stresses, but which has been developed using results which are not comparable (Meier (1960) and McRoberts (1975)). The review will be presented using the following outline:

1. strain-time curves;
2. flow law (short-term);
3. flow law (long-term);
4. factors influencing the flow law of ice.

2.4.2.1 Strain-time law

In Figure 2.4 the typical creep curves of a single crystal of metal and of polycrystalline metals is plotted. Four regions are shown associated with the deformation in the strain-time curve II. Figure 2.12 shows a set of creep curves for polycrystalline ice from Mellor and Testa (1969b). The important experimental parameters are contained in the Figure, and the plot illustrates that polycrystalline metals and equiaxial polycrystalline ice have creep curves of the same shape. For this reason much of the analysis of creep data of polycrystalline ice has been prepared using procedures outlined in textbooks on the creep of metals (Hult (1966), Odqvist (1966), and Conway (1967)).

The shape of the strain-time curve of ice has been studied and the region of decreasing strain-rate successfully fitted using a power law to relate the strain as a function of time (Glen (1955) and Barnes et al. (1971)). No author has established all the factors which influence the exponent applied to the time.

Glen (1955) used the Andrade one-third law to fit his experimental data and to predict a strain-rate at times beyond the limit of his experiments. Barnes et al. (1971) also used the Andrade one-third law to separate the primary

creep from the so called secondary creep in their experiments. This allowed the authors to determine the secondary or steady-state strain-rate from experimental results for which a true steady-state creep had not yet been achieved. These results and the validity of this approach will be discussed under the topic of short-term flow laws.

The use of the one-third law in analysing the primary creep behaviour of metals was first proposed by Andrade (1910). His experimental results on the time dependent behaviour of lead under constant load were analysed using this relation for the primary portion of the typical creep curve. As mentioned above, this method has made its way from the metal literature into the ice literature. Glen (1955) was the first author to use this relationship to analyse the strain-time behaviour of ice. The shortcoming of this function is its inability to separate the steady-state creep region from the primary region shown in Figure 2.4. The above authors have assumed that superposition of the deformation from each of the initial three regions of the creep curve is valid from the beginning of the experiment. Recently, two more elaborate strain-time relationships have been proposed for use in analysing the polycrystalline ice results (Michel (1978), and Sinha (1978)).

Michel (1978) develops a strain-time relationship using a model of the deformation behaviour of discrete ice crystals. This model accounts for the creep behaviour of the individual ice crystals with its strong dependence on the

orientation of the c-axes. This information, plus the requirement that a collection of ice crystals with randomly oriented c-axis must deform in a compatible fashion are the governing conditions of the model. The strain time behaviour of deformed ice has been modelled very closely using this procedure (Michel (1978), and Michel (1979a). The model requires that five parameters be determined to predict the strain-time response of an ice sample under a given loading condition. The use of this model requires extensive computer analysis and time to establish these parameters (Michel (1979b)). This is a shortcoming of the approach at this time, but with future development this model appears to hold promise in predicting the time dependent deformation behaviour of polycrystalline ice.

Sinha (1978) has presented a simple rheologic model for the prediction of the time-dependent deformation behaviour of polycrystalline ice from initial application of load to the onset of tertiary creep (Figure 2.4). His model has been verified using experimental results of columnar grained ice under short-term loading condition (Sinha (1978) and Gold and Sinha(1979)). The model has not yet been used to verify that it will predict the strain-time behaviour of equiaxial polycrystalline ice in the same manner as it predicts the columnar grained ice behaviour. The model must also be tested using the results from long-term loading of ice to compare the predicted behaviour and the actual experimental behaviour.

2.4.2.2 Flow law resulting from short-term loading

The majority of creep experiments presented in the literature have strain-rate data determined before the inflection point on the strain-time curve (Figure 2.4). All the data reviewed in this section has been obtained from laboratory experiments of short-term loading condition. The loading configuration used in the majority of the experiments was uniaxial compression, but tension and shear loading were also used (Steinemann (1958) Butkovich and Landauer (1958)). The discussion will be restricted to the flow laws determined by various authors in the stress range of 10 kPa to 1000 kPa. Only the influence of the applied stress on the strain-rate which results from these creep experiments will be outlined. The detailed influence of all the other factors on the flow law will be discussed in a later section of this review. The review of the literature of the flow laws will be presented in approximate chronological sequence.

The early workers showed that polycrystalline ice deformed plastically under load, but they did not establish the flow law which governed its behaviour (Reush (1864) and McConnel and Kidd (1888)). During the period from the late 1800's until the mid 1940's experimenters were analysing the load and strain-rate curves of ice using a Newtonian fluid model (Weinberg (1907), Somigliana (1921), and Lavrov (1947)). The earlier work by McConnel and Kidd had shown that ice was not a Newtonian fluid, since the strain-rate

was not proportional to the applied stress. In the late 1940's researchers with experience in the creep of metals became interested in the creep of ice. Orowan (1947) and Nye (1951) proposed that the behaviour of ice be analysed as an ideally plastic material, in a manner similar to that used in the study of metals. This was the important push that was required as it brought people with varied backgrounds together to examine the behaviour of ice.

Glen (1952, 1953, 1955) presented the initial results on the creep of polycrystalline ice. He showed that the strain-time law of polycrystalline ice had a shape similar to the typical creep curve shown in Figure 2.4. He presented the flow law for polycrystalline ice as a simple power law relationship with the following form:

$$[de/dt] = A[\delta]^{n} \qquad (2.11)$$

where

$[de/dt]$ = minimum axial strain-rate

δ = axial stress

A = temperature dependent parameter

n = exponent

Glen (1955) presented data which upon analysis gave the exponent n equal to 3.17 ± 0.2 at temperatures warmer than $-2.0^{\circ}C$. These data were determined using the minimum strain-rate measured during the loading period of each experiment. The strain-rate recorded during these

experiments was not the lowest strain-rate for each given stress level, because some of the experiments were still undergoing primary creep. Glen's results showed a strong dependence of the strain-rate on the stress. In a plot of logarithm of strain-rate versus logarithm of stress, a straight line with a slope equal to 3.17 was the best fit through the data.

The second major contribution to the flow law of polycrystalline ice was made by Steinemann (1958). He showed that under extended periods of loading polycrystalline ice underwent an acceleration in strain-rate after passing through regions 1, 2 and 3 on the strain-time curve. This acceleration occurred beyond the inflection point and resulted in a region of nearly constant strain-rate in the tertiary portion of the strain-time plot. This second constant strain-rate region will be discussed later in Section 2.3.2.3.

Steinemann's research showed that the flow law at low stress was not linear in a logarithm strain-rate versus logarithm stress plot. Figure 2.13 shows the data of Steinemann at various temperatures and under both tensile and compressive loading conditions. It must be noted that the non-linearity in the flow law plot is a result of the data from the tension experiment. This data was the first indication from laboratory experiments that the flow law of ice may not be linear throughout the complete stress range in the strain-rate versus stress plot. Steinemann studied

many other factors which influence the flow law of ice but these will be discussed in Section 2.3.3.

Butkovich and Landauer (1958 and 1960) studied natural polycrystalline ice from the Thule area of Greenland under laboratory conditions. Their experimental results show that the strain-rate of polycrystalline ice is about 100 times slower than the strain-rate of single crystals subjected to easy glide. Their flow law using a simple power law had an exponent of n equal about 1 for the test conditions. This data has been criticized because of the short time of loading and the fact that each sample only contained a few individual ice crystals (Mellor and Testa (1969b) and Mellor (1979)). The criticism resulted because the samples had too few crystals to be considered an isotropic material (Mellor (1979)). Therefore, the data of Butkovich and Landauer should not be compared to the data of Glen and Steinemann in establishing a flow law.

Voytkovskiy (1960) reported results of creep experiments conducted on polycrystalline ice under a condition of torsional shear. He established a stress level [δp] called the "limit of prolonged creep" as the stress level above which no continous steady-state strain-rate is possible within an ice specimen. He established the following values of [δp] for different experimental temperatures:

δp	Temperature

kPa	°C
160	-1.2
200	-1.8
300	-4.0

All ice samples stressed to a higher level would undergo a period of decreasing strain-rate, then an inflection point and finally an acceleration in the strain-rate to rupture. He states that no steady-state strain-rate would exist above this stress level. He used this evidence to dispute the validity of the flow law proposed by Glen (1955) with the exponent n equal to 3.17. He says,

"In most of Glen's experiments the stresses exceeded the limit of prolonged creep and there was no stage of steady creep, while Glen compared minimum rates of deformation without consideration of the character of the creep curves."

Votykovskiy presents his flow law of the steady-state strain-rate as a function of the applied stress as :

$$[dV/dt] = K[S\delta]^{\underline{n}} \qquad (2.12)$$

where

[dV/dt] = shear strain-rate

K = constant

Sδ = shearing stress

He found that the exponent n of this flow varied between 1.6

and 2.2. The low value of the exponent n should be noted as it contrasts with the value reported by Glen (1955) and Steinemann (1958). It should also be noted that these experiments were conducted under a torsional shear loading condition in contrast to unaxial compression and tension used in Glen (1955) and Steinemann (1958).

Weertman (1963) presented a theoretical relationship which predicted that the strain rate of polycrystalline ice was related to the applied stresses raised to the third power. This relationship was based on the resolved shear stress actually applied to the basal plane of a single ice crystal. In a polycrystalline aggregate of randomly oriented single crystals the applied stress to the sample would exceed the resolved shear stress on the basal plane of a single crystal. Therefore, the strain-rate associated with a polycrystalline ice mass must be less than the strain-rate associated with a single crystal in which the applied stress was equal to the resolved shear stress. Weertmann's relationship predicted a slower strain-rate in a polycrystalline ice than in a single crystal, but the calculated strain-rate was still about an order of magnitude faster than the experimentally measured strain-rate for polycrystalline ice. To explain this Weertman suggested that the ice crystals supported a portion of the applied load depending on their crystal orientation. The crystal aligned for easy glide supported less of the load, whereas a less favourably oriented crystal supports a higher portion of the

load. This would reduce the theoretical strain-rate to approximately that observed in the experiments. Weertman's relationship has not been accepted within the ice literature to date, but it does lend theoretical support to the view that the power law exponent equals 3.0 as proposed by Glen (1955).

Dillon and Andersland (1967) conducted experiments on the creep of ice under high stresses and in the temperature range -10°C to -14°C. They compiled a summary of the data of other authors to establish a flow law using a hyperbolic sine relationship. This type of relationship results from the chemical rate process theory, presented by Kauzmann (1941) to explain the deformation of metals from an atomic point of view. The hyperbolic sine relationship showed a good fit to the experimental data over a wide stress range as shown by Dillon and Andersland (1967). The hyperbolic sine relationship was also used by Barnes et al. (1971) to extend the stress range of the flow law of ice to very high stresses and will be discussed later.

Mellor and Smith (1967) conducted experiments on snow ice samples with density less than pure ice. Their data can be converted to densities of pure ice, as illustrated in Budd (1969) and the strain-rate and stress results obtained. The results give a non-linear flow law which is best described as a two term flow law as follows:

$$[de/dt] = A^1[\delta] + A^2[\delta]^{n^1} \qquad (2.13)$$

where

$[de/dt]$ = strain-rate

δ = axial stress

A^1 & A^2 = constants dependent on temperature and ice type

n^1 = exponent determined from experiment

A similar bilinear flow law as given by Equation 2.13 was initially proposed by Meier (1960) to describe the combined results of laboratory studies and glacier deformation studies. His results will be discussed in Section 2.4.2.3.

The results of Mellor and Smith (1967) have been questioned because of the decrease in the stress dependence of the strain-rate at low stresses. The criticism is that the experiments were not loaded for a long enough period to produce sufficient strain within the sample to cause a minimum strain-rate to be achieved (Mellor and Testa (1969b)).

Mellor and Testa (1969a and 1969b) conducted an extensive study of the influence of temperature and low stresses on the flow law of polycrystalline ice. They showed that at a constant axial stress of 43 kPa the strain-rate results of three samples showed that ice is not a viscous fluid. The strain-time curve from the final load application is plotted in Figure 2.12. From these experimental results they determined an exponent n equal to 1.8 using a simple power law relationship between strain-rate and stress. The

authors suggest that their experiments may not have been conducted to large enough strains to establish a true secondary strain-rate, and this would mean that the true exponent for the ice flow law would increase above the experimental value of 1.8. The experimental results of Mellor and Testa (1969b) are very important since they show that the flow law of ice will not have a linear relationship between stress and strain-rate at low stresses at a temperature of -2.0°C.

Colbeck (1970) studied the deformation of polycrystalline ice samples cut from an ice tunnel in the Blue Glacier. He conducted the experiments within the ice tunnel to ensure a controlled experimental environment. These tests were conducted at low stresses and at the pressure melting temperature of the glacier. The author checked the experimental data against various flow laws to establish the best fit to his data. In a published paper, Colbeck and Evans (1973), presented the following flow law for the experimental data from the Blue Glacier:

$$[de/dt] = A\,[\delta] + B\,[\delta]^3 + C\,[\delta]^5 \qquad (2.14)$$

where

$[de/dt]$ = strain-rate

δ = axial stress

A, B, C = constants determined from data

The use of this flow law to represent the behaviour of ice

at low stresses and at its pressure melting point has been questioned by Roggensack (1977), because each experiment was only conducted for about 200 hours and the total strain of each sample was very small. In view of the findings of Mellor and Testa (1969b) concerning the flow law at low stresses it is questionable if the flow law of ice should contain a linear term. Mellor and Testa's (1969b) experiments also illustrated that the loading time of the experiments reported by Colbeck (1970) and by Colbeck and Evans (1973) was too short to have established a minimum strain rate at the applied stress used during their test program.

A major experimental study of artificially prepared polycrystalline ice samples was reported by Barnes et al. (1971). In this study a large number of creep experiments were conducted over a wide stress range (100 kPa to 10,000 kPa) and a wide temperature range (0 to -48°C). A hyperbolic sine flow law was found to best describe the data over the complete stress and temperature range. This flow law has the following form to relate stress and temperature to the strain-rate:

$$[de/dt] = [A \sinh(\delta n)]\{\exp(-Q/KT)\} \qquad (2.15)$$

where

$[de/dt]$ = strain-rate

δ = axial stress

A & n = constants

Q = activation energy

K = Boltzmann's constant

T = temperature (K)

Equation 2.15 also simplifies to the following relationship if the stress range of interest is limited to the range 100 kPa to 1000 kPa.

$$[de/dt] = [A'(\delta)\underline{n}]\{\exp(-Q/kT)\} \qquad (2.16)$$

Equation 2.16 reduces to a simple power law relationship if the flow law at a particular temperature is examined. The above authors found that their data were best represented using an exponent n equal to 3.0. They also discuss the mechanism of creep under different loading and temperature conditions, but this will be discussed later in Section 2.4.3 where all the factors other than stress which influence the creep law will be reviewed.

To this point in the review the flow laws presented by various authors in the literature have been discussed. These flow laws have all been based on experimental studies in which the accumulated strain in the sample was less than that required to reach the inflection point shown in Figure 2.4. These flow laws, therefore, are only one of the two which have been outlined for polycrystalline ice (Glen (1975)). The flow law determined under conditions which cause large strains in the sample will now be examined.

2.4.2.3 Flow law resulting from long-term loading

The literature related to long-term loading presents results of deformation studies on glaciers, on ice caps and on ice shelves. Steinemann (1958) conducted a number of laboratory creep experiments on polycrystalline ice to large strains. These laboratory data are comparable to the field loading data, since they were obtained under similar loading conditions.

To establish the stress and strain conditions in a field loading condition Nye (1951) introduced the invariants of the deviator stress and strain-rate tensor. The invariants are called the "effective shear stress" [σe] and "effective strain-rate" ([dE/dt]e). The two invariants are defined as:

$$\sigma e = 1/2(\sigma ij \cdot \sigma ij)^{0 \cdot 5} \qquad (2.17a)$$

$$[dE/dt]e = 1/2([de/dt]ij \cdot [de/dt]ij)^{0 \cdot 5} \qquad (2.17b)$$

where

σij = deviatoric stress tensor

$[de/dt]ij$ = strain-rate tensor

It should be pointed out that the effective shear stress as defined above will not reduce to the uniaxial stress condition, but will reduce to the pure shear stress condition. In later sections and chapters this shortcoming of the invariant will be discussed and the shortcoming of

the effective stress defined in this manner pointed out.

Steinemann (1958) presented laboratory data from constant stress experiments. The strain-time plots for these data have the shape of curve 1 in Figure 2.4. He calculated the strain-rates from the tertiary portion of each creep curve. This data from Steinemann (1958) at a temperature of -1.9°C and -4.8°C are contained in Table 2.7 and shown plotted in Figure 2.14. The flow law which results from the best fit line through this data at -1.9°C is:

$$[de/dt] = 0.001\ (\sigma/162.0)^{3.45} \qquad (2.18)$$

where

$[de/dt]$ = strain-rate (%/hours)

σ = axial stress (KPa)

This best fit flow law gives an exponent equal to 3.45 on the stress. This information is very important and will be discussed in detail in Chapter 4.

The glaciological literature contains reports of field measurements of ice movement made on glaciers, ice caps and ice shelves. Budd (1969) outlines the information which must be gathered on each ice body in order to analyse the deformation behaviour. He and Raymond (1978) state that all the information required for a complete analysis of an ice body is never available; therefore, assumptions must be made to establish the deformations. A detailed discussion of the

methods of analysis and the assumptions required is beyond the scope of this thesis. For this information the reader is referred to Budd (1969), Thomas (1973a) and Raymond (1978). In this thesis some of the results presented by the above authors are discussed and in so doing a flow law which is representative of the behaviour of ice under long-term loading will be established.

The above three authors (Budd, Thomas and Raymond) are used as sources of information on the deformation of natural ice bodies. From each, information on the deformation of natural ice bodies has been extracted. These analysed deformation measurements of natural ice bodies have produced a number of flow laws for the ice. The data are plotted in Figure 2.16. Superimposed on the data is the flow law of polycrystalline ice determined in the laboratory by Glen (1955), and Barnes et al. (1971). The laboratory data are included to establish a comparison with the field measurements.

The comparison of the results in Figure 2.16 show that both the field measurements and the extrapolated laboratory data at approximately the same temperature are parallel. The deformation data determined from measurements on glaciers are both faster and slower than the laboratory experimental data on ice. The deformation studies of the ice shelves at both -16°C and -6°C show that the ice in the field deforms slightly faster at a given stress than the polycrystalline ice tested in the laboratory (Thomas (1973b)). Not

withstanding these differences in the data at a particular value of stress the lines which best describes the flow laws for both the ice shelf and the laboratory experiments are parallel. This suggests that the exponent for both the short-term and long-term loading condition are approximately equal.

The fact that the ice shelf deformation data deforms at a faster rate than the laboratory data at the same temperature supports the finding of Steinemann (1958). He found that when ice was subjected to a loading condition which strained the ice beyond the inflection point the ice deformed at a faster rate than ice strained to less than the inflection point, for the first time.

In Figure 2.16 the borehole deformation study by Hansen and Landauer (1958) indicates the opposite to the above behaviour at -24°C. Their results show that the ice in the field deforms at a slower rate than ice measured in the laboratory at the same stress. This contradictory evidence occurs because of the difficulty in determining a strain-rate from deformation measured in a borehole. Budd (1969) and Raymond (1978) explain that the complicated stress state surrounding boreholes in ice is not fully understood and has not been completely accounted for in establishing the flow law. Therefore, the data which results from this field data should not be used to establish a flow law.

2.4.3 Factors affecting the flow law of ice

In this section the influence of factors other than stress on the flow law of polycrystalline ice are reviewed. An extensive study of all the factors influencing the flow law of ice has not been conducted, but data are available which allow the evaluation of the factors with a major influence. The following factors are reviewed in this section:

1. temperature,
2. crystal size,
3. crystal orientation,
4. type of stress application,
5. confining pressure,
6. density of specimen.

The influence of the temperature of the polycrystalline ice on the flow law has been studied extensively by Glen (1955), Steinemann (1958), Mellor and Testa (1969a) and Barnes et al. (1971). Glen (1955) first introduced the use of the Arrhenius equation to analyse the temperature influence. The simple power law given in Equation 2.11 is rewritten as follows to account for temperature:

$$[de/dt] = (A\,[\delta]^{n})\{\exp(-Q/kT)\} \qquad (2.19)$$

where

$[de/dt]$ = strain-rate (%/hr)

δ = axial stress (kPa)

Q = activation energy (KJ/mol)

K = Boltzmannn's constant

T = Temperature (K)

Equation 2.19 assumes that the creep within the polycrystalline material is governed by a thermally activated process. The concept of a thermally activated process governing the creep mechanism was presented by Kauzmann (1941). He showed this to be a valid representation of the temperature influence on the creep of crystalline material. Jones and Burnet (1978) found that Equation 2.19 is valid between -0.2°C and -20°C for the deformation of single crystals of ice. This has been reviewed in Section 2.2.2.

Barnes et al. (1971) established that the Arrhenius equation represented the influence of temperature on their research results. These authors combined their results with those of Glen (1955) and Steinemann (1958) and found that Equation 2.19 fits the creep data only at temperatures colder than -8°C for polycrystalline ice. At temperatures warmer than -8°C the equation would predict the temperature influence provided the value of the activation energy was increased from 78 kJ/mol to 120 kJ/mol. The findings at temperatures warmer than -8°C showed there is a change in the creep mechanism which is responsible for the deformation of the polycrystalline ice. Barnes et al. (1971) discussed this finding in detail. Since there is a change in the creep mechanism and an associated change in the activation energy,

the Arrhenius equation will not predict the complete influence of the temperature on the flow law of polycrystalline ice.

Mellor (1979) discussed the use of the Arrhenius relationship for describing the temperature influence of polycrystalline ice. He outlined that much of the mathematical power of this relationship is lost at temperatures warmer than -10.°C. On this basis and on the basis of the findings of Mellor and Testa (1969a) that the activation energy of ice changes above -10°C he suggests not using it above -10°C. Barnes et al. (1971) suggest that its use warmer than -2.8°C is invalid, but with proper selection of the activation energy it can be used between -2.8°C and -10°C.

Is the use of the Arrhenius equation justified? In the above review, the authors give different regions over which they feel its use is valid. In the study of the creep of ice at temperatures below -10°C its use has been justified by considering that one deformation process controls the creep of polycrystalline ice. This view is difficult to understand, since the material is composed of discrete ice crystals which are joined by grain boundaries. Thus the creep within the material must be controlled by deformation within the discrete crystals as well as deformation at the grain boundaries.

The Arrhenius equation was developed using the concept that the deformation in material is controlled by a single

process. Thus the activation energy determined from creep studies should be unique to one deformation process. This has not been shown to be the case, so the use of Arrhenius equation is questionable. Close to 0°C its use has been found to be invalid by Glen (1955), Mellor and Testa (1969) and Barnes et al. (1971).

Voytkovskiy (1960) used an inverse relationship between strain rate and temperature given by Royen to relate the temperature influence. The use of this relationship was not based on a physical process but on the fact that it fitted the creep data at warm temperatures. The relationship Voytkovskiy used was:

$$[de/dt] \text{ proportional to } (1 / 1+T) \qquad (2.20)$$

where

[de/dt] = strain-rate

T = temperature below the melting point.

Equation 2.19 and Equation 2.20 are the relationships which have been used to describe the temperature influence on the flow law of polycrystalline ice. Neither relationship predicts this influence over the complete temperature range of all the experiments. Voytkovskiy's relationship describes the influence at temperatures close to 0°C and the Arrhenius relation at temperatures colder than -10°C. As previously discussed the use of the Arrhenius relationship should not be associated with an unique creep mechanism, but should be

used for its mathematical convenience only.

The influence of grain size on the creep of polycrystalline ice has not been studied systematically Mellor (1979). Baker (1978) reported that the flow law of polycrystalline ice varied with the grain size in the only study to date. Figure 2.15 contains a plot of the data reported by Baker. His data has been corrected to a constant stress level and temperature level for comparison purposes. This data shows that the strain rate decreases with decreasing grain size to a minimum strain-rate at an optimum grain size. The strain-rate then increases as the grain size decreases from the optimum size. This behaviour is consistent with results in the metal literature reported by Shahinian and Lane (1953) for polycrystalline metals.

Butkovitch and Landauer (1958, 1960) found that samples with large initial crystal sizes deformed at a faster rate than samples with smaller crystal sizes. Rigsby (1957) has shown that under shear the ice crystals decrease in size in the region subjected to shear. Thus all these authors have found an influence of crystal size on the flow law.

During creep experiments it has also been noted that the deformation rate increases in the tertiary region of the creep curve. The second important influence on the flow law of ice related to the ice crystal is the orientation of the ice crystal. In the review of the deformation of single ice crystals it was found that a ice crystal deforms much faster, if the shear stress is aligned parallel to the basal

plane than if the shear stress is aligned normal to the basal plane. Steinemann (1958), Rigsby (1960), Kamb (1972) have shown that ice crystals within a sample subjected to load tend to align themselves so that the resolved shear stress and the basal plane of the crystal become aligned for easy glide. The sample must be subjected to stress for a prolonged period in order for this realignment to take place. This change in orientation of the ice crystal under load explains why a polycrystalline ice sample enters the tertiary creep region.

When the ice sample subjected to large enough strains enters the tertiary region, the ice crystals within the sample undergo re-orientation of the optic-c axis and recrystallization occurs within the crystals. This contributes to the increase in deformation rate measured. Preferred orientation of optic axis of the ice crystal under field loading conditions has been recorded by Rigsby (1955, 1960), Kamb (1961), Gow (1973), and Hudleston (1977). This demonstrates that the induced crystal orientation caused by deformation is a very important factor influencing the flow law of polycrystalline ice.

Kamb (1972) studied the induced preferred crystal orientation in laboratory samples under a condition of torsional shear. He determined that the preferred orientation of the c-axis is largely a function of the total strain the sample under goes rather than the applied stress or time the sample has been subjected to the load. These

experiments were all conducted between -0°C and -5°C. Hudleston (1977) using studies from a shear zone on the Barnes Ice Cap extended the findings of Kamb (1972) that the degree of preferred orientation of the c-axis is dependent on the total strain. This build-up of preferred crystal orientation results in the basal planes of each crystal becoming aligned with the shearing stress within the ice. The alignment allows the ice to become softer as the total strain is increased. These results illustrate that the laboratory creep behaviour in the tertiary region can be extended using field behaviour, since under both conditions the change in crystal orientation is similar.

Other authors have reported changes in the ice crystal pattern or structure during laboratory experiments. The loading conditions applied during each experiment follows. Steinemann (1958) used a type of torsional shear. Glen (1955) and Mellor and Testa (1969a) used uniaxial compression, while Sego and Morgenstern (1977) used a punch to indent the sample. Each of these experiments resulted in a change of ice crystal size which induced a change in the orientation of the ice crystals within the deformed zone of the sample. In each experiment, the change in the ice crystals occurred in a zone which showed that the uniformly applied stress to the sample produced a non-uniform zone of stress within the sample. The stresses within each disturbed zone could not be determined hence the exact stress state which caused the change in the ice crystal could not be

evaluated. This is a shortcoming of the present methods of testing but it also raises an important question. Is it valid to directly compare data determined using different loading conditions? When the above results are compared after converting the stresses to an invariant stress are the results still comparable? Are tension experiments comparable to compression experiments for establishing the flow law of ice?

Mellor (1979) points out that from plastic yielding theory both the results from compression and tension should be equal in the ductile zone. Thus from an ideal material behaviour point of view they should be comparable. The experimental procedure used to test ice in tension, however, causes many problems. Hawkes and Mellor (1972) point out the difficulties of tension testing at high strain-rate. During the experiments the bonding of the ice specimen to the loading platens is difficult to maintain. In creep experiments these problems are increased, since, if the properties of the bonding ice are different from the ice being tested the stresses transferred from the platens to the sample will not be uniform. Steinemann (1958) also encountered difficulty in conducting tension experiments at high applied stress levels because of problems in mounting of the samples. However, he states that the tension samples were ideal for low applied stress experiments. These statements do not seem compatible. If one has difficulty at a high stress level, a similar problem would be expected at

a low stress level. Therefore, the results at low stresses in tension must be used with caution and possibly excluded from determination of a flow law for ice.

The state of stress at a point in an ice mass controls the deformation properties of the ice just as it would of any other material. The influence of stresses in different directions must be studied to properly understand the deformation behaviour. In the most general condition, the state of stress at a point is described using a second order tensor with nine values of stress. The deformation or strain behaviour is also described using a second order tensor. In the study of the properties of materials the stress and the deformation are related in order to determine the deformations for a given a stress change.

The six independent components of the second order stress tensor can be examined using three invariants. It is common in material behaviour studies to relate the invariants of the strain tensor to those of the stress tensors and thus develop a flow law for the material. Nye (1953) first proposed using plasticity as a basis for relating the stress and strain at a point. He suggested that flow law of ice should be written as follows:

$$[dE/dt]e = f(\delta e) \qquad (2.21)$$

where

[dE/dt] is defined in Equation 2.17b

δe is defined in Equation 2.17a

Equation 2.21 shows that the flow law of ice is only a function of the second deviatoric stress and strain-rate invariant. The first and third invariants do not influence the flow law of ice in Equation 2.21. This follows because Equation 2.17a and 2.17b for the effective shearing stress and the effective strain-rate are defined using only the second invariant of each tensor.

The physical implication of this statement is that the confining pressure applied to ice will not influence the deformation of the ice. Steinemann (1958) and Rigbsy (1960) showed that the flow law of polycrystalline ice is independent of variations in confining pressure or the first deviatoric stress invariant. Nye's flow law also states that the flow law is independent of the third invariant of the deviatoric stress tensor.

Byers (1973) presents evidence that the flow law of polycrystalline ice, within the accuracy of his experimental results, is independent of the third invariant of the stress deviator. He conducted experiments using a torsional shear apparatus in which both a vertical stress and confining pressure could be applied. This allowed Byers to vary the deviator stress invariants during his experiments and study the deformation response of the ice. These results confirm that only the second invariant of the deviator stress tensor controls the deformation of the polycrystalline ice.

In experimental studies on the flow law of ice reported

in the literature the ice samples have densities very close to that of pure ice. The slight variation in density is due to the preparation method used in making the samples. The influence of the density of the ice sample on the flow law has not been studied in detail. Mellor and Smith (1967) present data on the influence of the density variation of snow specimens on their deformation behaviour. Figure 2.17 reproduced from Budd (1969) shows that as the density of the snow samples increase the secondary strain-rate decrease rapidly. This influence can be used to analyse data of experiments under similar loading conditions for difference in the flow law due to density variations within the samples.

This need for comparison of data under similar density conditions is illustrated in Figure 2.18 in which is plotted data close to 0°C from Glen (1955), Mellor and Testa (1969a) and Colbeck (1970). Except for a variation in the density of the test samples all the data contained in Figure 2.18 were determined using similar experimental conditions. The data plotted in Figure 2.18 are contained in Table 2.7. This shows a large variation in the strain-rate at each stress level. This is due to the difference in the densities of the samples from which the results are plotted.

2.4.3.1 Reanalysis of creep data

In this section the results of early experimental studies reported in the literature will be used to determine

a flow law for polycrystalline ice. The data was obtained from experimental creep curves which had not yet reached the inflection point. Thus the data only pertains to experiments which have undergone small strains as outlined in Section 2.4.2. In this section, only the influence of stress on the strain-rate will be reviewed. The influence of the other factors has been discussed previously.

To minimize the influence of temperature on this flow law only experimental results close to -2.0°C will be used. This temperature was selected, since Glen (1955), Steinemann (1958), and Barnes et al. (1971) conducted extensive studies on the deformation behaviour of polycrystalline ice at this temperature. The creep experiments conducted during this research program were also conducted close to -2.0°C. This temperature is important when one discusses the design of foundation in the North, since at temperatures warmer than about -2.0°C artificial methods would normally be used to maintain the ground frozen. Thus -2.0°C is about the warmest ground temperature at which a foundations would be designed without using artifical methods to maintain this or a colder temperature (Morgenstern et al. (1979)).

Throughout this thesis, the simple power flow law presented by Glen (1955) and contained in Equation 2.11 will be rewritten in a more general form. The general form was presented in the geotechnical literature by Ladanyi (1972). This flow law is also in the form suggested by Hult (1966) and Odqvist (1966) in relation to analysis of creep in

metals. Ladanyi's relationship is:

$$[de/dt]/[de/dt]c = [\delta/\delta c]^{n} \qquad (2.22)$$

where

[de/dt] = strain-rate (%/hr)

[de/dt]c = proof strain-rate (%/hr)

δ = axial stress (kPa)

δc = proof stress (kPa)

The proof strain-rate ([de/dt]c) is a convenient strain rate against which all the experimental results are normalized. Ladanyi suggests the use of [de/dt]c equal to 0.001 %/hr in presenting results in Geotechnical Engineering. The proof stress δc is the stress level which will produce the proof strain-rate under the given experimental conditions. This proof stress is a function of all the factors which will influence the flow law except the stress. Equation 2.22 should be compared with Equation 2.11 used by Glen (1955) to represent his data at -2.0°C. The A parameter from Glen (1955) is equal to ([de/dt]c/{[δc]^{n}}).

In order to present the flow law under short-term loading conditions the experimental results of Glen (1955), Steinemann (1958) and Barnes et al. (1971) are tabulated in Table 2.5. The data has been plotted in Figure 2.19. This shows that the data from the three authors are comparable and can be used to determine a flow law for polycrystalline ice at -2.0°C. It must be noted that the data from

Steinemann (1958) only includes the compression results. The tension results were not included. Figure 2.13 contains the plot of strain-rate versus axial stress of all of Steinemann data. This illustrates that the results of the tension experiments under low stress produce a non-linear flow law. Immediately the question of the validity of comparison of the tension and compression data must be posed. Is the non-linearity a result of the test configuration or an actual material behaviour?

The answer to the above question may be determined by examining the data of Steinemann in Figure 2.13 and Figure 2.19. The curvature of the flow law at a temperature -1.9°C in Figure 2.13 is based on the results of two tension experiments under low stress. These two data points show a wide scatter in values and reflecting uncertainty in the experiments. The experimental data under tension loading at -4.8°C again shows a similar scatter in the results in Figure 2.13. If one examines just the compression data one would have a linear flow law parallel to the results at -1.9°C. This would suggest that the flow law for polycrystalline ice may be different under conditions of compressive and tensile loading. At this time insufficient data are available to establish the flow law of ice under tensile loading, hence until more data becomes available, the flow law should be determined only using data from compression experiments.

The flow law of polycrystalline ice was determined

using a least squares fit through the data contained in Table 2.5. The flow law determined using the data of each author will be presented along with the flow law of the combined data. The parameters will have the same meaning as in Equation 2.22. The flow law resulting from Glen (1955) is:

$$[de/dt] = 0.001\ [\sigma/147.9]^{2.96} \qquad (2.24)$$

The data from Steinemann (1958) results in the following flow law:

$$[de/dt] = 0.001\ [\sigma/184.5]^{3.10} \qquad (2.25)$$

Analysis of the data from Barnes et al. (1971) results in the following:

$$[de/dt] = 0.001\ [\sigma/295.1]^{3.25} \qquad (2.26)$$

The combination of all the data results in the following:

$$[de/dt] = 0.001\ [\sigma/157.7]^{2.93} \qquad (2.27)$$

The flow law determined from the analysis of the data of each author and the combined flow law agree very closely. These results show that the combined flow law based on thirty five data points is the flow law of polycrystalline

ice at -2.0°C under compression loading conditions. This flow law is valid between the stress range of 100 kPa and 1000 kPa for loading conditions which produce strains less than the inflection point in the strain-time curve. This law is, therfore, valid for the short-term loading condition of Glen (1975).

Table 2.1

Authors and experimental conditions used to determine the elastic properties of ice.

Authors	Method	Temp. °C	Frequency Hz
Jona and Scherrer (1952)	Vibrating quartz crystal a standing elastic wave This gives rise to a Laue-type diffraction pattern from which shear and longitudinal elastic waves are found.	-16.0	$15\text{-}18\times10^{6}$
Green and McKinnon (1956)	Ultrasonic pulse technique	-16.0	
Bass et al. (1957)	Resonant frequency of plates and bars	-2 to -26	$5\text{-}50\times10^{3}$
Dantl (1968)	Supersonic pulse-echo technique and double-pulse interference	0 to -140	$5\text{-}190\times10^{6}$

Table 2.2

Dynamic elastic constants of single crystals of ice at -16°C (units 10^4 bars)

Reference	C^{11}	C^{12}	C^{13}	C^{33}	C^{44}
Penny (1948)	15.2	8.0	7.0	16.2	3.2
Jona and Scherrer (1952)	13.85 ±0.018	7.07 ±0.12	5.81 ±0.16	14.99 ±0.08	3.19 ±0.03
Green and McKinnon (1956)	13.33 ±0.018	6.03 ±0.72	5.018 ±0.72	14.28 ±0.08	3.26 ±0.08
Bass et al. (1957)	13.33 ±0.080	6.3 ±0.8	4.6 ±0.9	14.2 ±0.7	3.06 ±0.015
Zarembovitch and Kahane (1964)	13.94 ±0.09				
Dantl (1968)	13.20 ±0.04	6.69 ±0.13	5.84 ±0.41	14.42 ±0.06	2.89 ±0.02

Table 2.3

Relationships used to fit strain time data of single crystals of ice in easy glide

Author	Test Type	Relationship
Griggs and Coles (1954)	compression	$\dot{e}=[\ 0.62(\delta c-Tc^2)]^2 t^2$ e = strain(%) δc = stress(bar) Tc = temperature ($^\circ C$) t = time (hours)
Jellinek and Brill (1956)	tension	$e=4.1\times10^{-1^\circ}\ t^2 + 10^2(\delta/C)$ e = strain (%) δ = stress (bars) t = time (seconds) C = 4.9×10^4 bar
Butkovich and Landauer (1958)	shear	$e=(\text{Constant})\ t^{1\bullet7}$ e = strain (%) t = time (seconds)
Glen and Jones (1967)	tension	$e=(\text{constant})t^{1\bullet4\pm^\circ\bullet2}$ e = strain(%) t = time(seconds)

Table 2.4

Parameters used to relate shear strain rate to shear stress in single crystal studies.

Reference	Test type	Large A	Strain n	Temperature °C
Steinemann (1954)	shear	---	1.3-1.8	-2.3
Butkovich and Landauer (1958)	shear	1.34×10^{-4}	2.49	-5
Wakahama (1962)	constant strain rate	$7.3 \times 10^{-?}$	3.0	-10
Higashi et al. (1964)	constant strain rate	---	1.53	-15 to -40
Readey and Kingery (1964)	constant strain rate	---	1.50	0 to -42
Higashi et al. (1965)	constant stress	---	1.58	-5 to -40
Jones and Glen (1968)	constant strain rate	---	2.13	-10 to -50

Table 2.5

Data summary of authors from literature

Sample Name	Sample Temp. ?(C)	Axial Stress (kPa.)	Grain Size (mm)	Sample Diameter (mm)	Strain rate (%/hr.) 10^{-3}
Glen(1)	-1.50	90.00	1.00	50.80	0.48
Glen(2)	-1.70	151.00	1.00	50.80	0.77
Glen(3)	-1.30	153.00	1.00	50.80	1.66
Glen(4)	-1.30	168.00	1.00	50.80	0.98
Glen(5)	-1.60	183.00	1.00	50.80	2.52
Glen(6)	-1.50	187.00	1.00	50.80	1.28
Glen(7)	-1.10	240.00	1.00	50.80	2.69
Glen(8)	-1.50	246.00	1.00	50.80	4.07
Glen(9)	-2.10	278.00	1.00	50.80	4.39
Glen(10)	-1.50	367.00	1.00	50.80	8.90
Glen(11)	-1.30	380.00	1.00	50.80	26.20
Glen(12)	-1.30	413.00	1.00	50.80	26.00
Glen(13)	-2.00	632.00	1.00	50.80	107.00
Glen(14)	-1.20	635.00	1.00	50.80	81.60
Glen(15)	-1.40	930.00	1.00	50.80	247.00
St(1)	-1.90	186.00	0.85	30.00	1.20
St(2)	-1.90	267.00	0.85	30.00	3.20
St(3)	-1.90	332.00	0.85	30.00	7.20
St(4)	-1.90	506.00	0.85	30.00	18.00
St(5)	-1.90	670.00	0.85	30.00	52.90
St(6)	-1.90	740.00	0.85	30.00	58.70
St(7)	-1.90	850.00	0.85	30.00	95.80
St(8)	-1.90	942.00	0.85	30.00	164.20
St(9)	-1.90	1080.00	0.85	30.0	225.00

Glen(1) from Glen (1955) St(1) from Steinemann (1958)

Table 2.5 (cont.)

Data summary of authors from literature

Sample Name	Sample Temp. ?(C)	Axial Stress (kPa.)	Grain Size (mm)	Sample Diameter (mm)	Strain rate (%/hr.) 10^{-3}
St(10)	-1.90	1270.00	0.85	30.00	334.40
St(11)	-1.90	1323.00	0.85	30.00	460.80
St(12)	-1.90	1323.00	0.85	30.00	586.80
St(13)	-1.90	1462.00	0.85	30.00	532.80
St(14)	-1.90	1462.00	0.85	30.00	716.40
St(15)	-1.90	1553.00	0.85	30.00	1033.20
Barnes(1)	-2.00	181.80	////	/////	1.40
Barnes(2)	-2.00	276.00	////	/////	5.90
Barnes(3)	-2.00	473.5	////	/////	33.50
Barnes(4)	-2.00	619.7	////	/////	60.80
Barnes(5)	-2.00	688.10	////	/////	110.20
Barnes(6)	-2.00	861.10	////	/////	165.60
Barnes(7)	-2.00	927.70	////	/////	165.60
Barnes(8)	-2.00	1030.00	////	/////	261.00
Barnes(9)	-2.00	1127.00	////	/////	360.00

St(1) from Steinemann (1958)
Barnes(1) from Barnes et al. (1971)

Table 2.6

Data summary of creep result in tertiary creep region from Steinemann(1958)

Sample Name	Sample Temp. °(C)	Axial Stress (kPa.)	Strain rate (%/hr.) 10^{-3}
St(1)	-1.90	342.0	21.6
St(2)	-1.90	518.6	51.8
St(3)	-1.90	561.0	101.9
St(4)	-1.90	698.0	136.4
St(5)	-1.90	771.0	211.3
St(6)	-1.90	886.0	296.6
St(7)	-1.90	978.8	458.6
St(8)	-1.90	1147.2	860.4
St(9)	-1.90	1292.0	1044.0
St(10)	-1.90	1292.0	1468.4
St(11)	-1.90	1456.0	2061.7
St(12)	-1.90	1515.0	2894.4
St(13)	-1.90	1399.0	3189.2
St(14)	-1.90	1545.0	3688.0
St(15)	-1.90	1640.0	5989.4

Table 2.7

Data summary of showing influence of density all experiments at about 0.0°C

Sample Name	Sample Density (kg/m^3)	Axial Stress (kPa.)	Strain rate (%/hr.) 10^{-3}
Glen(1)	0.91	70.0	20.2
Glen(2)	0.91	68.0	7.4
Glen(3)	0.91	156.0	31.5
Glen(4)	0.91	159.0	21.2
Glen(5)	0.91	238.0	26.5
Mellor(1)	0.88	49.0	116.2
Mellor(2)	0.86	49.0	219.2
Mellor(3)	0.86	49.0	112.9
Mellor(4)	0.86	73.6	81.9
Mellor(5)	0.86	73.6	128.8
Mellor(6)	0.86	98.1	100.2
Mellor(7)	0.86	122.6	152.4
Mellor(8)	0.86	147.1	134.1
Mellor(9)	0.86	196 1	134.5
Mellor(10)	0.86	245.1	191.7
Mellor(11)	0.86	245.1	265.1
Mellor(12)	0.86	294.1	242.7
Mellor(13)	0.86	294.1	196.0
Mellor(14)	0.86	392.3	193.2
Mellor(15)	0.86	392.3	225.8
Mellor(16)	0.86	392.3	220.1

Glen(1) from Glen (1955)
Mellor(1) from Mellor and Testa (1969a)

Table 2.7 (cont.)

Data, summary of showing influence of density all experiments at about 0.0°C

Sample Name	Sample Density (kg/m^3)	Axial Stress (kPa.)	Strain rate (%/hr.) 10^{-3}
Mellor(17)	0.86	490.4	247.0
Mellor(18)	0.86	490.4	466.9
Mellor(19)	0.88	784.6	550.2
Mellor(20)	0.86	784.6	506.9
Mellor(21)	0.87	784.6	441.8
Colbeck(1)	0.91	46.4	1.1
Colbeck(2)	0.90	56.4	1.9
Colbeck(3)	0.89	47.0	1.1
Colbeck(4)	0.89	59.4	1.8
Colbeck(5)	0.88	57.5	3.5
Colbeck(6)	0.90	58.3	2.4
Colbeck(7)	0.89	76.3	3.9
Colbeck(8)	0.91	74.5	2.3
Colbeck(9)	0.89	79.5	4.5
Colbeck(10)	0.89	96.3	4.6
Colbeck(11)	0.90	96.8	2.8

Mellor(1) from Mellor and Testa (1969a)
Colbeck(1) from Colbeck (1970)

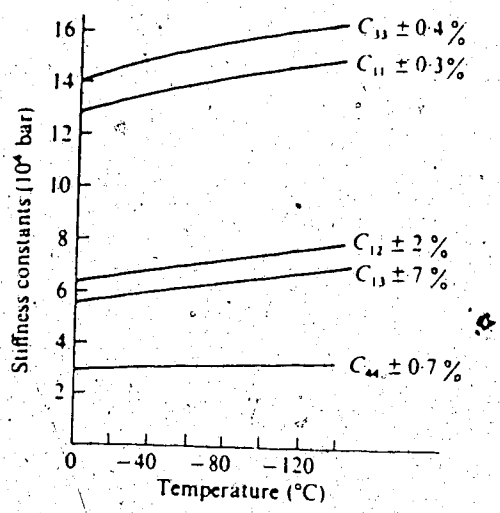

Figure 2.1: Dynamic stiffness constants of aged single crystals of ice versus temperature at frequency of 30 MHz. Dantl (1968).

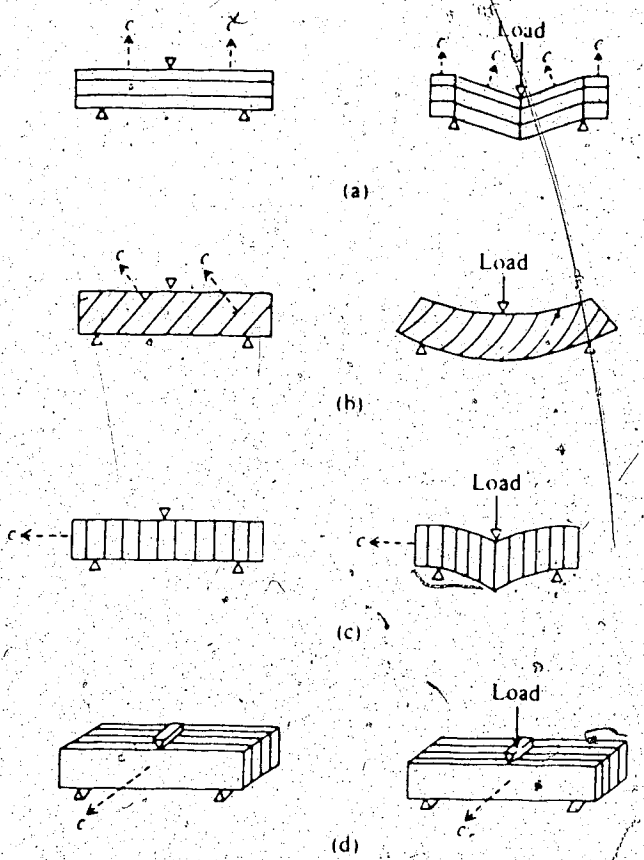

Figure 2.2: Schematic diagrams representing types of bending of single crystals of ice under load. Parallel lines are basal planes. Hobbs (1974)

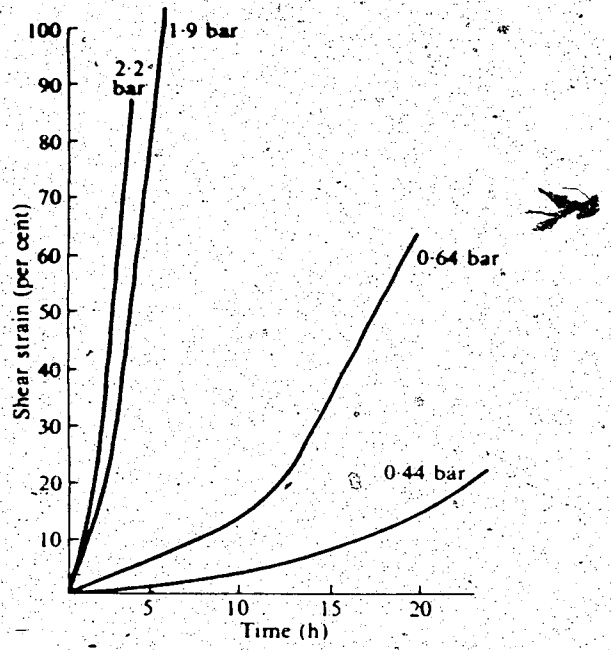

Figure 2.3: Creep of single crystal of ice at -2.3°C under constant applied stress on the basal plane Steinemann (1954).

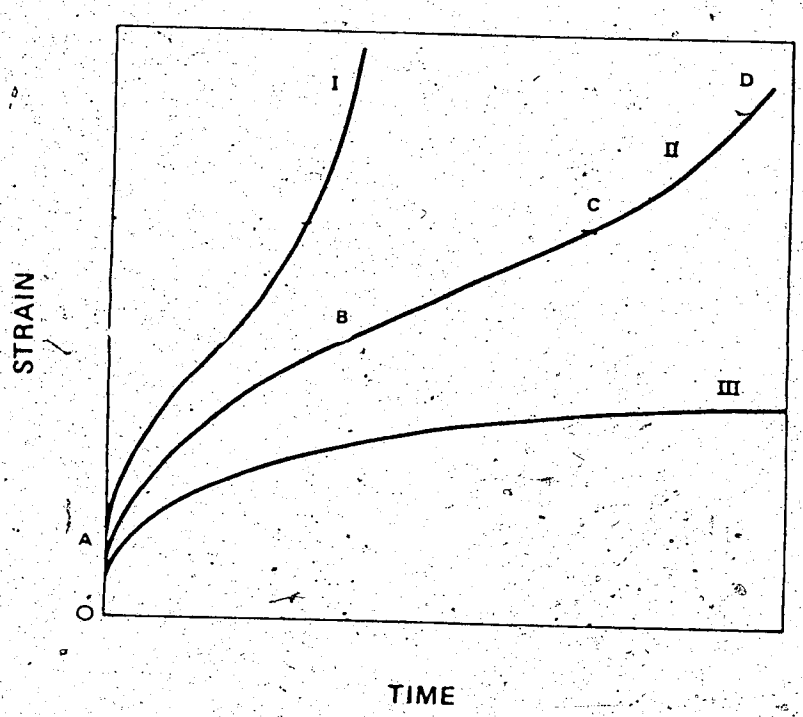

Figure 2.4: Typical creep curves of polycrystalline material at a constant temperature and applied stress Roggensack (1977).

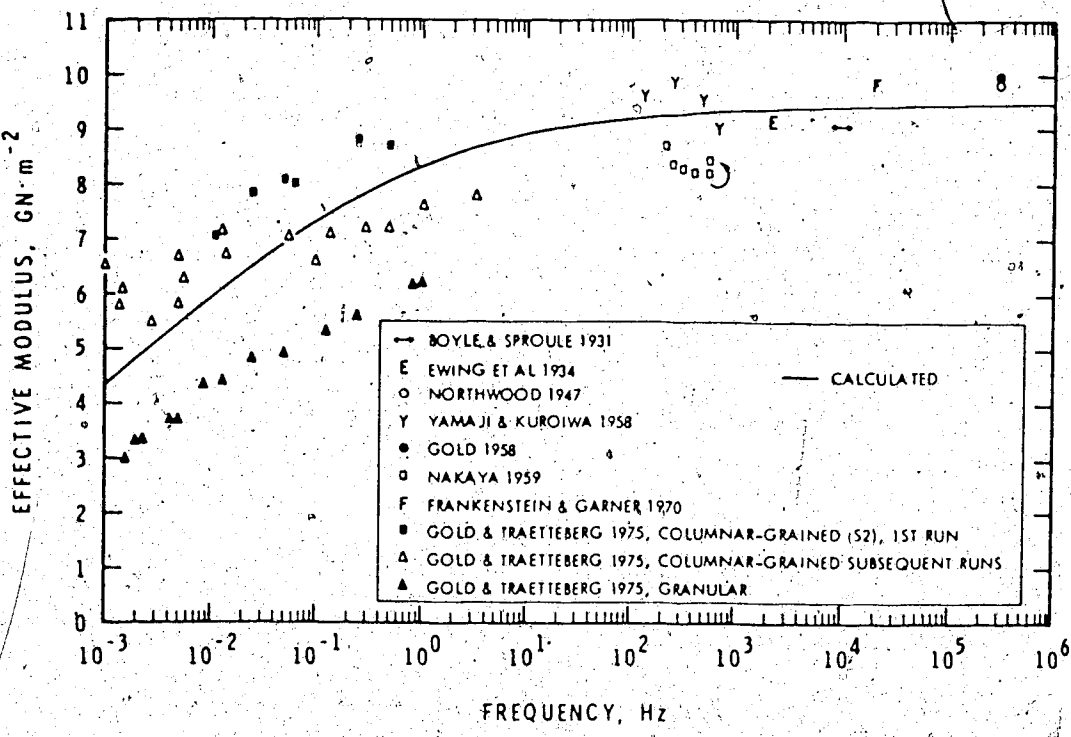

Figure 2.5: Frequency dependence of Effective Young's Modulus for polycrystalline ice at -10.°C Sinha (1978).

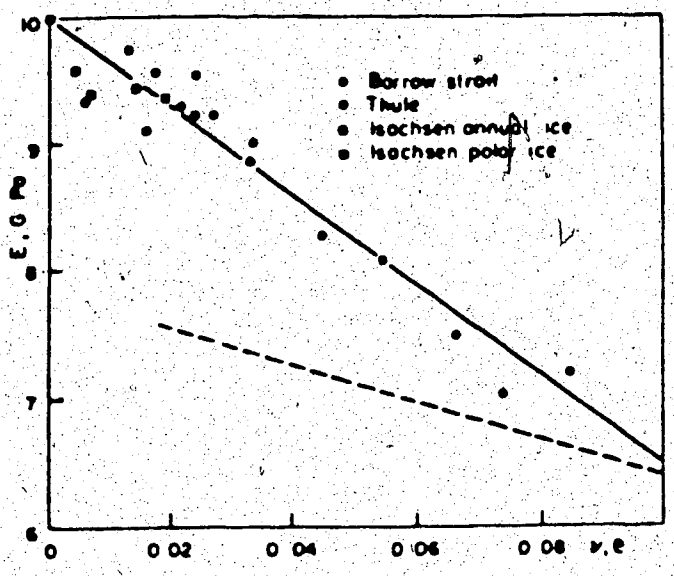

Figure 2.6: Young's Modulus as a function of brine volume (v) or porosity (e) Michel(1978).

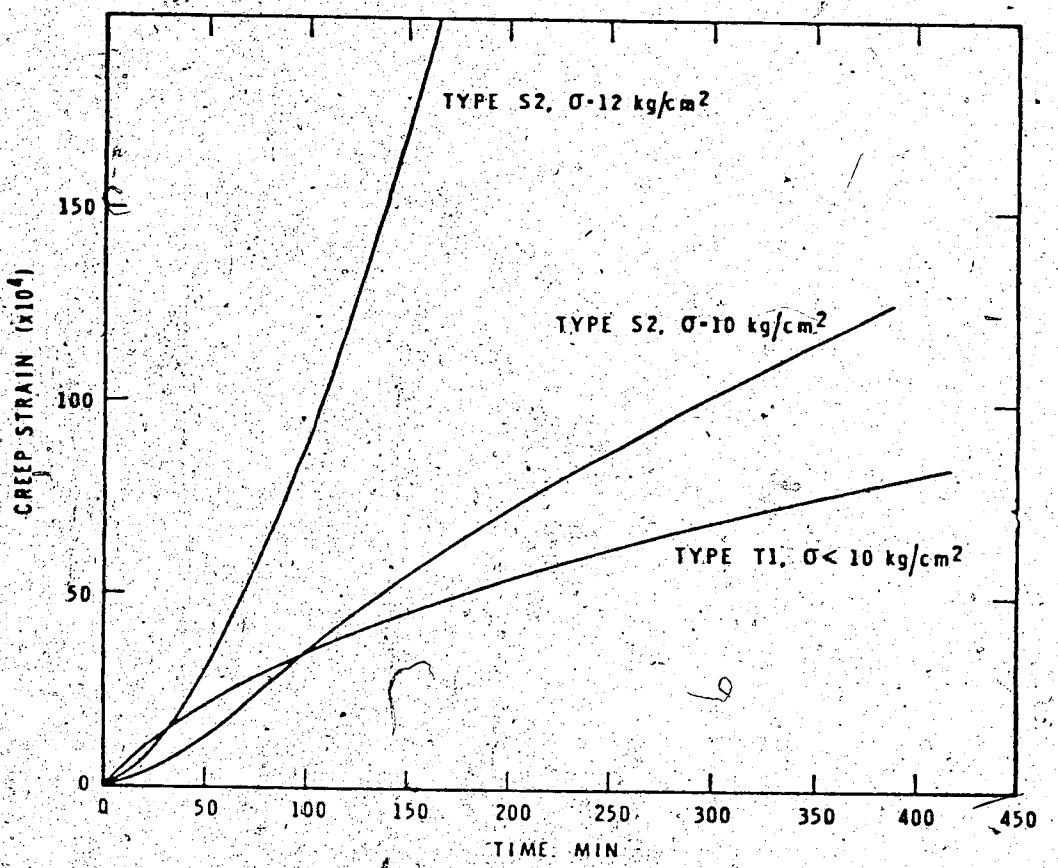

Figure 2.7: Typical creep curve of columnar grained ice with comparison to polycrystalline ice (T1) Gold (1965).

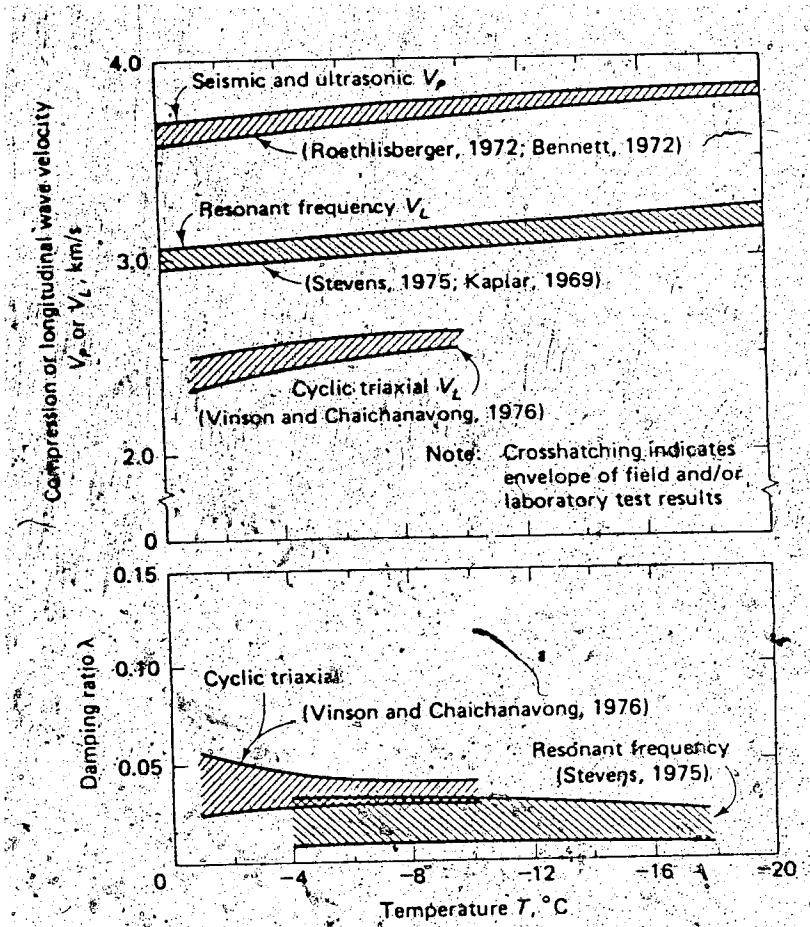

Figure 2.8: Longitudinal-wave velocity and damping ratio of ice versus temperature Vinson (1978).

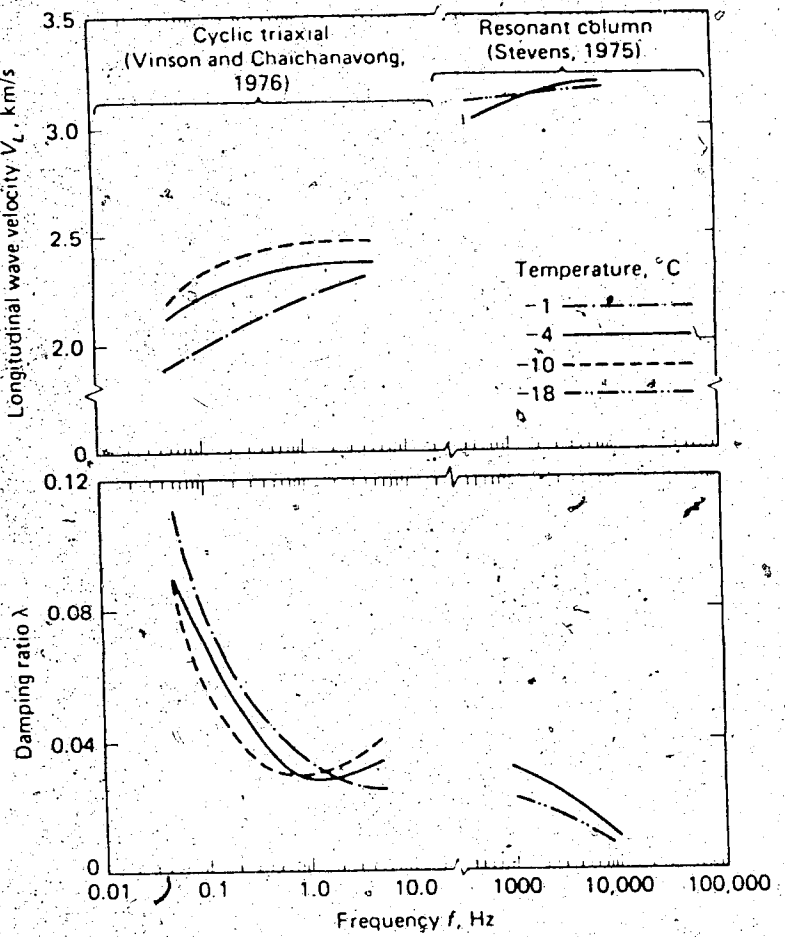

Figure 2.9: Longitudinal-wave velocity and damping ratio of ice versus frequency Vinson (1978).

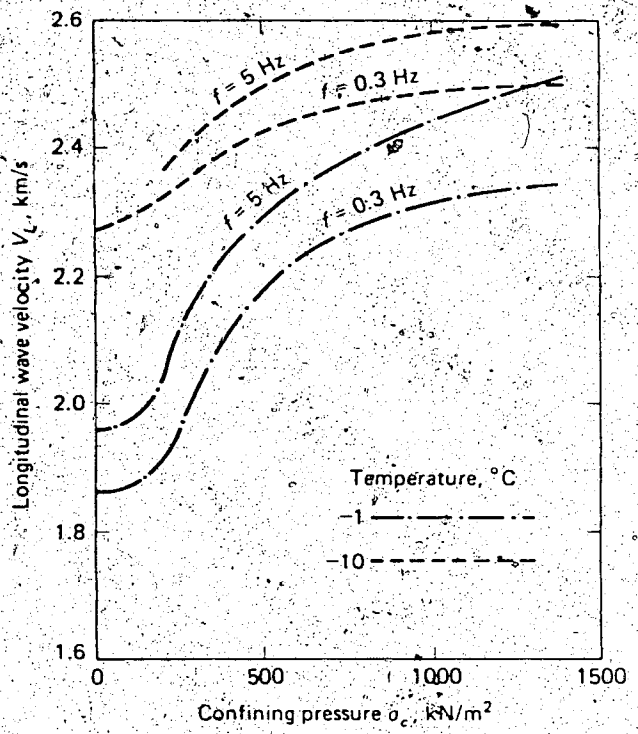

igure 2.10: Longitudinal-wave velocity of ice versus confining pressure Vinson (1978).

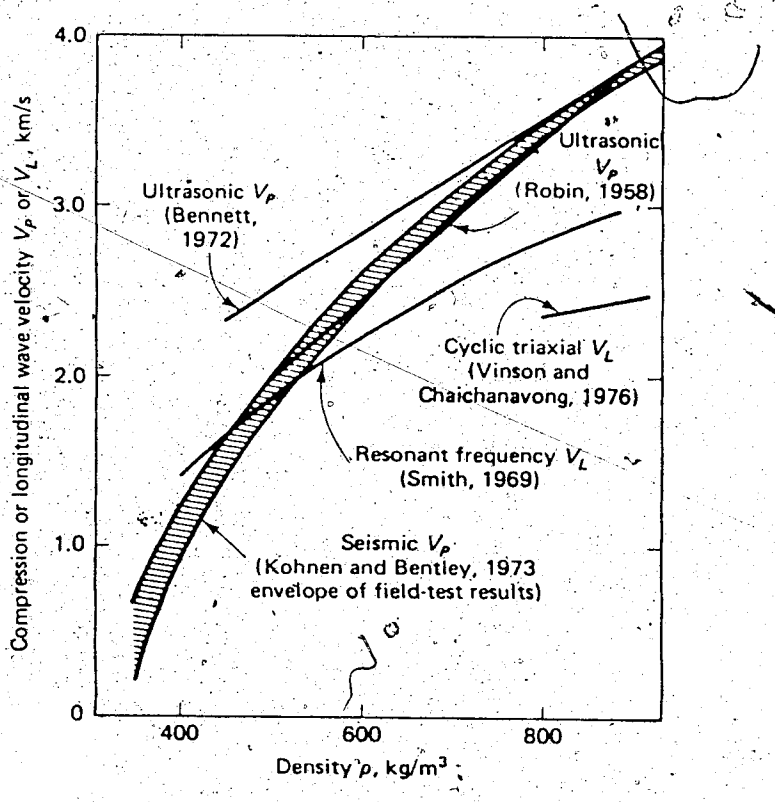

Figure 2.11: Longitudinal-wave velocity of ice versus ice density Vinson (1978).

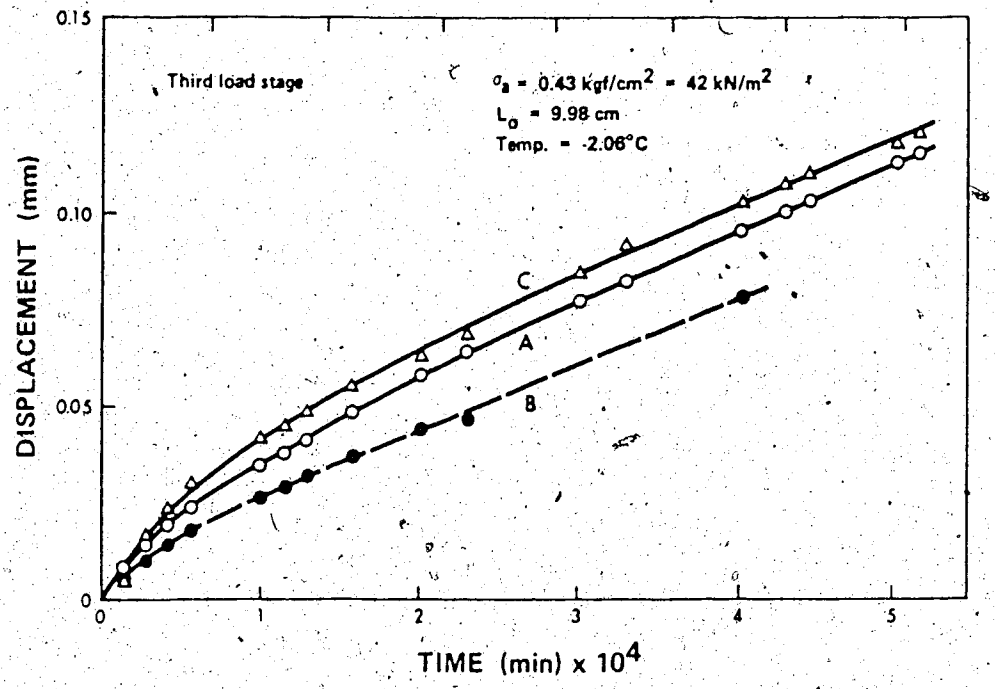

Figure 2.12: Constant stress creep of polycrystalline ice Mellor and Testa (1969)

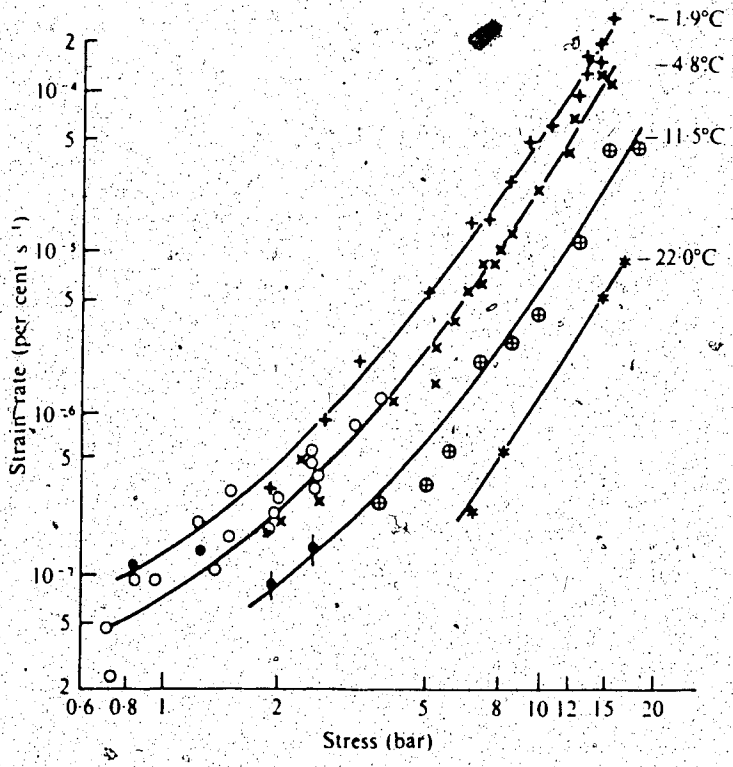

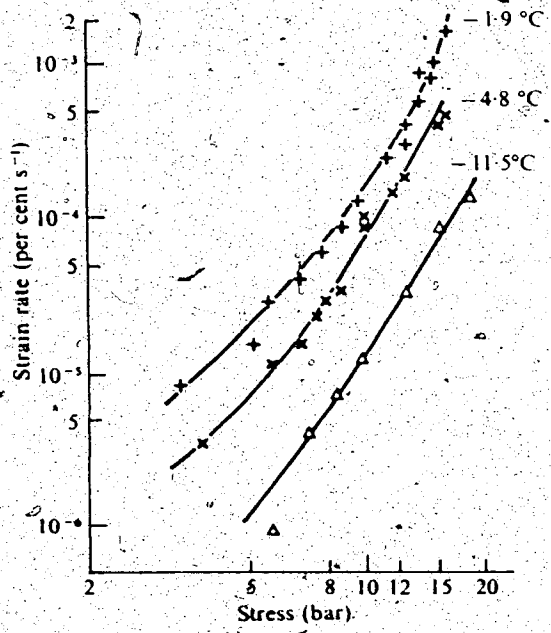

igure 2.14: Steady state strain rate versus stress of polycrstalline ice during tertiary creep Steinemann (1958)

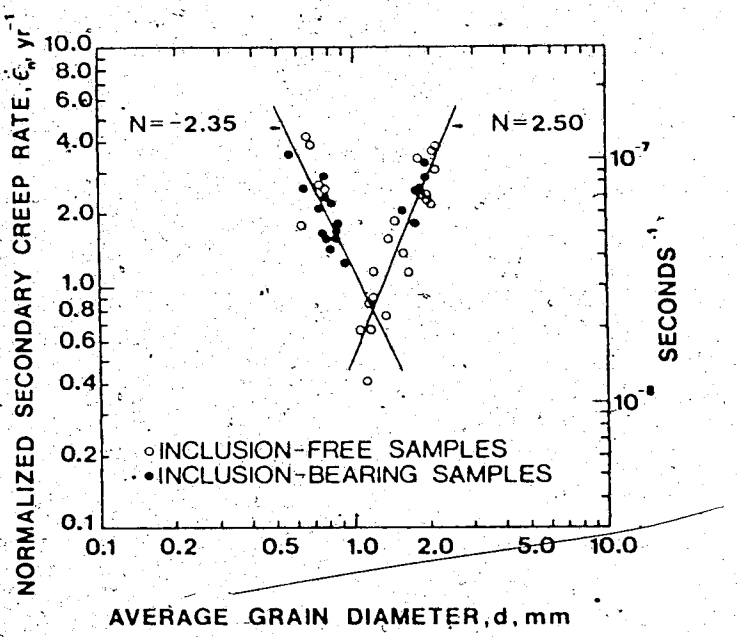

Figure 2.15: Normalized secondary-creep rate versus average grain diameter for both inclusion-free and inclusion-bearing polycrystalline ice Baker(1978).

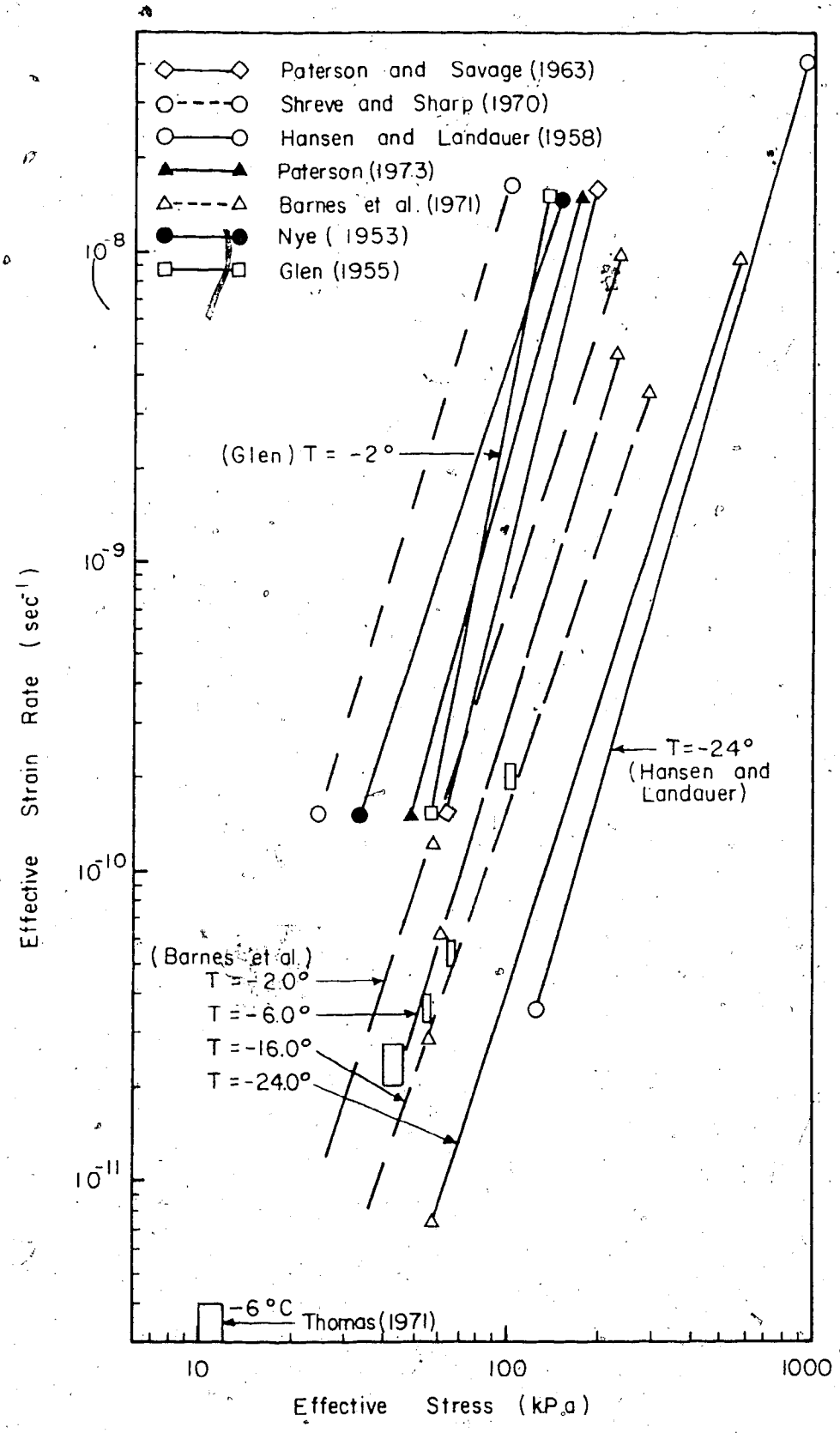

Figure 2.16 Compiled strain rate versus stress creep data of field and selected laboratory data.

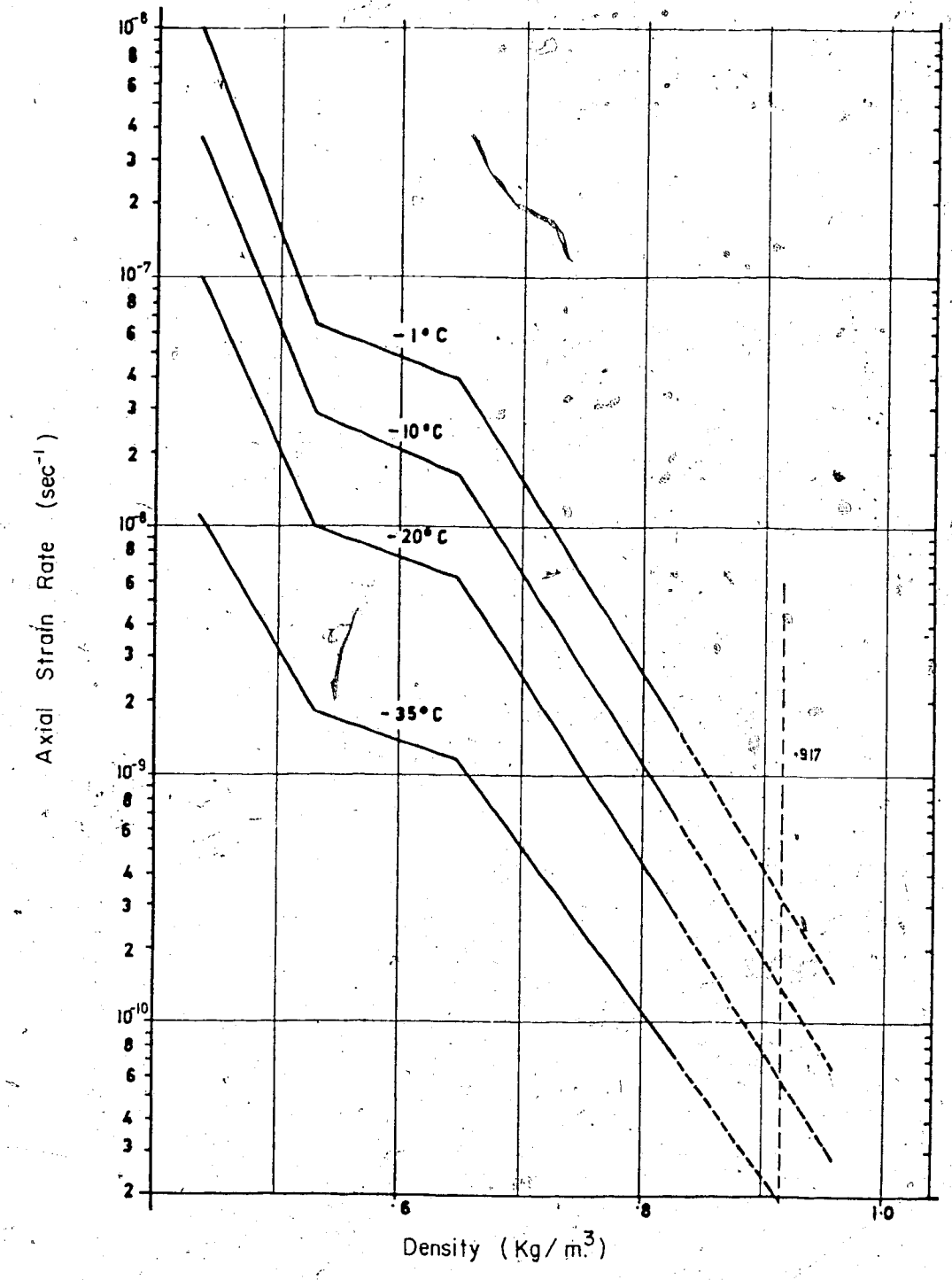

Figure 2.17: Strain rate versus density for snow and ice samples from Mellor and Smith (1966) and extrapolated to density of pure ice. From Budd (1969).

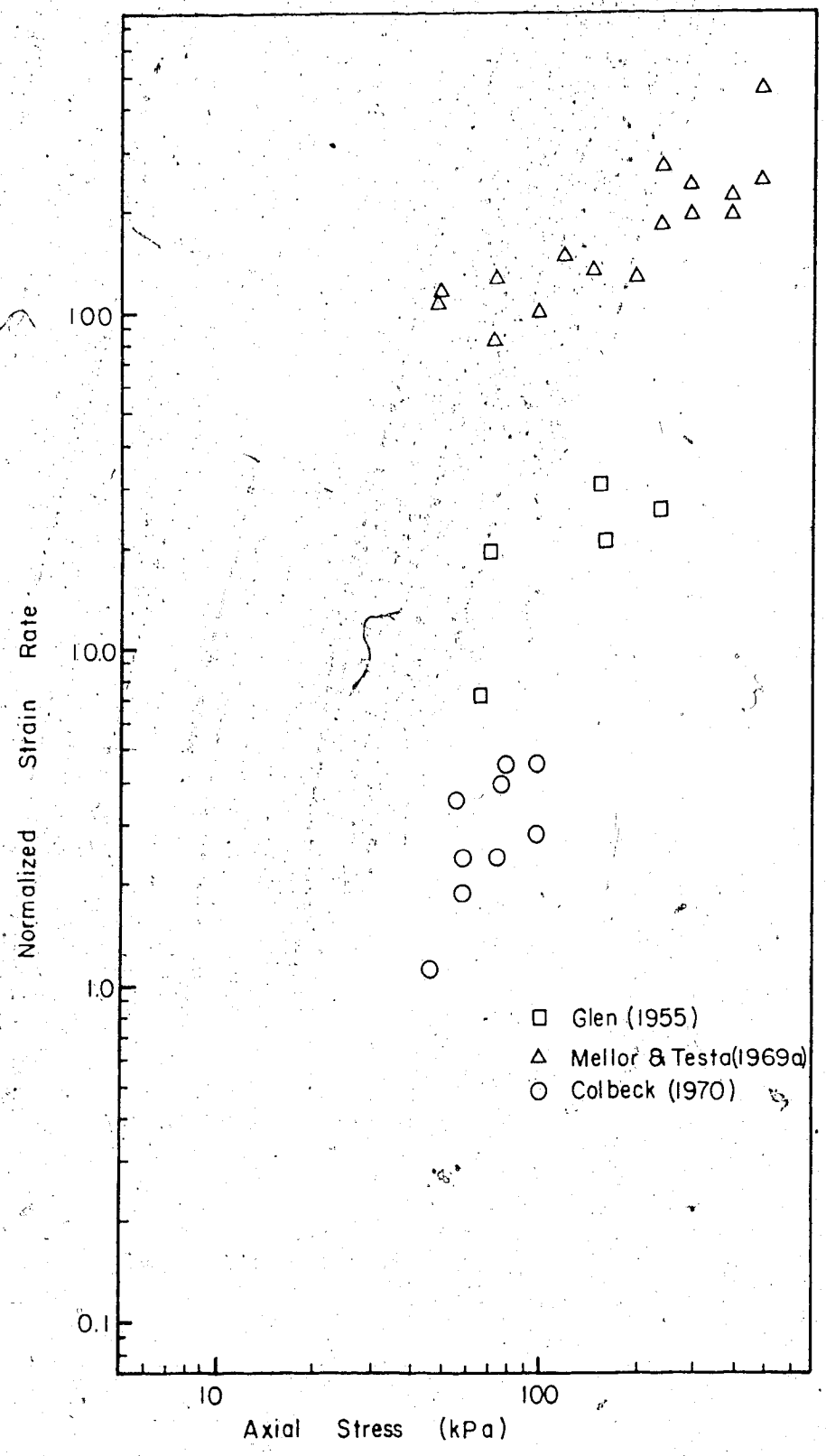

Figure 2.18 Normalized strain rate versus axial stress of polycrystalline ice at different densities.

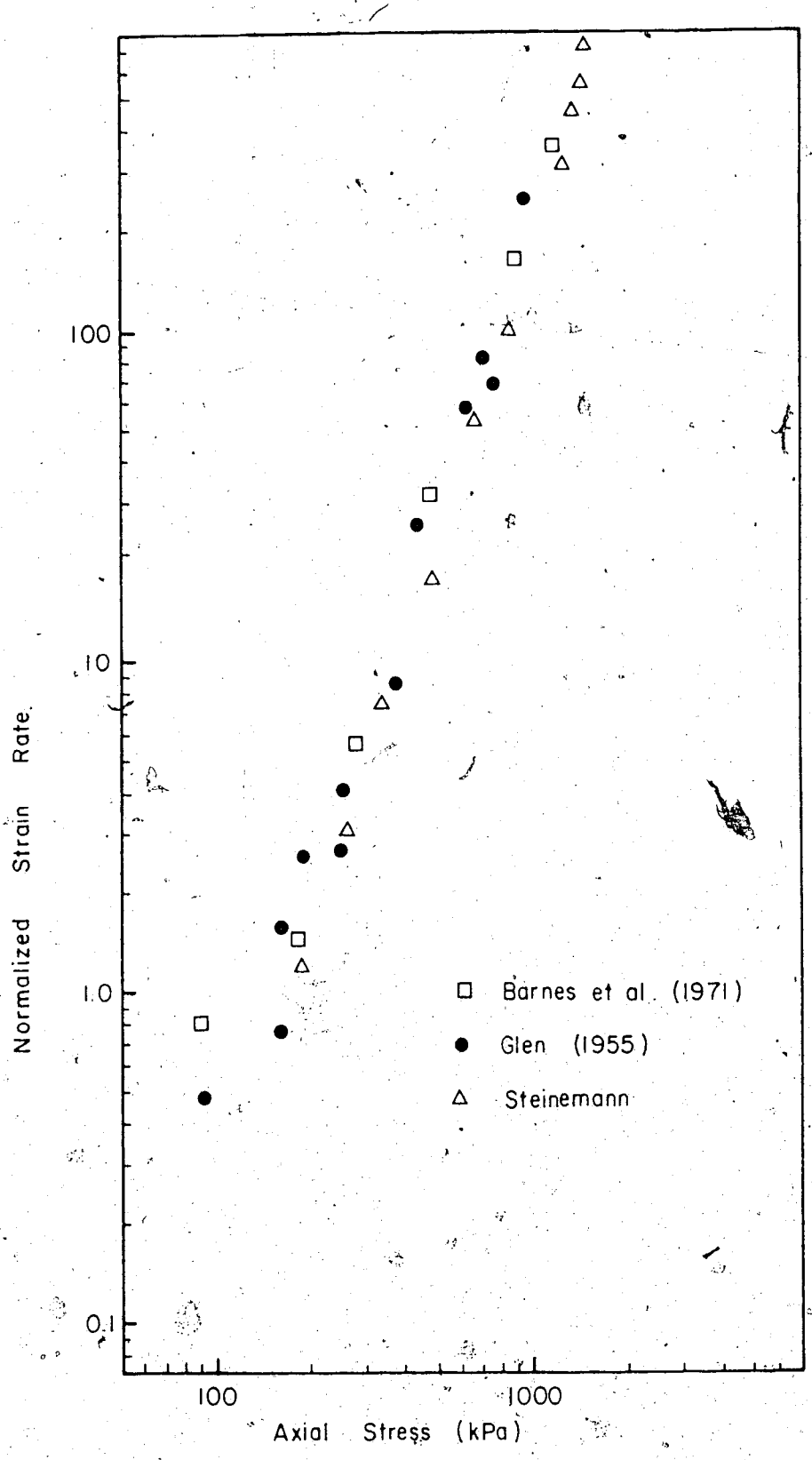

Figure 2.19 Normalized strain rate versus axial stress of of polycrystalline ice at -2.0°C.

CHAPTER 3

Test Equipment and Test Procedure

3.1 Ice Sample Preparation

3.1.1 Introduction

The ice used in this research program was prepared artifically. The procedure used to prepare this polycrstalline ice was developed after studying those used by Glen (1955), Dillon and Andersland (1967), Mellor and Testa (1969a and 1969b) Barnes et al. (1971), and Hawkes and Mellor (1972). The ice produced has a uniform cloudy appearance with fine air bubbles dispersed throughout the sample. The specimens contained randomly oriented ice crystals which were of uniform grain diameter. This type of ice has been used in laboratory studies to determine a flow law of ice used in the analysis of glacier flow (Hawkes and Mellor (1972)).

The samples required to conduct a study of the flow law of ice under various loading conditions must meet the following requirements:

1. Be reproducible.
2. Be homogeneous and isotropic with crystals that are randomly oriented.
3. Be small enough in grain size so that the bulk properties of the ice may be determined using a small test sample.

In order to meet these requirements the laboratory procedure

was developed to make bulk ice samples with the above qualities from which the test specimens were trimmed.

For an ice sample to meet the above three requirements it must have characteristics that differ from ice formed in nature. Natural ice usually has a preferred crystal orientation and a preferred crystal growth direction, it is therefore anisotropic and will not meet the second and third requirements. Air bubbles are trapped within natural ice, but they do not have a uniform distribution, hence the first requirement is difficult to fulfill. Ice formed in nature also usually is subjected to large thermal strains during formation which cause cracks to form. These cracks are non-uniformities which fail to meet the second requirement. Ice prepared in a laboratory is formed under controlled conditions and can meet the above requirements.

In order to have a laboratory sample which is consistently reproducible and uniform, the sample must have as few contained air bubbles as possible. The number and size of the air bubbles within the ice can be reduced by using de-aired water. The water may be de-aired using one of the following methods:

1. Boiling the water to reduce the solubility of air in the water which allows the air to escape. The water is then cooled under a saturated water vapour with the container sealed so no air dissolves in the water.
2. Placing the water in a mechanical deaerator which uses the cavitation principle to release the air from the

water and a vacuum above the water to draw off the air.

3. Placing a vacuum above the water within a bottle to remove the air.

Each of the first two methods has been used during this research project to remove air from water. Figure 3.1 presents the time required to de-air water using the mechanical deaerator and the vacuum method alone. This shows that the mechanical system saves time. Hence, it was used during this research instead of the vacuum method.

To ensure that the ice sample does not crack during formation, the thermal strains associated with freezing of the sample must either be relieved or reduced. The thermal strains were reduced by having a large portion of the sample consist of small ice crystals which do not undergo a phase change. Thus only the water which fills the voids between the crystals undergoes volumetric strain during the phase change. The volumetric strain which does occur in the sample was relieved by allowing the top plate of the ice making apparatus to displace upward during expansion of the sample on freezing. This is illustrated in Figure 3.2 which shows how the upper plate forms a seal and also allows the sample to expand during freezing. The above method of relieving the thermal strains is applicable only to a freezing apparatus which undergoes one-dimensional freezing.

The requirement of randomly oriented ice crystals was fulfilled by filling the sample mould with ice crystals. The ice crystals were poured into the mould after passing

through a sieve to ensure that each crystal met a certain size restriction. The individual ice crystal has a preferred crystal orientation depending on the condition during its formation (Michel (1979)). When these crystals were placed into a mould the large number of crystals and the random method of placement ensured that the ice sample had a random crystal orientation. The random nature of the crystal orientation in this type of sample has been well documented (Glen (1955), Mellor and Testa (1969b), Kuo (1972) and Byers (1973).

These seed ice crystals were used to control the average grain diameter of ice crystals in an ice sample. As mentioned, the mould was packed with ice crystals which were sieved through a set of sieves and only crystals of a given size range were placed in the mould. Thus the size of the seed crystals was controlled. The voids between the seed crystals were then flooded with de-aired water which freezes within the mould using each individual crystal as a nucleation point. Each crystal grows slightly in size but the large number of seed crystals which are the nucleation points prevented one preferred crystal orientation from dominating within the sample. This procedure developed a randomly oriented crystalline material which had a uniform grain diameter throughout. Figure 3.3 demonstrates the uniform grain size throughout each sample

In order to describe fully the ice-making equipment and the ice making procedure, each will be discussed in detail

in the following sections. The equipment used to make the ice has been illustrated in Figure 3.2 and Plate 3.1.

3.1.2 Equipment Used in Ice Making

The mould was developed in two phases. Initially a 104 mm diameter by 204 mm high mould was used to provide specimens compatible with test equipment. With the construction of new test equipment and modification to the sample preparation equipment, a larger sample was required. At this point the 150 mm diameter by 400 mm high mould was designed and constructed. Each mould used the same principle for preparing the ice sample but the method of removing the sample from the mould differed. The details of each mould are given in Figure 3.2.

The principles of the ice making method around which the equipment was designed are as follows:

1. The mould must have a base plate which will allow ready access of cooled de-aired water to the interior of the mould;
2. The base plate must be removable and also capable of sealing a vacuum inside the mould;
3. The base plate must conduct heat readily to freeze the sample.
4. The upper plate must seal a vacuum and be able to allow volume expansion of the sample to take place during freezing; and
5. The mould must allow for removal of the completed sample

easily.

The two moulds shown in Figure 3.2 meet these requirements and allowed samples of high quality to be prepared for the laboratory testing program.

The only difference between the two moulds is in the actual body of the mould and in the method used to remove the sample. The 104 mm diameter mould was constructed of P.V.C. plastic and consisted of a split barrel. The 150 mm diameter mould was constructed of a tapered aluminum barrel. The sample was removed by attaching a heat tape to the outside of the barrel and heating it until the sample could slide out. The second method proved to be superior because the split barrel developed problems in maintaining the vacuum required during preparation of the ice. The split barrel, however, has advantages for sample removal.

The base plate was constructed of aluminum. An O-ring seal between the mould barrel and the base plate allowed the mould to maintain a vacuum. An inlet was machined through the side of the base plate to its center to allow cooled de-aired water to enter the mould through the base. The inlet hole was separated from the sample by two layers of .001 mm stainless steel mesh. This mesh kept the ice crystals from filling the inlet port and it also dispersed the inflowing water through the voids in the sample. The bottom of the base plate was machined to fit onto the cooling plate so that the sample could be frozen from the bottom upward. The upper plate was machined to house an

O-ring seal which allowed a vacuum to be maintained within the mould. It has an outlet port in the center through which the water escaped from the sample when saturated. The vacuum pump was also attached to the mould via the port in the top plate. This plate was made of P.V.C. plastic and details of it are contained in Figure 3.2. The upper plate was designed with a thickness of 25 mm to allow for volume expansion of the sample during freezing without the plate being pushed out of the mould.

The remainder of the equipment consisted of the vacuum pump, the container of cooled deaired water, and the constant temperature bath for freezing the sample. Each of these pieces of equipment was attached to the sample mould by lines or a cooling plate. The details of the line connection are given in Plate 3.1.

The snow crystals were sieved through a set of standard U.S. sieves to ensure a uniform size of seed ice crystals. No. 20 and 40 sieve sizes were used to ensure that the ice crystals in the sample would be about 1 mm in diameter. The crystals were sieved by hand so that each crystal passed the No. 20 sieve and only the crystals retained on the No. 40 sieve were placed in the mould.

The vacuum within the mould was achieved by attaching a vacuum pump to the mould as illustrated in Plate 3.1. The de-aired water was allowed to cool within a cold room in a Pyrex glass bottle which had a plastic cover to maintain a saturated vapour above the water level. This container was

also attached to the mould as illustrated in Plate 3.1. A vacuum gauge was used to ensure that before the water was transferred from its container to the mould, no leaks existed in the mould. The details of the steps followed in the use of this equipment will be discussed in Section 3.1.3.

To ensure one-dimensional rapid freezing of the sample within the cold room, a Hot Pak constant temperature bath was attached to a lower cooling plate. This allowed the cooling plate to be maintained at -30°C by circulating an ethylene glycol mixture from the constant temperature bath through the cooling plate. During freezing of the sample the sides of the mould were insulated to reduce the radial heat flow from the sample. This set up an approximately one dimensional heat flow pattern so that only about 5 mm of the outside of each sample was affected by radial heat flow. This thin zone of ice may be seen in Plate 3.2. The thin zone of nonuniform ice was machined away before a sample was used for an experiment.

3.1.3 Ice Making Procedure

The procedure outlined below is detailed to ensure that the ice making procedure can be followed by other researchers who may wish to reproduce the ice to compare data. The non-reproducibility of samples has, in the past been, one of the pitfalls in comparing the data presented by different authors. The procedure for producing ice samples

used in this research, is simple and requires only equipment which is readily available in most laboratories.

The actual procedure will be discussed under the following topics; preparatory ice sample making, and ice sample making. Each of these will be further subdivided.

I. Preparatory ice sample making.

1. Mould:

a. The mould was washed to remove all dirt and grease. It was then rinsed using distilled water and dried.

b. The inside walls were greased with a fine coat of petroleum jelly to prevent the sample from freezing to the mould.

c. The upper and lower plates were also washed, rinsed, and dried.

d. The O-ring seals were cleaned to remove any dirt and grease.

e. The O-rings were coated with a film of vacuum grease to ensure a proper seal could be made.

f. The mould and the base plate were assembled. The top of the mould and top plate were wrapped in plastic to prevent dirt from contaminating the exposed surfaces.

g. The mould was placed in the cold room and allowed to reach an equilibrium temperature. This usually required a period of 5 to 6 hours.

2. Seed Ice Crystal:

a. All the ice crystals used in the ice sample wer

obtained by scraping the hoar frost from exposed cooling plates in a separate cold room. This cold room had been set aside to produce only hoar frost for this research program. The seed ice crystals may also be obtained by crushing ice made from distilled water. Walker (1970) also obtained seed crystals by injecting water into liquid nitrogen to freeze the crystals.

b. These ice crystals were then placed in a plastic bag to keep the ice from being contaminated.

c. The bag of ice crystals was placed in the sample preparation cold room and the temperature of the snow crystals allowed to stablize at -5°C for twenty-four hours.

NOTE: The sample preparation was conducted in a room which was also used to trim permafrost samples. This required that special precautions be taken to keep the samples from being contaminated. The work area had to be kept extremely clean and free of dust. To achieve this, all trimmings were removed from the cold room immediately, the room was vacuumed to keep the dust down, the ice-making equipment was stored in plastic bags and all exposed surfaces were kept covered.

3. De-airing of the Water:

a. A 6 liter sample of deionized distilled water was placed in a mechanical deaerator.

b. The water was subjected to 10 minutes of mechanical cavitation under a slight vacuum. This brought the dissolved oxygen content down to 1 ppm. as illustrated in Figure 3.1.

c. The water was then drained to a Pyrex glass bottle ensuring that no mixing of air and water occurred. The bottle was filled in this manner until its neck was full. This minimized the exposed surface area of the water to the atmosphere.

d. The top of the bottle was secured with plastic film to reduce the possibility of air dissolving in the water.

e. The bottle containing the de-aired water was placed inside the cold room and the water allowed to cool to 0°C.

f. The water bottle was not disturbed during this period and the water was cool enough for use in the ice sample preparation when dendritic ice crystals started to grow along the edge of the bottle.

g. Supercooling of the water was evident during the sample preparation, since upon placing the stainless steel inflow tube into the water a large volume of the water nucleated to form ice crystals. This loss of water never interfered with the sample preparation.

4. Cooling Plate:

a. The constant temperature bath was started and set to

maintain a constant temperature of -30°C.

b. The fluid was circulated through the cooling plate to maintain it at -30°C.

At this point, the ice crystals and each component of the ice-making equipment was ready to make up the ice sample. The mould and the ice crystals were at the cold room temperature. The water was at its freezing point or just slightly below it, and the cooling plate was at a constant temperature. The ice making could now take place.

II. Ice Sample Making.

1. The sieves were removed from the protective plastic bag, and stacked so that the sieve openings decreased in size downward from the top sieve. The order followed was No. 10, No. 20, No. 40, and the pan.
2. Approximately 400 grams of snow crystals were placed on the No.10 sieve from the plastic bag.
3. Aggregates of snow crystals were broken up by rubbing the piece of snow against the mesh of the sieve.
4. The sieve was vibrated by hand to ensure that all the ice crystals passed through the sieve openings.
5. Once the vibrating was completed the ice crystals retained on the appropriate sieve were poured into the mould.
6. The outside of the mould was tapped to densify the ice crystals.
7. The steps from 2 to 6 were repeated until the mould was filled with snow crystals.

8. The upper plate was fitted into the top of the mould, and pushed down to seal the ice crystals inside of the mould.
9. The mould was fitted with the piping necessary to attach the vacuum pump and the bottle containing the de-aired water. This is illustrated in Plate 3.1.
10. The vacuum pump was attached and the vacuum gauge monitored to ensure that a minimum vacuum of 700 mm of mercury was applied to the mould.
11. The requirement that the mould seal a minimum vacuum of 700 mm of mercury was strictly enforced to ensure that little or no air would be trapped inside of the sample. If the seals on the mould could not be adjusted to meet this requirement the sample was abandoned and the procedure was repeated.
12. If step 11 was met, the vacuum was maintained on the sample for about 15 minutes to evacuate all the air.
13. The valve on the inlet line was closed, the vacuum gauge was removed, and the stainless steel tubing was attached to the inlet line and placed in the bottle of de-aired water.
14. Once the tubing was submerged, the inlet valve was opened. The arrangement of the tubing is illustrated in Plate 3.1.
15. The vacuum applied to the mould drew the water into the mould and through the voids in the ice crystals. The fine wire mesh over the inlet port in the base dispersed

the incoming water through the voids.

16. The vacuum was maintained on the mould until the water escaped through the outlet port in the top plate. At this time the vacuum pump was isolated from the mould by closing the outlet valve shown in Plate 3.1.
17. The water was allowed to flow through the sample for two minutes under the reducing pressure differential then the inlet valve was closed.
18. The outlet line attached to the top plate was now removed which placed the water in the mould under hydrostatic pressure.
19. The mould was moved to the cooling plate and immediately surrounded with 125 mm of Zonalite insulation. Immediately, the heat within the sample started to flow towards the cooling plate and a smaller portion flowed radially to the walls of the mould.
20. The sample was left for a minimum of 36 hours to ensure that the sample was completely frozen before it was removed.

The sample was removed from the mould and stored in a freezer until it was required for use.

3.1.4 Sample Storage

The ice samples were not all required for testing immediately after preparation. Therefore, some were stored in a freezer and to reduce ablation the sample was wrapped in plastic film manufactured by F.D.E. of Canada. The first

layer of plastic was firmly attached to the sample with masking tape. The sample was identified by writing the sample information on the masking tape. Details of the sample preparation were written on a sample form which was kept for future reference. A card containing the sample information was also attached to the plastic film surrounding the sample. The joints in the plastic film were sprayed with a mist bottle to form a layer of ice over the joints to guard against further ablation of the sample. The sample was wrapped with a second layer of plastic film and this layer taped tightly to the sample. The joints in the film were taped also.

The sample was then placed in the deep-freeze. Each sample was completely covered with about 5 cm of crushed ice or snow. The location of the ice sample within the freezer was noted on the form for future retrieval. This method of sample storage has been used successfully to store permafrost samples for extended periods of time (Roggensack (1977)). Ice samples have also been stored for extended periods using this procedure.

3.2 Ice Thin Section

In order to determine the size of individual ice crystals within a sample, a thin section of the ice specimen was be prepared. The thin section when viewed under crossed polarized light gives details of the crystal shape, the crystal size, grain boundaries, the impurities and the air

bubble pattern (Langway (1958)). The c-axis orientation of the ice crystal can also be established. The method and equipment used has been described by Nuttall (1974). The equipment was initially designed to make large thin sections and to view these with the naked eye. Photographing of each section using a camera mounted above the polarizing light table is also possible. Plate 3.3 gives details of the light table and equipment used in preparing the thin sections.

3.2.1 Ice Thin Section Equipment

The equipment used in preparing and viewing the thin sections consisted of a band saw, smooth aluminum hot plate, 5 cm by 5 cm glass plates, and a cross polarizing light table. The cross polarizing light table and the aluminum hot plate are shown in Plate 3.3.

3.2.2 Procedure Used in Preparing Thin Sections

To prepare a thin section of an ice sample the following steps were followed:

1. A slab of ice of about 10 mm thick was cut from the ice sample at the desired location.
2. The orientation of the sample was noted and the sample number and thin section number were recorded on the glass plate.
3. The temperature of the aluminum hot plate was adjusted using a variable resistor to maintain a surface temperature of about +2°C.

4. The ice slab was placed on the hot plate.
5. The ice was melted to form a flat surface, and the ice slab was slid off the hot plate onto a clean glass plate. This required care to ensure that no air became trapped between the ice surface and the glass plate.
6. The ice slab and the glass plate were allowed to cool in the cold room to freeze the slab to the glass plate.
7. The orientation of ice slab relative to the sample on the glass plate was checked, as was the sample number and thin section number.
8. The ice slab was placed on the hot plate and slowly melted to reduce the thickness of the ice slab to approximately 1 to 2 mm.
9. The thickness of the thin section was maintained constant by rotating the slab of ice on the warm smooth plate. The thin section throughout this operation could be checked between the cross-polarized plates for clarity of the crystal structure.
10. The thin section was removed from the hot plate when the crystal contrast was sufficient to distinguish individual crystals and grain boundaries.
11. The thin section was now wiped with a lint-free paper towel to remove excess water from the thin section before it froze.
12. The temperature of the thin section was allowed to stabilize and the water film between the glass plate and thin section allowed to freeze completely.

13. The thin section was photographed using a camera mounted above the cross-polarized table.
14. Immediately after the thin section was photographed it was placed between two separate layers of plastic film. It was then placed in a one gallon paint can and covered with a layer of snow to reduce the ablation. The can was sealed and stored in a freezer.

3.3 Constant Displacement Rate Loading Test

3.3.1 Introduction

The constant displacement rate load tests were performed to establish the stress-strain behaviour of the ice under various constant displacement rates. The effect of confining pressure on the stress-strain behaviour of the ice was also established.

3.3.2 Equipment

The constant displacement rate tests were performed using a 18 kN capacity Wykeham Farrance constant displacement rate loading press. The displacement rate could be varied between 1.2 mm/minute and 0.00049 mm/minute. The maximum diameter of sample was limited to 70 mm because of spacing restriction between the bars of the reaction frame. This restriction limited the triaxial cell diameter which could be used in this test program.

The triaxial cells used required extensive modification to obtain temperature control, temperature measurement, reduction of friction on the platens, and centering of the

sample on the platen. Plate 3.4 shows the triaxial cell used in the testing program.

The triaxial cell was selected since it allows for a cell fluid to surround the sample which reduces ablation of the sample. The cell fluid employed was a light paraffin oil similar to the fluid used by (Glen (1955) and Iverson and Moum (1974)). This fluid also acts as thermal mass surrounding the sample which helps maintain a constant temperature in the sample during the experiment.

The temperature of the sample was maintained constant by circulating a mixture of ethylene glycol and water through the cooling coils, which act as heat exchangers, mounted within the triaxial cell. The temperature of the ethylene glycol mixture was maintained constant during the experiment by circulating the fluid through a Hot Pak constant temperature apparatus. This apparatus was capable of maintaining the temperature of the circulating fluid constant for prolonged periods of time.

The temperature of the triaxial cell fluid was measured using a temperature measuring probe located at the mid-height of the sample between the sample and the copper cooling coil. The temperature measuring probe was constructed using a stainless steel tube and an Atkin #3 thermistor bead. The details of its construction and calibration is given by Roggensack (1977).

Plate 3.5 shows that the base of the triaxial cell was isolated from the load frame by a cooling plate mounted

between the cell and the frame. The cooling fluid from the Hot Pak apparatus was circulated through this plate. The triaxial cell and measuring equipment were isolated from the temperature fluctuation of the cold room by being housed in an insulated cabinet as illustrated in Plate 3.5.

The measuring instruments used in these experiments were a linearly variable displacement tranducer(LVDT), thermistor, and temperature compensated strain gauge load cell. The Hewlett Packard 24 DCDT LVDT was capable of measuring deformations accurately to .0013 mm The load cells were capable of measuring a load of 18 kN. The thermistors were calibrated using a quartz thermometer to ± 0.001°C; therefore, the thermistor measured a temperature 0.01 ± .005°C.

3.3.3 Sample Preparation

The ice sample selected for testing was removed from the storage freezer, placed in the sample preparation cold room and allowed to come to equilibrium with a room temperature of -5°C for about twenty-four hours.

It was then unwrapped and all loose snow was removed. The sample was described visually in detail. The ice color, bubble content and bubble dispersion were noted.

A slab of ice was cut from each end of the sample for use as an initial indicator of the crystal character. This slab usually measured about 1 cm in thickness and was the full diameter of the sample. Each slab was used to prepare

an ice thin section as described in Section 3.2.2. The crystal character was examined under polarized light to ensure that the crystals were of approximately equivalent diameter and that ice crystal orientation appeared random. The random orientation of the ice crystals was assessed by noting color variation between crystals appearing in the thin sections. Each sample required that about two centimeters of ice be cut away from each end before an acceptable thin section meeting the above requirement could be produced.

The ice samples contained a zone of ununiform ice at each end because the water under a pressure head flowed into and out of the sample as the ice crystals were flooded during preparation (Section 3.1.3). This reduced the usable length of each sample for testing to approximately 270 mm from the initial length of 356 mm. At this point a final set of thin sections were prepared showing the crystal size, shape, and orientation. The sample was now ready for preparation as a constant displacment rate test specimen.

The ice sample was placed in the rotary table mounted on the bed of the milling machine (Plate 3.6). This table was used because it facilitates the machining of a circular sample using a shell mill cutter in the milling machine. The rotary table fixes the central axis of the sample at a fixed distance from the central axis of the shell mill. Thus a sample can be trimmed to any diameter, if it will fit into the rotary table. The shell mill allows a cut into the

sample of one centimeter radially and five centimeters in length to be made. A circular sample could also have been obtained using a lathe, however, the cutting tool must be properly designed and great care exercised during trimming, or the sample could be chipped. The shell mill provided more flexibility in sample preparation, since it does not chip the sample, and thus is preferred when working with ice.

The sample was machined to 70 mm diameter for testing in the cells available for constant displacement rate experiments. In order to machine the sample to the required length a multiple number of passes were required with the shell mill. This was easily accomplished with the milling m[illegible]cause of the vertical travel of the cutter head a[illegible]ble. Therefore, a sample length of 200 mm could be pre[illegible] without adjusting the sample in the rotary table. This [illegible]lowed all constant displacement rate samples to be mach[illegible]ed to the required diameter and length. Each sample was [illegible]epared with a minimum length to diameter ratio of 2.0. After machining of each sample, the ends of the sample were ready for preparation.

The shell mill cutter (Plate 3.7) was designed to cut both in the vertical plane and the horizontal plane; thus the ends of each sample were trimmed using this cutter. Since the initial ice sample was longer than the length required for the constant displacement rate sample, the unmachined portion was saved for future tests. This required removin[illegible] the sample from the rotary table and use of a band

saw to cut the machined portion of the sample away from the unmachined portion.

To prepare the ends the machined sample was placed in the rotary table jaws and tightened to hold the sample securely. A fine initial cut was made on the end of the sample, removing about 0.02 mm of ice. This cut was used as a check on the mounting of the sample. If the sample was not mounted properly the cutter would cause it to vibrate slightly or would not cut the upper face uniformly. If the sample was not secured properly it was now readjusted. This precaution prevented the time-consuming mishap of chipping or cracking a partially prepared sample because of improper mounting.

The ends of the sample were machined at right angles to the vertical axis of the sample. Generally two passes of the shell mill were required to prepare one end of the sample. A final cut of about 0.02 mm was made. The shell mill was then passed over the sample a minimum of two times to ensure that no cutter marks were protruding from the sample. These cutter marks would be stress concentration points during the loading of the sample. The sample was removed from the rotary table and turned end-for-end and remounted in the rotary table. The sample was checked to ensure that it was securely mounted and then machined to the required length for testing. The final steps in preparing the sample were the same as above. The sample was now weighed and the dimensions recorded.

In order to ensure reproducibility in all measurements from sample to sample, a guide was established for the measurements of each sample. The dimensions of each sample were established by taking three measurements of the sample length and three measurements of the sample diameter. The diameter was measured at the top, middle and bottom whereas the length was takened at three independent locations on the sample. The sample was weighed allowing the bulk density to be calculated. With the dimensions established, the sample was ready to have the centering holes drilled and to be mounted in the cell.

A centering hole was drilled in the top and bottom of each constant displacement rate sample to facilitate centering of the sample during setup. This was required because each end platen had a securly attached Teflon friction reducer which caused aligning problems during sample set up.

The sample was again mounted in the rotary table and secured. The shell mill was removed and replaced with a cutter head of 3 mm diameter. The center of the sample was located and a centering hole drilled to a depth of 6 mm. The sample was removed and turned end-for-end and remounted. The center again was located and the centering hole drilled. The sample was removed from the rotary table and was ready for mounting in the test cell.

The sample and the test cell platen were wiped clean to ensure that no grit was lodged between the sample and the

Teflon-coated load platen. The lower load platen was coated with paraffin oil to further reduce the friction, and the sample was placed on the platen using the centering hole as a guide. The upper platen was lowered on the sample using the same procedure as above. The cell was then assembled around the sample and filled with paraffin oil using a tank under low pressure to force the oil into the cell. The sample was ready for testing in the constant displacement rate test frame.

3.3.4 Test Procedure

The constant displacement rate experiments were conducted in a cold room maintained at -3±.5°C. The experiments were all conducted at test temperatures warmer than the room temperature. This required that the fluid circulating through the cooling coils be heated above the ambient room temperature. The experiments were performed with these temperature conditions to ensure that the sample would cool down if a constant temperature bath failed. This temperature condition also ensured that heat flowed radially outward from the cell to the cold room. The radial heat flow away from the cell helped to reduce temperature fluctuations of the sample.

The cell containing the sample and the confining fluid was transferred from the preparation cold room maintained at -5°C to the sample testing cold room at -3°C. The cell was placed inside the insulated cabinet, on the cooling plate

which separated the test frame from the cell (Plate 3.5). The fluid lines from the constant temperature bath were attached to the cell. The fluid temperature in the bath was checked to ensure that it was at the desired test temperature. The variable resistor dial on the constant temperature bath was locked at this dial setting. The temperature measuring probe was placed into the cell and attached to the data recorder. The cell temperature was recorded and the pump on the constant temperature bath activated. The ethylene glycol mixture circulated through the cooling coil within the cell and the cooling plate beneath the cell.

While the cooling fluid was being circulated, the LVDT and the load cell were adjusted to their zero position for the experiment. This was accomplished using an electronic monitor within the cold room. The insulated cabinet surrounding the cell was closed. The cell and the sample were allowed a minimum of twenty-four hours to establish an equilibrium temperature. During this period the temperature of the cell was recorded and it was noted that the sample reached a stable temperature in about 10 hours.

The displacement rate used during each experiment was selected using the nominal rates applicable for each set of gears on the testing machine. The press was then started and all the measuring devices were recorded to establish their zero readings and zero time at the start of the press. The zero time of the experiment had to be adjusted during data

reduction because no seating load had been applied to the specimen. The true time zero was determined by extrapolating the load time plot to a zero load and using this as zero time. This method was preferred to that using the zero time established when the press was started, since the gears require a certain time to become engaged and begin loading the specimen. The time zero value for the LVDT was selected as the above value.

The deformation of the sample was checked at regular time intervals to ensure that it was being loaded at a constant rate of displacement. The output of the LVDT, the load cell, the thermistor, and the time clock were recorded at regular time intervals during the experiment on a remote data acquisition system located outside the cold room. The data were recorded using a Techtran cassette recorder. The data were reduced using a Fortran computer program and the results plotted using a Calcomp bed plotter. The data plots are contained in Appendix A.

The test was continued until the stress versus time plot stabilized at a constant stress and until the sample had undergone a strain of greater than 15%. Figure 3.4 shows a typical plot of stress versus time of a constant displacement rate sample. The reasons these two requirements were imposed on the experiment will be discussed in Chapter 4.

Upon termination of testing each sample was removed from the test cell. The final dimensions were taken and the

shape sketched. The sample was weighed to determine if any weight loss had occurred during the experiment. Thin sections of the sample were then prepared to determine th affect of the the deformation of the sample on the initial ice crystal structure. The thin sections were prepared according to section 3.2.2.

3.4 Constant Displacement Rate Punching Test

3.4.1 Introduction

In this experiment a circular punch was forced into a cylindrical ice sample at a constant displacement rate. The load required for the punch to penetrate the ice was recorded. These experimental results will be analysed using the flow law of the ice to develop a clear understanding of the material behaviour. Ladanyi and Johnston (1974) and Ladanyi (1976) used the expansion of a spherical cavity to predict the punch resistance. The results of these experiments will be analysed in Chapter 5.

3.4.2 Equipment

The constant displacement rate penetration equipment was similar to the constant displacement rate loading experiment equipment. A constant displacement rate Wykeham Farrance 100 kN capacity press was used. The press used a double gear box system and was able to achieve displacement rates between 6 x 10^{-6}mm per minute and 6 mm per minute. A cell capable of holding a 100 mm diameter sample was easily

accommodated within the triaxial press.

The 100 mm diameter triaxial cell also was modified to contain cooling coils for maintaining temperature control. A temperature probe was also fitted through the top of the cell. The lower platen was coated with a Teflon sheet to reduce friction. The cell was similar to the 70 mm triaxial cell illustrated in Plate 3.4.

The temperature control and temperature measurements were accomplished using the same equipment as in the constant displacement rate loading experiments.

The vertical deformation of the punch was measured using a 24 DCDT Hewlett Packard LVDT with a measurement accuracy of .0012 mm. The load cell was a Hemisphere temperature compensated load cell capable of measuring a load change of 1 N. The thermistor probe was the same as used in the constant displacement experiment.

3.4.3 Sample Preparation

The dimensions of the sample used in the punch experiment had a minimum sample height and diameter of five times the punch diameter. This required that the height and diameter of the sample be at least 100 mm. This fulfilled the requirement of ensuring that all the plastic flow occurs within the sample as outlined by Bishop et al. (1956). The sample preparation was the same as the constant displacement rate sample to the point where the dimensions and weight of the sample were obtained.

At this point the penetration sample was secured in the rotary table and checked to ensure that the sample was properly mounted. The shell mill was removed from the milling machine and replaced by a 20 mm diameter cutter. The centre of the sample was located in the same manner as in Section 3.3.3 and the cutter was advanced into the ice cutting a circular opening to the required depth. The hole was slightly larger in diameter than the punch to minimize the friction on the sides of the 19.05 mm diameter punch. This hole was used to embed the punch below the surface at the beginning of the experiment. The sample was again weighed and this weight was used as a check against weight loss during the experiment. The penetration sample was now ready for mounting in the cell.

The lower platen and the sample were wiped clean. The Teflon face of the lower platen was lubricated with paraffin oil and the sample centered on the bottom platen. The punch was inserted into the embedment hole and the cell body lowered around the punch rod. The cell body was securely attached to the base. The space surrounding the sample in the cell was then filled with light paraffin oil using the same pressurized tank as used in the constant displacement rate loading test. The cell containing the sample was then transferred to the cold room in which the tests were performed.

3.4.4 Test procedure

The cell was placed in the insulated cabinet on the cooling plate which separates the cell base from the loading frame. Plate 3.5 shows the constant displacement rate loading system. The temperature measuring probe was inserted to the mid-height of the sample between the cooling coil and the sample via the hole in the top of the triaxial cell. The lines used for circulating the ethylene glycol mixture were attached to the inlet ports of the cell. The constant temperature bath was checked to ensure that the cooling fluid was at the correct temperature, and that the variable resistor dial was locked. The cell temperature was recorded. The pump was then started to circulate the ethylene glycol mixture through the cooling plate and the cooling coil in the cell.

As the cooling fluid circulated, the cell temperature was monitored using a remote read-out device in the cold room. The LVDT and the load cell were adjusted to their zero position for the experiment. The zero reading for each piece of measuring equipment was recorded both manually and remotely on the Techtran cassette recorder. The insulated cabinet surrounding the cell and the instruments was sealed from the cold room. The sample was allowed twenty-four hours to establish its equilibrium temperature before the experiment was started. The temperature was monitored during this period to ensure that an equilibrium temperature was established within the cell.

At the end of this period, the sample was ready for testing. The cell was adjusted within the loading frame to bring the punch and ball just in contact with the load cell (Plate 3.5). The zero reading of the LVDT was checked, as was the zero reading of the load cell. The gears of the load frame were adjusted to set the displacement rate at the desired rate. The press was then started and the zero time of the experiment was recorded. During data reduction the zero time was readjusted using the procedure discussed in Section 3.3.4.

The output of the temperature probe, LVDT and the load cell were monitored manually during the first few hours of the experiment to ensure that the punch was advancing in the correct direction. The output throughout the experiment was recorded automatically at regular time intervals on the Techtran cassette recorder. The data were reduced and plotted using a Fortran program and the Calcomp bed plotter. The data plots are contained in Appendix A.

The reduced data were plotted while the experiment was being conducted to see the shape of the punch resistance versus time plot. The punch experiments were continued until a constant punch resistance versus time plot was established. The punch penetration also was restricted to generally no more than 25 mm to ensure that the plastic flow was contained within the elastic body as proposed by (Bishop et al. 1956). Figure 3.5 shows a plot of a typical set of data from a penetration test. When these two criteria were

met the experiment was terminated.

The sample was removed from the apparatus. Its weight determined, and a thin section of the sample taken to study the deformation of the the ice crystals during loading. The sample was sectioned to give one section near the bottom platen and one thin section through the vertical mid-plane of the sample. Thus one section would be in the low stressed region of the sample and one would be in the highly stressed region surrounding the penetrating punch. The procedure used in making these sections was the same as outlined in Section 3.2.2.

3.5 Constant Stress Loading Test

3.5.1 Introduction

In this experiment a sample was loaded with a constant load and the deformation of this sample was recorded with time. This is the classical creep experiment used to establish the deformation versus time plot for a constant load. Since the cross-sectional area increases with deformation, a slight adjustment to the load must be made if a constant stress on the sample is desired. This experiment was performed to establish the deformation versus time relation for a stress range of interest. These experiments were conducted for comparison with the data of other authors.

3.5.2 Equipment

The constant stress experiments were conducted using a lever-assisted loading frame to apply a constant load. The lever for this dead load frame was copied from the Wykeham Farrance constant displacement rate direct shear apparatus. This gave a mechanical advantage of five times, thus reducing the amount of dead load required for each experiment. The loading system is illustrated in Plate 3.9. The dead load system of applying a constant load to a sample has been used by all previous authors working on the creep of ice. It was also used in this program because a constant load can be maintained indefinitely.

The cells used were designed to hold the sample and surround each sample with paraffin oil to reduce ablation. The cells contain a copper cooling coil through which a cooling fluid was circulated to maintain a constant temperature. The upper and lower platens were coated with Teflon to reduce the friction between the sample and the platen. The details of the constant stress cell are shown in Plate 3.8. The cells were not designed to maintain a confining pressure, thus no cell cover was constructed.

The system of transferring the load from the lever system to the upper platen was similar to the transfer system in the direct shear apparatus. The transfer mechanism was designed to fit around the outside of the insulated cabinet which housed the measuring equipment and constant stress cell. The LVDT holder also held the temperature

measuring probe and was attached to the load ram. The sample displacement was thus measured from the ram and not the top of the sample. All the instruments were housed within the insulated cabinet to reduce temperature fluctuations. Plate 3.10 shows the details of the constant stress load frame and the cell.

Each load transfer system was aligned to ensure that the load ram and the lever housing were acting on a plumb line in order that no lateral loads were applied to the sample during testing.

The temperature of the sample was maintained constant by circulating an ethylene glycol mixture through the copper cooling coils mounted in the cell. The cooling coils act as heat exchangers and thus maintain the paraffin oil surrounding the sample at a constant temperature. As in the previous tests the temperature was maintained constant by circulating the fluid through a Hot Pak constant temperature bath. The temperature of the paraffin oil surrounding the sample was also measured at the sample mid-height. The temperature of the sample was taken as the oil temperature, since all heat would be conducted radially outward from the cell. The base of the cell was separated from the loading frame using a block of Bakelite, rather than a cooling plate. It was designed in this fashion to reduce the number of constant temperature cooling baths which were required for the experimental program. The outward flow of heat from the cell reduced the temperature fluctuations of the

samples.

The measuring instruments used were a LVDT, and a temperature measuring probe. The Hewlett Packard 24 DCDT LVDT was capable of measuring deformations accurately to 0.001 mm. The thermistors were calibrated using a quartz thermometer which measured the fluid temperature surrounding the thermistor probe to a temperature of .001°C thus the probes would be accurate to 0.01±.005°C.

3.5.3 Sample Preparation

The constant stress specimen preparation was similar to the constant displacement rate experiment. The constant stress samples were, however, much larger. Their average diameter was 120 mm and the height averaged 250 mm. This height of sample required that during machining each sample be rotated end-for-end in order to machine the full length of the sample. This operation required extra care to ensure that the sample alignment was correct and that the sample and the shell mill cutter were aligned before each pass of the cutting head.

The ends of each sample were prepared in the same manner as the constant displacement samples. After the dimensions and weight of each sample were determined the centering holes were drilled. In the constant stress sample the holes were 6.0 mm diameter and 10.0 mm deep. The sample was then ready for mounting in the constant stress cell. This cell is illustrated in Plate 3.8.

The ends of the sample and the upper and lower platen were wiped to remove any grit. The sample was lowered onto the lower platen using the centering hole as a guide. The upper platen was then lowered onto the ice sample. The cell was filled with paraffin oil, until the upper platen was covered and then the cell was moved from the preparation room into the cold room.

3.5.4 Test Procedure

The cell containing the constant stress sample was placed on the Bakelite platen and centered. The lines for circulating the ethylene glycol mixture were attached to the cooling coils in the cell. The temperature measuring probe was placed in the oil at approximately mid height of the sample. The constant temperature bath was checked to ensure that the ethylene glycol mixture was at the appropriate temperature and the variable resistor was locked to maintain this temperature. The pump on the bath was started and the fluid allowed to circulate through the cooling coils. The insulated cabinet containing the cell and sample was sealed, and the sample allowed twenty-four hours to establish an equilibrium temperature. The LVDT was also attached to the power supply and housed in the insulated cabinet to allow it to establish an equilibrium temperature.

In order to reduce the equipment required, four constant stress cells were attached to one constant temperature bath. Thus, in order to have each sample at an

equilibrium temperature, no experiment was started until each sample attained an equilibrium temperature. Figure 3.6 shows the temperature records of four cells connected to one constant temperature bath for an extended period of time. The temperature difference in the plot is due to varying lengths of pipe leading to each cell and the associated radial heat loss from these pipes. The slight temperature difference has a minor influence on the deformation. Each sample was ready for testing when the equilibrium temperature was established in all four cells.

The steps in setting up each constant stress experiment were quite different from the constant displacement experiments since the load transfer to the sample was via a lever and dead load system. This required that the various components of the loading system be assembled and that the load be applied to the lever. The complete system is illustrated in Plate 3.9 and Plate 3.10. The assembly of the loading frame and the load transfer system required a certain time, therefore no attempt was made to obtain the instantaneous elastic deformation of each sample.

The load transfer ram with the LVDT and thermistor holder was placed on the steel ball on the upper load platen. The ram was attached to the hanger which transfers the load from the lever to the ram. The load of the hanger and the ram were applied to the load platen (a seating pressure of about 5 kPa). At this point the LVDT was zeroed, the reading was recorded both manually and on the Techtran

cassette recorder. The temperature measuring probe was moved to the sample mid height and the reading recorded. The above procedure required that the insulated cabinet be opened for a period of time. Therefore, the box was resealed and the sample temperature allowed to re-establish itself. This time allowed the upper platen to become seated under the low seating pressure and ensured that the temperature of the sample was re-established. During this period of approximately one hour, the deformation of each sample was recorded on the cassette recorder at time intervals of ten minutes. The change in the LVDT reading during this time was negligible and therefore this was not considered as part of the sample deformation. The temperature was monitored to ensure that it remained constant and then the sample was ready to have the total load applied.

The load to be applied to each sample had previously been determined so that a pre-selected constant stress would be applied on each sample. The weights were selected and placed beside the load frame on the floor. The load transfer frame was adjusted to ensure that it was in line with the lever transfer pivots in order that the load was applied vertically. Time zero was now established and the LVDT reading recorded. The lever arm and hanger were applied and the LVDT and time recorded. The load was then placed on the hanger and the vertical deformation and the time were recorded. This load transfer operation required about 30 seconds.

The vertical deformation of the sample was recorded at one minute time intervals using the manual scan of the data acquisition system. The lever arm of the loading apparatus was monitored to ensure that it remained level. This was determined using an oil-filled spirit level and any necessary adjustments could be made by adjusting the screw on the load transfer assembly. The data recording interval was increased to ten minutes after one hour. This allowed the recording of the reading to be made on the Techtran cassette recorder attached to the data acquisition system. Ten minute recording intervals were continued for a period of twenty-four hours.

For the duration of each experiment the LVDT and temperature probe readings were recorded at one hour intervals using the Techtran recorder. The recorded data were reduced using a Fortran program and plotted on a Calcomp bed plotter. The resulting data plots are contained in Appendix A.

The computer processed data were plotted while the experiment was running to study the characteristics of the displacement (strain) versus time plot. Each experiment was continued until the displacement time plot showed an inflection point and accelerated deformation rate. The load was removed when the tertiary mode of creep was well defined but before instabililty of the sample occurred. A typical strain versus time plot for a experiment is contained in Figure 3.7.

The cell was not disconnected from the constant temperature bath at this point because this would change the equilibrium temperature regime of the other samples connected to the constant temperature bath. The unloaded sample was not removed from the cell. Thus, it was allowed to undergo stress relief. This required the final thin sections and final dimensions of the sample be taken when all the constant stress samples attached to the circulating bath were unloaded.

3.6 Simple Shear Loading Test

3.6.1 Introduction

A special apparatus was designed and constructed to conduct constant stress creep tests on an ice sample under a complex stress state. The constant stress tests yields the deformation behaviour under the uniaxial stress state, and a constant strain rate experiment will yield the influence of varying the confining pressure on the flow law. The simple shear device applies a constant vertical stress and also a constant shearing stress to the sample. This imparts a more complex stress state within the sample to examine the influence of this on the flow law of ice.

3.6.2 Equipment

The simple shear tests were performed in a cell designed and constructed for this purpose. The details of the cell and loading system are shown in Figure 3.8. The

basic principle of the testing system is illustrated in Figure 3.9 which shows that a normal load and a shear load are imparted to the upper platen and then transferred to the sample via a set of serrated grip plates on the top and bottom of the sample.

The cell and loading apparatus was constructed in the workshop of the University of Alberta. A shear load can be applied to the upper load platen. This causes a shear distortion within the sample which can be measured by measuring the horizontal displacement of the upper load platen. The shear load is applied by a horizontal ram which passes through a Thomson linear bearing in the cell wall. A constant load is applied to this horizontal rod by passing a steel cable attached to the rod over a pulley and placing a dead weight on this hanger. The total shear load is measured by a load cell attached to the loading ram and the upper load platen within the cell. The horizontal load is transferred into a shearing stress applied to the sample by a serrated plate between the upper load platen and the top of the sample Figure 3.9. This serrated plate is melted into the sample to ensure that it is in intimate contact with the ice.

The vertical load is applied to the sample through a vertical loading ram which passes through the top of the cell cover. This load is transferred to the upper load platen through a set of roller bearings which allow the load platen to move horizontally without placing a lateral thrust

on the vertical ram. The vertical load on the upper platen is also transferred from the upper load platen to the sample via the serrated plate.

This load transfer through the serrated edges of the plate causes stress concentrations and some pressure melting of the sample at the tips of the serrations.

The temperature control in this cell was achieved in a similar fashion to each of the other test cells used in the experimental program. Cooling coils were placed around the outside perimeter of the cell and a cooling plate was placed above and below the sample. These acted as heat exchangers to maintain the paraffin oil and thus the sample at a constant temperature. The ethyelene glycol mixture circulating through each heat exchanger was maintained at a constant temperature by being circulated through a Hot Pak constant temperature bath.

3.6.3 Sample preparation

The preparation of the simple shear test specimen differed from the preparation of the other specimens. After the ice sample was selected for testing it was mounted in the rotary table of the milling machine. The sample was machined to the required radius and height following the same procedure as used in the constant displacement rate loading specimens. The dimensions and the weight of the specimen were determined. At this point the preparation procedure varied from that of the constant displacement rate

sample preparation procedure.

The sample was again mounted in the rotary table. The serrated end plates which were cleaned and maintained at 22°C were brought into the cold room. The top plate was placed on the top of the ice sample and it immediately melted the serrated edges into the ice surface. Dry ice was placed on the top of the plate and the melted ice surrounding the serrated surface was refrozen. Thus the serrated plate was frozen into the top of the sample. The sample was immediately inverted and the bottom plate placed on the sample in the same fashion as above. The serrated plates were kept aligned at 90° to the axis of the sample and parallel by using the rotary table and the milling machine spindle in the placement of the plate. The sample height was remeasured to determine the new height of the specimen.

The sample was fitted into the upper and lower loading platens as shown in Figure 3.8. The loading platen was then placed on the sample followed by the cooling plate. The shear load ram was connected to the transfer mechanism. The vertical loading ram was connected and the cover placed on the test cell. The cell was filled with paraffin oil and was now ready for testing.

3.6.4 Test procedure

The sample was allowed to come to an equilibrium temperature by circulating ethylene glycol through the

cooling coils within the cell. Twenty-four hours were allowed for the sample to reach the equilibrium temperature.

The horizontal and vertical LVDT's were attached to the loading rams, and a zero reading taken. The total dead load required to apply the constant vertical stress was applied on the vertical hanger system. The shear load was placed on the shear load hanger to impart a constant shear stress on the sample. The zero time was recorded and the zero reading of the horizontal LVDT, and the vertical LVDT, and the shear load cell were recorded. The temperature at the mid-height of the sample was also recorded.

The reading of each of the above recording devices was taken at one minute intervals for the first hour. The recording interval was increased to ten minutes for the next twenty-four hours, and then one hour thereafter. The data was recorded automatically on the Techtran cassette recording. The recorded data were processed using a Fortran computer program. The data plots are contained in Appendix A.

The computer processed data were plotted throughout the experiment to determine the displacement versus time plot for the sample. The experiment was stopped after the displacement versus time plot showed a steady state portion or when tertiary creep was established. Figure 3.10 gives a typical set of data from this experiment.

Table 3.1

Summary of Bulk Density and Average Grain Diameter

Sample Number	Bulk Density Mg/m?	Grain Diameter mm
15	8.96	0.98
16	////	0.83
18	8.92	0.92
19	////	0.92
20	8.89	1.06
25	8.85	////
29	8.85	0.90
30	8.91	1.19
31	8.98	0.59
32	8.85	1.19
33	8.92	1.08
34	8.92	0.94
35	8.94	0.62
37	8.91	0.86
38	////	0.86
39	8.89	1.06
41	8.88	1.06
42	8.89	0.85
43	8.85	1.09
44	8.91	////
45	8.91	////
46	8.92	0.82
47	8.91	////
48	8.89	1.10
51	8.90	0.94
52	8.90	1.18

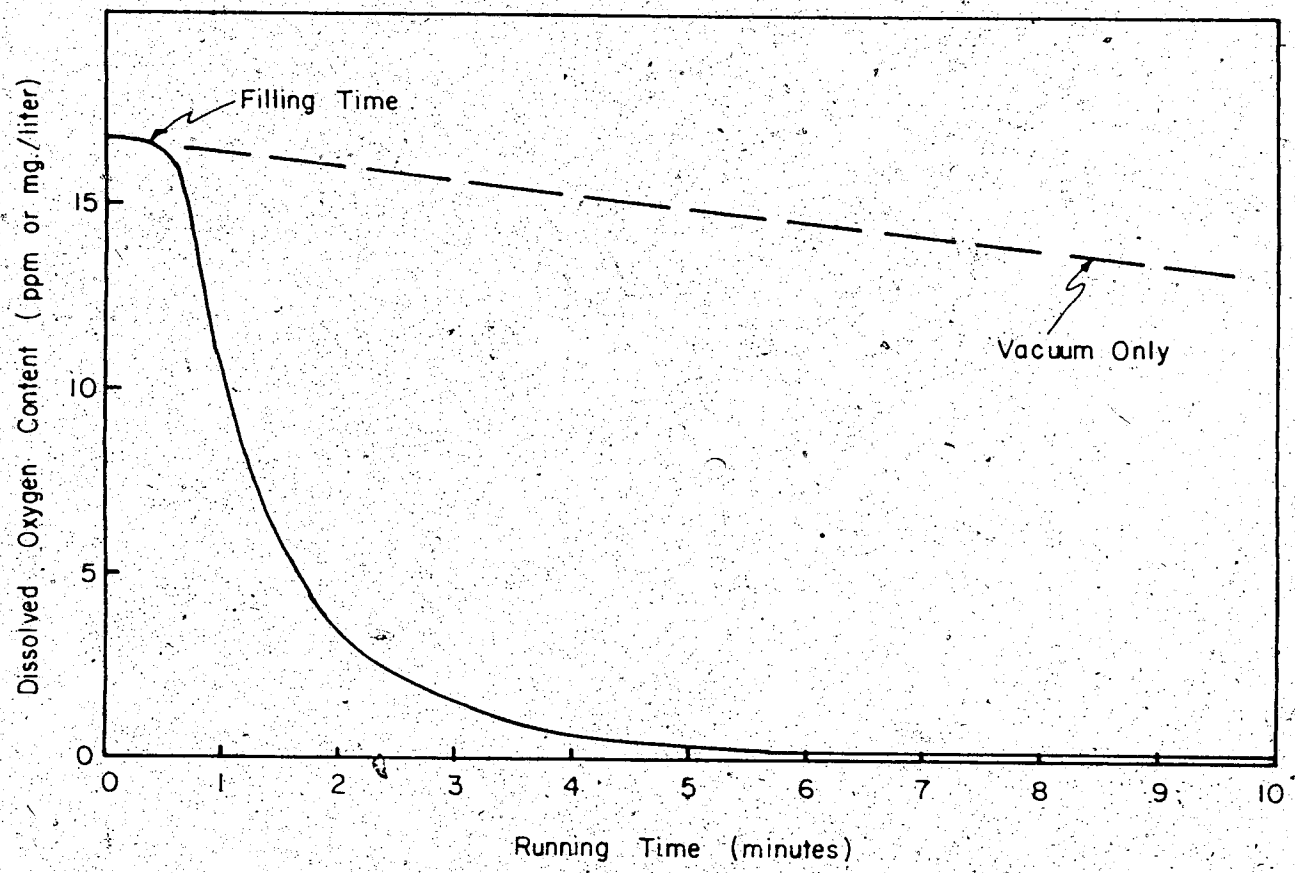

Figure 3.1: Dissolved oxygen versus time required to deair 6 liters of water

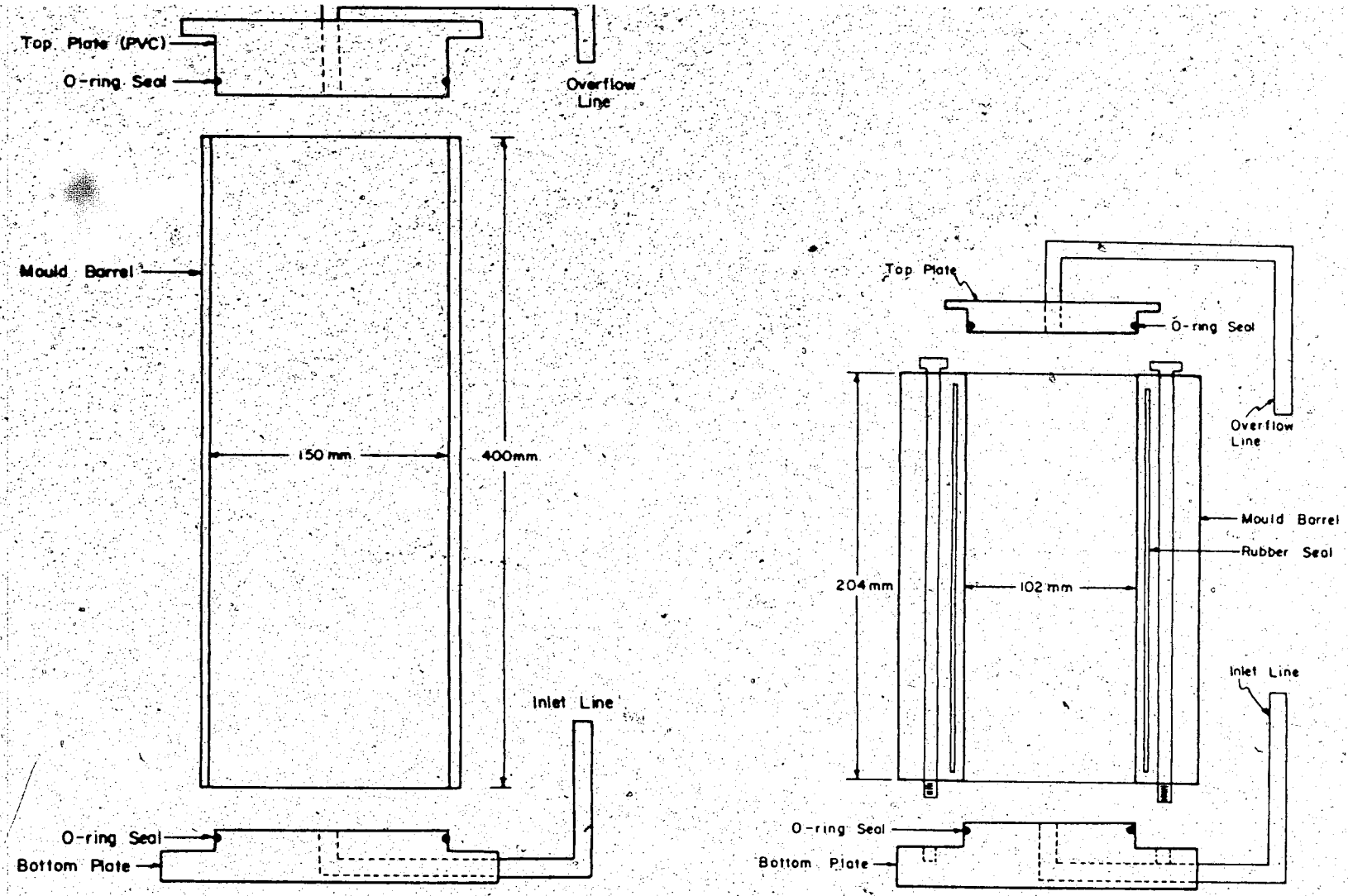

Figure 3.2 Moulds used for making ice samples

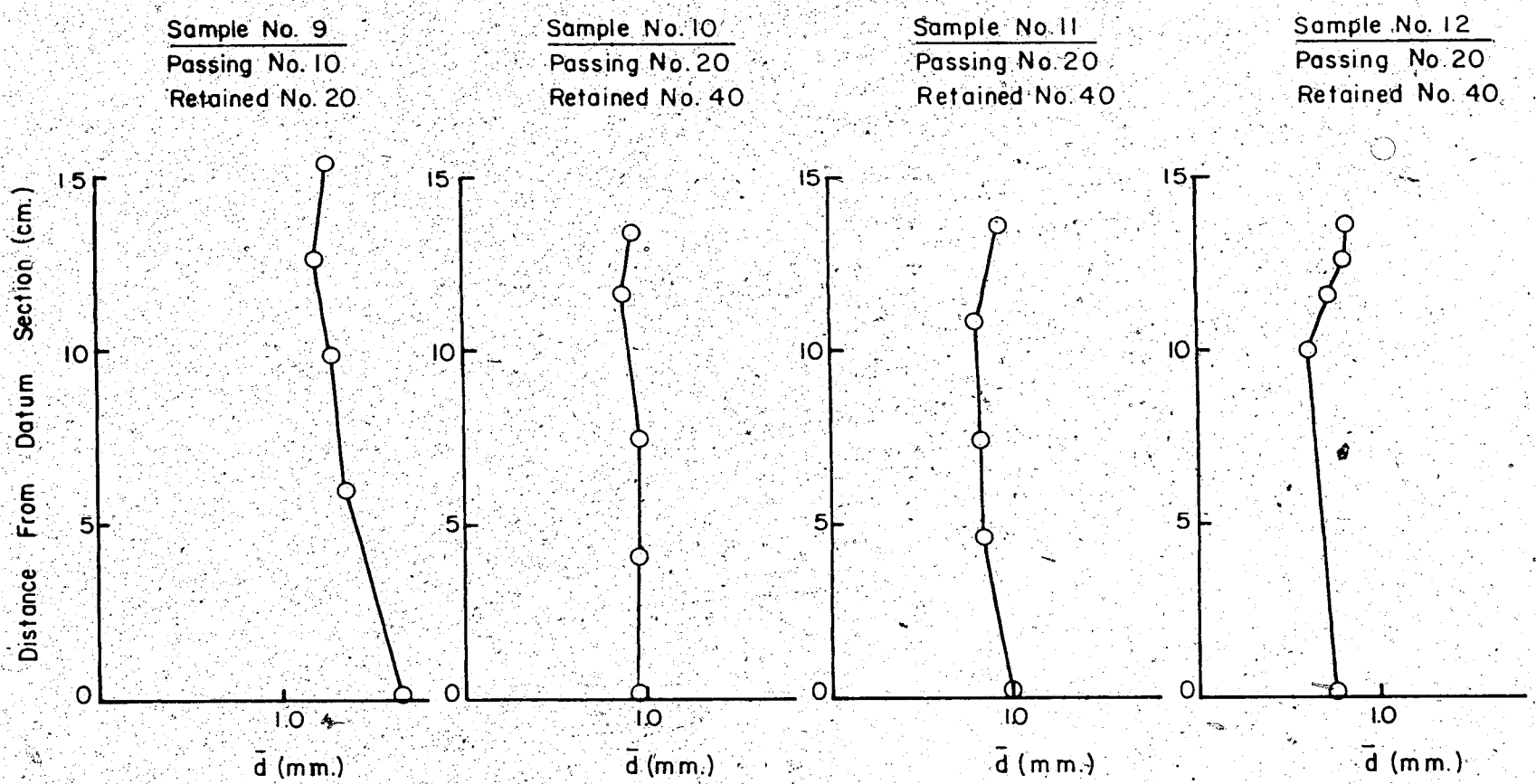

Figure 3.3 Average crystal diameter (d) versus distance from datum of thin section.

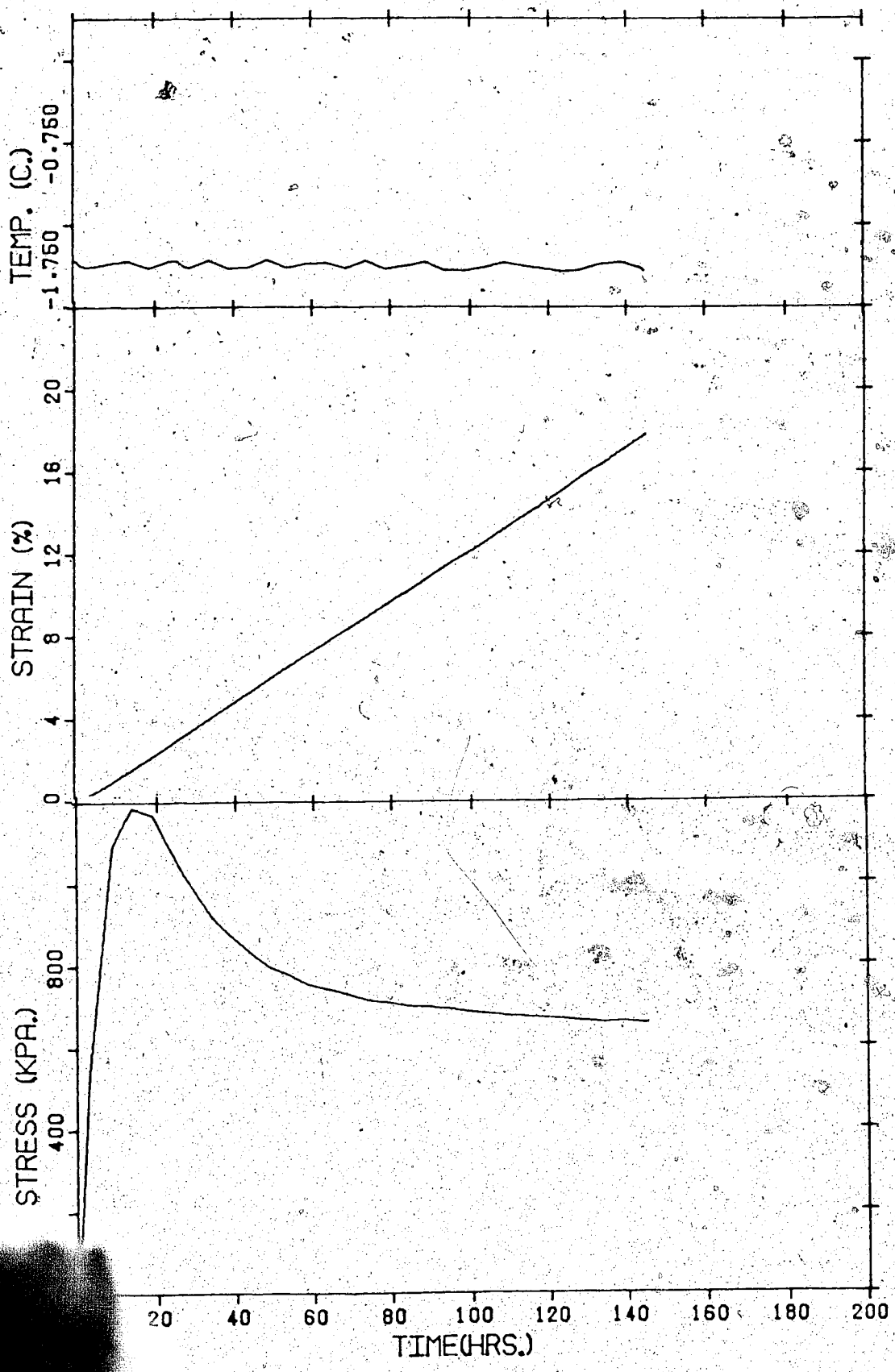

4 Typical plot of data from the constant displacement rate experiment

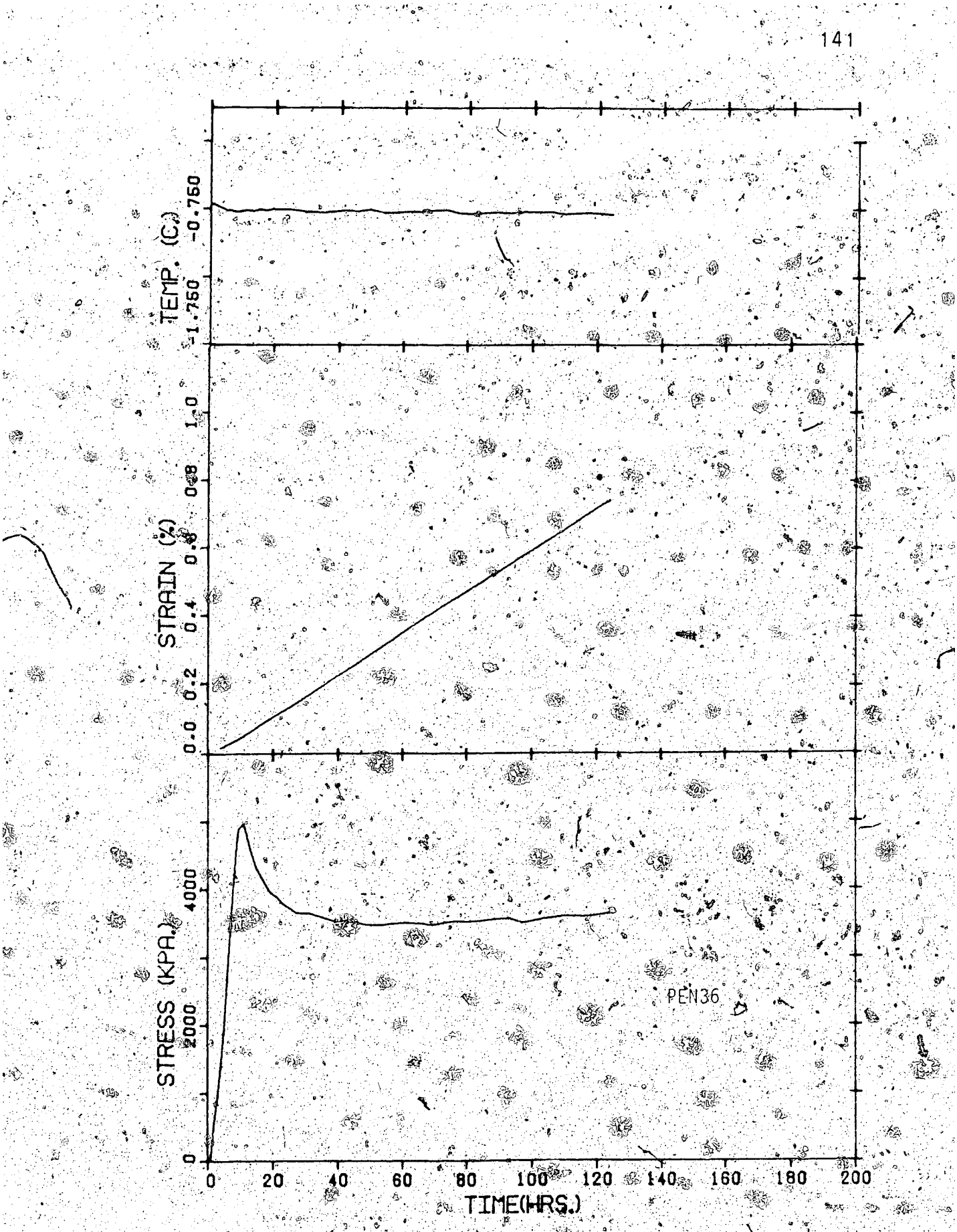

Figure 3.5 Typical plot of data from the constant displacement rate penetration experiment

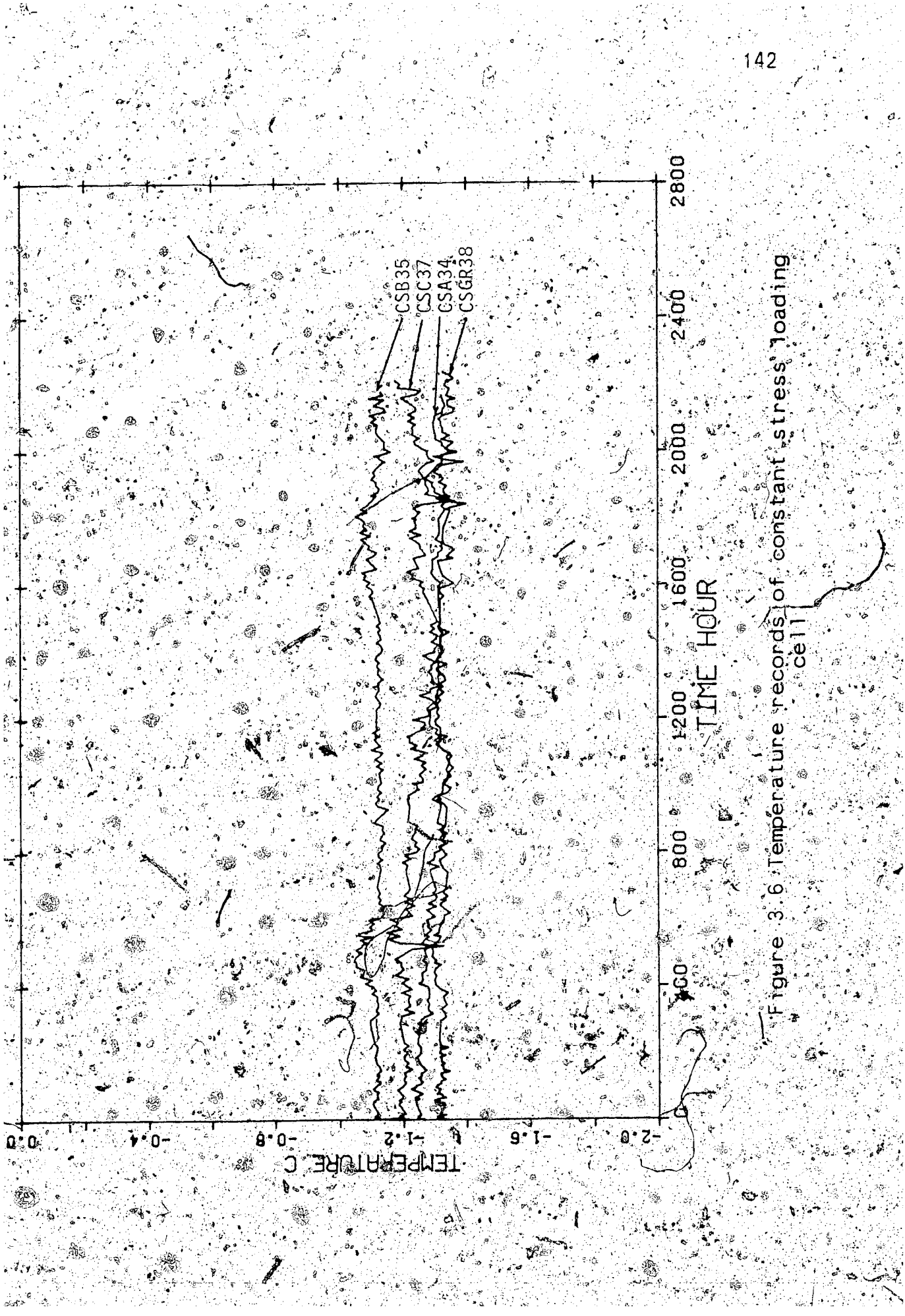

Figure 3.6 Temperature records of constant stress loading cell

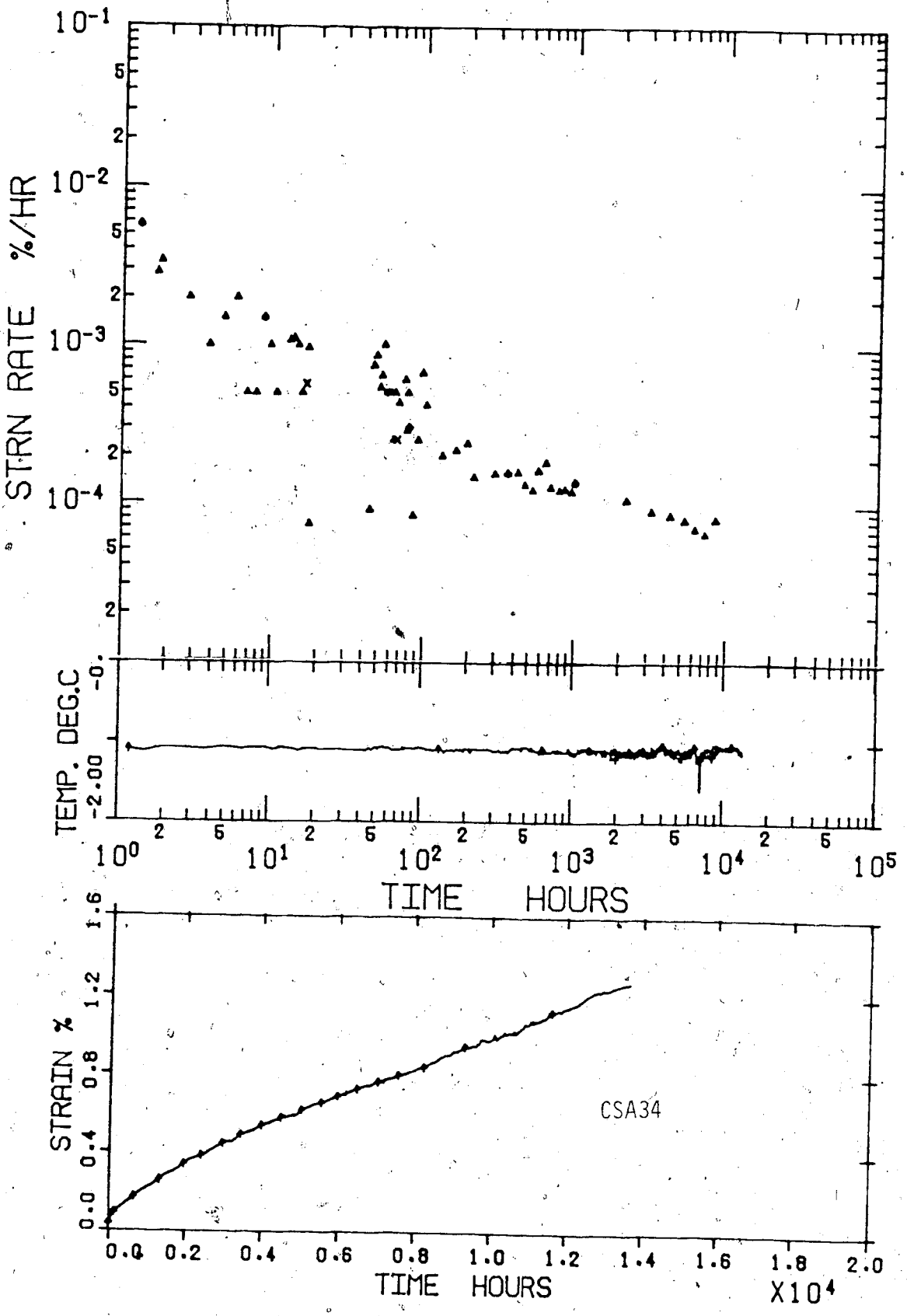

Figure 3.7 Typical plot of data from the constant stress loading experiment

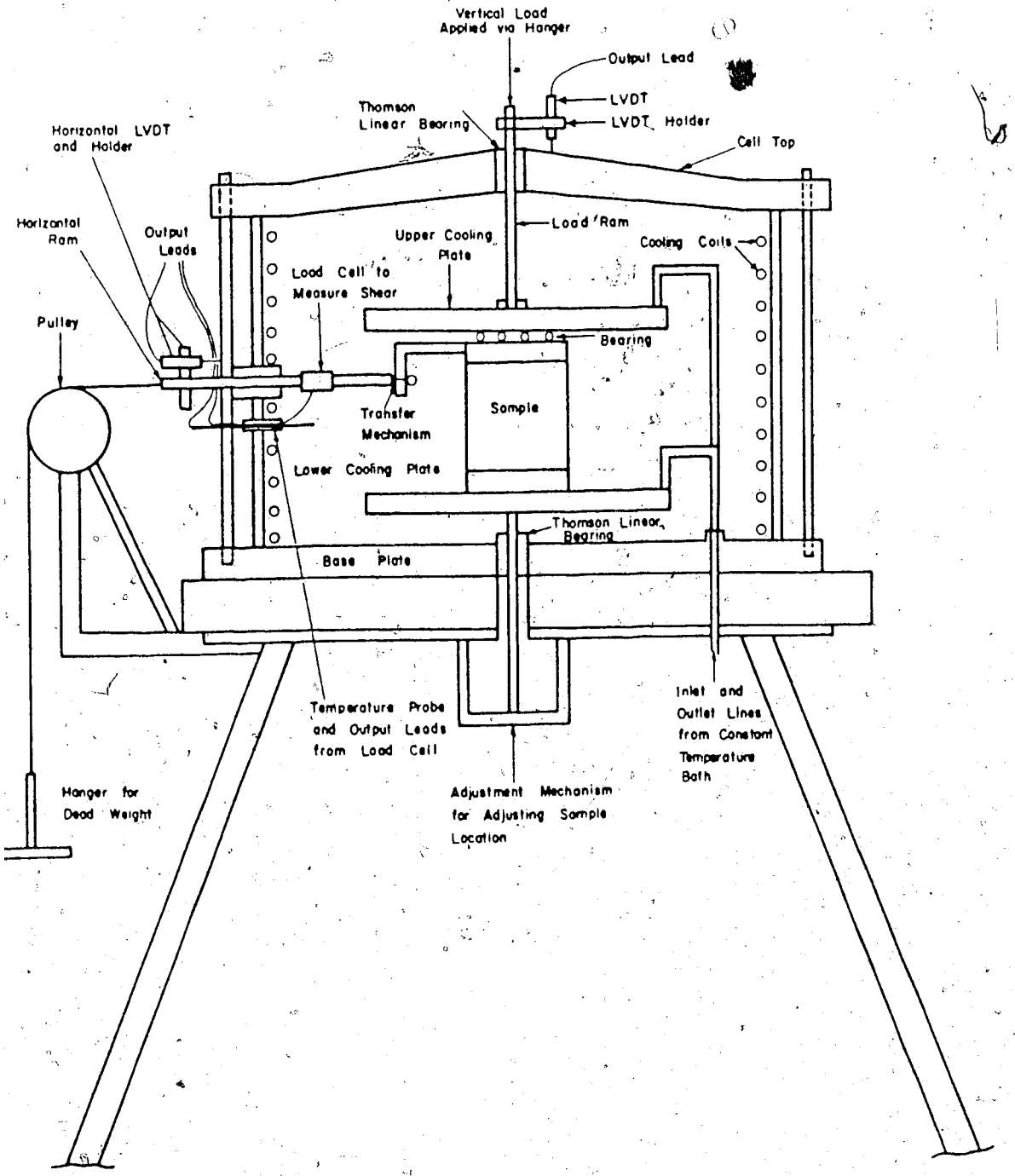

Figure 3.8 Simple shear loading system

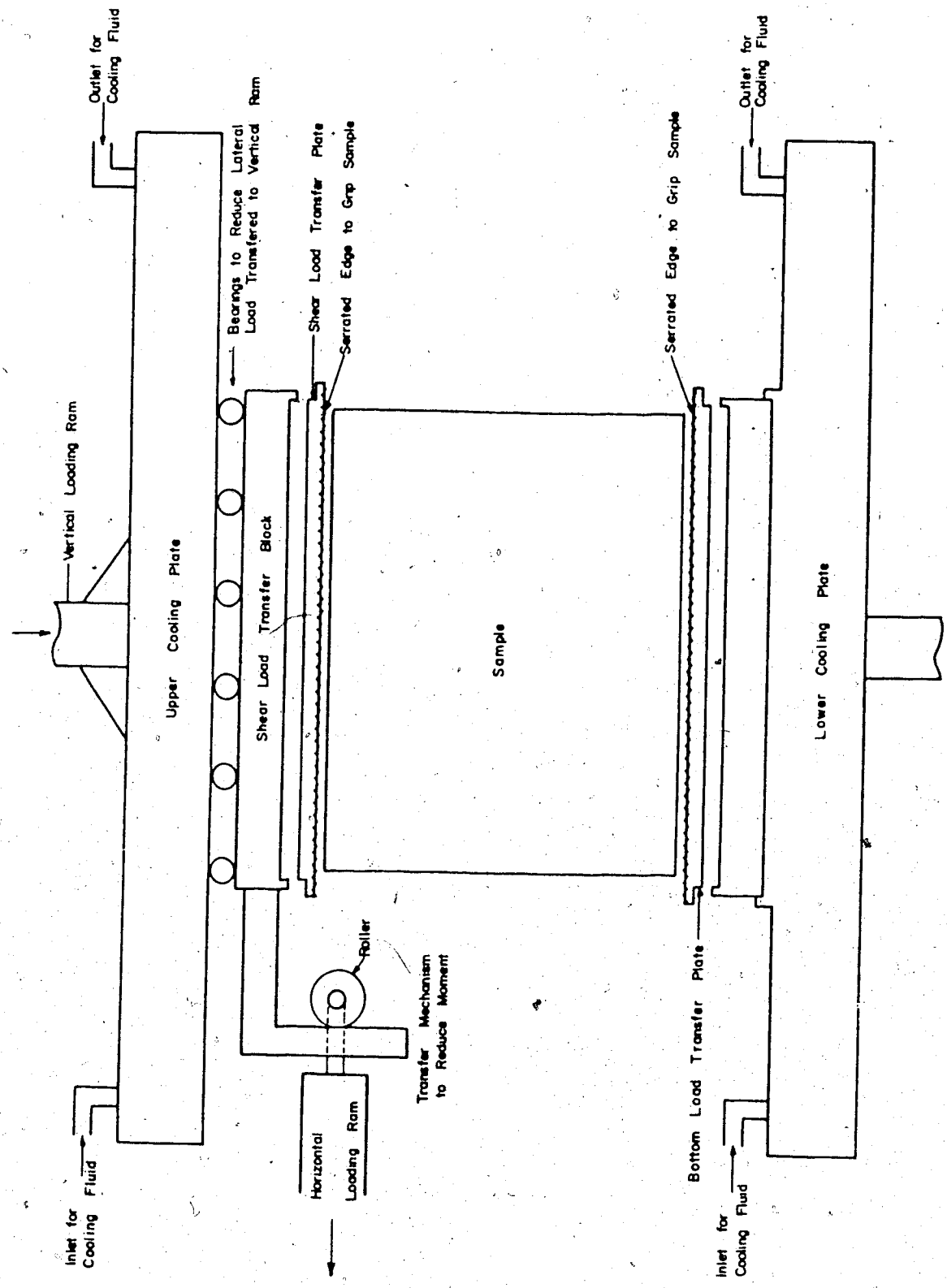

Figure 3.9 Detail of loading system in simple shear experiment

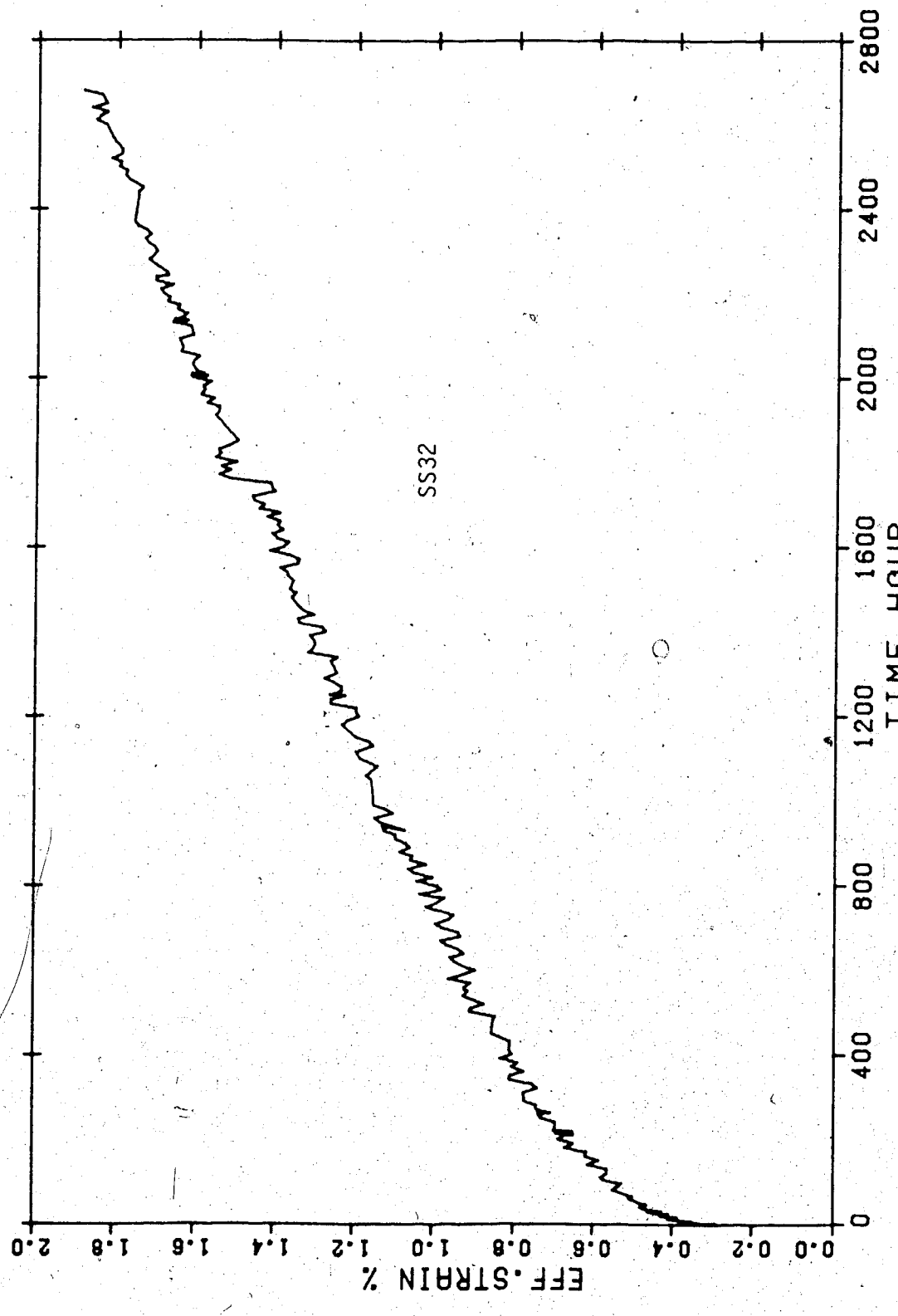

Figure 3.10 Typical plot of data from the constant stress simple shear loading experiment.

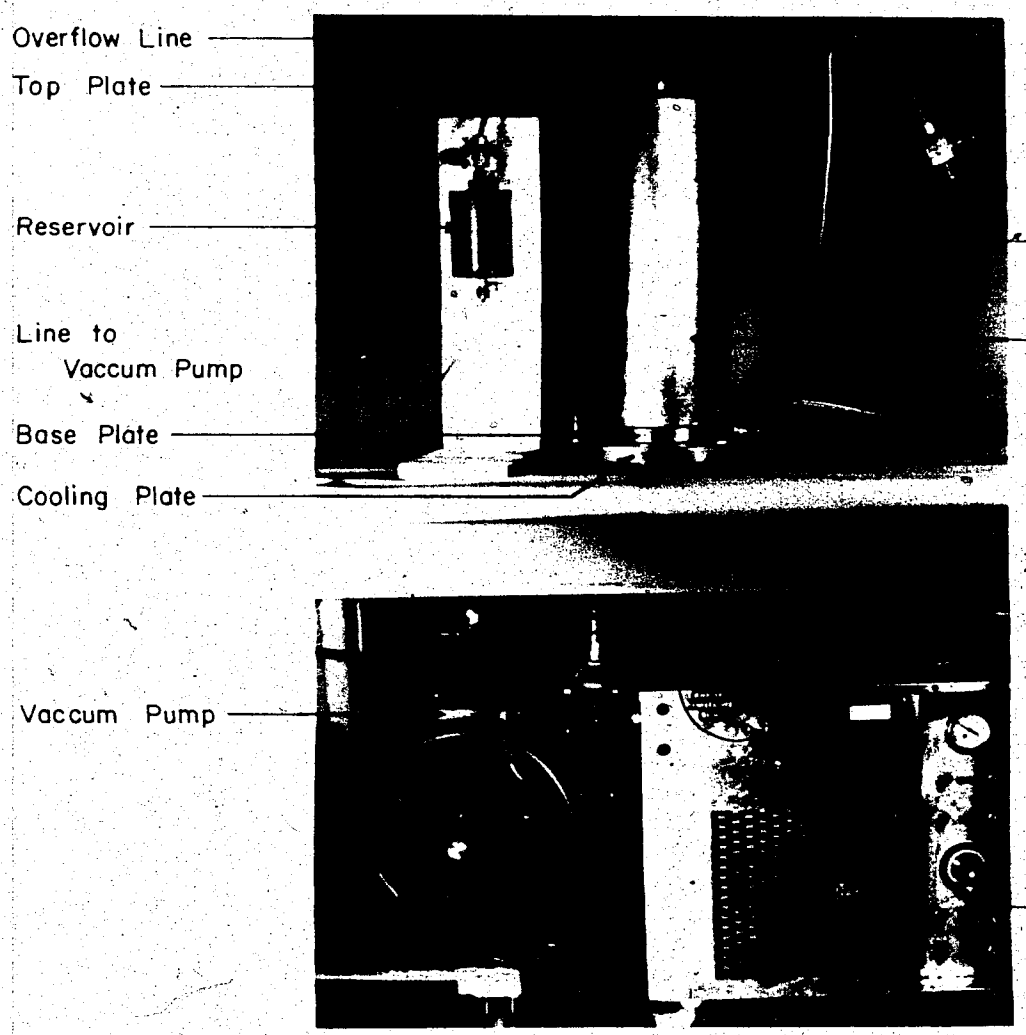

Plate 3.1: Ice making equipment.

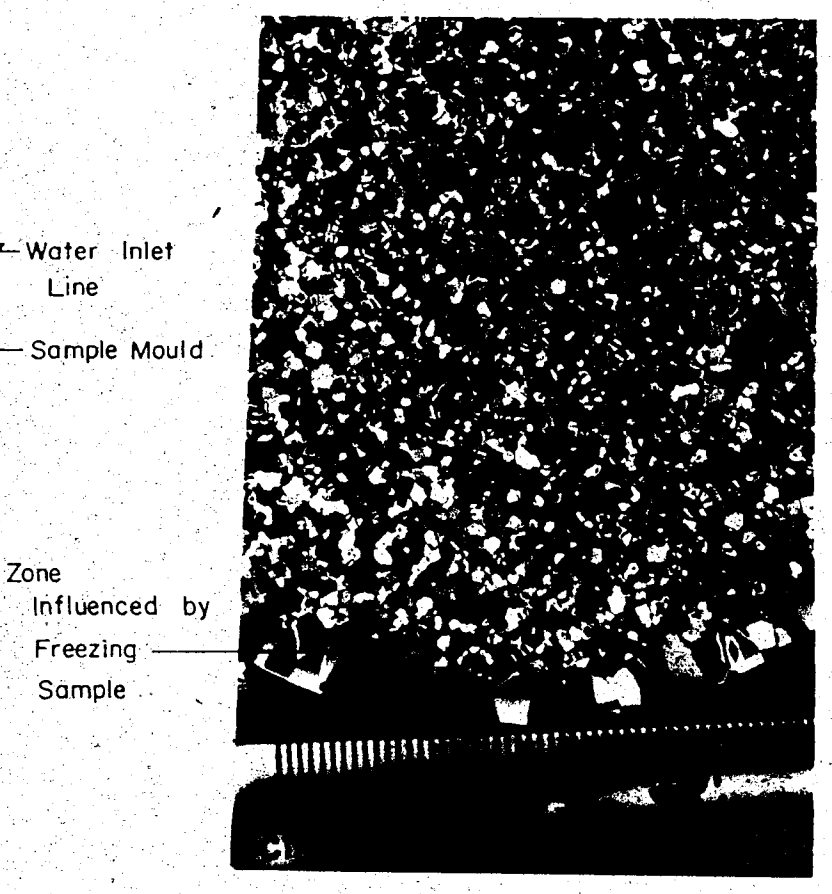

Plate 3.2: Thin section of ice sample region affected during freezing

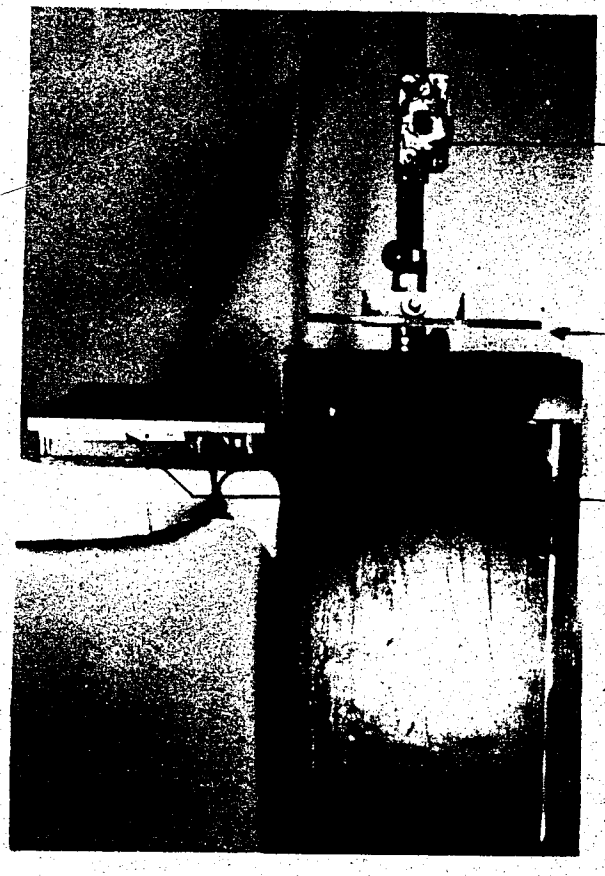

Plate 3.3: Thin section equipment.

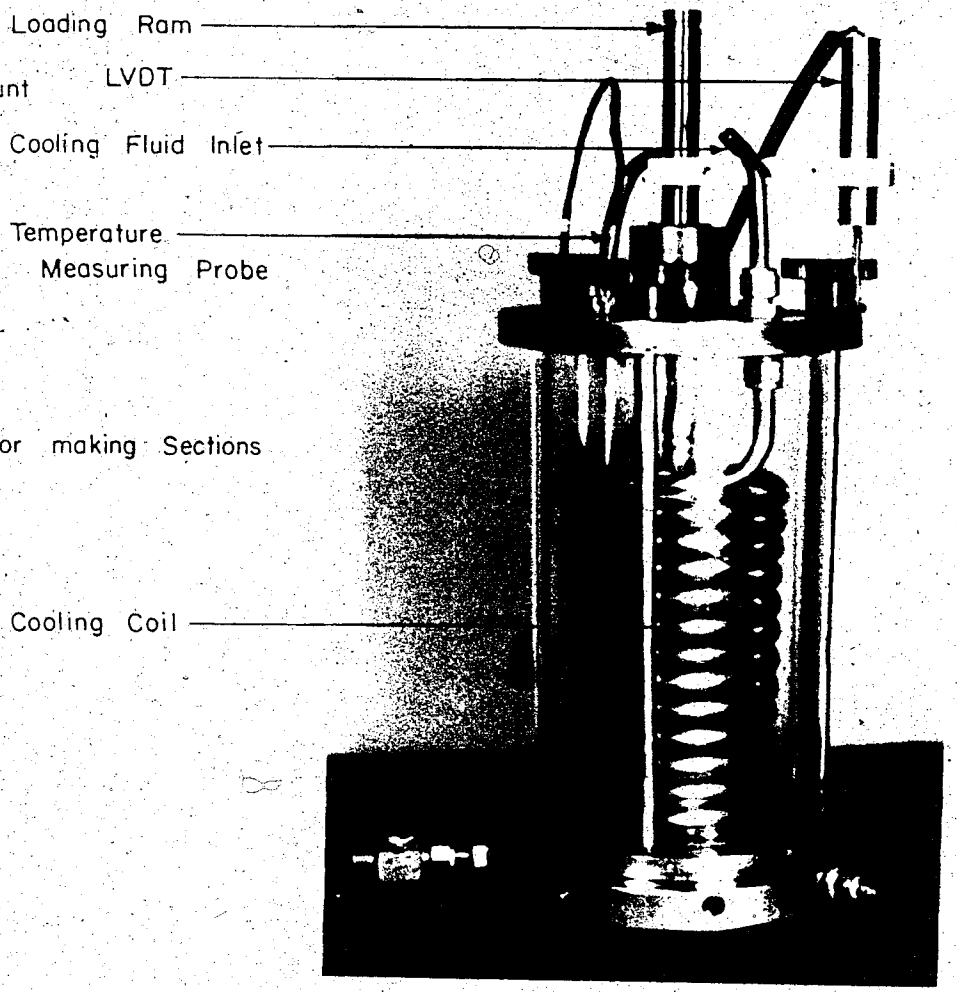

Plate 3.4: Constant displacement rate triaxial cell.

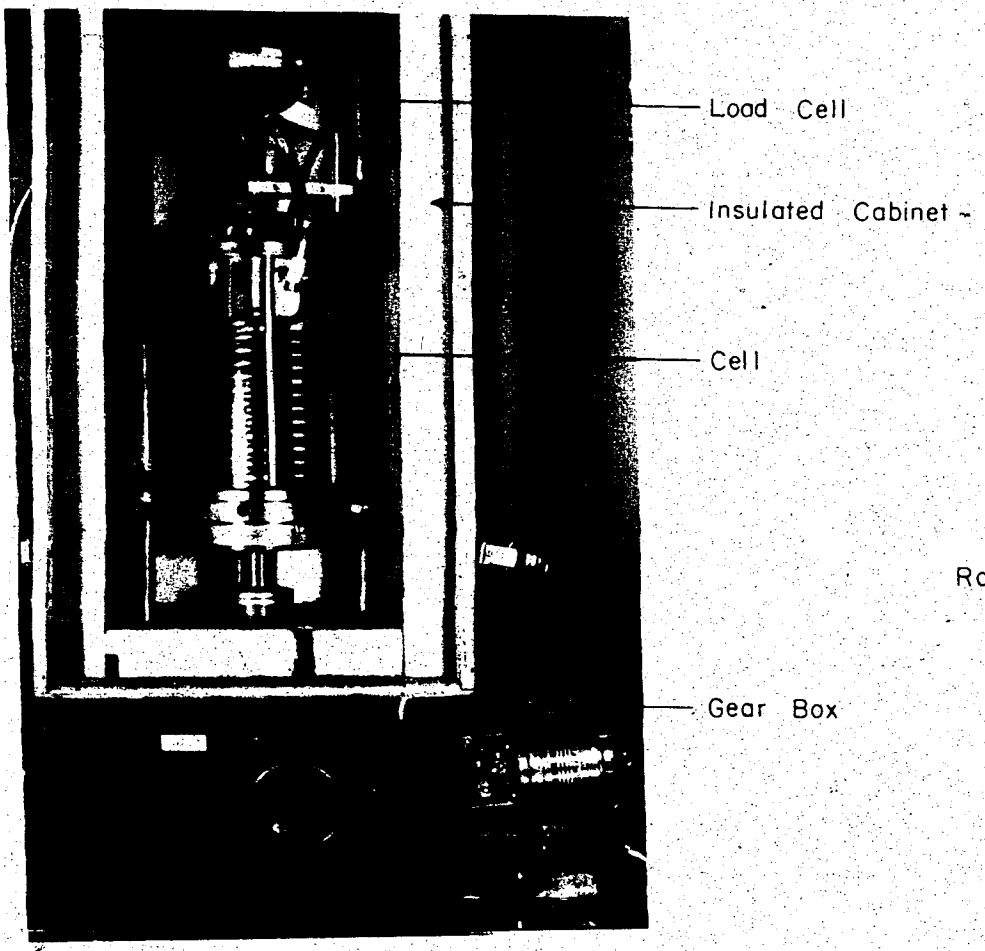

Plate 3.5: Constant displacement rate loading system.

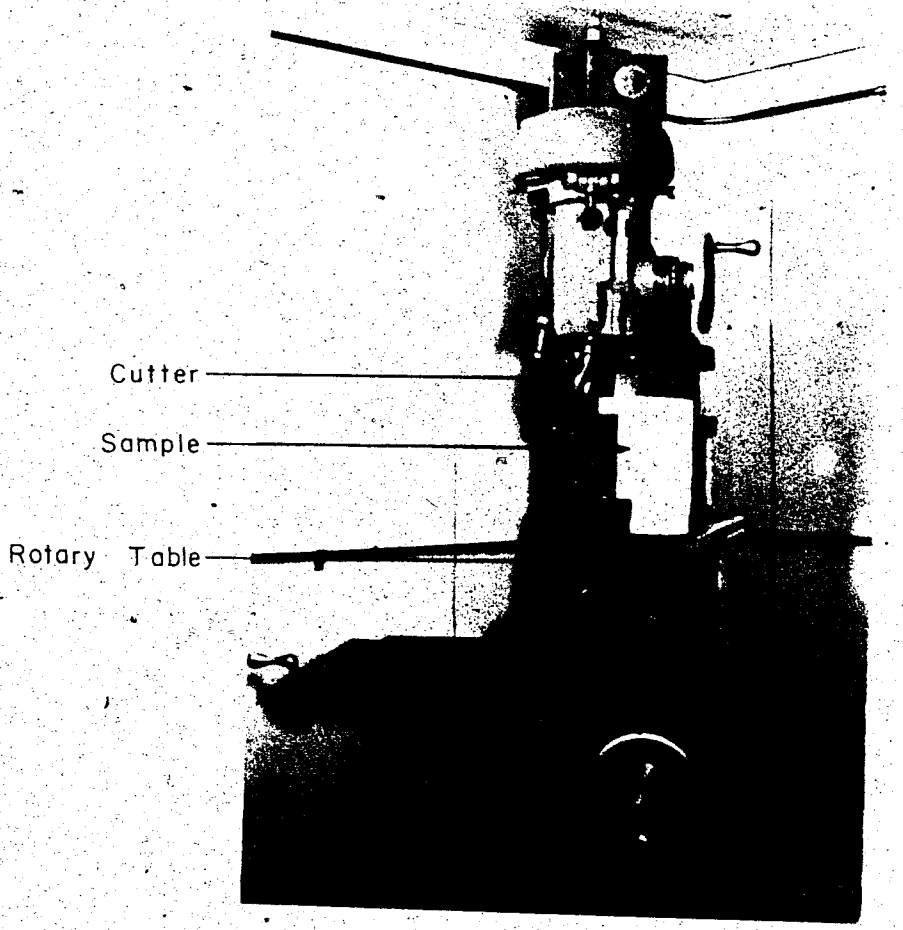

Plate 3.6: Milling machine used to trim ice samples.

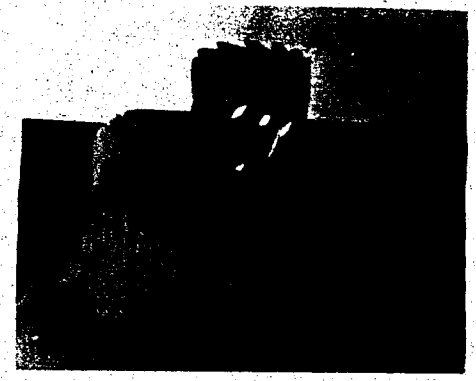

Plate 3.7: Shell mill cutter used to trim ice.

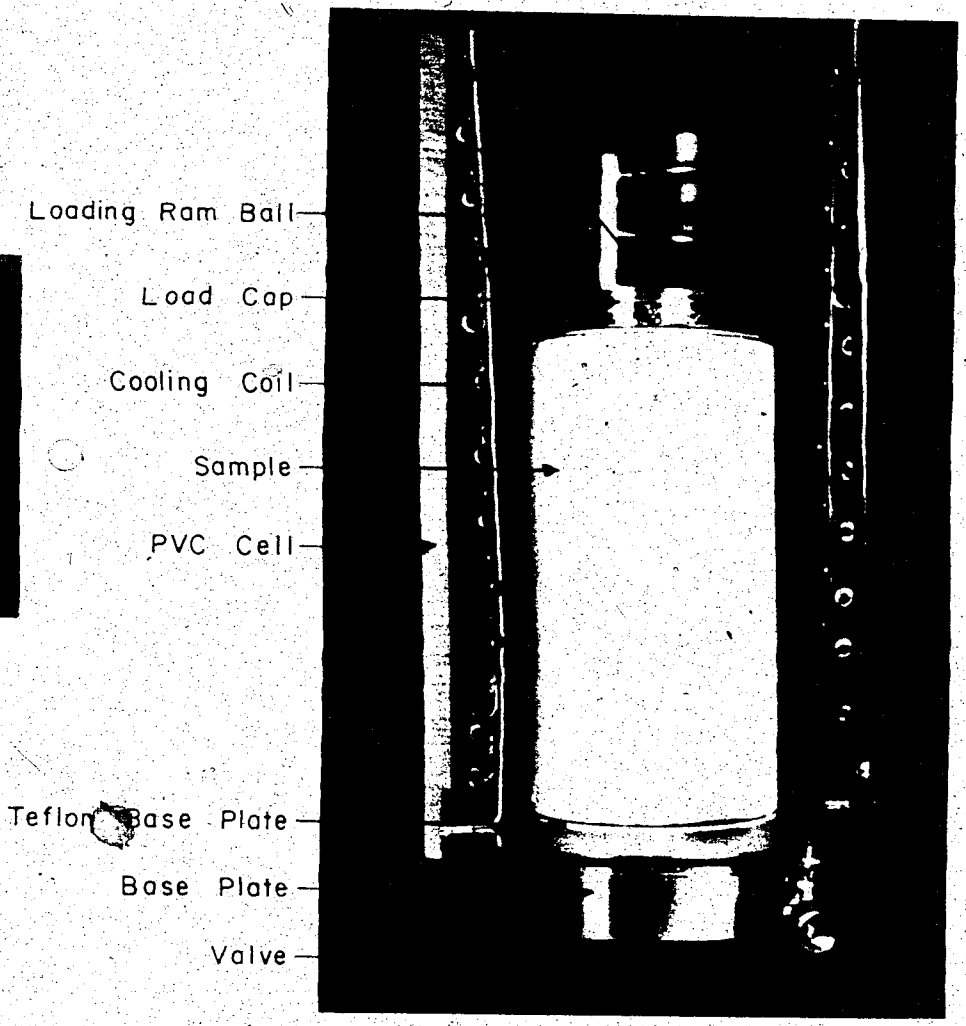

Plate 3.8: Constant stress cell.

Plate 3.9: Constant stress loading system.

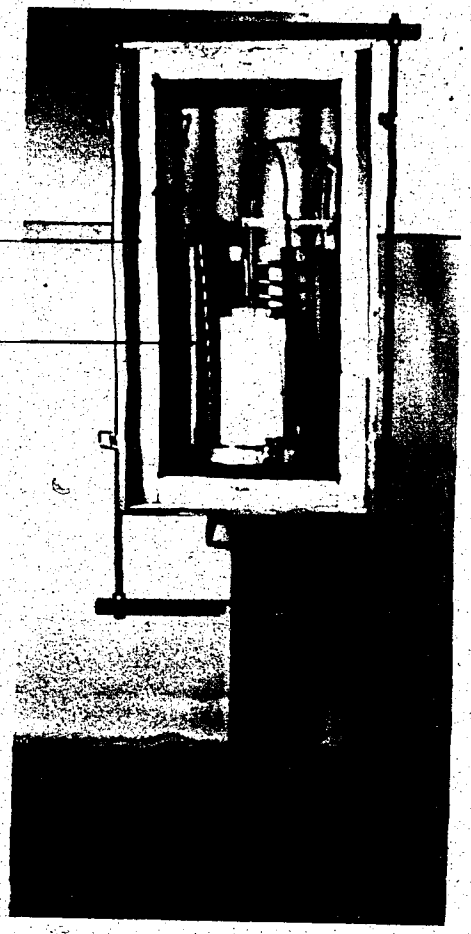

Plate 3.10: Constant stress loading system with cell and sample.

CHAPTER 4

Analysis of Laboratory Creep Data

4.1 Introduction

In this chapter the results of the constant stress and constant strain-rate tests will be analysed. The method used to predict the strain-time law for ice under a constant stress will be discussed, and the power law relationships used in this study will be outlined. The minimum strain-rate determined from each experiment is used to relate the minimum strain-rate with stress to develop a flow law. These data will be compared with test results available in the literature and the influence of various factors on the minimum strain rate will be evaluated. Finally, a method of predicting how long a constant stress creep test must be loaded so that a true minimum strain-rate can be determined from the test results will be given.

4.2 Experimental results of constant stress tests

The creep curves of the six constant stress tests conducted at -1.2°C are contained in Figure 4.1. This Figure is a compilation of the strain-time curves of the constant stress experiment. Figure 4.2 contains the plot of the strain versus time, the temperature versus time, and the strain-rate versus time plot for sample CSGR38. This is a typical set of experimental data determined during the research program. The plots and data for the other

experiments are contained in Appendix A.

The strain-rate versus time plot in Figure 4.2 shows a continual decrease of strain-rate with time, then a levelling out of the strain-rate to a minimum strain-rate value and subsequently an acceleration in the strain-rate during the tertiary portion of creep. The various regions of the typical creep curve have been explained in Section 2.4.2.1.

Not all of the constant stress creep experiments showed a distinct tertiary region in their strain-time curves. Figure 4.1 illustrates that sample CSA34 and CSB35 have not reached a tertiary mode of deformation. The data from experiment CSB35 are presented in Figure 4.3 and it illustrates the levelling off of the strain rate with time under a constant applied stress of 100 kPa. After being loaded for 14,000 hours tertiary creep has not yet been achieved in this experiment.

The data for sample CSA34 contained in Appendix A illustrate that the strain rate has not yet reached a minimum constant value. This plot and the other plots contained in Appendix A do not show a steady-state strain-rate during the experiments. These results are in contrast to those of Glen (1955), Mellor and Testa (1969), and Colbeck (1970) which had a steady-state strain-rate over a portion of the experiment. The strain-rate of each sample of this research program attains a minimum value and then fluctuates about this minimum value. The fluctuation in

strain-rate results because the data points have not been smoothed by averaging or selection of data points. The method used to calculate the strain-rate of each sample will be discussed in Section 4.3.

Figure 4.2 and Figure 4.3 illustrate that time duration for which each sample maintains a minimum strain-rate varies. The time duration is a function of the applied stress during the experiment and is followed by an acceleration in the strain-rate. This minimum strain-rate is not a prolonged steady-state rate in the classical creep theory, because of its short duration.

4.3 Data reduction

As discussed in Chapter 3, all the reduction of the voltage output signal from the experimental measuring equipment was accomplished using a computer program. This program calculates the time, the deformation the sample has undergone, and the temperature measured at the sample mid-height. Using this information, the true strain of the sample is calculated and the strain-time curve plotted. This calculated information is also stored within the computer for use in analysing the experimental data.

The plots contained in Appendix A and Figure 4.2 and Figure 4.3 have each been prepared using this stored data. The strain versus time plot and the temperature versus time plot are produced directly from the data. The strain-rate versus time plot is prepared after the data are analysed to

determine the strain-rate at a particular time. The strain-rate has been calculated using a linear regression analysis through data points at three different times after the experiment began. The points through which the linear regression analysis is fitted are at fixed intervals to reduce some of the fluctuation in the calculated strain-rate.

It must be explained that a reading of the LVDT and thermistor output was taken every hour throughout the experiment. The data file for each experiment was compiled by taking data readings at 10 hour intervals from the master file of hourly readings. The initial portion of the strain-time curve was established using recording intervals of 10 minutes and then 1 hour. This allows the correct shape of the strain-time curve to be established for the short loading times. As the experiment progressed the time interval used in establishing the strain-time curve was increased to 10 hours. This usually occurred after the first 100 hours of loading. This increase in the data sampling interval was justified since very small changes in the output voltage were recorded by the LVDT during this time period.

As mentioned above, the strain-rate was established using a linear regression fit through the data. If the strain-rate was calculated using each data point, a large fluctuation in the strain-rate value resulted. This is a consequence of the fact that during a short time interval

the deformations recorded are so small that it is difficult to separate the sample deformation from the noise of the electronic instrument. Therefore, to have strain-rate calculations which reflect the true behaviour of material, one must ensure that this noise is eliminated for during the data reduction.

The method selected here was to record the data at fixed time intervals and then vary the time interval used to calculate the strain-rate. This reduced the need to select the data used and kept the complete data file available for future analysis. It does require a selection of the proper time interval to be used in calculating the strain-rate for each set of data. This time interval also must vary during the experiment since in the early stage rapid deformation is taking place, and at later times the deformation decreases, therefore, longer time intervals are used in calculating the strain-rate, so that the influence of the recording noise is minimized.

The strain-rate for the experiments was calculated using a data interval of one between time zero and 100 hours. The data interval was five between 100 hours and 1000 hours and at times larger than 1000 hours the data interval was twenty. The program used to calculate the strain-rate data was developed by P.K. Kaiser, in the Department of Civil Engineering to analyse time dependent deformation in rock (Kaiser (1979)).

4.4 Strain-time relationships

In this section the method of determining the strain-time relationship from the test data are outlined. The best fit relationship from this data are given and a comparison of this relationship with the actual recorded data are presented.

To determine initially the most appropriate curve fitting method to use in establishing the strain-time relationship a review of the metal literature and the ice literature was undertaken. The widely used methods of establishing the strain-time relationship for ice have been discussed in Chapter 2. Conway (1967) gives an extensive review of functional relationships used to fit the strain-time curves in metals. He suggests the following four methods as being the most successful for metals:

1. Parabolic representation;
2. Andrade One-third law representation;
3. Logarithmic representation;
4. Hyperbolic Sine representation.

In addition, he discusses both graphical and numerical methods which can be used to fit these relationships to the strain-time data. Each method was tested by fitting the experimental data to the functional relationship and each gave varying results. The fit of each relationship to the data of sample CSA34 is illustrated in the following Figures:

1. Parabolic representation - Figure 4.4;

2. Andrade one-third law representation - Figure 4.5;

3. Logarithmic representation - Figure 4.6;

4. Hyperbolic Sine representation - Figure 4.7.

The fit of each relationship to the experimental data met with varying success. The parabolic relationship does not fit the data at small times but gives a good fit to the data at times greater than 400 hours. The Andrade one-third law gave a very good fit for times less than 350 hours, but did not fit the data at greater time. The logarithmic relationship was applicable only for times up to 100 hours and was not able to fit the data at times greater than 100 hours. The hyperbolic sine relationship gave a good fit to the data as shown in Figure 4.7. This relationship recovered the data for times up to 3000 hours but did not fit the data beyond this time. The lack of fit of a single relationship to the strain-time curve suggests that a different approach than that used in the metal literature was required to establish a strain-time law.

In the ice literature, superposition of the various deformation modes has been advocated. (Voytkovskiy (1960) and Barnes et al. (1971)). Voytkovskiy (1960) suggests that the strain-time law be fitted by adding the initial elastic deformation, the primary creep behaviour and the quasi-steady-state creep behaviour. Barnes et al. (1971) suggests use of the Andrades one-third law to fit the primary region of the strain-time curve. They add the instantaneous elastic deformation and quasi-steady-state

creep deformation to the primary deformation. This relationship for fitting the strain-time curve is called the Cottrell-Aytekin relationship and has the form:

$$e = e^0 + x \cdot t^{0 \cdot 33} + [de/dt]s \cdot t \qquad (4.1)$$

where

e^0 = instantaneous strain

x = constant.

[de/dt]s = true secondary creep rate.

t = time

This relationship may be rewritten in a more generalized form as follows:

$$e = e^0 + A(t+1)\underline{m} + [de/dt](min)(t+1) \qquad (4.2)$$

where

e^0 = instantaneous strain

A = derived parameter from data

$\underline{m}$ = exponent which is a derived parameter from the data

[de/de](min) = minimum strain-rate

t = time

The relationship was generalized, so that the constants A and m could be determined from the actual laboratory data and not taken from the literature. The generalization was necessary since the Andrade one-third law did not fit the

laboratory data as shown in Figure 4.4. The time from Equation 4.1 was changed to (t+1) to allow examination of the data on the logarithmic plot at time equal to zero. This generalization to the Cottrell-Aytekin relation was proposed by Roggensack (1977), but without the (t+1) term in the relationship.

The relationship given by Equation 4.2 requires good data for the instantaneous elastic strain. As mentioned, under the discussion of test procedure in Section 3.5.4 no attempt was made to measure the initial elastic strain for each experiment. Since the initial elastic strains were not determined, experimental data will be analysed using the experimental strain-rate. The differential form of Equation 4.2 is:

$$de/dt = A \bullet m\ (t+1)\underline{x} + [de/dt](min) \qquad (4.3)$$

which may be rewritten as

$$de/dt = B(t+1)\underline{x} + [de/dt](min) \qquad (4.4)$$

where

$$B = A \bullet m$$

$$x = m-1$$

If Equation 4.4 is rearranged, and the logarithm taken of both sides:

$$\log.(de/dt-[de/dt](min))=\log. B + x \log.(t+1) \qquad (4.5)$$

The constants B and x may be determined from a plot of the logarithm (de/dt-[de/dt](min)) versus logarithm (t+1). This approach was used to develop the strain-time relationship.

4.4.1 Determination of parameters for strain-time relationship

The strain-rates as determined in Section 4.3 were used to prepare the strain-rate versus time plot used to determine the parameters of Equation 4.4. Figure 4.8 shows the plot of the logarithm (de/dt - [de/dt](min)) versus logarithm (t+1) for sample CSB34. The constants A and m are given in the Figure. The plots of the data from the other test samples which were used to determine the constants A and m are contained in Appendix A. The constants determined from the Figures in Appendix A are summarized in Table 4.1 along with other important experimental information.

To determine if the constants in Equation 4.2 are a function of stress, both the constants A and m were plotted versus stress. Their variation with stress is shown in Figure 4.9 and Figure 4.10. A line fitted to the data in Figure 4.9 gives the following equation for the influence of stress on the constant m:

$$m = 0.32 - 0.00033 \bullet \sigma \qquad (4.6)$$

where

σ = axial stress (kPa.)

Equation 4.6 demonstrates that Andrade one-third law is a close approximation to the laboratory data but will not fit the data over the complete stress range of these experiments.

The variation of the parameter A with stress is illustrated in Figure 4.10. It illustrates that at the temperature of these experiments and over the applied stress range, A is dependent on the applied stress. In Figure 4.10 a large variation in the A parameter is shown at a stress of 300 kPa. To determine the relationship of the A parameter with stress the value of the parameters determined from sample CSD39 and sample CSE42 at a stress of 300 kPa have been averaged. The relationship for A in terms of applied stress is:

$$A = 0.0021 \bullet \sigma \qquad (4.7)$$

where

σ = axial stress (kPa).

Equation 4.6 and 4.7 show that both m and A are dependent on the applied stress. Insufficient data are available to determine the temperature variation of each parameter.

Two experiments at -3.8°C with applied stresses of 250 kPa and 300 kPa were conducted. The parameters determined

from the plots of strain-rate difference versus time at -1.0°C are contained in Table 4.2. The data in Table 4.2 illustrates that at a given stress level the m parameter is independent of the temperature for the limited range. The information on the A parameter is insufficient to draw a conclusion concerning any temperature influence. However, it is expected that the A parameter would decrease with decreasing temperature to explain the findings of a decrease in deformation associated with a decrease in temperature.

The above analysis of the laboratory data gives a strain-time relation as follows:

$$e = e^{o} + [de/dt](min) \bullet (t+1) + A \bullet (t+1)^{\underline{m}} \qquad (4.8)$$

where

e= strain (%)

e^{o}= instantaneous strain (%)

[de/dt](min) = strain-rate (%/hour).

δ = axial stress (kPa.).

t = time (hours).

m is given by Equation 4.6.

A is given by Equation 4.7.

The minimum strain-rate [de/dt](min) in Equation 4.8 is a function of stress, temperature, and ice crystal size as outlined in Chapter 2.

The relationship between the minimum strain-rate and the constant applied stress was evaluated using a linear

regression analysis on the data. This analysis provided the best fit straight line through the experimental results when plotted in a logarithm strain-rate versus logarithm stress plot. The general form of the flow law relationship has been discussed in Section 2.3.3.1 and given in Equation 2.22. The best fit flow law through the present data is:

$$[de/dt](min) = 0.001 \left(\sigma/266.5 \right)^{2 \bullet 55} \qquad (4.9)$$

where

$[de/dt](min)$ = strain-rate (%/hour)

σ = axial stress (KPa.).

Only the data for the constant applied axial stress experiments have been used to establish Equation 4.9. The data used to obtain this relationship are given in Table 4.3. Figure 4.11 is a plot of the experimental results and has the best fit line plotted through the data points. Figure 4.11 shows that Equation 4.9 predicts the minimum strain-rate in terms of stress accurately for these experimental data over the range of applied stress.

When the relationship between minimum strain-rate and stress given by Equation 4.9 is substituted into Equation 4.8 the following strain-time relationship is obtained:

$$e = e^{o} + 0.001(\sigma/266.5)^{2 \bullet 55}(t+1) + A \bullet (t+1)^{\underline{m}} \qquad (4.10)$$

where each symbol has the same meaning as given in Equations

4.8 and 4.9.

The usefulness of Equation 4.10 in predicting the strain-time curve of this experimental data must be examined. As mentioned earlier, the initial elastic deformation of the sample was not measured.

To evaluate the importance of the initial elastic strain at these low applied stresses, the magnitude of the strain will be evaluated. To calculate the instantaneous elastic strain in each sample, a simple elastic analysis was used. The analysis consisted of calculating the strains associated with a uniform stress condition within the sample. To evaluate the strain associated with each applied stress the appropriate Young's Modulus of polycrystalline ice is required. Michel (1979) presents the dynamic Young's Modulus of T1 ice as 8.92×10^6 kPa. The dynamic value of Young's Modulus is an appropriate value to use since it does not vary in the high frequency range (Figure 2.5). The instantaneous elastic strains using this analysis are .0011% and .0033% strain at applied stresses of 100 kPa and 300 kPa respectively. These strains are very small compared to the measured strains. This demonstrates that the elastic strain can be neglected when comparing the laboratory strain-time data and the strain-time curve resulting from Equation 4.10.

The comparisons of the predicted and actual strain-time plots are shown in Figures 4.13 to 4.16. Each figure shows the comparison between Equation 4.10 and the measured experimental data recorded for different applied axial

stresses. The solid line is the strain-time plot of the experimental data and the dashed line the strain time plot given by Equation 4.10. In Figure 4.13 it is seen that Equation 4.10 overpredicts the strain-time curve of sample CSB35 but closely agrees with the curve of sample CSA34 at an applied stress of 100 kPa. Figure 4.14 shows excellent agreement between the data of sample CSGR38 and Equation 4.10 at an applied stress of 150 kPa. The strain-time curve of sample CSC37 is overpredicted slightly by the strain-time relationship, as is shown on Figure 4.15. The strain-time curves, under an applied stress of 300 kPa, have a agreement which is similar to the curves of the 100 kPa experiments. This is given in Figure 4.16.

It is seen that the strain-time relationship established using the laboratory data fits the actual laboratory data well over the complete time range of each experiment. This analysis shows that the principle of superposition and a simple data fitting technique yields good agreement between the actual strain-time plots and the experimental obtained strain-time relationship.

Equation 4.10 shows that the Andrade one-third law does not recover the strain-time curves of this data over the complete applied stress range. This is a result of the fact that the exponent m in Equation 4.10 is a function of the stress applied during the experiment. Andrade's law does not account for this stress dependence of the exponent applied to the time.

Using the principle of superposition and a simple curve fitting method suggested by Roggensack (1977) the strain-time fit of these laboratory data has been developed. The data from this research program show that both the A and m parameters in the Equation 4.2 are dependent on the applied stress. The m parameter is independent of temperature but the data supporting this are very limited. The A parameter appears to be temperature dependent.

4.5 Flow law determination

4.5.1 Introduction

In this section the flow law established from the experimental results of both the constant stress experiments and the constant strain-rate experiments will be presented. The correspondence between the results of these two experimental procedures are discussed. The flow law of the experimental data will be presented and the influencing factors on the flow law outlined. A comparison of the experimental flow law with the experimental data of Glen (1955), Steinemann (1958), and Barnes et al. (1971) is contained in Section 4.6.3.1. This comparison will be used to establish the influence of sample size on the flow law for ice.

4.5.2 Correspondence of constant stress and constant strain-rate experimental data

During the experimental program, samples of ice were subjected to constant applied stress and to constant strain-rate loading conditions. These experiments were conducted at a temperature of -1.2°C. Each experiment was conducted under a sufficiently low applied stress or strain-rate as to be in the ductile range of ice deformation (Figure 4.17), thus, similar physical properties of the ice must be measured from each test.

The procedure used to conduct each experiment is given in Section 3.3.4 and Section 3.5.4. The important question is at what point on a typical constant stress creep test curve and on a constant strain rate curve are the same material properties being measured. Hawkes and Mellor (1972), Michel (1978), and Mellor (1979) suggest that the maximum stress from a constant strain-rate experiment corresponds to the inflection point on a typical constant stress creep curve (Figure 2.4). The location of these points on the two typical curves has been discussed in Chapter 2. On each curve, the suggested point is the maximum of the (σ/[de/dt](min)) ratio. Each point on the creep curve, therefore, measures the material behaviour under a similar physical condition although the path to achieve this condition is different.

The inflection point on a typical constant stress creep curve corresponds to the minimum strain-rate during this experiment. Beyond the inflection point the ice crystals within the sample begin to recrystallize and as a result the

strain-rate accelerates (Glen (1955)). Thus the physical characteristics of the ice crystals within the sample begin to change beyond the inflection point, and the overall properties of the ice sample also change. The crystals within a constant strain-rate sample also undergo a change in crystal size and orientation of the optic c-axis beyond the yield point. The change in the crystal structure within the sample is evident from the stress time curve in Figure 4.18. The resistance of the ice decreases beyond the yield point and gradually levels out at a stress lower than the yield stress. The weakening of the ice in the constant strain-rate experiment results from cracking and/or recrystallization of the individual ice crystals within the sample.

The step-by-step change in the crystal characteristic during the various portions of the strain-time curve or stress-strain curve has not been studied extensively. Glen (1955), Steinemann (1958), Rigsby (1960) and Mellor and Testa (1969b) have documented this recrystallization of ice under load but it has not been studied at various times during a load history. Correspondence between the two types of experiments therefore exists at the yield point and at the inflection point, but beyond the inflection point the correspondence is uncertain.

Mellor (1979) speculates that at strains of about 10% the constant strain-rate test and the constant stress test again have a direct correspondence between the material

properties being measured. At this strain, the constant strain-rate curve shows a leveling off of the stress time curve at a constant stress value. This is again illustrated in Figure 4.18. The results of constant stress tests carried out to large strains, shows that the sample approaches a constant strain-rate under the applied stress (Steinemann (1958) and Mellor (1979)). At this point in a constant stress experiment, the ratio of ($\delta/[de/dt]$) would have the lowest value beyond the inflection point and would correspond to the constant strain-rate test conducted to large strains. This correspondence has not been checked experimentally because of the difficulty in taking a constant stress experiment to large strains and the long time involved in conducting these experiments.

4.5.3 Flow law determined from constant stress experiments

The experimental flow law determined from the constant stress uniaxial compression tests has been discussed in Section 4.4. The experimental data are tabulated in Table 4.3 and the logarithm strain-rate versus logarithm stress plot presented in Figure 4.11. The minimum strain-rate determined in each experiment has been plotted against the axial applied stress to determine this flow law. The flow law from the constant stress experiments is given by Equation 4.9 and is repeated below as:

$$[de/dt](min) = 0.001 \left(\delta/266.5 \right)^{2.55} \qquad (4.9)$$

where

$[de/dt]_{(min)}$ = strain-rate (%/hr.)

δ = axial stress (kPa.)

The small variation in the temperature among experiments has not been accounted for in determining the above flow law. The large amount of equipment and time required to conduct the experiments were the reasons that the influence of the temperature was not examined extensively. All the uniaxial compression tests were conducted at a temperature maintained close to -1.2°C throughout the loading. This temperature was selected because it was close to that used by Glen (1955), Steinemann (1958), and Barnes et al. (1971). The method used to maintain temperature control has been discussed in Section 3.3 and Section 3.4.

4.5.4 Flow law determined from constant strain-rate experiments

The flow law from the constant strain-rate experiments was determined using the average strain-rate between the beginning of the experiment and the peak of the stress-strain curve. The stress used is the stress associated with the peak on the stress-time curve. Figure 4.18 shows a typical plot of a constant strain-rate experiment. The plots of the other constant strain experiments conducted during this research program are

contained in Appendix A.

Table 4.4 is a summary of the pertinent information from each of the constant strain-rate experiments. Figure 4.12 shows the logarithm strain-rate versus logarithm stress plot and the best fit relationship through the data points. The best fit relationship was determined using the method of least squares to fit the data points from Table 4.4. The relationship developed using the constant strain-rate data is:

$$[de/dt](min) = 0.001 \left(\sigma / 159.3 \right)^{2.47} \qquad (4.11)$$

where

$[de/dt](min)$ = strain-rate (%/hr.)

σ = applied stress (kPa.)

It is noted that the two test methods do not give identical flow laws. The constant strain-rate data predicts that the material will deform at a higher rate than predicted by the constant stress data. One would immediately suggest that the difference is due to the difference in the experimental method. However, the correspondence of the two experiments has been discussed in Section 4.5.2. which suggests that some other influence is contributing to the difference in the flow laws. Before discussing this influence, the flow law for the combined results from the constant strain-rate and constant stress data will be presented.

4.6 Flow law determined from combined data of constant strain-rate and constant stress tests

The data used in determining the combined flow law are contained in Table 4.3 and Table 4.4. Figure 4.19 contains the plot of the combined data with the best fit line through the data points. Again the curve fit has been accomplished using the method of least squares and the relationship for the resulting flow law is:

$$[de/dt](min) = 0.001 \left(\sigma/235.5 \right)^{3.14} \qquad (4.12)$$

where

$[de/dt](min)$ = strain-rate (%/hr.)

σ = applied stress (kPa.)

This is the flow law for the ice determined in this research if one does not separate the data as in Sections 4.5.3 and Section 4.5.4. This flow law applies over the stress range 100 kPa to 1200 kPa.

4.6.1 Factors influencing the flow law of ice

The review of plastic deformation of polycrystalline ice in Chapter 2 gave the following factors as influencing the flow law of ice:

1. Temperature;
2. Stress range;
3. Crystal size;
4. Crystal orientation;

5. Ice density.

The summary of the experimental data contained in Table 3.1 shows that the variation in ice crystal size and ice density is small between samples used in this research. The test temperature in all of the experiments was within ±0.2°C of -1.2°C. Each of the samples were prepared using the standard method presented in Section 3.1.3. hence no preferred crystal orientation should exist. Only two possibilities remain to explain the difference in the flow law: first, the different experiments are not comparable and second, some other factor influences the flow law of ice.

The correspondence between the two methods of conducting the test has been discussed in Section 4.5.2 and by Hawkes and Mellor (1972) and Mellor (1979). They presented data which is reproduced in Figure 4.17 that shows the smooth transition from the constant stress data to the constant strain-rate data. This smooth transition would not occur if the method of testing and the interpretation of the results of each of the experiments were different. The experimental data will be examined to determine if some other factor influences the flow law.

4.6.2 Grain size ratio

In Chapter 2 the influence of the ice crystal size on the minimum strain-rate and on the yield stress of ice was reviewed.

Muguruma (1969) showed that the yield stress during a

constant strain rate experiment varied inversely with the square of the average grain diameter. His relationship follows:

$$\delta(max) = 0.75 + 0.31\, d^{-0.5} \qquad (4.13)$$

where

$\delta(max)$ = yield stress (kg/cm^2)

d = grain diameter (mm)

This illustrates that as the grain diameter decreases the yield stress increases. That is the finer the ice crystal the harder the material is to deform in the ductile range of its behaviour. Muguruma tested columnar grained ice to establish this behaviour.

Baker (1978) gave a relationship between the steady-state strain-rate and grain size as follows:

$$[de/dt] = A \cdot d^{2.5} \qquad (4.14)$$

where

$[de/dt]$ = steady-state strain-rate (yr^{-1})

d = average grain diameter (mm)

A = parameter which is function of stress and temperature

Equation 4.14 predicts that the steady-state strain-rate decreases with decreasing grain size. Baker (1978) also found that as the grain size decreased below a certain

limiting size the strain-rate began to increase. This behaviour is illustrated in Figure 2.15. He has limited experimental evidence to support the increase in strain-rate below a certain grain diameter. These data are suspect for the following reasons:

1. He has only four experiments on pure ice;
2. The loading times of the experiment were so short it is questionable if these experiments attained a steady-state strain rate similar to the other experiments.

The short loading period may account for the increase in strain-rate instead of the decreasing crystal size.

Muguruma (1969) and Baker (1978) both show an increase in resistance of the ice to a decrease in grain size. These authors did not, however, vary the sample size during their experiments. Therefore their observations may be due not only to the individual crystal size, but also to a size effect which relates the crystal size to the test sample size.

In this research, each sample had about the same size of ice crystal, but a difference in the actual size of the sample tested existed. The constant strain-rate samples averaged about 70 mm in diameter whereas the constant stress sample averaged between 110 and 120 mm in diameter. It is suggested that the difference in the minimum strain-rate observed between the two sets of experimental data are due to a size effect and are not associated with a difference in

the experimental procedure.

To illustrate, a new parameter termed the grain size ratio (GSR) is defined as:

$$GSR = (Dc/Ds) \qquad (4.15)$$

where

Dc = average crystal diameter (mm)

Ds = average sample diameter (mm)

The GSR is a non-dimensional ratio of average crystal diameter to the sample diameter. Now using the grain size ratio, the data of the constant strain-rate experiments and the constant stress experiments will be analysed to evaluate any influence of the GSR on the flow law.

4.6.3 Influence of grain size ratio on minimum strain-rate

In order to assess the influence of the size effect on the minimum strain-rate, the influence of stress and temperature on the individual experimental data must be removed. As mentioned, the variation in temperature between the experiments was not studied extensively in this project. The laboratory data does not show a large influence of temperature over the stress range of these experiments as is illustrated in Table 4.1 and Table 4.2. The constant stress samples CSA34 and CSB35 do not have a difference in the minimum strain-rate at the same stress although the test temperatures differ by 0.2°C.

The minimum strain-rate as a function of the applied stress for the constant stress experiment is given by Equation 4.9 and for the constant strain-rate tests is given by Equation 4.11. Therefore, to study the influence of the grain size ratio, these two equations are used to correct the strain rate of each experiment to the value which corresponds to an applied stress of 100 kPa. The correction applied to each set of test data follows:

$$[de/dt](100)=(100/\sigma)^{n}\bullet[de/dt](\sigma) \qquad (4.16)$$

where

$[de/dt](100)$ = equivalent strain-rate at 100 kPa

n = 2.47 (constant strain-rate)

n = 2.55 (constant stress)

$[de/dt](\sigma)$ = strain-rate from test (%/hr)

σ = axial stress from test (kPa)

The normalized experimental strain-rate data and the grain size ratio are contained in Table 4.6. Figure 4.20 contains a plot of the data from Table 4.6 corrected to a stress of 100kPa. This Figure shows the variation of the normalized strain-rate with grain size ratio at a constant stress of 100 kPa. The best fit line through the data from Figure 4.20 gives the following relationship:

$$[de/dt]/[de/dt]c = B\ (GSR)^{1\bullet71} \qquad (4.17)$$

where

$[de/dt]c = .001$ (%/hr)

B = 446.4 when stress = 100 kPa

GSR = grain size ratio

Equation 4.17 shows the strong influence which the GSR has on the normalized strain rate. With a decrease in GSR the normalized strain-rate decreases at a constant stress of 100 kPa. This is an important finding, since it predicts that the normalized strain-rate is influenced by a relative crystal size and not just the crystal size.

Equation 4.17 shows that experiments conducted with small diameter samples with a constant grain size will result in a normalized strain-rate which is faster than strain-rates obtained from experiments conducted using a larger sample but the same crystal size. Extrapolating this to the field condition, suggest that ice in the field will be more resistant to deformation under a given stress than predicted from laboratory experiments because the GSR in the field is usually very small. This is an important conclusion, and would suggest that increasing the size of the loaded area of polycrystalline ice increases its resistance to plastic deformation even if the applied stress is maintained constant.

Now, to determine the flow law for ice, the data must be compared at a constant grain size ratio. This can be accomplished by correcting the strain-rate data at a constant stress of 100 kPa to a constant grain size ratio at

this stress level. This correction is made by using Equation 4.17 to set up a ratio of strain-rate and grain size ratio at a constant stress as follows:

$$[de/dt](d\text{-}grs.)/[de/dt](t\text{-}grs) = zz$$

$$zz = (d.grs/t.grs)^{1.71} \qquad (4.18)$$

where

$[de/dt](d\text{-}gsr)$ = strain-rate at desired GSR(%/hr)

$[de/dt](t\text{-}gsr)$ = strain-rate at test GSR (%/hr)

d-gsr = desired GSR

t-gsr = test GSR

The experimental constant stress and constant strain-rate data have been corrected to a grain size ratios 0.0075, 0.015 and 0.030.

At this point for each experiment the minimum strain-rate is corrected to a constant grain size ratio at the normalized stress of 100 kPa. In order to establish the flow law from these correcterd data at a constant grain size ratio the minimum strain-rate for the actual applied stress in each experiment is calculated using Equation 4.16. The stress and strain-rate data for both the constant strain-rate and the constant stress experiments at the grain size ratios are contained in Table 4.6. The corrected data are plotted in Figure 4.22 along with the uncorrected experimental data to illustrate that this correction procedure improves the comparison between the data. The

improved comparison is illustrated by the common proof stress of the data when analysed separately or together.

The data corrected to a constant grain size ratio in Figure 4.22 show more consistency between the data of the two experimental methods. The experimental strain-rates of the constant stress experiments have increased in magnitude as the correction for the grain size ratio is applied. Thus the data points in the low stress region of Figure 4.22 have been shifted upward. This results since all the constant stress experiments had low grain size ratio and the data in Figure 4.22 is being compared at a grain size ratio equal to 0.030 which shifts this low GSR da[illegible] upward.

The method of least squares again has been used to fit a straight line through the corrected data from the logarithm strain-rate and logarithm stress plot. This fit gives the following relationship for the data contained in Figure 4.22:

$$[de/dt](min) = .001\ (\sigma/158.8)^{2.53} \qquad (4.19)$$

where

$[de/dt](min)$ = minimum strain-rate (%/hr.)

σ = axial stress (kPa.)

Comparison of Equation 4.9 and Equation 4.19 gives the exponent of each equation as about 2.5. The proof stress in Equation 4.19 is 158.8 kPa and in Equation 4.9 is 266.5 kPa. The difference in the proof stress of each results, because

the data used to obtain each equation was compared at different grain size ratios. This illustrates that the proof stress is a function of the grain size ratio.

The influence of the grain size ratio on the proof stress and the exponent n will be examined. These two quantities have been defined in Section 2.4.3.1. To study this influence the data corrected to various grain size ratios and the flow laws resulting from the data must be compared.

The strain-rate data corrected to various grain size ratios are contained in Table 4.6. The method of least squares has been fitted through the logarithm of the stress and logarithm of the normalized strain-rate for this data at each different value of the grain size ratio. The values of the proof stress (δc) and the exponent (n) for the different grain size ratios are tabulated in Table 4.7. The data in Table 4.7 illustrates that the exponent n is independent of the grain size ratio, but that the proof stress (δc) is dependent on the grain size ratio. The proof stress versus the grain size ratio is plotted in Figure 4.21. This figure shows that for the experimental data the relationship between the grain size ratio and the proof stress is best expressed using the following power law relationship:

$$\delta c = 9.04/(GSR)^{0.68} \qquad (4.20)$$

where

δc = proof stress (kPa.)

GSR = grain size ratio (mm/mm)

With this relationship between proof stress and grain size ratio, Equation 4.20 can be substituted into Equation 4.19. Taking the value of the exponent n as 2.52, the minimum strain-rate can be written in terms of the applied stress and grain size ratio. This gives the following expression for the flow law:

$$[de/dt](min) = .001 \left[\sigma \cdot (GRS)^{0.68}/9.0 \right]^{2.52} \qquad (4.21)$$

where

[de/dt](min) = strain-rate (%/hr.)

GSR = grain size ratio

σ = axial stress (kPa.)

Equation 4.21 shows the important influence that the grain size ratio has on the flow law of ice, as found during this research.

4.6.3.1 Comparison of laboratory data and data from literature

In this section the laboratory creep data from this research project is compared to the laboratory creep data of Glen (1955), Steinemann (1958) and Barnes et al. (1971). The test results used are those presented by each author at temperatures between -1.5°C and -2.0°C. The data from each of the authors have been tabulated in Table 4.8.

The data from Table 4.8 are plotted in Figure 4.23. The experimental results of this research program which are uncorrected for the grain size ratio effect from Table 4.6 are also plotted in Figure 4.23. The data show that the experiments conducted at -1.2°C without being corrected for the grain size ratio in the stress range 100 to 300 kPa have the lowest minimum strain-rate. The strain-rates are between two and five times slower than those given by Glen (1955) and about three times slower than the strain-rate of Steinemann (1958). The only difference between the tests is the sample size. In this research program the samples have diameters which are between three and four times larger than those of the above two authors. This difference in the sample size is reflected in the grain size ratio for each test specimen. The grain size ratio of each sample can be compared using the data in Table 4.6 and Table 4.8.

The difference in the experimental strain-rate data are attributed to the grain size ratio difference between the various samples used. To check this influence the data in Table 4.6 have been corrected to a standard grain size ratio which is representative of Glen (1955), Steinemann (1958), and Barnes et al. (1971). The method outlined in Section 4.6.3 has been used. The data are given in Table 4.6 and the common grain size ratio of 0.030 has been used.

The data from Table 4.8 and the corrected data from Table 4.6 have been replotted in Figure 4.24. The data plotted in this figure are all at approximately the same

grain size ratio and thus are comparable. In Figure 4.24 the data are consistent with the expected behaviour of the material. The experiments at the colder temperature have a lower strain-rate at each given stress level. This shows that a study of the influence of test temperature on the minimum strain-rate is important. The influence of temperature on the flow law of ice has been discussed in Chapter 2. Before considering this influence on the minimum strain rate, the flow law of the combined data contained in Figure 4.24, without temperature corrections will be analysed to show that the temperature influence on the data is small. This influence will be observed by comparing the data before and after the correction is applied.

The method of least squares has been fitted through the data of Figure 4.24, yields:

$$[de/dt](min) = .001\ (\sigma/138.7)^{2.78} \qquad (4.22)$$

where

$[de/dt](min)$ = strain-rate (%/hr.)

σ = axial stress (kPa.)

The exponent of the flow law relationship is 2.78. This value of the exponent is slightly lower than 3.0 which is gaining acceptance in ice mechanics literature. It must again be pointed out that the temperature influence on the minimum creep rate has not been accounted for in Equation 4.22. This will now be considered.

4.6.3.2 Temperature influence on minimum creep rate

In discussing the method used to represent the influence of temperature on the quasi-steady-state strain-rate, it was mentioned that a preference for the Arrhenius equation has evolved in the study of ice deformation. This relationship has been used because most authors have described the creep of ice in terms of a thermally activated process. Mellor and Testa (1969), Jones and Burnet (1978), and Mellor (1979) found that this relationship is valid in ice monocrystals between 0°C and -60°C. However it is not valid at temperatures above -10°C. To describe the creep of polycrystalline ice (Mellor and Testa (1969), Barnes et al. (1971) and Mellor (1979)). Voytkovskiy (1960) used the following relation, first introduced by Royen, to give the variation of strain-rate with temperature:

$$[de/dt](min) \text{ proportional to } 1/(1+T) \qquad (4.23)$$

where

[de/dt](min) = strain-rate (%/hr)

T = number of degrees below 0°C.

Equation 4.23 has been fitted to the limited test data at various temperatures from this research. Only the constant stress experimental data has been used to study the temperature influence. These data have been corrected to a grain size ratio of 0.0075 and are contained in Table 4.9.

It has been plotted in Figure 4.25. The following relationship gives a good fit through the data:

$$[de/dt](min)/(.001(\delta/158.8)^{2\bullet53}) = zz$$

$$zz = .025 + 0.5(1/1+T) \qquad (4.24)$$

where

$[de/dt](min)$ = strain-rate (%/hour)

δ = axial stress (kPa)

T = number of degrees below 0°C.

Equation 4.24 is valid for the experimental data between the temperature of -0.7°C and -3.8°C. In order to establish a relationship which is valid for the complete temperature range of 0°C to -10°C a large number of experiments would be required at various temperatures. This was not undertaken since a study of the temperature influence on the flow law of ice was not part of this research program.

The influence of Equation 4.24 on the data contained in Figure 4.24 was also examined. This data was corrected using the following equation for the temperature influence:

$$[de/dt](min)\text{-}2.0°C = zz$$

$$zz = (0.192)/[0.025 + 0.5/(1/1+T)][de/dt](min)T \qquad (4.25)$$

where

$[de/dt](min)$-2.0°C = strain-rate at -2°C (%/hour)

T = number of degrees below 0°C

$[de/dt](min)T$ = strain-rate at -T°C (%/hour)

These data are contained Table 4.10 and plotted in Figure 4.26. It shows that the spread in the data of this research and from Table 4.8 observed in Figure 4.24 is reduced when the temperature correction is made. The flow law for the data shown in Figure 4.26 has been established using the same method as used previously. The relationship for the data corrected to a grain size ratio equal to 0.030 and at temperatures equal to -2°C is:

$$[de/dt](min) = .001 \left(\sigma/143.5 \right)^{2.80} \qquad (4.26)$$

where

$[de/dt](min)$ = strain-rate (%/hour)

σ = axial stress (kPa.)

This relationship shows that the exponent of the flow law approaches 3.0 when the temperature variation of the results are accounted for. Equation 4.26 is the flow law based on the combined data of Glen (1955), Steinemann (1958), Barnes et al. (1971) and this author.

Using Equation 4.26 and accounting for the influence of temperature on the proof stress a generalized equation for the flow law of ice at a constant grain size ratio of 0.030 can be written:

$$[de/dt](min) = zz$$

$$zz = [0.025 + 0.5 \ (1/1+T)].001 \ (\sigma/79.5)^{2.80} \qquad (4.27a)$$

where the parameters have the same meaning as in Equation 4.24 and 4.26. Using Equation 4.27 the flow law at temperatures of -1.0°C, -2.0°C and -3.0°C have been determined and plotted in Figure 4.27. This data is for a constant GSR of 0.030. This indicates that the temperature influence on the flow law is slight within this temperature range.

The flow law of polycrystalline ice that accounts for both the temperature influence and the grain size influence may be written as:

$$[de/dt](min) = [0.025 + 0.5\ (1/1+T)].001 \times [5\ (GSR)^{0.68}/7.32]^{2.80} \qquad (4.27b)$$

4.7 Method to predict length of experiment

When conducting creep experiments under a constant stress at a given test temperature, at what point in the experiment is the loading of the sample stopped? This is an important consideration, but one which has not received a great deal of study. One might answer the above question with "When the information of interest has been recorded". This being a logical answer one must establish what exactly is the "information of interest".

In the past, as mentioned in Chapter 2, most creep studies conducted on polycrystalline ice were interested only in establishing the flow law of ice. This information

was of interest primarily for the study of glacier movement. The early stages of the research were influenced very heavily by the glaciologist and physicist. They brought into the study of the deformation of ice the methods of analysis used in the study of polycrystalline metals. This was a logical extension, since a great deal of fundamental research was under way on deformation behaviour of metals at that time. It is at this point that the direction of the research appears to be inconsistent.

The typical creep curve given in Figure 2.4, has a primary, secondary and tertiary sections. The metal research was interested in the primary, secondary and the onset of tertiary, since in engineering design the onset of the tertiary behaviour is considered failure. Thus, the analytical methods and theories concerning creep of metals were related to these first two regions of the creep curve. The early creep studies of ice also examined only the primary and secondary portion of the typical creep curve of polycrystalline ice shown in Figure 2.4. The researchers, therefore, terminated their experiments when the strain versus time curve approached a linear portion establishing a quasi-steady-state strain-rate. These experiments were terminated at this point since the information needed to establish a flow law for ice had been obtained. The majority of the experimental data used to determine the flow law of ice was obtained using experiments terminated before the onset of tertiary creep (Glen (1955), Voytkovskiy (1960), and

Barnes et al. (1971)). An exception is the data presented by Steinemann (1958) which was determined from experiments conducted beyond the point of the onset of tertiary creep.

The data from the above authors has been used with the strain-rates determined from field measurements on glaciers to establish the flow law for ice (Meier (1960) and McRoberts (1975)). The typical creep curve (Figure 2.4) shows that beyond a certain strain the experiments enter the tertiary portion of the strain-time curve. In this region recrystallization of the ice crystals occurs and the fabric of the ice begins to change (Glen (1955), Steinemann (1958) and Kamb (1961)). Thus the deformation behaviour of ice is not the same in the regions before and after the onset of tertiary creep. Since ice within a glacier has been subjected to load for extended periods of time, this ice deforms in a similar manner to that within the tertiary region of the creep curve. As mentioned except for Steinemann (1958) the laboratory studies reported within the literature have not studied the creep behaviour in this tertiary region, therefore these laboratory results should not be compared with field results. Thus, the question, "What is the information of interest?".

For the analysis of the deformations of glaciers and ice shelves, only experiments conducted well into the tertiary region of the typical creep curve would be of value. These experiments must be conducted to large strains and would require very long loading times. To study the

deformations of interest to a foundation engineer, the primary region, the secondary region, and the onset of tertiary creep are of interest. The behaviour during the tertiary region is not of much interest since the structure will be considered to have failed at deformations associated with the onset of tertiary creep.

Therefore, in studies of the creep of ice for engineering purposes, the following are required:

1. the strain-time curve,
2. the minimum time the sample must be loaded to establish the minimum strain-rate,
3. the time at which the onset of tertiary creep occurs.

The time for the minimum strain-rate to be established is required to evaluate the length of time a creep experiment must be conducted to yield all the data of interest. The time to the onset of tertiary is very important since this is the time beyond which the deformations of a structure founded on ice will accelerate. The onset of tertiary creep has been defined as failure in frozen soil by Vialov (1965a) and should also be used in ice.

4.7.0.1 Prediction of time to achieve minimum strain-rate during testing

In the study of the flow law of ice, it is important to know at what time the sample has reached the minimum strain-rate. If the experiment is stopped before this strain-rate is achieved, the measured strain-rate will

overpredict the strain-rate as a function of stress for the experiment which will result in an incorrect flow law. This is a special problem when conducting experiments below about 300 kPa, since the required time to achieve a minimum strain-rate increases rapidly under low applied stresses. It is this difficult task of achieving a minimum strain-rate in an experiment under low stress which has caused much of the problem related to the flow law of ice at low stresses. In Chapter 2 the bilinear flow law established by many authors for ice in this stress region was reviewed.

This bilinear flow law has been developed using the results of laboratory experiments and field measurements (Meier (1960) and McRoberts (1975)). The field studies were conducted using borehole deformation and tunnel closure measurements from glaciers and ice shelves. These measurements were made within glaciers and ice shelves which have undergone extensive deformation over a long time period. Because of the long history of loading the ice within the glacier has passed the primary and secondary portion of the typical creep curve and is similar to the ice well within the tertiary region of the creep curve of Figure 2.4. The result is a higher strain-rate at a given stress level in this ice than in ice which is under load for the first time and has not reached the tertiary region of the strain-time curve. The difference in the strain-rate of ice in the secondary and tertiary region is shown by comparing Equation 2.18 and Steinemann's Equation 2.25 (1958).

The field data, therefore, should not be used with laboratory experimental data determined at strains below the inflection point to establish a flow law for ice. Two separate flow laws for the ice must be established. One law would relate experiments which have achieved a minimum strain-rate but have not yet reached the onset of tertiary creep. The second law would be based on experiments which have been carried well beyond the inflection point and have re-established a minimum or steady-state strain-rate within the tertiary region of the creep curve.

In this research program the data were used to establish the flow law of ice before the onset of tertiary creep hence the flow laws given in Equation 4.9 and Equation 4.11 are only valid for this condition. The experiments used in establishing these flow laws were all long-term creep experiments. The load was maintained for in excess of 14,000 hours (1.6 years) on two of the samples. The long loading periods were maintained to establish the true minimum strain-rate and to ensure that the onset of tertiary creep was established. The method used to determine the minimum strain-rate has been outlined in Section 4.3. The time at which this minimum strain-rate occurs has been recorded. This data will be used to establish the minimum time of loading required to reach the minimum strain-rate.

Table 4.11 contains the information on the time required to establish the minimum strain-rate. The data has been plotted versus the axial stress in Figure 4.28. This

data shows quite a scatter but the data can be enclosed with two straight lines. This gives a minimum time and a maximum time required to establish a minimum strain-rate in the laboratory experiment of this research program. The relationships used to bracket the data contained in Figure 4.28 are:

$$T_{max} = (1337.6/\sigma)^{2.94} \qquad (4.28)$$

and

$$T_{min} = (669.8/\sigma)^{3.32} \qquad (4.29)$$

where

T_{max} = maximum time to minimum strain-rate (hours)

T_{min} = minimum time to minimum strain-rate (hours)

σ = axial stress (kPa)

Equation 4.28 and Equation 4.29 can be used to predict the test time required to get useful data on the minimum strain-rate from constant stress experiments. These equations show that except for high stress experiments the time required to get useful information on the minimum strain-rate from an experiment is excessive.

This information confirms the findings of Mellor and Testa (1969b) that for previous experiments conducted below 100 kPa the experiments were terminated at too short a loading time to have established a steady-state strain-rate.

Therefore, this data will predict a smaller dependence of strain-rate on stress and should not be used to establish the flow law of ice . Equation 4.28 and 4.29 suggest that Mellor and Testa's tests under an axial stress of 43 kPa were not conducted for a long enough time to have established a minimum strain-rate. According to Equation 4.29, 5.5×10^5 minutes were required to establish the minimum strain-rate in these experiments. The loading applied in the experiment at a stress of 43 kPa was only maintained for 5.0×10^4 minutes.

These results suggest that the strain-rates published in the literature at low stress are too high. In each case, the strain-rates are determined from the primary portion of the creep curve and thus do not represent a minimum strain-rate for each experiment. The decrease in the exponent n from a power of approximately 3 in the stress region 100 kPa to 1000 kPa to a value approaching 1 at lower stresses is suspect. The laboratory data in this research program support the use of only a simple power law as given in Equation 4.26 to describe the flow law of polycrystalline ice.

In conclusion, constant stress experiments at stresses below 100 kPa require loading times in excess of 1000 hours to establish a minimum strain-rate. The data available in the literature from laboratory experiments at stress levels below 100 kPa are in question and should be used with caution in developing a flow law for ice. Thus, what is the

nature of the flow law at low stresses? This research project did not address this problem directly because of time constraints on the testing. However, using the results of this research, some guidance on this problem will be given in Section 4.7.1.

4.7.0.2 Time to failure

In order to design a foundation one must understand the deformation behaviour of the material. To this point, the deformation behaviour of ice as a function of time, stress, temperature, and grain size has been examined. These parameters have been incorporated into a deformation law for ice and this is contained in Equation 4.8 and 4.27. Now, failure of the ice will be defined.

In conventional soil mechanics, the peak of the stress-strain curve of a constant strain-rate experiment is defined as failure (Terzaghi and Peck (1967)). Failure is defined in terms of the peak stress. This allows the Mohr-Coulomb strength failure criterion to be used to establish the failure resistance of a soil. This definition of failure has carried over into ice mechanics. The strength of ice is defined as the peak stress from the stress-strain curve.

Mellor (1979) suggests that failure within the ice be defined using the strain at which the maximum ratio of [σ / [de/dt] (min)] occurs. He suggested the use of the strain definition for failure because the failure stress of ice in

uniaxial compression can vary by orders of magnitude depending on the strain-rate applied during the experiment, temperature, and grain size. The strain at failure is defined to occur at the peak in the constant strain-rate experiment and at the inflection point in the constant stress experiment. The strain at failure of polycrystalline ice varies only between 0.3% and 2.0% depending on the strain-rate (Mellor (1979)). This shows that the variation in the failure strain is greatly reduced compared to the variation in the failure stress of ice. The experimental conditions do not influence the strain at failure nearly as much as they influence the strength at the yield point.

It must be noted that the low strains to failure are associated with the high strain-rate experiments, which result in a brittle failure mode of the ice (Gold (1972)). The larger strains to failure are associated with a ductile failure in the ice. In the low stress experiments the ice retains some resistance to deformation after the yield point has been reached. In this work only the strains at failure in the ductile range will be discussed, (Figure 4.17).

The correspondence between the constant strain-rate experiment and the constant stress experiment has been outlined in Section 4.5.2. This showed that the peak of the constant strain-rate test corresponds to the inflection point of the constant stress creep curve. Therefore, if failure is defined at the peak in the constant strain-rate experiment, and the inflection point of the constant stress

experiment is also defined as failure. This definition of the inflection point as the failure is consistent with the definition given by Vialov (1965a) for frozen soil.

To examine this proposed failure condition, the relevant information from this research is tabulated in Table 4.12. The strain at failure is plotted versus the applied stress in Figure 4.29 which shows that the failure strain is slightly dependent on the applied stress in the ductile range. Figure 4.30 illustrates that the failure strain is only slightly dependent on the minimum strain-rate during the experiment. Figure 4.30 shows that, in the ductile range the failure strain is approximately equal to 1% over 2 1/2 orders of magnitude of axial strain-rate. This consistency in the strain at the failure point over the wide range of strain-rate supports the use of a strain failure criterion instead of a stress failure criterion.

In engineering design, the use of the design life or time to failure has been accepted (Conway (1967) and Mellor (1979)) as a valid failure criterion. Conway (1967) presents the time to failure as the time to cause rupture of the test specimen. Mellor (1979) defines the time to failure in ice as the time required to reach the failure strain. In the design of a foundation in permafrost or ice, as in conventional soil mechanics, failure is associated with first yield in the material. Thus Mellor's definition of the time to failure will be used in this research and not the time to rupture as used in metals.

The time to failure recorded for each experiment is included in Table 4.12. These data are plotted versus the axial stress at failure in Figure 4.31. This shows that the time to failure is related to the stress using a power law relationship. The best fit power law of the experimental data are:

$$Ty = B\,\sigma^{-2.22} \qquad (4.30)$$

where:

Ty = time to failure (hours)

B= 8.78×10^{7} (hour / $kPa^{2.22}$)

σ = axial stress (kPa)

Equation 4.30 allows the prediction of the time to failure for a given stress under a uniaxial loading condition. The time to failure under a more complex loading state was not studied in this research.

4.7.1 Comparison of laboratory and field flow laws

In this chapter, the laboratory flow law of polycrystalline ice determined during this research program has been presented and examined. The factors which influence this law have also been examined. The data from this research have been compared with data from (Glen (1955), Steinemann (1958) and Barnes et al. (1971)). The results of this study and the preceding three authors are plotted in Figure 4.26, which shows that the data compare very well.

The best fit straight line through the data gives a flow law expressed by Equation 4.26. As has been mentioned earlier this flow law was determined from samples tested to a total strain less than the failure strain. It is now necessary to compare this flow law with the flow law of polycrystalline ice from experiments conducted to large strains.

In Section 4.5.2, the correspondence of the constant strain-rate experiment and the constant stress experiment was examined. It was shown that the same flow law resulted when the data was compared at the yield point. In Section 4.7.0.2 it was established that the failure strain of each experiment was approximately 1%. However, the constant strain-rate experiments were conducted to strains greater than 5%. A typical set of data from one of these experiments is illustrated in Figure 4.18. The stress in the stress time plot increases initially to a peak value and then decreased. At large strains, the stress gradually levels out at a constant value. A flow law can be determined using the stress and strain-rate data from each experiment at large strains. This law will differ from the flow law based on the peak stress and strain rate data as given in Equation 4.26.

Table 4.13 tabulates the data from the constant strain-rate experiments which were conducted to large strains. The average stress was determined from each constant strain-rate test at a strain of 10%. This allows for direct comparison of the data conducted at different strain-rates. In Figure 4.32 the data determined at both the

peak strain and 10% strain from the constant strain-rate experimental curves are plotted. The flows laws determined at the two different strains for the laboratory ice are not the same. The flow law determined using the best fit line through data points at the peak strain is:

$$[de/dt](min) = 0.001\ (\sigma/159.3)^{2.47} \qquad (4.11)$$

The flow determined using the data at 10% strain is:

$$[de/dt](min) = 0.001\ (\sigma/138.9)^{3.18} \qquad (4.31)$$

where

$[de/dt](min)$ = minimum axial strain-rate (%/hr)

σ = axial stress (kPa)

Equation 4.11 and 4.31 show that the flow law determined using the two sets of data give different results. Although the exponent n is not equal in each set of data, its value is close to 3 within the stress range of these experiments. The prestrained ice is softer than the ice subjected to loading for the first time.

These data are very important when one considers the consequence of the finding. The ice is softening under continued applied load or accumulated strain. The resistance of the ice drops from a peak resistance at about 1% strain to an approximately constant resistance after 10% strain. This constant resistance of the ice at 10 % strain continues

as the strains increase.

In geotechnical engineering the behaviour of an overconsolidated clay is identical to the above behaviour of the ice. The resistance of the clay increases to a peak value and with continued deformation the material becomes weaker. The resistance of the clay decreases and approaches the residual strength of the clay at large strains. Structural changes take place within the clay during this straining (Skempton (1964) and Morgenstern and Tchalenko (1967)) which account for the decrease in shear resistance with strain.

An ice sample also undergoes changes within the ice crystals which accounts for the decrease in resistance in a manner similar to the clay. Recrystallization (Steinemann (1958)) and preferred crystal orientation (Rigsby (1960)) account for the weakening of the ice at strains greater than the peak strain. Colbeck (1970) suggests that no recrystallization occurs at strains of less than 1%, hence, one would not expect the crystal structure of the ice to change before the peak resistance of the ice were reached. Therefore, the laboratory specimens retained their initial crystal structure until the peak is reached during testing. After the peak, the crystal orientation and structure of the ice changes resulting in a decrease of the resistance. Thus, as pointed out in Chapter 2, two different flow laws for ice exist. It was also shown that from a crystal point of view, the ice is different for each loading condition.

Hence, artificially prepared laboratory ice under first time loading should not be used to develop a flow law for use in analysing the flow of glacier ice. This has been recognized within the glacier literature (Glen (1975)). However, many comparisons between laboratory flow laws and field flow laws have been made and presented in the literature. Meier (1960) combined field and laboratory results and developed a bilinear flow for ice as a result of not recognizing the difference. Thus, as a precaution, one should examine carefully the data base used to develop a flow law for ice which covers a wide range of stresses to ensure that similar ice is being compared.

Can a flow law for the field behaviour of polycrystalline ice be developed? Can the stress range applicability of the flow law developed from this research be extended? Figure 4.32 suggests that ice which has been deformed to large strains with the associated change in crystal structure, has a flow law which is approximately parallel to that of ice deformed at low strains. This has been pointed out in Chapter 2. For a given stress the ice which is deformed to large strains, however, undergoes strain rates which are between 3 and 5 times faster than ice deformed to strains below 1%. This behaviour suggests that within the stress range studied an exponent of n equal to 3 is valid for both types of ice. Figure 4.26 shows the data from this research project and the results of Glen (1955), Steinemann (1958), and Barnes et al. (1971) with a flow law

in which the exponent n is equal to 3.0. The equation of this flow law is:

$$[de/dt] = .001\ (\sigma/150)^{3.0} \qquad (4.32)$$

where

[de/dt] = strain-rate (%/hr.)

σ = axial stress (kPa.)

This combined flow law is a good representation of the data in Figure 4.26. Figure 4.33 is a plot of the data from this research program in which a flow law with an exponent equal to 3 is established through the laboratory data. The equation for the flow law is:

$$[de/dt] = .001\ (\sigma/110)^{3.0} \qquad (4.33)$$

where

[de/dt] = axial strain-rate (%/hr.)

σ = axial stress (kPa.).

Figure 4.33 also contains the flow law expressed by Equation 4.32 which is the best fit through the combined data plotted in Figure 4.26.

The plot of a constant strain-rate experiment in Figure 4.18 shows that the resistance of the ice remains nearly constant at strains greater than 5%. This would suggest that the flow law determined at large strains from laboratory prepared ice would approximate that of clean ice deformed to

large strains in the field. This behaviour suggests that field data could be used to extend the flow law of polycrystalline ice into the low stress range. However, it must be recognized that the field data will only extend the flow law which has been determined from laboratory experiments conducted to a large strain. Since these experiments have not been conducted over a wide temperature range the preceding finding would at first appear to be of little help in extending the flow law of ice using field data.

An important finding of this research is that the preceding two flow laws are approximately parallel, therefore, field measurements can be used in conjunction with the laboratory data to extend the flow law to the low stress range. The field results and the creep experiments at large strain can be used to predict the exponent of the flow law of ice deformed to large strains. Then, as a consequence of the curves in Figure 4.32 being approximately parallel, the flow law for polycrystalline ice which has been strained to a value less than the yield point can be extended into the low stress range. This supports the findings of Thomas (1971) and Roggensack (1977) that the flow law for ice over the stress range 10 kPa and 1000 kPa shall be represented using a simple power law relationship. The exponent n equal to 3 can, therefore, be used to extend the laboratory data to low stresses for design purposes.

These findings now make it possible to extend the

laboratory flow law to the low stress region, but one must ask is this the flow law required for design? This research has shown the flow law is a function of grain size ratio, temperature and the strain the material has undergone. In a natural ice body it would be difficult to determine the grain size ratio and the strain it has already undergone in the field. Therefore, to determine the appropriate flow law for design, one must use field methods because many factors influence the flow law determined in the laboratory for it to be used for design. In the next Chapter a method will be examined which should be very useful in determining the flow law of ice in the field for design purposes.

4.8 Conclusion

The use of superposition of the elastic, time-dependent and quasi-steady-state components of strain produce a strain-time law which fits the experimental data. A parabolic form of a strain-time relationship was used to describe the primary portion of the creep curves. It was found that the exponent on the time was dependent on the applied stress. This shows that at a stress of 100 kPa, the Andrade one-third law fits the laboratory data, but as the stress increases this relationship fails to reproduce the data well. The temperature influence on the complete strain-time law was not determined in this research program.

The correspondence between the constant stress experiment and the constant strain-rate experiment was

discussed and used to establish the flow law of polycrystalline ice. It was found that the flow laws from the two test methods correspond only when the data are compared at a constant grain size ratio. The experimental data illustrate the importance of the ratio of the ice crystal size to sample size on the flow law of ice. This finding is important since it demonstrates that a size effect in the creep testing of polycrystalline ice exists which has not been recognized before. The findings must be used to relate data from various laboratory programs in which the grain size ratios are different. The temperature influence on the flow law shows that at temperatures warmer than -5°C this influence can be described using an inverse temperature relationhip.

When the grain size ratio and the temperature of the tests are standardized, a flow law with an exponent n equal to 2.8 is the best fit using a linear regression through all the data. The data used to obtain this relation is from this research project, Glen (1955), Steinemann (1958) and Barnes et al. (1971).

The importance of using the proper test information to determine the flow law was discussed. It is improper to use laboratory creep experiments not conducted well into the tertiary region to develop an ice flow law for comparison with field data. The flow laws developed in the laboratory and from the analysis of field data are not comparable except that the exponent in both situations is approximately

equal to 3.0.

Failure in the two types of experiments used in this research program is defined as occurring at the peak stress in a constant strain rate experiment and at the onset of tertiary creep within the constant stress experiment. This effectively divides the material into *before* and *after* failure conditions.

Table 4.1

Summary of strain time parameters at various stress levels

Sample Number	Axial Stress (kPa)	Temp °C	B (%/hr.)	x	A	m	Strain Rate (%/hr.)
CSA34	100	-1.3	0.0077	0.68	0.024	0.32	0.00008
CSB35	100	-1.1	0.0065	0.74	0.025	0.26	0.00008
CSGR38	150	-1.3	0.0041	0.73	0.015	0.27	0.00027
CSC37	200	-1.2	0.0060	0.88	0.05	0.24	0.0004
CSD39	300	-0.7	0.0050	0.76	0.021	0.24	0.0012
CSE42	300	-1.0	0.020	0.80	0.105	0.20	0.0016

Table 4.2

Summary of strain time parameters at various temperatures and constant axial stress of 300 kPa.

Sample Number	Temp °C	B (%/hr.)	x	A	m	Strain Rate (%/hr.)
CSD39	-0.7	0.0050	0.76	0.021	0.24	0.0012
CSE42	-1.0	0.020	0.80	0.105	0.20	0.0016
CSD45	-3.8	0.0044	0.78	0.02	0.22	0.00063

Table 4.3

Summary of constant stress data

Sample Number	Test Temp. °C	Axial Stress (kPa)	Minimum Strain Rate (%/hr.) 10^{-3}
CSA34	-1.3	100	0.08
CSB35	-1.1	100	0.08
CSGR38	-1.3	150	0.27
CSC37	-1.2	200	0.40
CSD39	-0.8	300	1.20
CSE42	-1.0	300	1.60

Table 4.4

Summary of constant strain rate data

Sample Number	Test Temp. °C	Axial Stress (kPa)	Minimum Strain Rate (%/hr.) 10^{-3}
UC15	-1.1	572.7	24.9
UC19	-1.5	643.7	31.5
UC20	-0.9	563.7	29.2
UC29	-0.8	1380.0	249.0
UC31	-1.0	697.7	26.0
UC43	-1.5	1181.0	124.3
UC48	-1.5	1177.0	139.9

Table 4.5

Summary of data used to study influence of grain size ratio

Sample Number	Test Temp.	Axial Stress	Minimum Strain Rate	Crystal Diameter Dc	Sample Diameter Ds	Grain Size Ratio
	°C	(kPa)	(%/hr.) 10^{-3}	(mm)	(mm)	(Dc/Ds)
CSA34	-1.3	100.0	0.08	0.94	119.8	0.0079
CSB35	-1.1	100.0	0.08	0.62	115.5	0.0054
CSGR38	-1.3	150.0	0.27	0.86	124.1	0.0069
CSC37	-1.2	200.0	0.40	0.86	126.0	0.0068
CSD39	-0.8	300.0	1.20	1.00	123.2	0.0081
CSE42	-1.0	300.0	1.60	0.85	125.7	0.0067
UC15	-1.1	572.7	24.9	0.98	68.0	0.014
UC19	-1.5	643.7	31.5	0.92	63.0	0.015
UC20	-0.9	563.7	29.2	1.06	65.9	0.016
UC29	-0.8	1380.0	249.0	0.90	70.3	0.013
UC31	-1.0	697.7	26.0	0.59	69.0	0.009
UC43	-1.5	1181.0	124.3	1.09	69.0	0.016
UC48	-1.5	1177.0	139.9	1.10	70.8	0.015

Table 4.6

Summary of data corrected for grain size.

Sample Number	Grain Size Ratio (Dc/Ds)	Sample Strain Rate (%/hr.) 10^{-3}	GRS= 0.015 Rate (%/hr.) 10^{-3}	GRS= 0.030 Rate (%/hr.) 10^{-3}	GRS= 0.0075 Rate (%/hr.) 10^{-3}
CSA34	0.0079	0.08	0.239	0.783	0.073
CSB35	0.0054	0.08	0.458	1.500	0.140
CSGR38	0.0069	0.096	0.845	3.330	0.310
CSC37	0.0068	0.068	1.540	5.040	0.470
CSD39	0.0081	0.097	4.582	14.980	1.400
CSE42	0.0067	0.072	4.704	5.390	1.440
UC15	0.014	24.90	27.99	91.600	8.560
UC19	0.015	31.50	31.500	103.100	9.630
UC20	0.016	29.200	26.170	85.600	7.990
UC29	0.013	149.100	318.200	1041.000	97.300
UC31	0.009	26.000	62.200	203.600	19.000
UC43	0.016	124.300	111.200	363.800	33.800
UC48	0.015	139.900	39.900	457.800	42.800

Table 4.7

Summary of data of proof stress and exponent related to GRS

GRS	σ_c	n
0.0075	251.3	2.52
0.015	158.8	2.53
0.030	97.9	2.52

Table 4.8

Data summary of authors from literature

Sample Name	Sample Temp. °(C)	Axial Stress (kPa.)	Grain Size (mm)	Sample Diameter (mm)	Strain Rate (%/hr.) 10^{-3}
Barnes(1)	-2.00	181.80	///	////	1.40
Barnes(2)	-2.00	276.00	///	////	5.90
Barnes(3)	-2.00	473.50	///	////	33.50
Barnes(4)	-2.00	619.70	///	////	60.80
Barnes(5)	-2.00	688.10	///	////	110.20
Barnes(6)	-2.00	861.10	///	////	165.60
Barnes(7)	-2.00	927.70	///	////	165.60
Barnes(8)	-2.00	1030.00	///	////	261.00
Barnes(9)	-2.00	1127.00	///	////	360.00
Glen(1)	-1.50	90.00	1.00	50.80	0.48
Glen(2)	-1.70	151.00	1.00	50.80	0.77
Glen(3)	-1.30	153.00	1.00	50.80	1.66
Glen(4)	-1.30	168.00	1.00	50.80	0.98
Glen(5)	-1.60	183.00	1.00	50.80	2.52
Glen(6)	-1.50	187.00	1.00	50.80	1.28
Glen(7)	-1.10	240.00	1.00	50.80	2.69
Glen(8)	-1.50	246.00	1.00	50.80	4.07
Glen(9)	-2.10	278.00	1.00	50.80	4.39
Glen(10)	-1.50	367.00	1.00	50.80	8.90
Glen(11)	-1.30	380.00	1.00	50.80	26.20
Glen(12)	-1.30	413.00	1.00	50.80	26.00
Glen(13)	-2.00	632.00	1.00	50.80	107.00
Glen(14)	-1.20	635.00	1.00	50.80	81.60
Glen(15)	-1.40	930.00	1.00	50.80	247.00

Table 4.8 (cont.)

Data summary of authors from literature

Sample Name	Sample Temp. °(C)	Axial Stress (kPa.)	Grain Size (mm)	Sample Diameter (mm)	Strain Rate (%/hr.) 10^{-3}
St(1)	-1.90	186.00	0.85	30.00	1.20
St(2)	-1.90	267.00	0.85	30.00	3.20
St(3)	-1.90	332.00	0.85	30.00	7.20
St(4)	-1.90	506.00	0.85	30.00	18.00
St(5)	-1.90	670.00	0.85	30.00	52.90
St(6)	-1.90	740.00	0.85	30.00	58.70
St(7)	-1.90	850.00	0.85	30.00	95.80
St(8)	-1.90	942.00	0.85	30.00	164.20
St(9)	-1.90	1080.00	0.85	30.00	225.70
St(10)	-1.90	1270.00	0.85	30.00	334.40
st(11)	-1.90	1323.00	0.85	30.00	460.80
St(12)	-1.90	1323.00	0.85	30.00	586.80
St(13)	-1.90	1462.00	0.85	30.00	532.80
St(14)	-1.90	1462.00	0.85	30.00	716.40
St(15)	-1.90	1553.00	0.85	30.00	1033.20

Table 4.9

Summary of data showing temperature influence

Sample	Temp. T °C	Stress (kPa.)	Strain Rate (%/hr.)	Strain Rate (%/hr.) GRS=0.0075	(1+T)	1/(1+T)
CSA34	-1.3	100	0.073	0.235	2.3	0.43
CSB35	-1.1	100	0.140	0.450	2.1	0.48
CSGR38	-1.3	150	0.311	0.359	2.3	0.43
CSC37	-1.2	200	0.470	0.262	2.2	0.45
CSD39	-0.7	300	1.40	0.280	1.7	0.57
CSE42	-1.0	300	1.43	0.286	2.0	0.5
CSE45	-3.8	300	0.63	0.126	4.8	0.21

Table 4.10

Summary of temperature corrected data from this research. Temperature=-2.0°C

Sample No.	Test Temp. °C	Axial Stress (kPa.)	Axial Strain Rate (%/hr.)	Temp. Correction	Axial Strain Rate (%/hr.)
CSA34	-1.3	100	0.783	0.79	0.62
CSB35	-1.1	100	1.50	0.72	1.08
CSGR38	-1.3	150	3.33	0.79	2.63
CSC37	-1.2	200	5.04	0.76	3.83
CSD39	-0.7	300	14.98	0.59	8.84
CSE42	-1.0	300	15.39	0.69	10.62
UC15	-1.1	572.7	91.6	0.72	65.90
UC19	-1.5	643.7	103.1	0.85	87.60
UC20	-0.9	563.1	85.6	0.66	56.50
UC29	-0.8	1380.0	1041.0	0.63	655.80
UC31	-1.0	698.0	203.6	0.69	140.50
UC43	-1.5	1181.0	363.8	0.85	309.20
UC48	-1.5	1177.0	457.8	0.85	389.10

Table 4.11

Summary of times to minimum strain rate

Sample Number	Axial Stress (kPa)	Time (hours)
CSA34	100	2000
CSB35	100	500
CSGR38	150	300
CSC37	200	50
CSD39	300	30
CSE42	300	80

Table 4.12

Summary of test data on yield within each experiment

Sample Number	Yield Stress (kPa)	Yield Strain (%)	Experimental Time to Failure (hours)	Calculated Time to Failure (hours)
CSC37	200	0.73	1270	1825
CSD39	300	0.8	240	666
CSE42	300	0.4	250	250
UC15	572.7	1.05	57.7	42.2
UC19	643.7	0.58	19.4	18.4
UC20	563.8	1.02	43.17	34.7
UC29	1380.0	1.78	10.83	7.1
UC43	1185.8	1.44	14.0	11.5
UC48	1178.0	1.85	22.83	13.2

Table 4.13

Summary of constant strain rate experimental data at a strain =10%

Sample Number	Test Temp °C	Peak Stress (kPa)	Constant Stress (kPa)	Constant Strain Rate (%/hr) 10^{-3}
UC15	-1.1	572.7	399.0	24.9
UC18	-1.5	////	370.0	24.9
UC19	-1.5	643.7	403.0	31.5
UC20	-0.9	563.1	360.0	29.2
UC29	-0.8	1380.0	825.0	249.2
UC31	-1.0	698.0	390.0	26.0
UC43	-1.5	1181.0	705.0	124.3
UC44	////	/////	230.0	3.1
UC48	-0.7	/////	545.0	127.0
UC33	-0.7	/////	650.0	/////

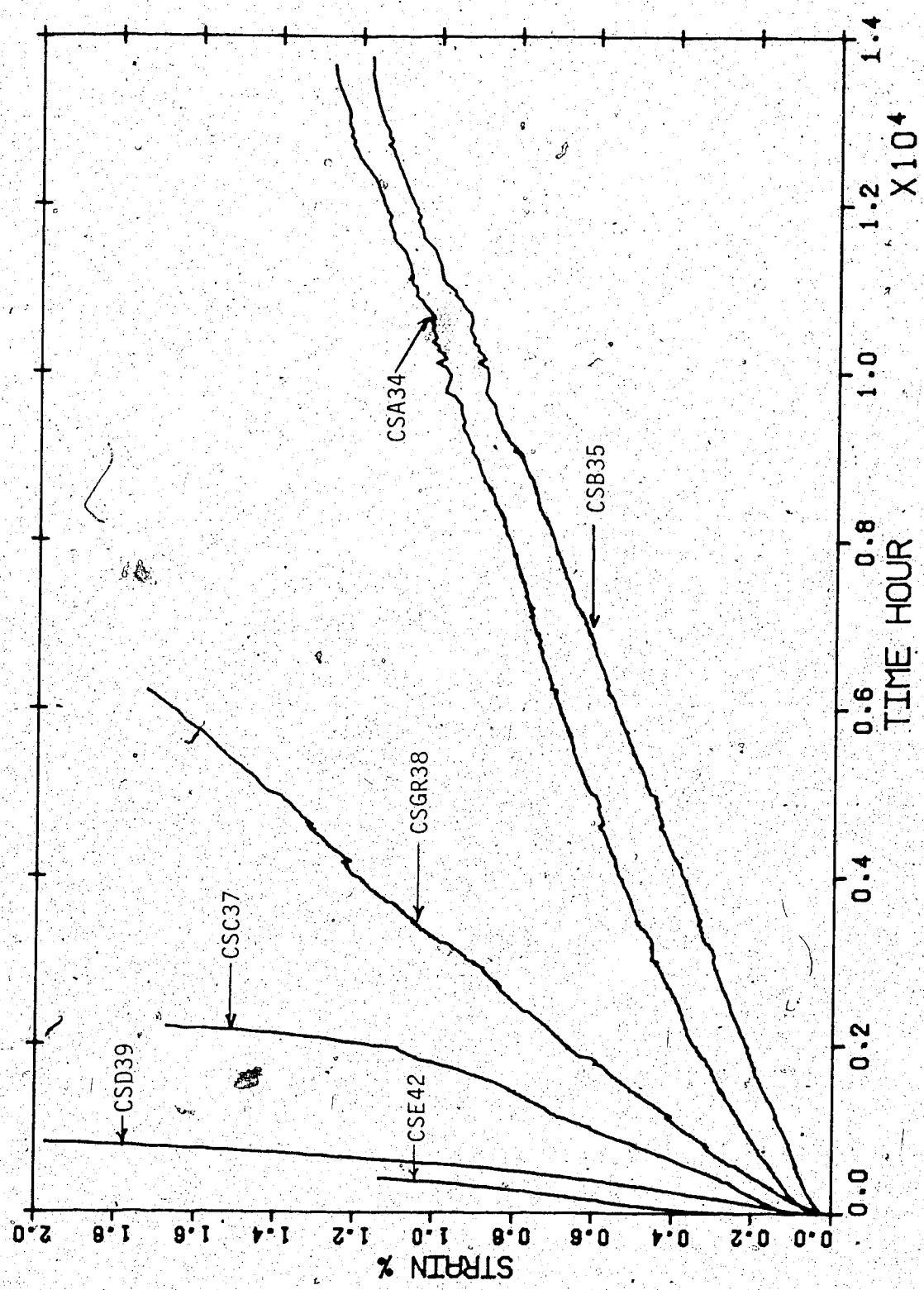

Figure 4.1 Compiled plot of strain-time curves of constant stress experiments

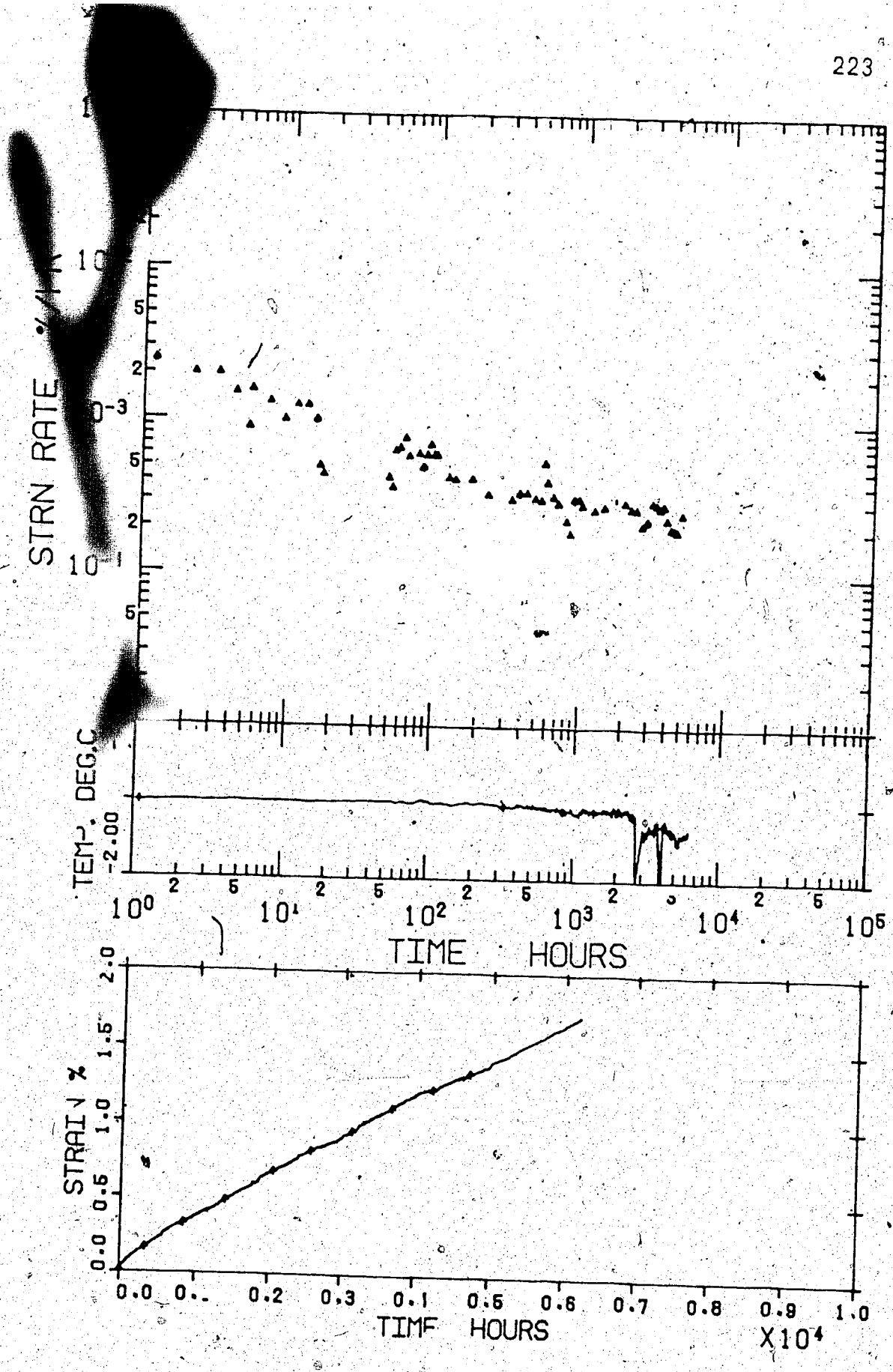

Figure 4.2 Data plot of constant stress sample CSGR38.

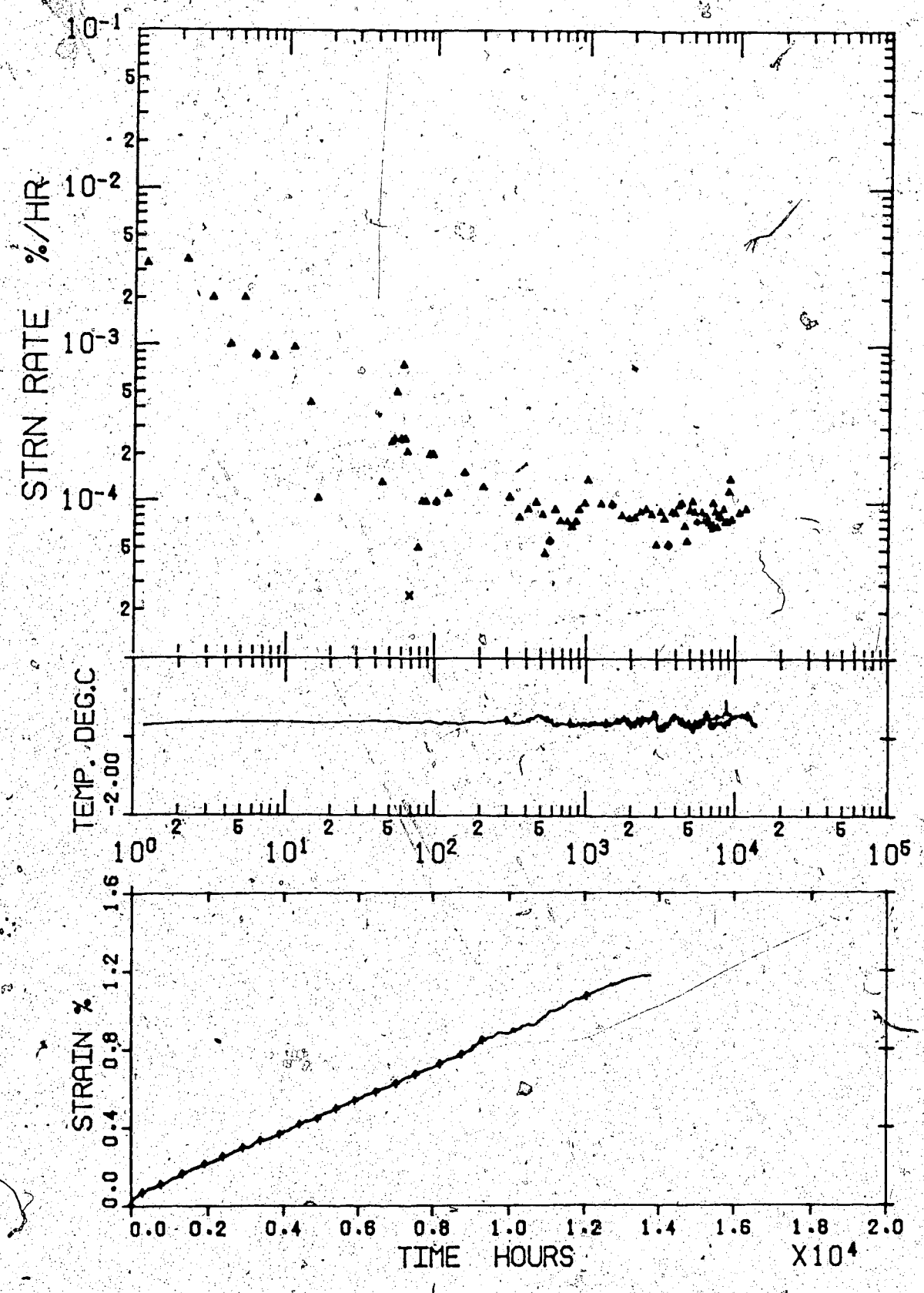

Figure 4.3 Data plot of constant stress sample CSB35.

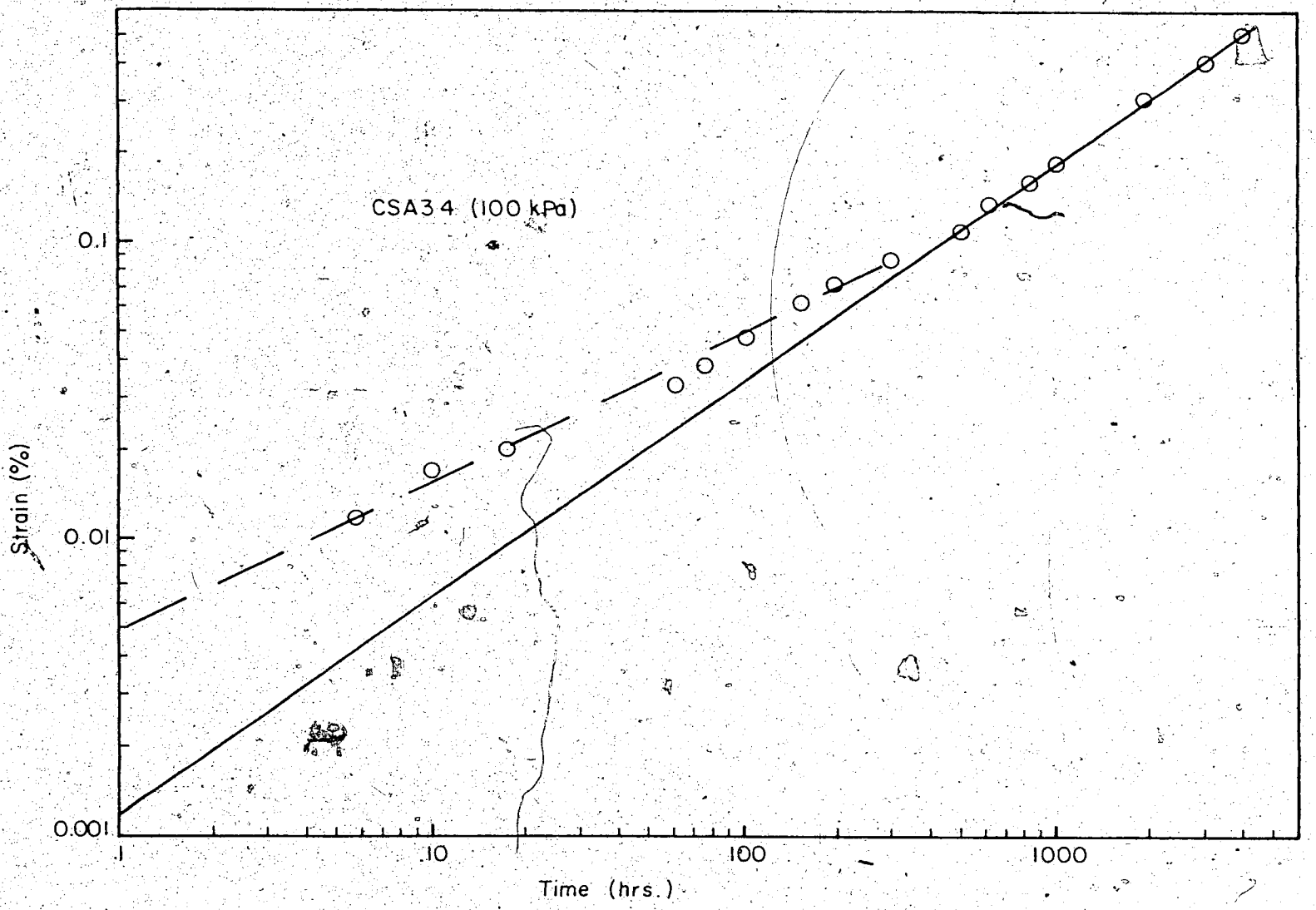

Figure 4.4 Comparison of parabolic strain-time relation and laboratory measured data.

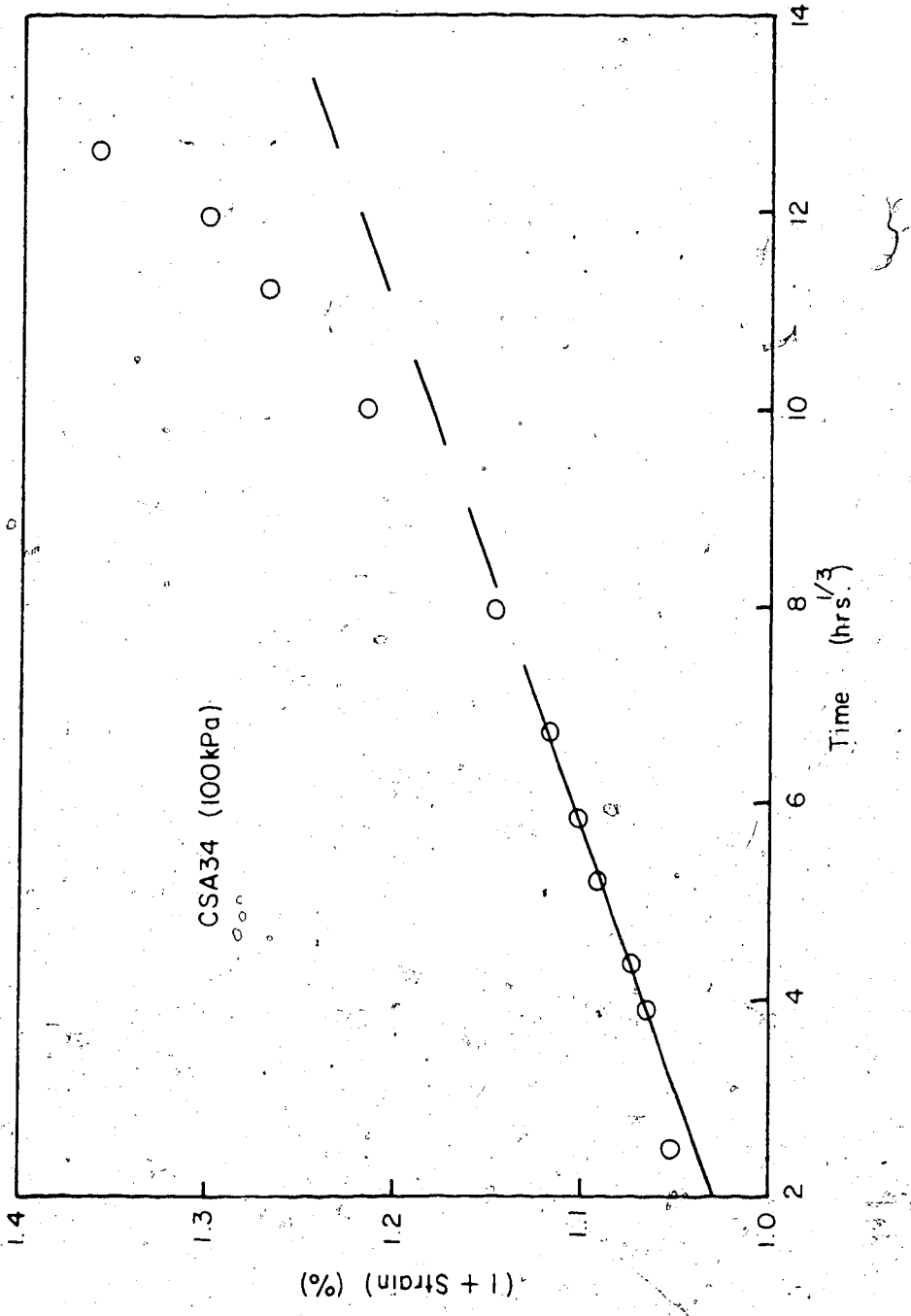

Figure 4.5 Comparison of Andrade one-third relation and laboratory measured data.

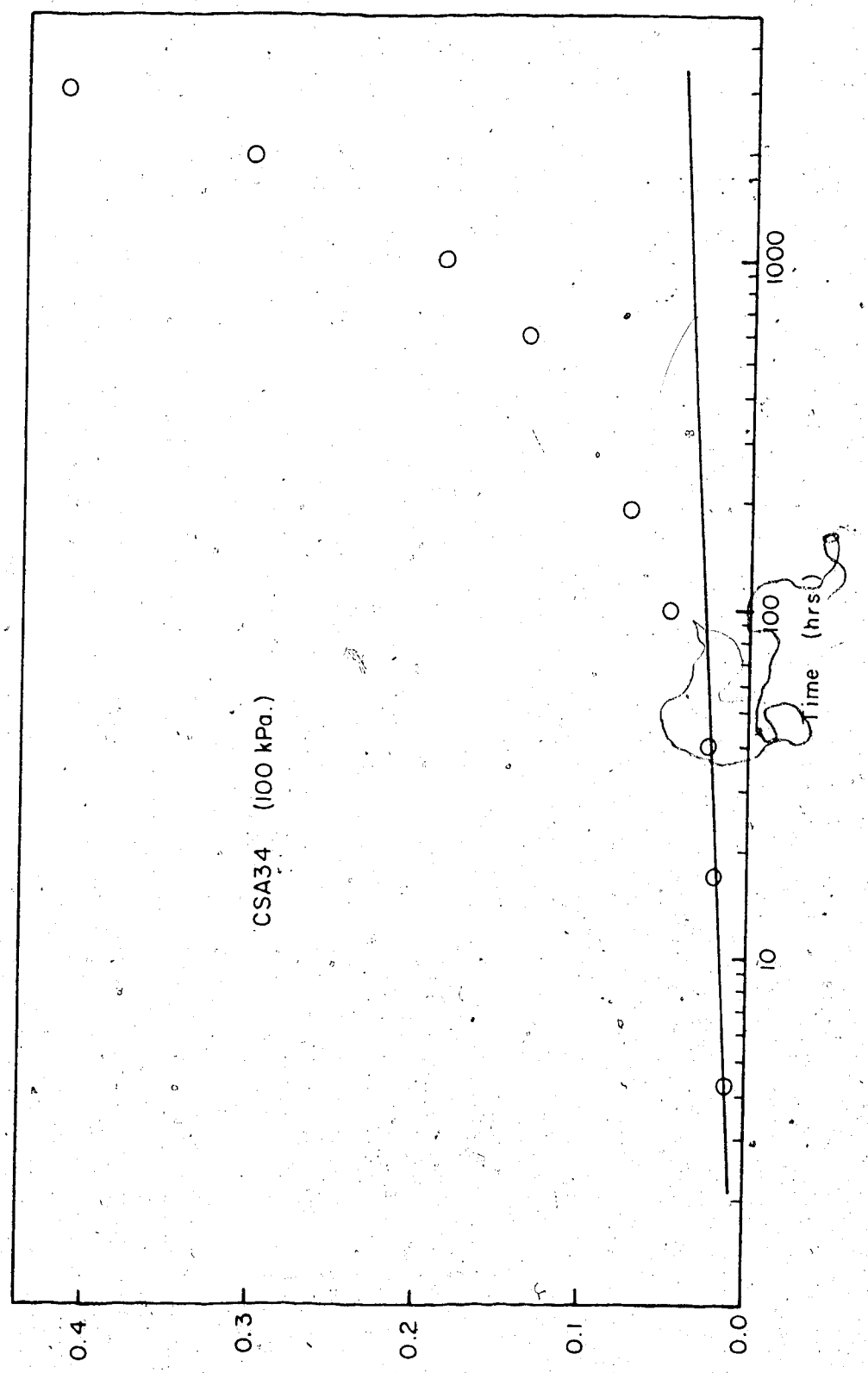

Figure 4.6 Comparison of logarithm strain-time relation and laboratory measured data.

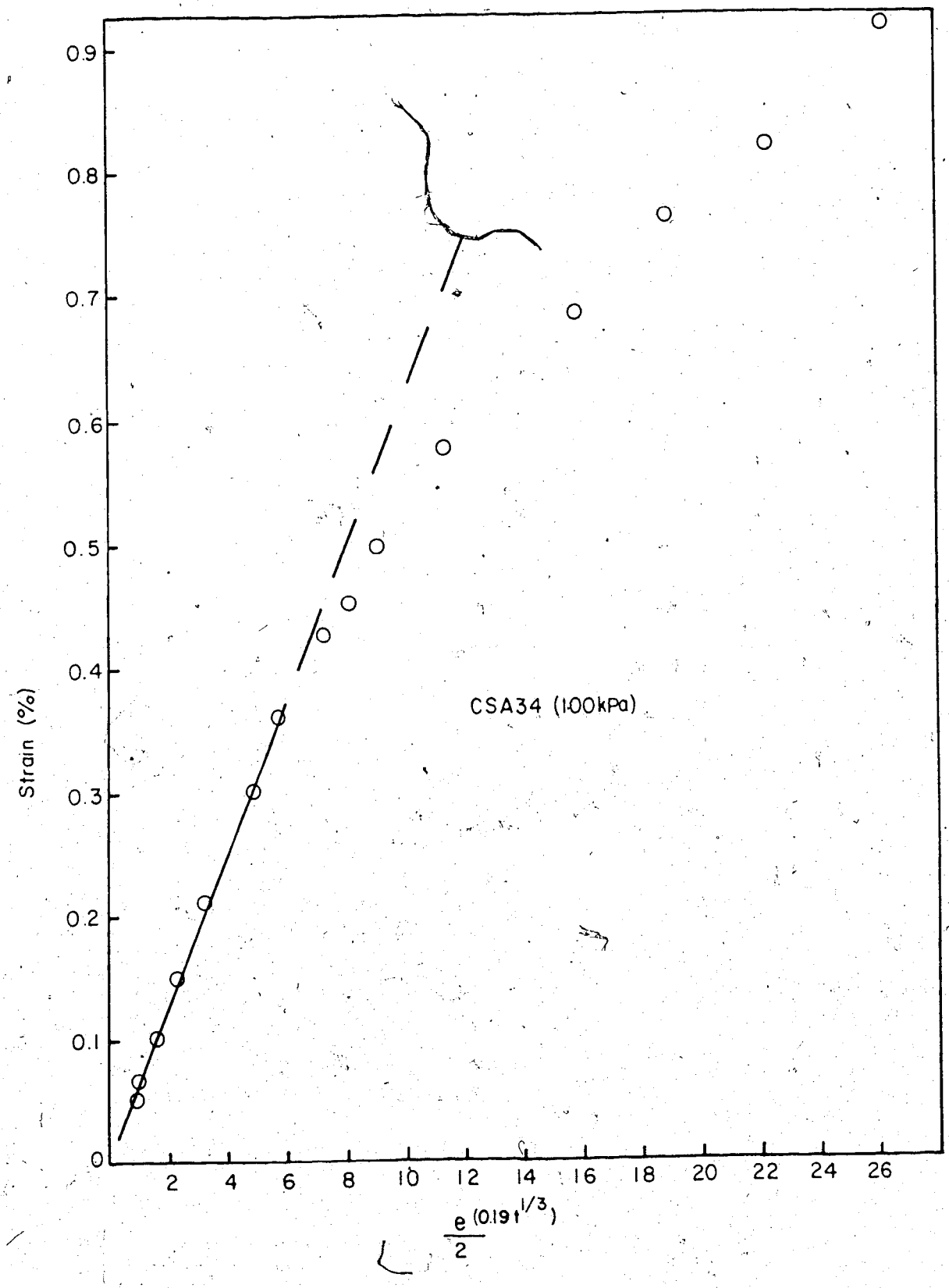

Figure 4.7 Comparison of hyperbolic sine relation and laboratory measured data.

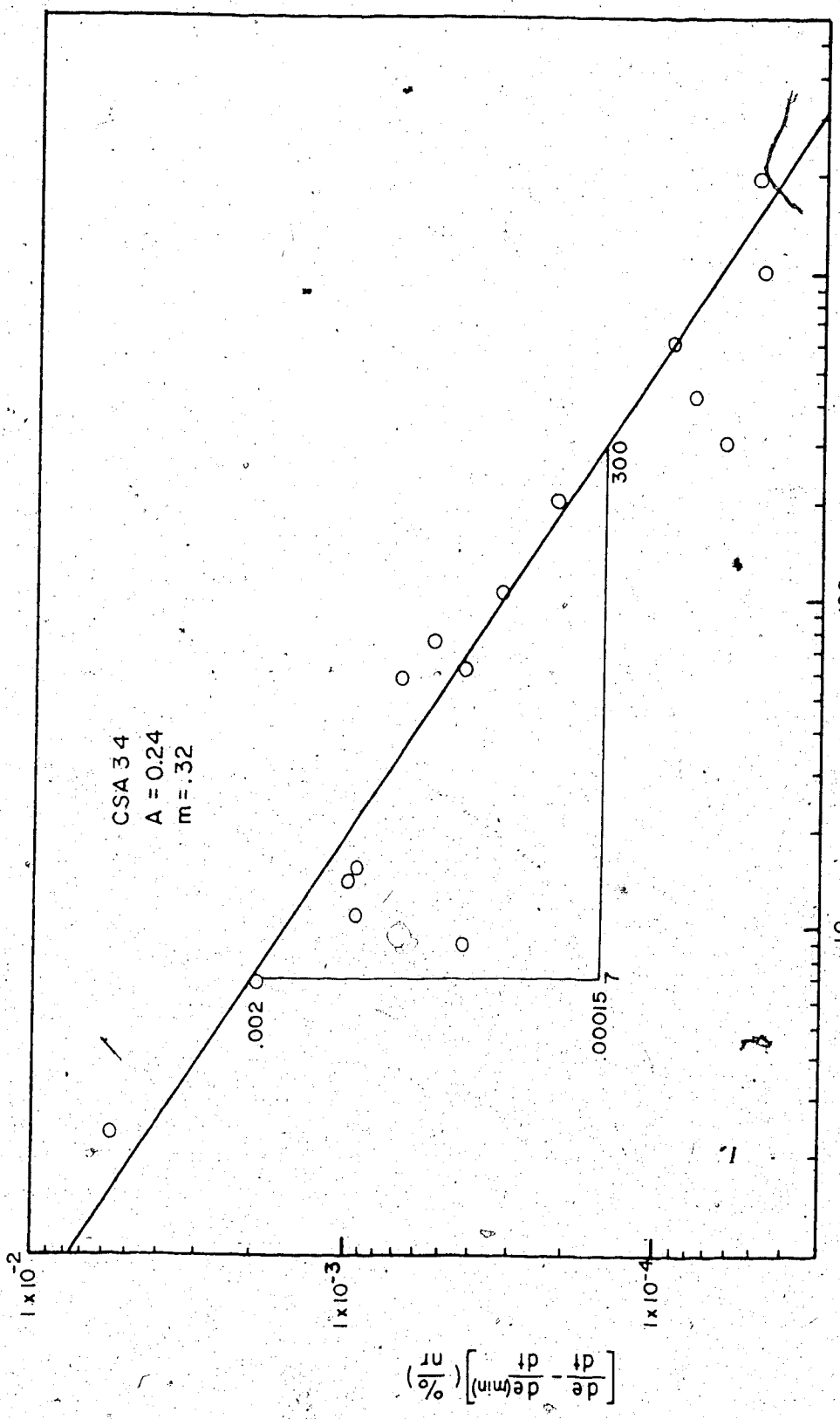

Figure 4.8 Logarithm strain rate versus logarithm (t+1) of sample CSA34.

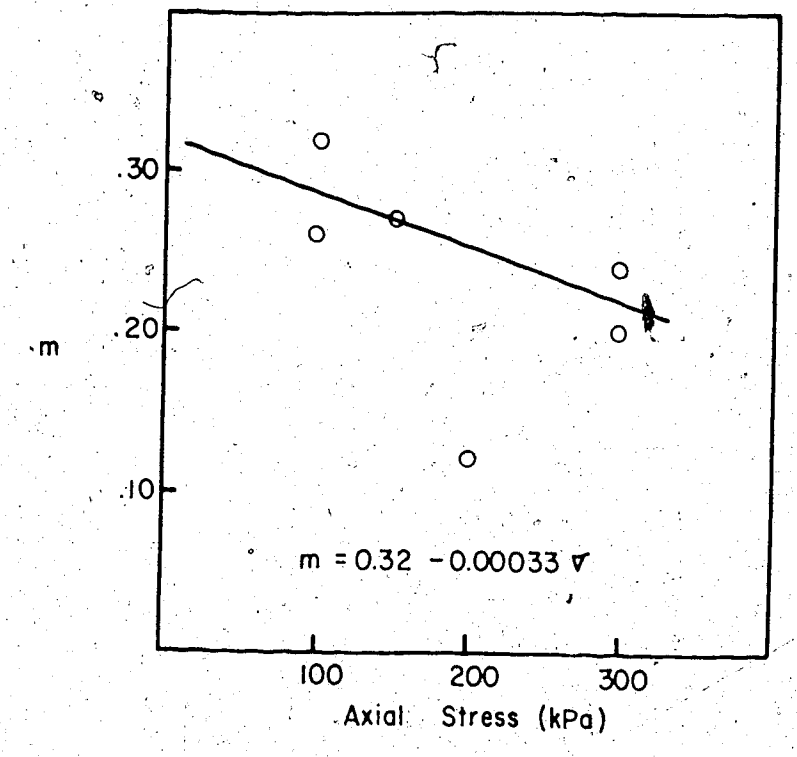

Figure 4.9 Applied stress versus m parameter of constant stress experiments.

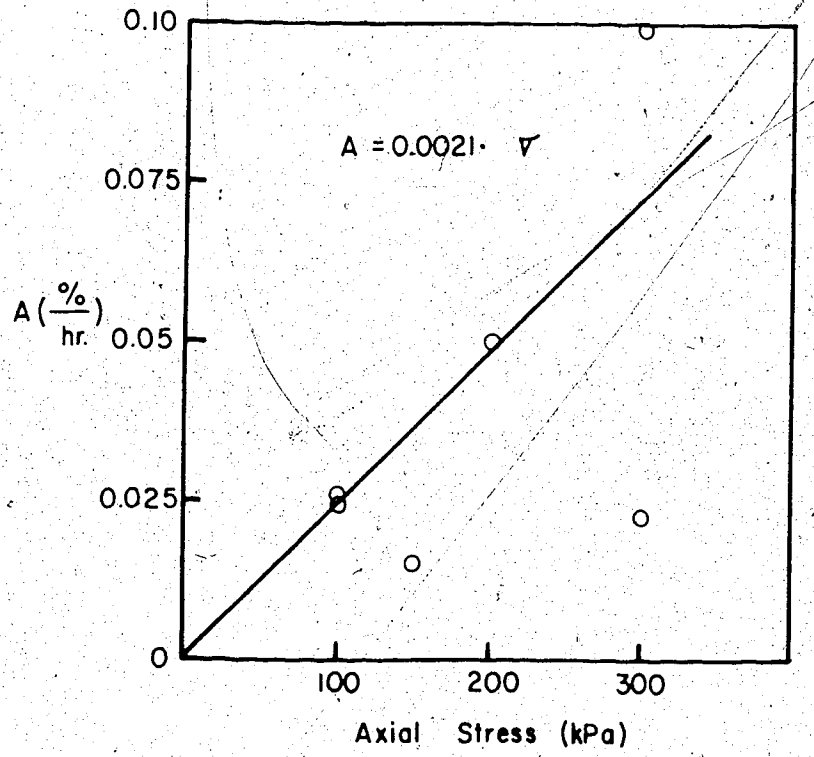

Figure 4.10 Applied stress versus A parameter of constant stress experiment.

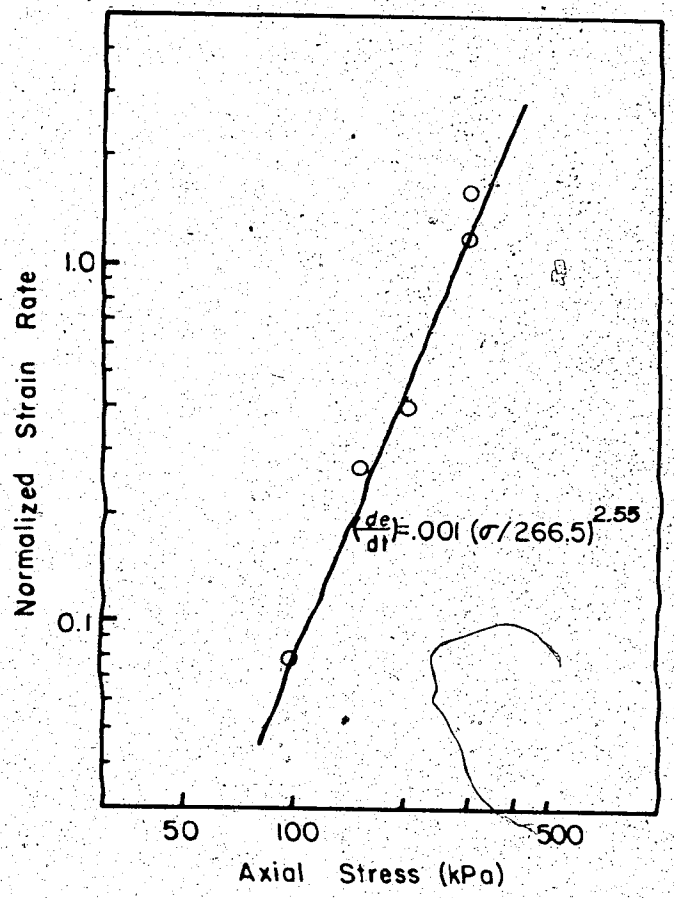

Figure 4.11: Normalized minimum strain rate versus applied stress of constant stress experiments.

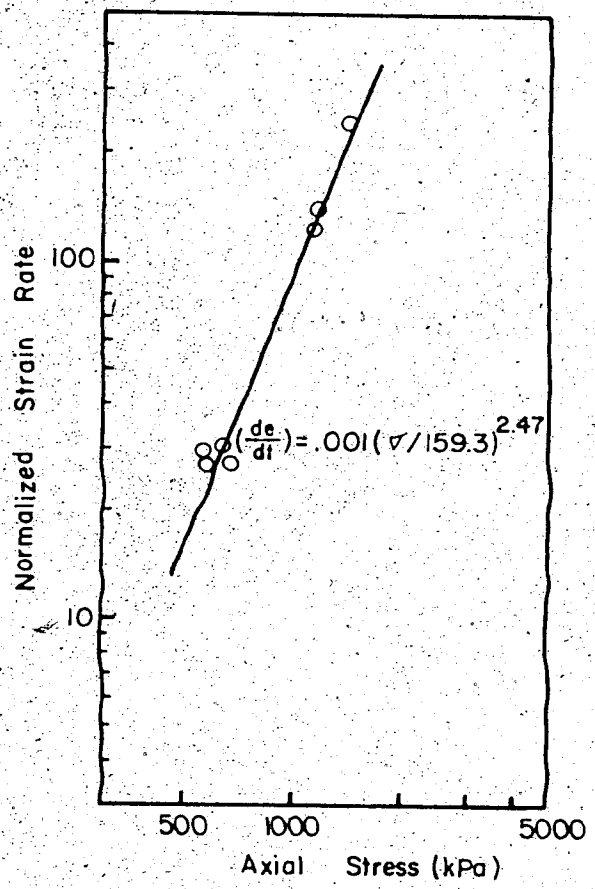

Figure 4.12: Normalized minimum strain rate versus peak stress of constant strain rate experiments.

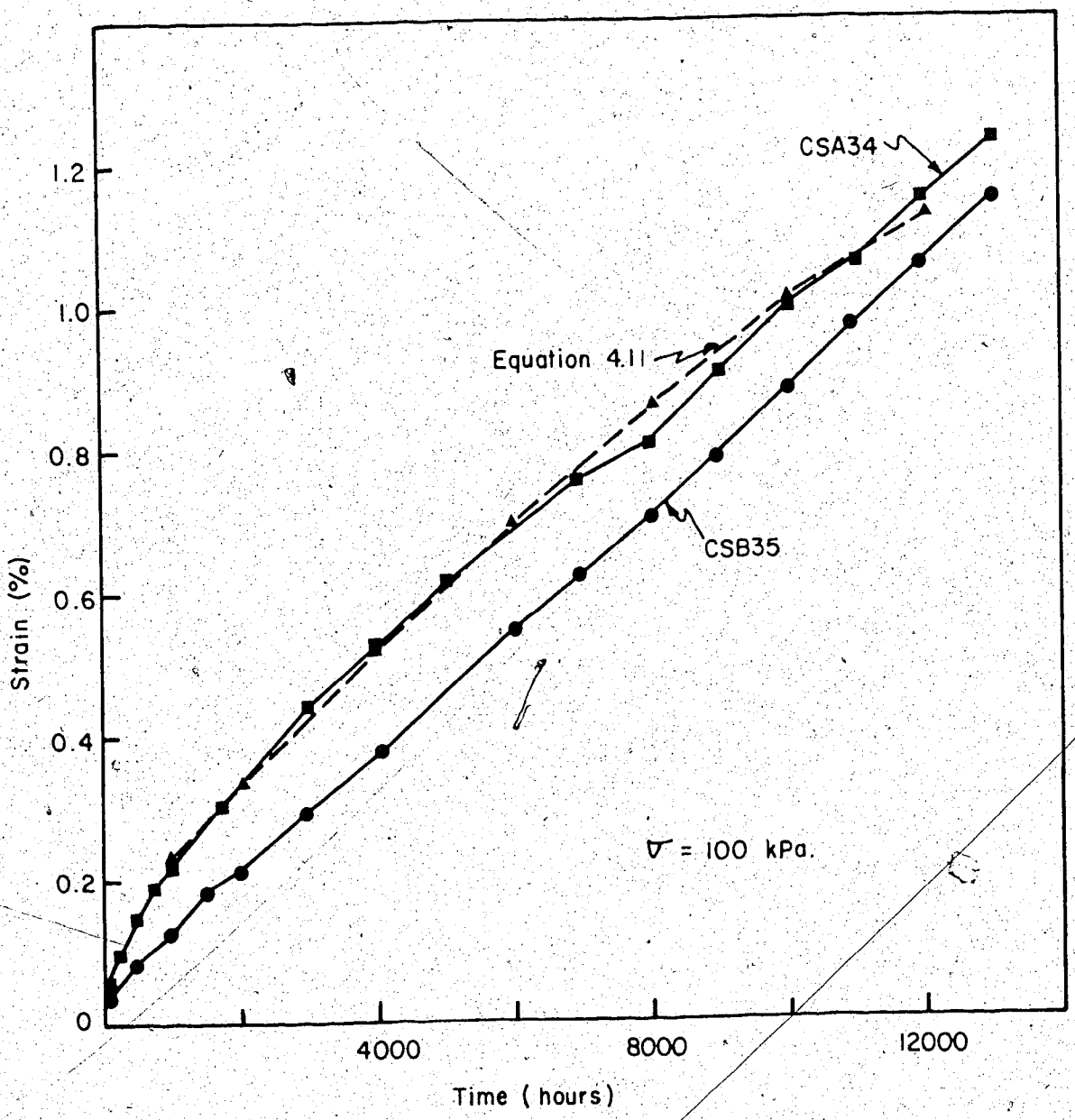

Figure 4.13 Comparison of Equation 4.11 and the strain-time data measured at a constant stress of 100 kPa.

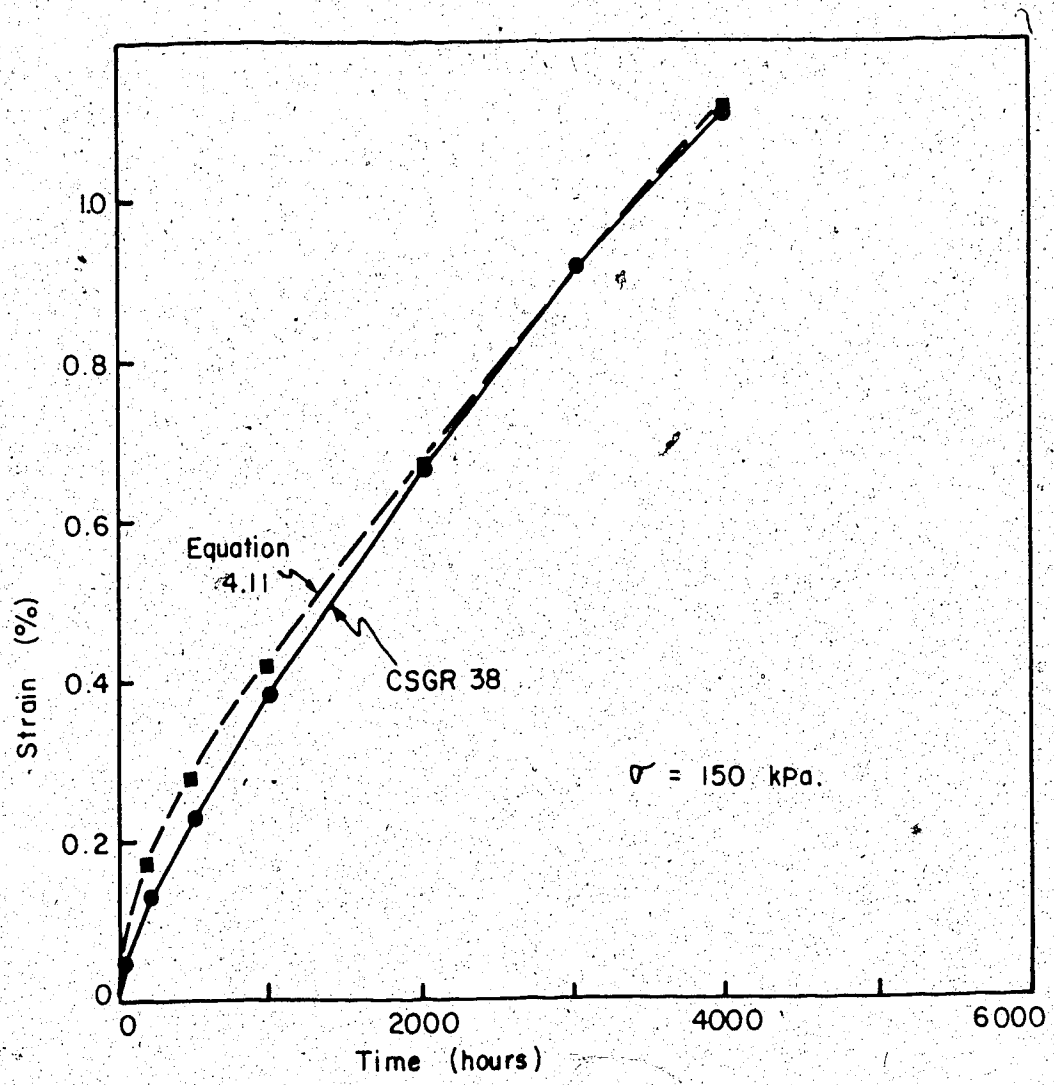

Figure 4.14 Comparison of Equation 4.11 and the strain-time data measured at a constant stress of 150 kPa.

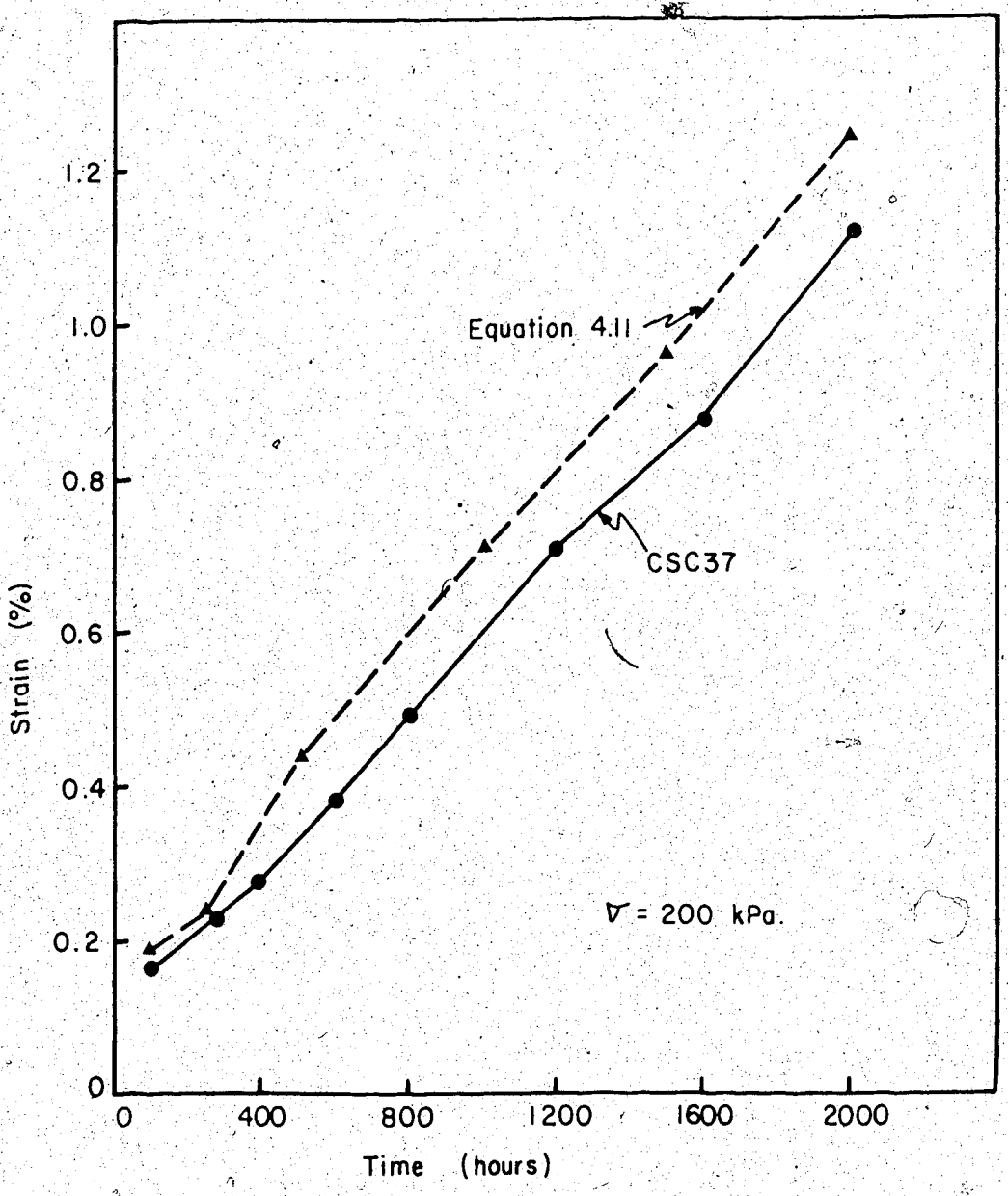

Figure 4.15 Comparison of Equation 4.11 and the strain-time data measured at a constant stress of 200 kPa.

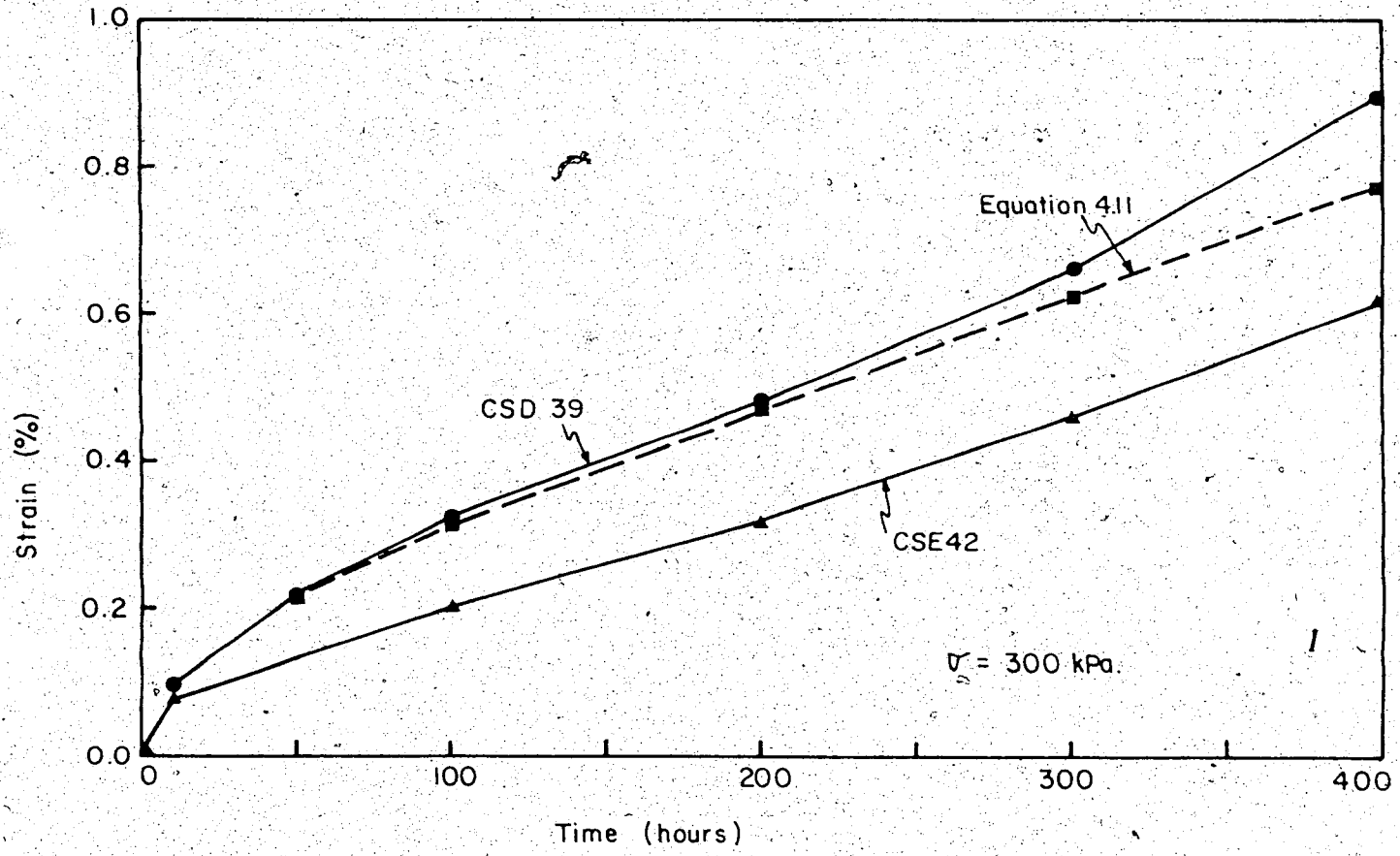

Figure 4.16 Comparison of Equation 4.11 and strain-time data measured at a constant stress of 300 kPa.

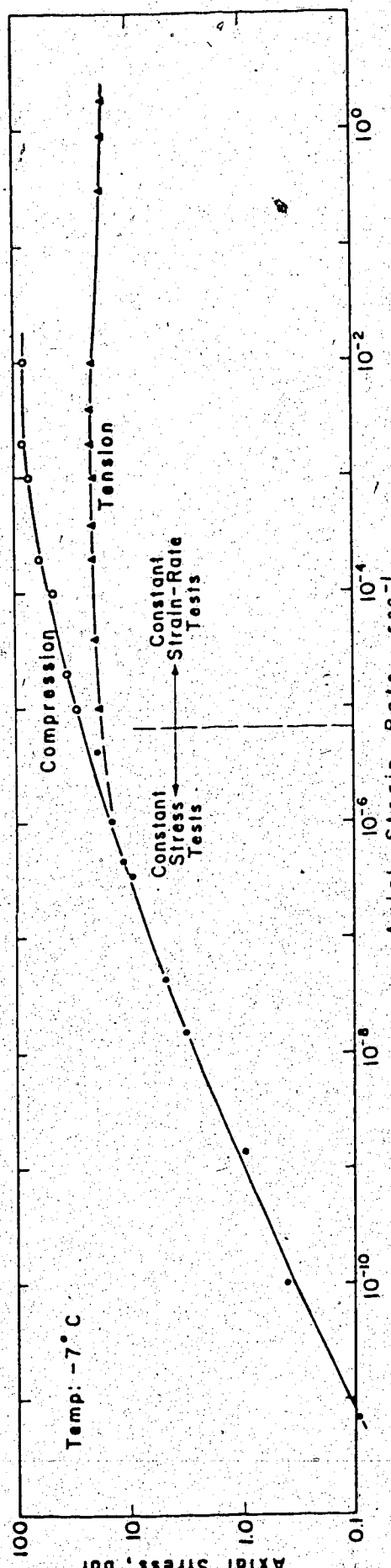

Figure 4.17 Axial stress versus axial strain reate for ice illustrating data in the ductile, transition and brittle zone.

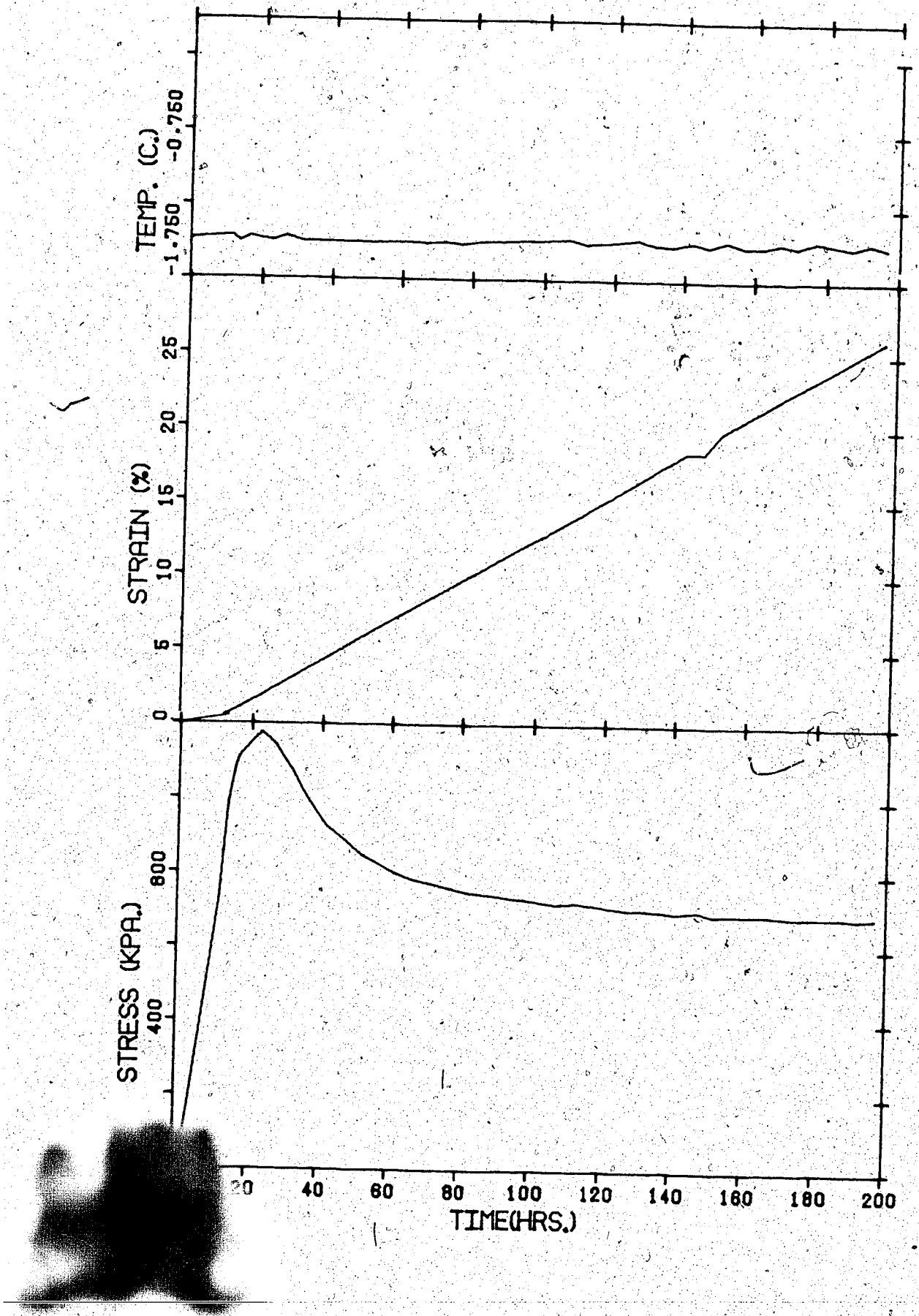

Figure 4.18 Data plot of constant strain rate sample UC48

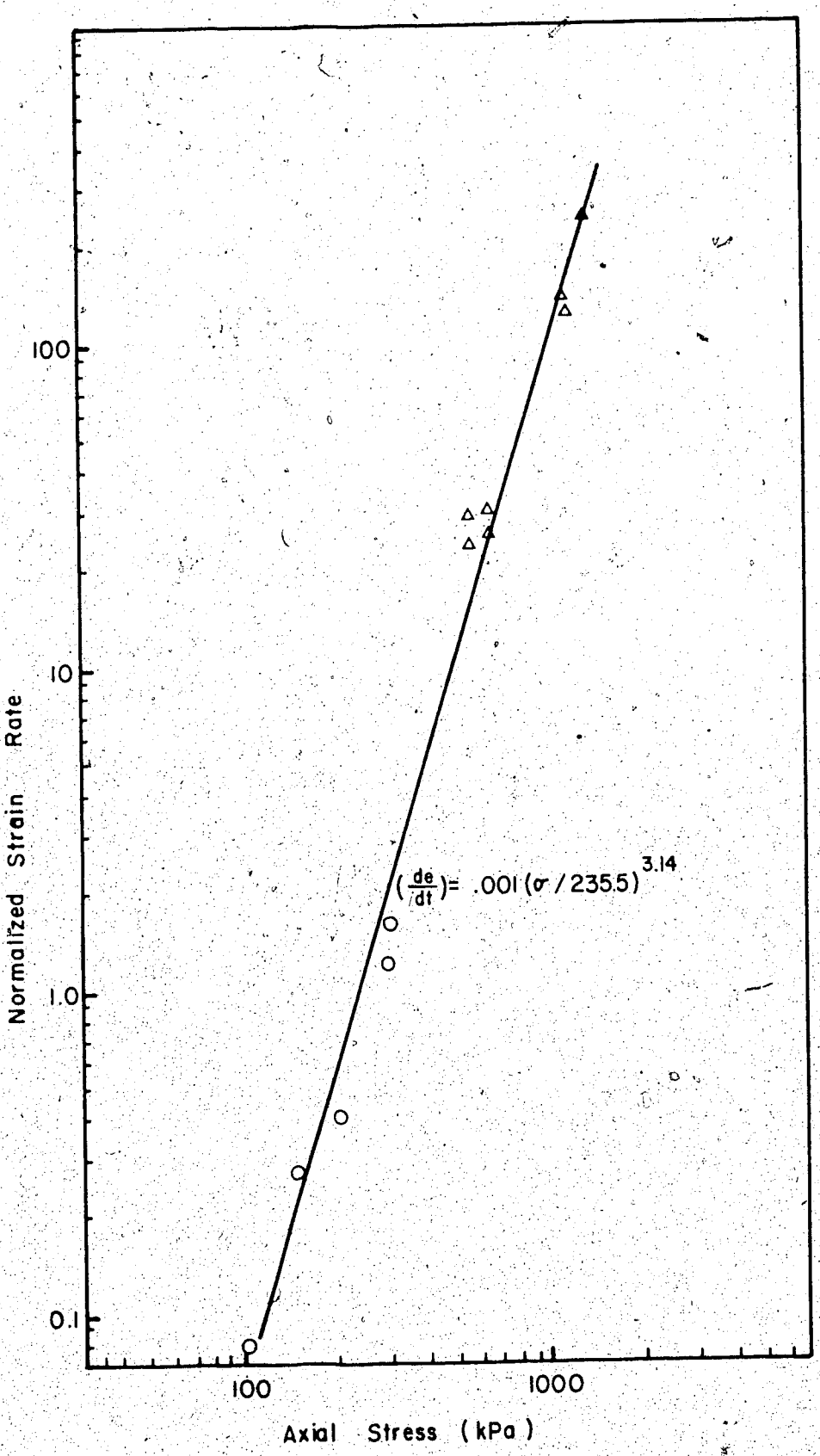

Figure 4.19 Normalized strain rate versus axial stress of combined constant stress and constant strain rate data.

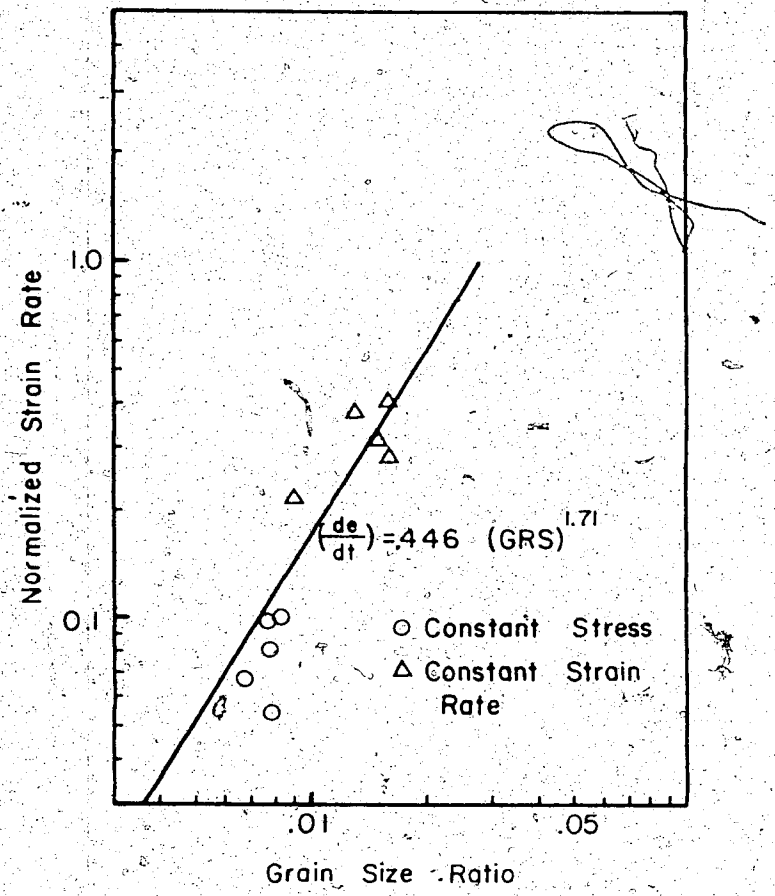

Figure 4.20 Normalized strain rate versus GSR.

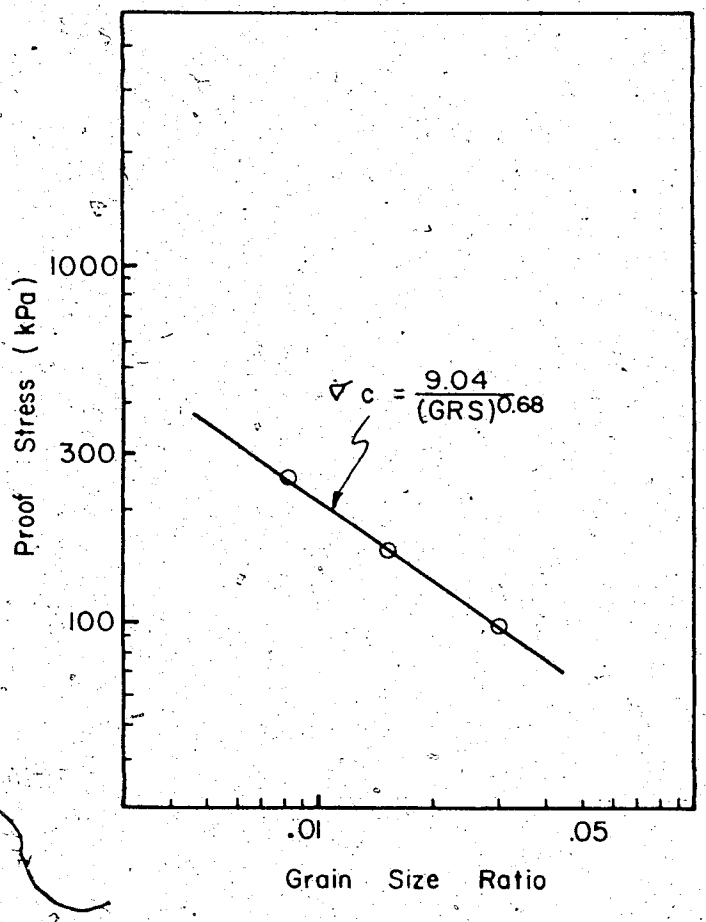

Figure 4.21 Proof stress versus GSR.

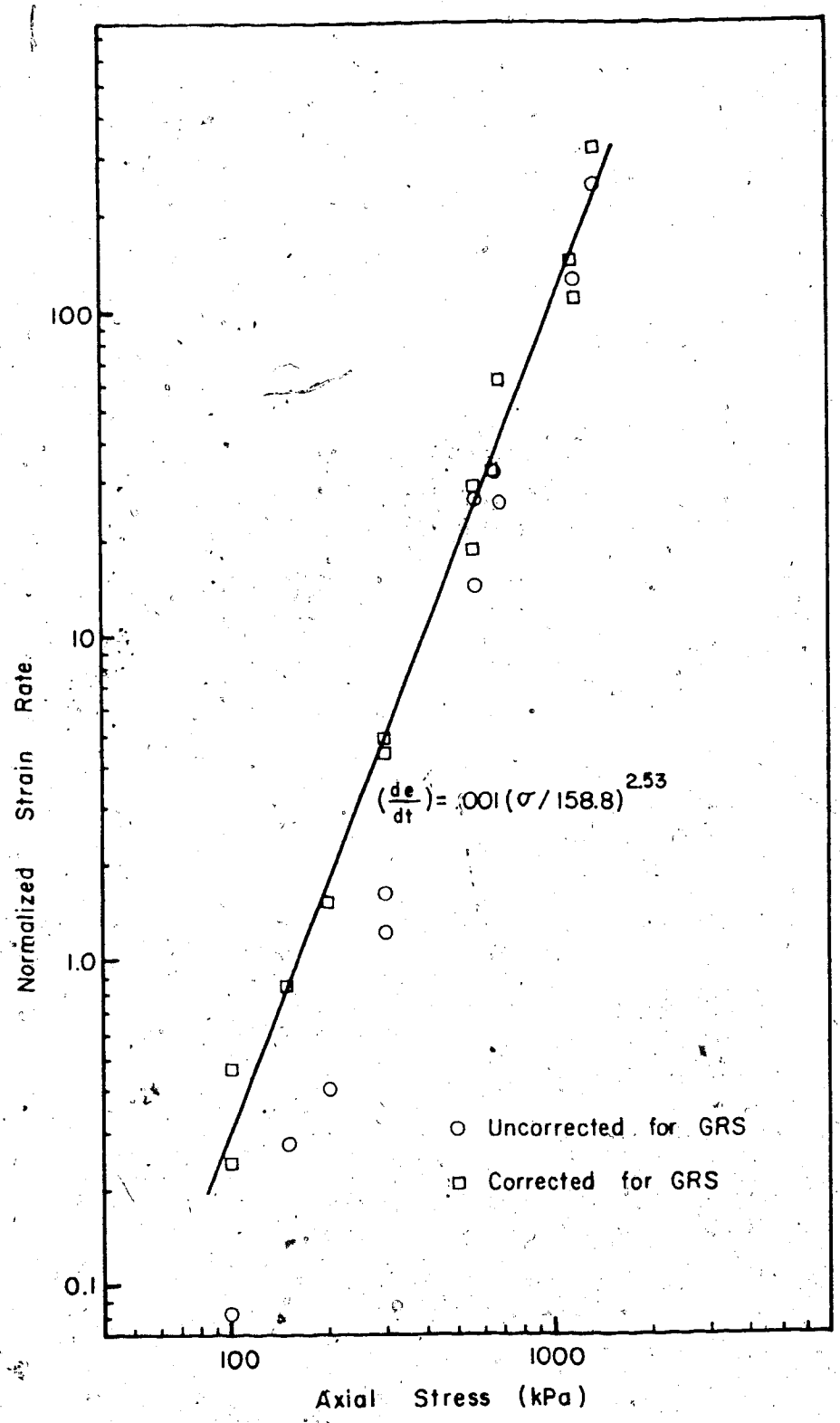

Figure 4.22 Normalizedstrain rate versus axial stress showing comparison of laboratory data corrected to GSR=0.015 and data not corrected.

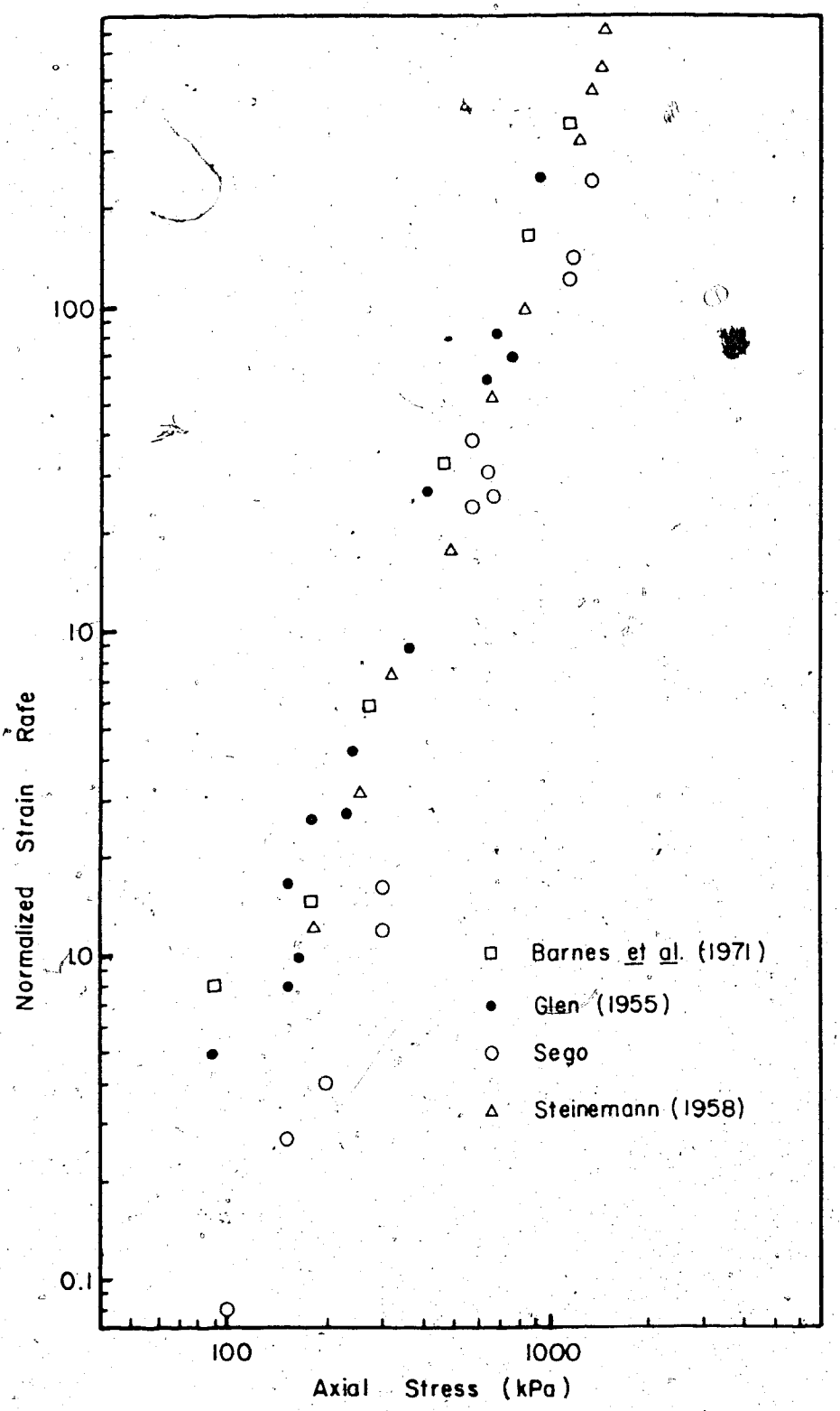

Figure 4.23 Normalizedstrain rate versus axial stress of laboratory data and data available from the ice literature.

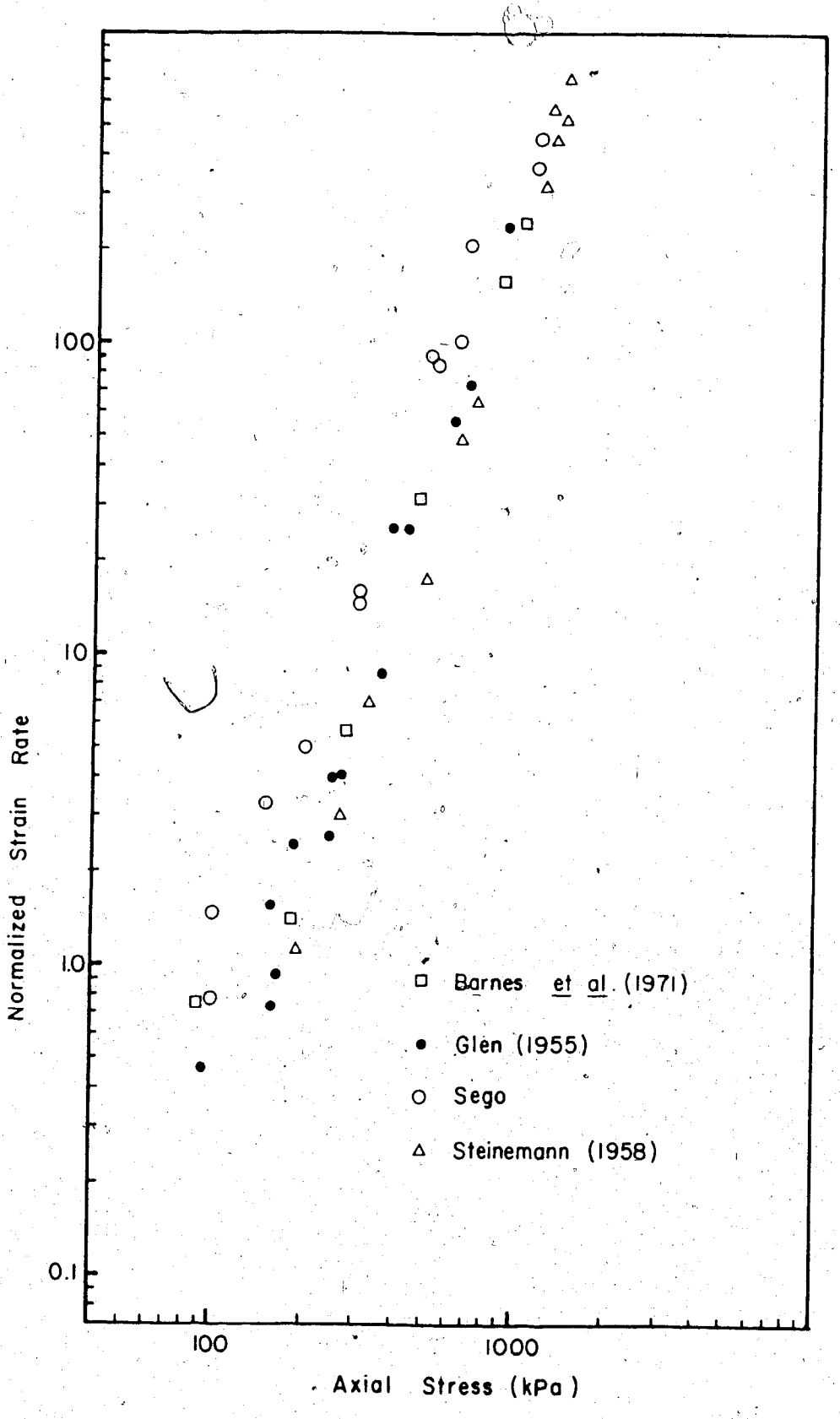

Figure 4.24 Normalizedstrain rate versus axial stress of laboratory data corrected to GSR=0.03 and data available from ice literature.

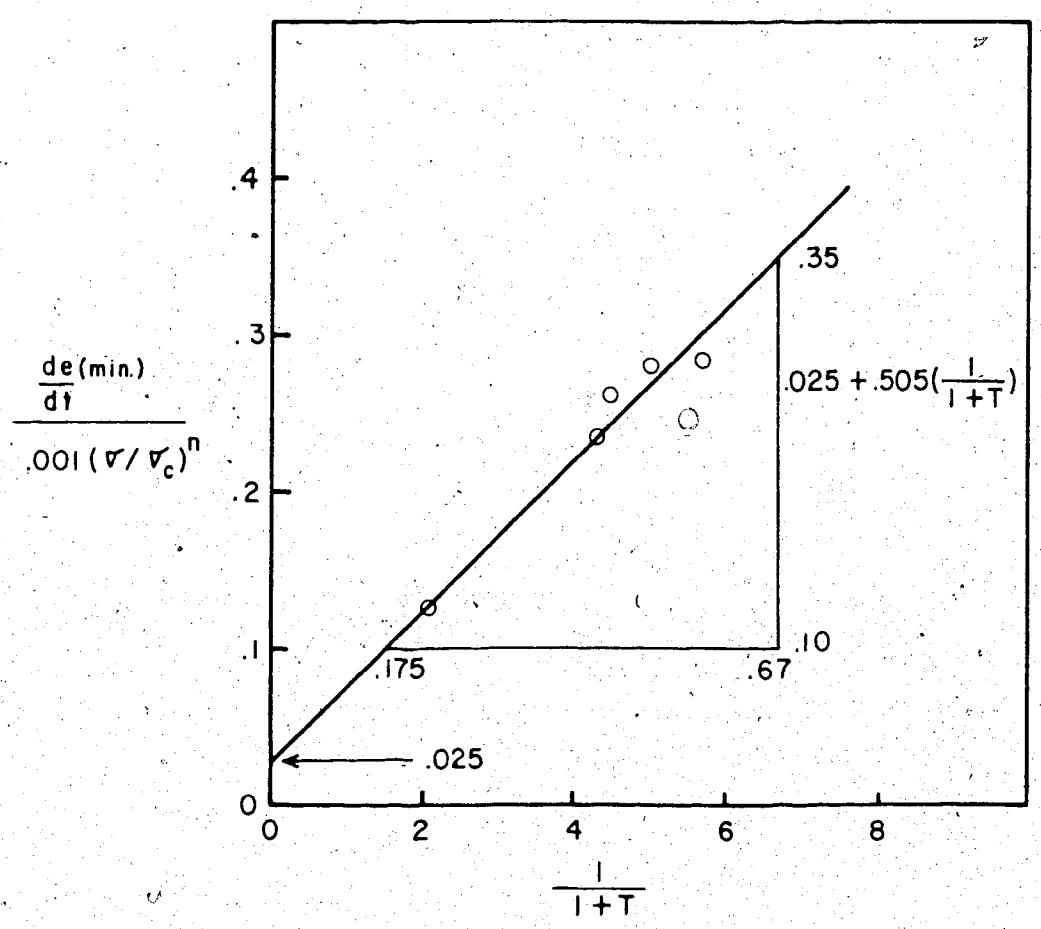

Figure 4.25 Normalize strain rate versus [1/1+T] at a constant stress of 300 kpa.

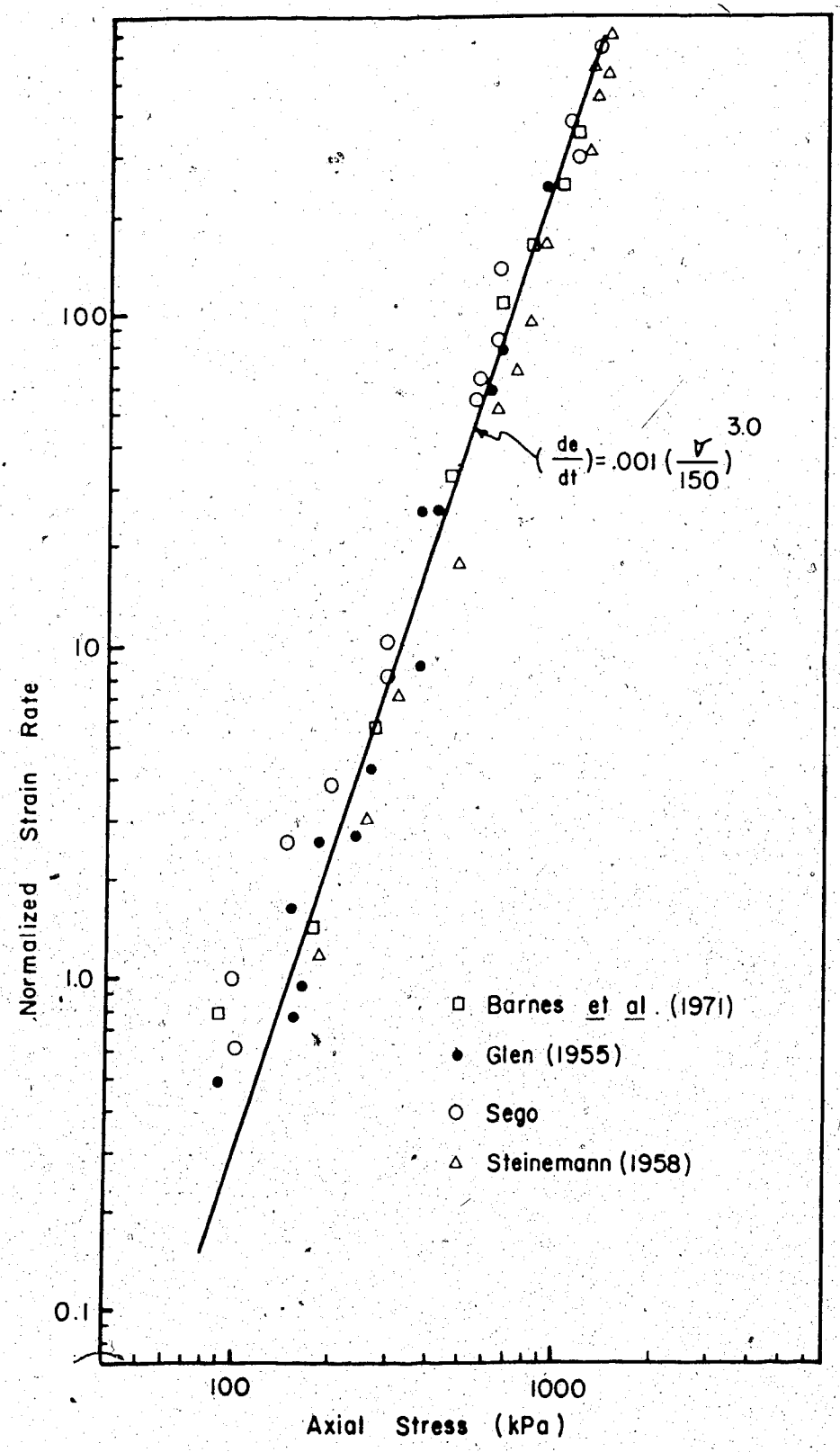

Figure 4.26 Normalize strain rate versus axial stress of laboratory data corrected to a GSR=0.03 and temperature equal to -2.0°C. and the data available from the ice literature.

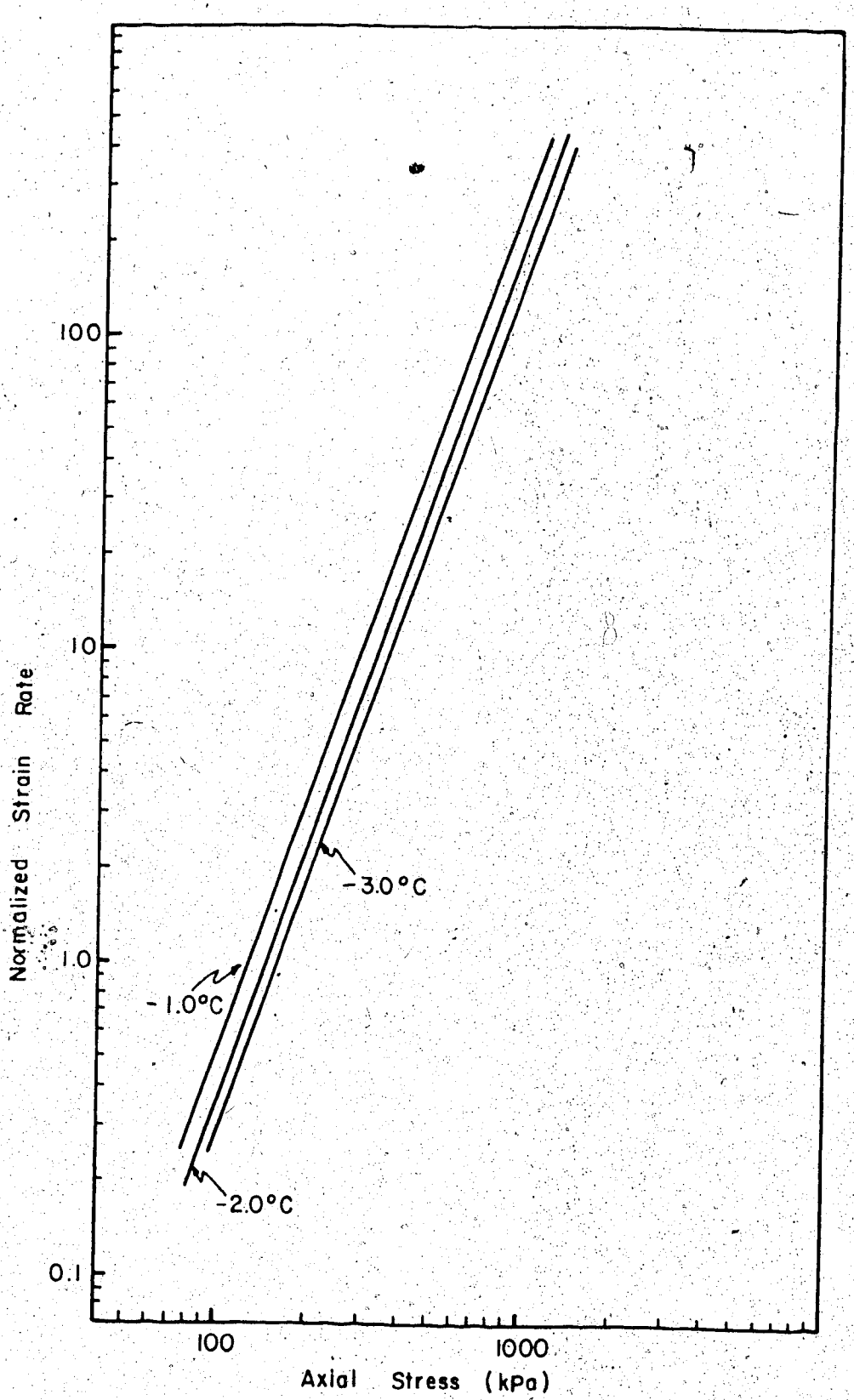

Figure 4.27 Normalizedstrain rate versus axial stress showing influence of temperature on the flow law of ice

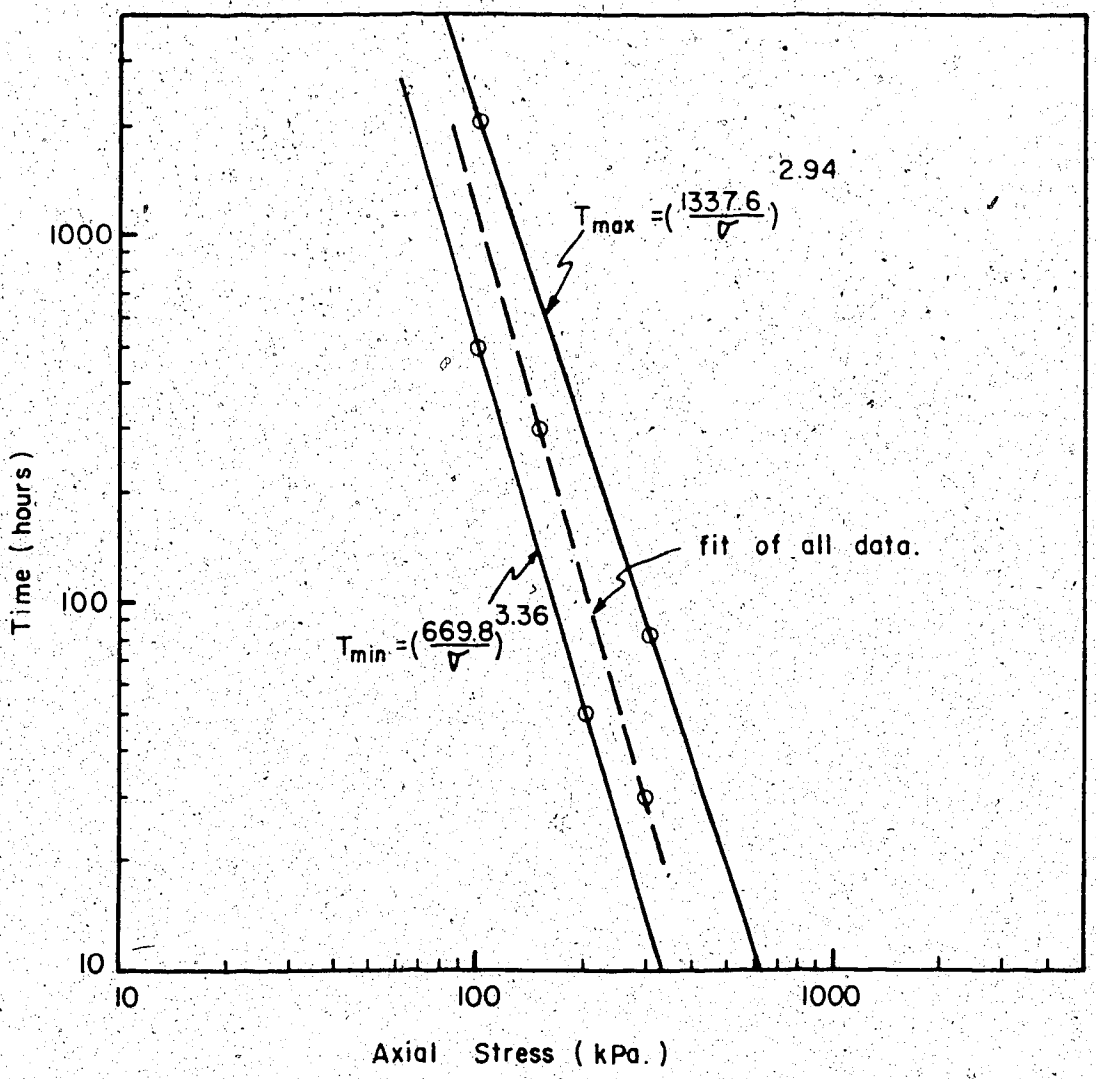

Figure 4.28 Time to minimum strain rate versus axial stress.

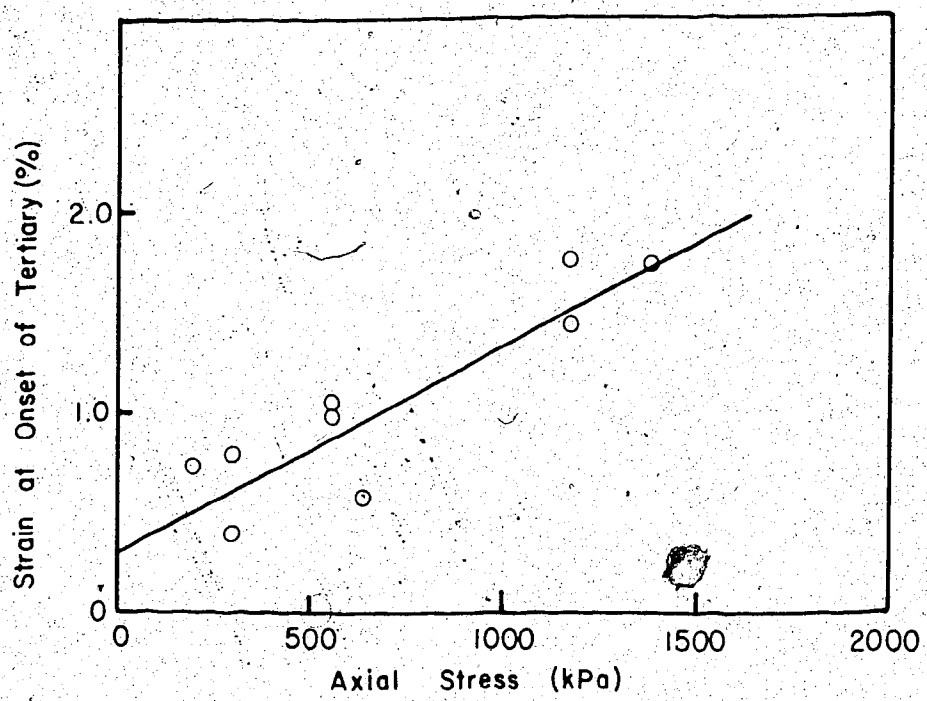

Figure 4.29 Axial strain at the onset of tertiary creep versus applied stress of laboratory data.

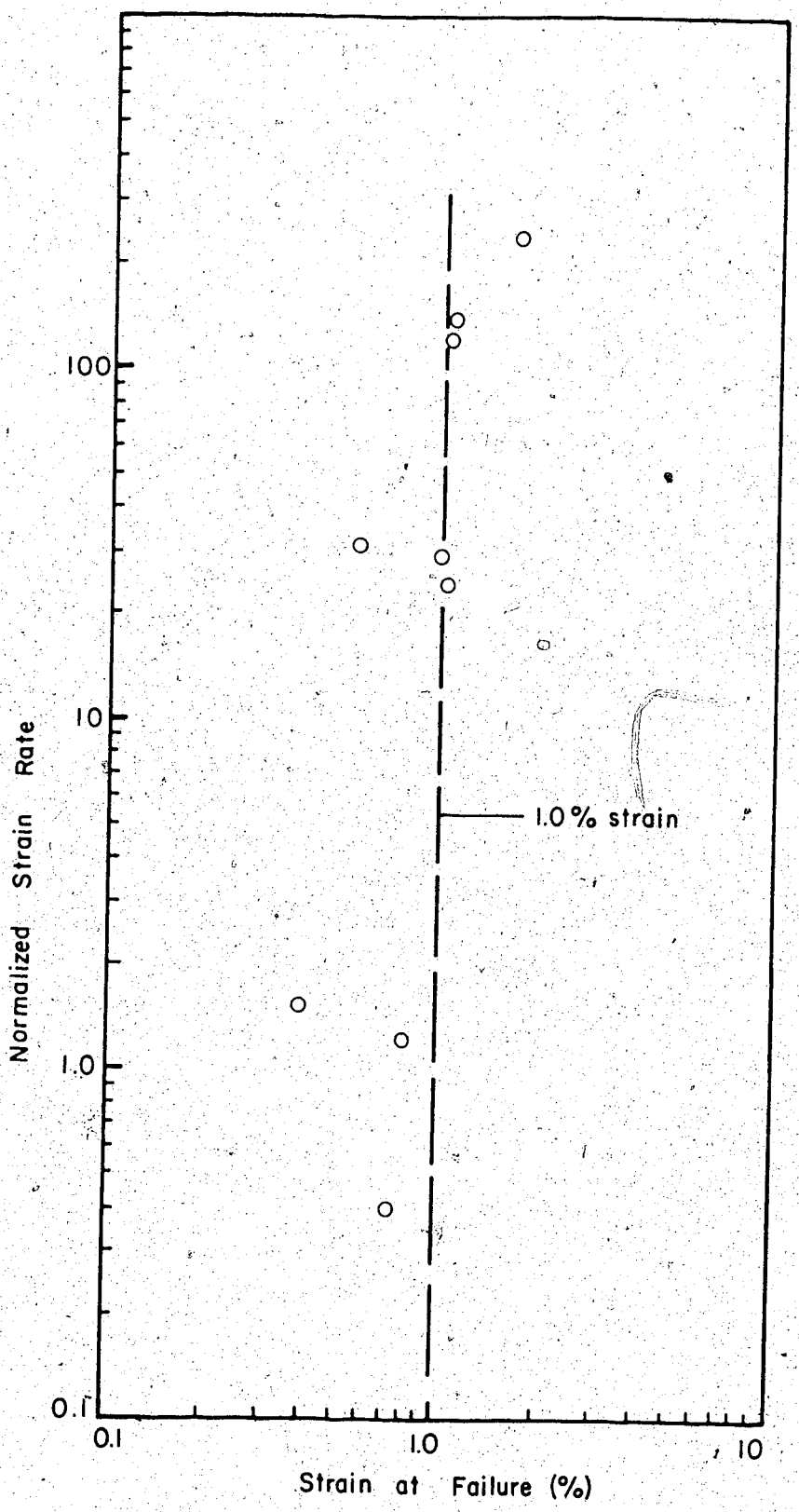

Figure 4.30 Normalize strain rate versus axial strain at the onset of tertiary creep of the laboratory data.

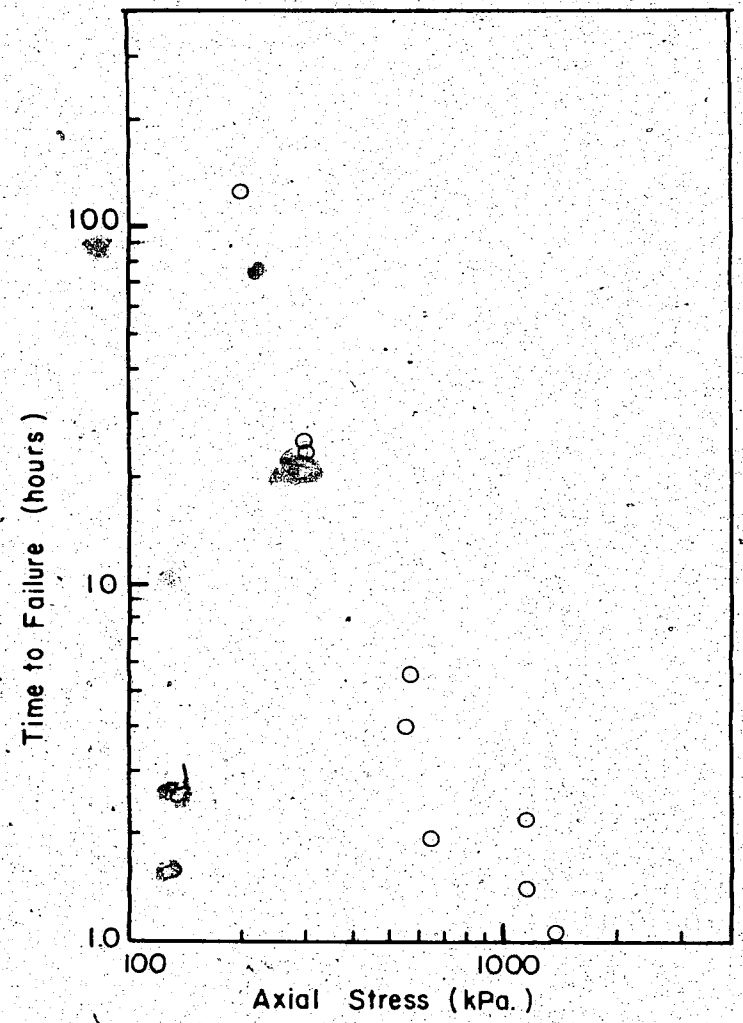

Figure 4.31: Measured time to failure versus axial stress for experimental laboratory data.

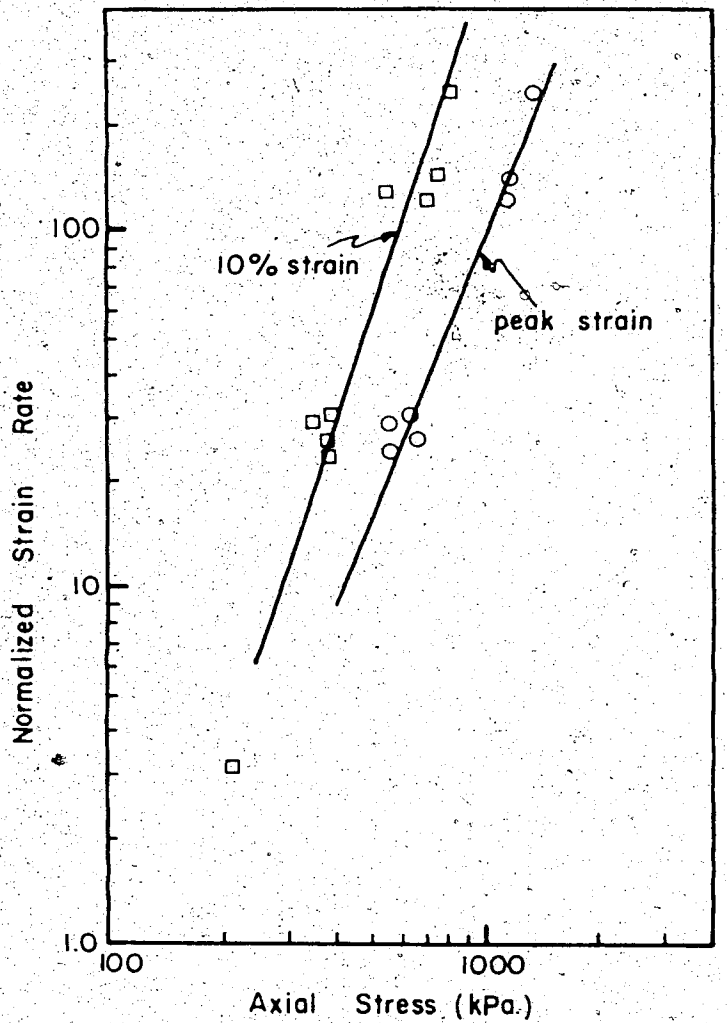

Figure 4.32: Normalized strain rate versus axial stress of laboratory data for both the condition of peak strain and at a total strain of 10%.

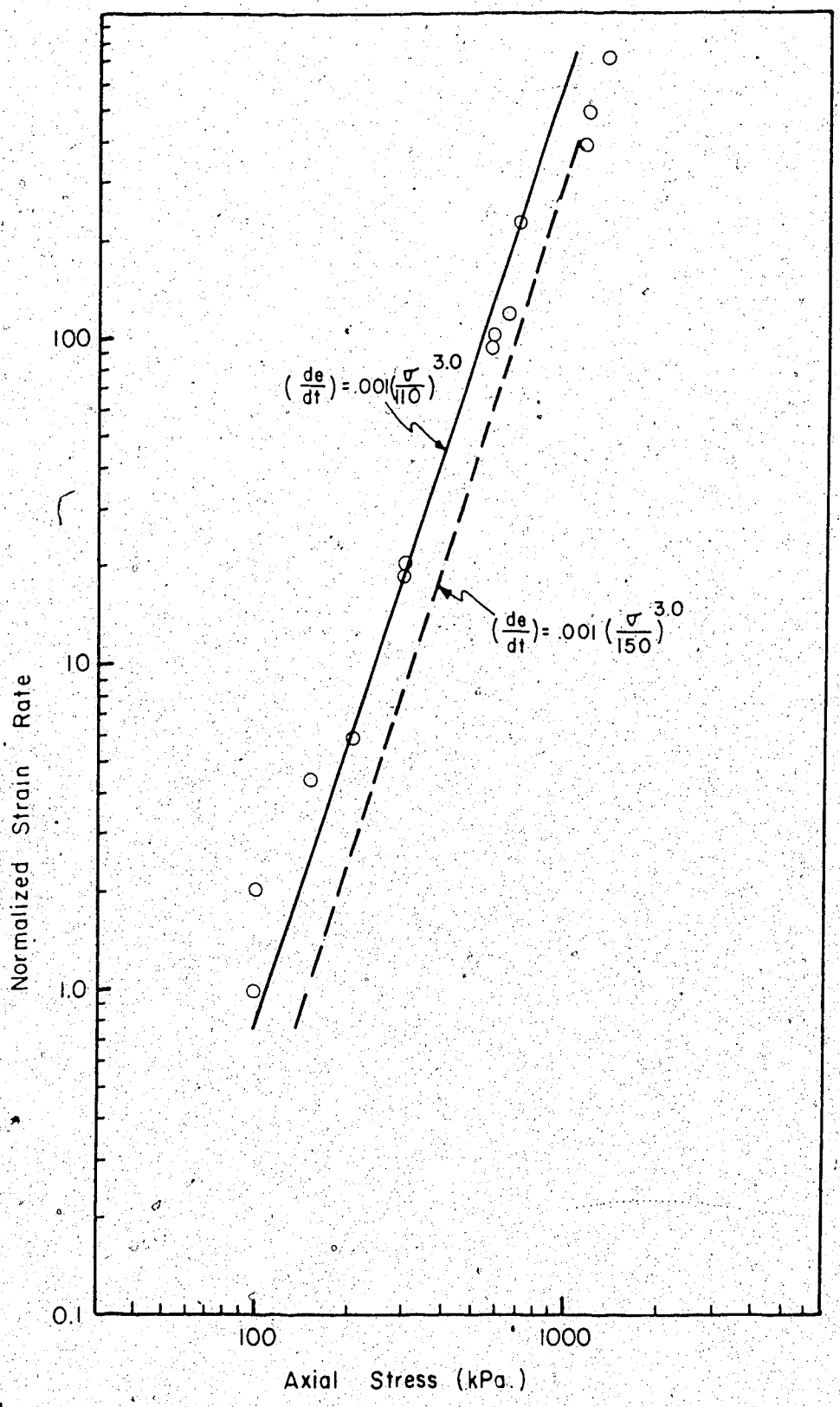

Figure 4.33 Normalized strain rate versus axial stress of laboratory data illustrating comparison of flow law with exponent equal to 3.0 and Equation 4.32.

CHAPTER 5

Analysis of Data under Complex Stress States

5.1 Introduction

In Chapter 4 the flow law of polycrystalline ice was established and the factors which influence this law were studied. The experimental data obtained in this study compared well with the laboratory experimental data reported in the literature for polycrystalline ice.

In this Chapter a technique which can be used to determine the parameters which describe the flow law of ice without having to conduct an extensive set of laboratory experiments will be examined. The method consists of penetrating a circular punch into an ice sample at a constant displacement rate while measuring the displacement and load acting on the punch.

The penetration of circular punches into ice has been used by various Russian authors such as Vialov et al. (1973) and Vyatkovskiy (1960) to examine foundation behaviour. In these studies, footings of various diameters were used to establish the influence of footing size on the deformation. A shortcoming in these studies has been the lack of development of a theory which relates the penetration of the circular foundation to the deformation behaviour of the ice. The authors also have not included the experimentally determined deformation law of the ice used during the research program. The lack of this information has hindered

the development of a consistent theory with which these results could be analysed.

In this Chapter a theory which combines the foundation material behaviour and punch penetration results will be outlined. The theory was developed after years of research work related to the penetration of punches into metals (Bishop et al. (1945), Hill (1950), and Hirst and Howse (1969)). The analysis has also been extended to the end bearing capacity of piles in soils (Gibson (1950), Skempton et al. (1953), Ladanyi (1959, and 1966) and Vesic (1972)). Each of these authors has used the expansion of a spherical cavity beneath the punch or pile to analyse their experimental results. Ladanyi and Johnston (1974) present the complete theory for analysing the behaviour of a circular punch penetrating into a material whose behaviour is governed by a flow law as follows:

$$[de/dt] = [de/dt]c\ (\delta/\delta c)\underline{n} \qquad (5.1)$$

In Chapter 4 it was shown that the flow law of the polycrystalline ice used in this research is governed by an equation which is similar to Equation 5.1. Thus the flow law of this research can be used with the theory of Ladanyi and Johnston (1974) to predict the punch resistance versus the penetration rate for a circular punch penetrating in polycrystalline ice. These experiments were conducted as part of the research program to evaluate the influence of a

complex stress state on the flow law of ice.

The results of a laboratory study of punch load and penetration rates will be presented and compared with the predicted behaviour using Ladanyi and Johnston's theory. The comparison will be discussed and the factors which may influence the data examined. It will be shown that the experimental results suggest that the theory applies to circular loaded punches near the surface as well as at depth. This finding is supported by data from Ladanyi and Paquin (1978). Their data showed no influence of increasing the depth of burial on the measured resistance in frozen sand. The applicability of the theory of expansion of a spherical cavity beneath a circular footing will also be illustrated using photographs of thin sections obtained from within the disturbed zone beneath the punch and remote from the disturbed zone.

5.2 Theory of expansion of a spherical cavity

The expansion of a spherical cavity beneath a deep circular punch was first used as a model of the penetration behaviour of a punch in metals by Bishop et al. (1945). This model was used since the complete solution of indentation of a hard punch into an elastic-plastic material is rather complex. The exact solution to this indentation problem has not been found, so the simplifying assumption of the cavity expansion is used to establish an approximate solution to the problem. This approximate solution is used to analyse

the results of experiments.

A recent study by Hirst and Howse (1969) related the material properties and the punch geometery to models which can be used to approximate the behaviour of the punch penetrating into a material. Their study (Figure 5.1) showed that the deformation behaviour beneath the punch and the method used to analyse the punch resistance was dependent on the material properties and the wedge angle of the punch. When a material had a high ratio of Young's Modulus to the yield stress (E/Y) for all wedge angles the plastic rigid model from Hill (1950) was applicable and the punch caused the material to yield plastically. As the (E/Y) ratio decreased and the punch became blunter the deformation pattern beneath the punch changed. The material beneath the punch under this condition compresses and forms a radial compression zone (Mulhearn (1959)). The material no longer yielded as a rigid plastic material and under the new condition a cavity expansion model predicted the resistance of the punch. As the (E/Y) ratio decreased and the material behaved more as an elastic material, the cavity model no longer was valid. This change in behaviour resulted from the fact that the elastic materials sustained little permanent deformation when loaded by a punch. The findings of Hirst and Howes (1969) suggest that the use of a cavity expansion model to analyse the penetration of a flat punch into ice is valid since it has a ratio of (E/Y) between 500 and 2000 (Hawkes and Mellor (1972)).

material properties and the punch geometry to models which can be used to approximate the behaviour of the punch penetrating into a material. Their study (Figure 5.1) showed that the deformation behaviour beneath the punch and the method used to analyse the punch resistance was dependent on the material properties and the wedge angle of the punch. When a material had a high ratio of Young's Modulus to the yield stress (E/Y) for all wedge angles the plastic rigid model from Hill (1950) was applicable and the punch caused the material to yield plastically. As the (E/Y) ratio decreased and the punch became blunter the deformation pattern beneath the punch changed. The material beneath the punch under this condition compresses and forms a radial compression zone (Mulhearn (1959)). The material no longer yielded as a rigid plastic material and under the new condition a cavity expansion model predicted the resistance of the punch. As the (E/Y) ratio decreased and the material behaved more as an elastic material, the cavity model no longer was valid. This change in behaviour resulted from the fact that the elastic materials sustained little permanent deformation when loaded by a punch. The findings of Hirst and Howes (1969) suggest that the use of a cavity expansion model to analyse the penetration of a flat punch into ice is valid since it has a ratio of (E/Y) between 500 and 2000 (Hawkes and Mellor (1972)).

pi = pressure required to expand a cavity in the material

q = pressure applied to the punch to penetrate the material

c = time-dependent strength of ice

ϕ = angle of cone of ice beneath punch

Z = parameter which relates punch displacement to the soil strength mobilized.

The location and direction at which each pressure within the model of a punch penetrating ice is illustrated in Figure 5.2. In Equation 5.2 the pressure applied to a punch (q) just causes the ice to fail under the cavity pressure (pi). In this study the punch displacements are large hence Equation 5.2 will be valid and may be used to relate the applied punch pressure to the pressure required to expand the cavity within the ice.

Ladanyi and Johnston (1974) have presented the theory used to develop the expansion of a cavity in a frictionless material. They used Hoff's analogue (Hoff (1954)) to justify analysing a non-linear creep problem as a non-linear elasticity problem in their development. The use of this analogue permitted the authors to develop a solution which gives the rate of cavity expansion under a constant applied internal pressure within the cavity. This relationship is then used to relate the settlement of a punch to the volume change of an expanding spherical cavity. The solution is

based on the following assumptions:

1. the material is homogeneous;
2. the material is initially isotropic;
3. the initial isotropic stress tensor (po) exists within the material.
4. volume strains are negligible; and,
5. temperature and time-dependent behaviour of material can be represented using a flow law as given in Equation 5.1.

The presentation of Ladanyi and Johnston (1974) is detailed and need not be repeated here. Only those equations which are required to determine the rate of punch settlement in terms of the cavity expansion will be presented.

The settlement rate of the circular punch is related to the displacement rate of the cavity by:

$$[ds/dt]/B = (1/3)\bullet[1 - [du/dt]i/ri]^{-3} - 1) \qquad (5.3)$$

where

[ds/dt] = settlement rate of the punch

B = diameter of the circular punch.

[du/dt]i = displacement rate at the boundary of the spherical cavity.

ri = radius of spherical cavity at which the internal pressure pi is applied.

The displacement rate of the boundary of the spherical cavity is related to the pressure in the cavity and within

the material during the cavity expansion by:

$$[du/dt]i/ri = [de/dt]c(1/2)[(pi-po)/(2n\sigma c/3)]^{\underline{n}} \qquad (5.4)$$

where

$[de/dt]c$ = proof strain rate from the flow law of material

σc = proof stress from flow law of material

n = exponent from flow law of material

pi = internal pressure in spherical cavity

po = initial stress tensor in material.

Equation 5.3 reduces to the following under the condition of small radial displacement rates expected in the experiments:

$$[ds/dt]/B = ([du/dt]i)/(ri) \qquad (5.5)$$

Substituting Equation 5.4 in Equation 5.5, the following relationship is obtained for the settlement rate in terms of the pressure required to expand the cavity:

$$[ds/dt]/B = [de/dt]c(1/2)[3(pi-po)/2n\sigma c]^{\underline{n}} \qquad (5.6)$$

If Equation 5.2 is substituted in Equation 5.6, the relationship for the settlement rate in terms of the applied pressure to the footing, material parameters, and initial stress conditions within the material is as follows:

$$[ds/dt]/B = [de/dt]c(1/2)(3/2n\delta c)\underline{n}[q-Z\bullet c\bullet\cot(\phi)-po]\underline{n} \quad (5.7a)$$

Each term in Equation 5.7a has been defined in the previous equations and they had the same meaning as used in Equation 5.1 through Equation 5.6. Equation 5.7a can be simplified for use in this research since for this material $\phi=45^{\circ}$, $Z=1$ due to displacement of the punch, and of $po = 0$ in the experiments. The equation which results from these simpifications is as follows:

$$[ds/dt]/B = [de/dt]c(1/2)(3/2n\delta c)\underline{n}[q-1\bullet c]\underline{n} \quad (5.7b)$$

Equation 5.7b allows the settlement rate of a circular punch to be predicted in terms of the pressure applied to the punch provided the flow law of the ice is known.

5.3 Material properties required to predict punch data

To predict the punch settlement versus applied pressure relationships, the appropriate material properties are required. Ladanyi (1976) discussed the problem of determining an appropriate time to failure of an element of material located beneath the circular punch. In ice, the time to failure is dependent on the stress applied to the sample. Figure 4.31 demonstrates that the material properties which are appropriate for the loading conditions of the ice must be selected in order to model the ice

behaviour. Ladanyi (1976) defined the time to failure of an element of ice below the punch as the time required to increase the strain acting on this element from a negligible value to the failure strain of ice. He presented the following relationship for the time to failure of the element of ice below the punch:

$$tf = 0.5([e^{00}]^{-0.33} - 1)(SHf)^{-0.33}\{B/[ds/dt]\} \qquad (5.8)$$

where

tf = time to failure

e^{00} = usually 1% of failure

SHf = shear strain at failure in compression experiment

B = diameter of punch

ds/dt = settlement rate of punch.

He then presents the average strain rate of the ice beneath the punch as follows:

$$[dE/dt]av = \{[Ef](tri)\}/tf \qquad (5.9)$$

where

[dE/dt]av= average strain rate beneath punch

Ef(tri) = failure strain under triaxial loading.

tf = time to failure

Equation 5.9 gives the strain rate within the ice beneath the punch. The flow law to be used in analysing the punch

data must be the flow law at the strain rate which is applied to the ice beneath the punch. This will be discussed in Section 5.5 in which the analysis of the data is presented.

5.4 Laboratory punch data

The experimental procedure used to determine the punch data reported in this research has been discussed in Section 3.4.4. Figure 5.3 contains a typical plot of the punch resistance versus time for one of the experiments conducted during this research. The temperature measured at the mid-height of the sample is also shown in Figure 5.3 to illustrate the temperature control achieved. Similar plots for each experiment conducted during this research are contained in Appendix A.

Table 5.1 summarizes the results of the punch experiments and includes the peak punch resistance and the asymptotic resistance for each experiment. The peak punch resistance and asymptotic data from Table 5.1 are plotted versus the punch settlement rate in Figure 5.4. Each set of the laboratory data plotted in Figure 5.4 had a linear regression analysis performed on the data to establish the best fit straight line through the data. The resulting relationship between the peak punch resistance and the settlement rate is

$$[ds/dt]/[ds/dt]c = (q/2300.)^{3.31}; \qquad (5.10)$$

While the best fit relationship through the asymptotic punch data is

$$[ds/dt]/[ds/dt]c = (q/1936.)^{3.31}; \qquad (5.11)$$

where

[ds/dt] = punch settlement rate (cm/hr.)

[ds/dt]c = proof displacement rate of (.001 cm/hr).

q = punch resistance measured, (kPa.)

The exponent of the simple power law which is the best fit through each set of data is 3.31 and hence the best fit lines through each set of data are parallel.

Ladanyi (1976) presents the relationship between the normalized settlement rate of a deep circular punch and the normalized punch resistance as:

$$([ds/dt]/[ds/dt]c) = (q/qc)^{n} \qquad (5.12)$$

where

qc = proof punch resistance

n = exponent of settlement rate versus punch resistance relationship

The exponent n is the exponent which relates the stress to the strain rate from the flow law of the material into which the punch is penetrating. Throughout the thesis the results of the punch experiments will be presented in a form similar

to Equation 5.12. This presentation will be used in order to maintain a consistant presentation of punch data results in the literature.

5.5 Analysis of punch data using laboratory determined flow law

In this section the laboratory determined relationship of the punch data will be predicted using the theoretical relationship from Section 5.2 combined with the flow law for ice established in Chapter IV. Equation 5.7b gives the punch resistance using the expansion of a spherical cavity model in terms of the punch settlement rate.

To determine the theoretical relationship between the applied pressure on the punch and its settlement rate the following material properties are required from Chapter 4:

1. The axial failure strain of uniaxial compression creep experiments from which the shear strain at failure can be evaluated (Figure 4.27).
2. The flow law for polycrystalline ice (Equation 4.19).

The data from 1 and 2 above was used in Equation 5.8 to calculate the time to failure of an element of ice beneath the punch. Equation 5.9 was then used to calculate an average strain rate within the ice. This information was substituted into Equation 5.7 (Ladanyi and Paquin (1978)) to obtain the following theoretical relationship between punch resistance and settlement rate:

$$[ds/dt]/[ds/dt]c = (q/1713)^{2.53} \quad (5.13)$$

Equation 5.13 has been plotted on Figure 5.4 for comparison with the measured laboratory punch data and Equations 5.10 and 5.11. It is seen that Equation 5.13 underestimates the punch resistance of the ice at normalized settlement rate below 2. Above this settlement rate, the theoretical relationship given by Equation 5.13 will slightly overestimate the measured punch resistance. The difference between Equation 5.10 and 5.13 is in the proof punch pressure (qc) and the exponent n hence each of these will be examined to establish its influence on the results.

First, the influence of the exponent n on the data will be examined. The exponent n equal to 3.31 was determined from a regression analysis through the actual laboratory data and it is the best fit to the limited experimental data. In many creep studies conducted on polycrystalline ice, the exponent n has been evaluated as equal to 3.0 (Glen (1975)). In Figure 5.5 the experimental punch data and a straight line which has a slope equal to 3.0 have been fitted to the laboratory data. The following relationship is plotted in Figure 5.5 and compared with the experimental data:

$$[ds/dt]/[ds/dt]c = (q/2300)^{3.00} \quad (5.14)$$

Equation 5.14 fits the data at the slow normalized settlement rate but underestimates the laboratory data at the fast normalized settlement rate. Thus, in order to fit the actual punch data at both the slow and fast settlement rate, the proof punch pressure would have to be varied. This is shown by Equation 5.15 plotted in Figure 5.5 which is defined by

$$[ds/dt]/[ds/dt]c = (q/1900)^{3.00} \qquad (5.15)$$

Equation 5.15 gives a close fit to the experimental punch data at both the slow and fast normalized settlement rates and thus is a better fit to the data than Equation 5.14. Equation 5.15 also compares favourably with the theoretically predicted punch resistance versus punch settlement relationship shown as a dashed line in Figure 5.5. The theoretical relationship is given by Equation 5.13.

Figure 5.5 illustrates that the theoretical relationship between the punch resistance and the normalized punch settlement rate, predicts a lower punch resistance value than the laboratory measured resistance of the punch at each normalized settlement rate. This behaviour is unexpected from the assumptions used in determining the theoretical relationship between the expansion of a spherical cavity and the punching resistance. In the theoretical analysis, it was assumed that the expanding

spherical cavity was restrained completely within an undeformed ice body which would predict a higher punch resistance for a deeply embedded punch than a punch near the surface. The higher punch resistance for the deeply embedded punch results because the ice into which it is penetrating is confined and thus should increase its resistance. The data in Figure 5.5 show the opposite behaviour.

Figure 5.6 shows the influence of punch resistance versus depth of embedment as predicted using a purely cohesive material and the bearing capacity relationship presented by Brinch Hansen (1961). This relationship of Brinch Hansen was developed for a rigid plastic material using plasticity theory to predict the capacity of punch at the surface. The influence of the embedment was then added to this. The theoretical resistance of a deep punch using the expansion of a spherical cavity as a model is also included in Figure 5.6 for comparison. As expected, it predicts a higher resistance than the bearing capacity relationship at all values of depth ratios. This finding of a higher theoretical punch resistance than the resistance predicted by a bearing capacity relationship has important implications for the experimental results.

As the punch experiments at a given applied pressure gave a lower settlement rate than predicted by the cavity expansion model, this would imply that the ice used in the punching experiments was stiffer than the ice used in the creep experiments. Equation 5.13 compared to Equation 5.15

illustrates this. If the ice is the same, some other aspect of the experiment is causing the ice in the punch experiments to behave in a stiffer manner than in the creep experiments. Since this difference cannot be due to the ice, the difference must be associated with the loading applied to the ice or the experimental method.

To examine the influence of loading of the ice during the punching experiment, recall that in Section 4.6.3 the influence of the grain size ratio on the deformation of polycrystalline ice was established. The grain size ratio was defined as the ratio of the average grain diameter to the sample diameter. Figure 4.21 showed that as the ratio decreased at a given applied stress the ice behaves as a stiffer material. The influence of the grain size ratio must be included in the flow law of ice used to predict the experimental punch data. To do this requires that the appropriate grain size ratio be established for the ice during the punch penetration.

A method of determining the grain size ratio in a punching experiment must be established. During the penetration of a punch into the ice a hemispherical cavity expands outward in front of the penetrating punch (Figure 5.2). In the uniaxial compression experiment, the grain size ratio was calculated by dividing the grain diameter by the sample diameter. During the punch experiment, a hemispherical surface applies the load to the ice as the punch advances. Therefore, to compare the punch experiments

with the uniaxial compression experiments, the circumference of the hemisphere must be used in place of the diameter in the uniaxial compression experiment to establish the grain size ratio. The punch samples had an average grain size of 1.1 mm, which produced a grain size ratio of 0.018. To compare the measured and theoretical punch resistance, the flow law of ice must be corrected to this grain size ratio.

The flow law for the ice given by Equation 4.19 was determined at a grain size ratio of 0.030. To correct this data to 0.018, Equation 4.20 must be used to adjust the proof stress to this grain size ratio. Using this relationship to correct Equation 4.19 results in the following flow law:

$$[de/dt = .001 (5/221)^{2.53} \qquad (5.16)$$

The theoretical settlement rate versus punch resistance relationship using the flow law described by Equation 5.16 instead of Equation 4.19 is:

$$[ds/dt]/[ds/dt]c = (q/2380)^{2.53} \qquad (5.17)$$

The theoretical punch resistance now predicts a higher resistance at a given settlement rate when compared to Equation 5.13. This is to be expected because the flow law for a grain size ratio of 0.018 has a higher proof stress and would behave in a stiffer manner than if the grain size

ratio were 0.03.

Equation 5.16 is the flow law for ice at a temperature of -2.0°C. The influence of the temperature on the punch resistance must now be examined to account for the variation between Equation 5.17 and Equation 5.10.

5.5.1 Temperature influence on laboratory punch data

The influence of temperature on the tip resistance measured during the punching experiments was studied only over a small temperature range. During the punching experiment on Sample P25, the test temperature was varied to establish the influence of small temperature changes. The asymptotic punch resistance at three different temperatures from this experiment are plotted in Figure 5.7. This data illustrates that the punch resistance is linearly related to the temperature between -0.5°C and -1.3°C. A decrease in the test temperature of 1°C results in an increase in the punch resistance of 180 kPa according to this data. Using this information, the experimental punch resistance data has been corrected to a test temperature of -2.0°C. At this temperature the theoretical punch resistance calculated using the flow law established at -2.0°C (Equation 5.16) and the measured punch resistance corrected to -2.0°C can be compared.

The punch data corrected to a temperature of -2.0°C and the theoretical punch resistance given by equation 5.17 are plotted in Figure 5.8. Equation 5.17 agrees favourably with

the actual experimental punch data and illustrates that the expansion of the spherical cavity models the punch data well, provided the flow law for ice is known. Its use to relate the resistance of circular punches to the flow law of the ice is therefore valid.

5.5.2 Analysis of asymptotic punch resistance

In the previous discussion of the analysis of punch resistance using the expansion of a spherical cavity, only the punching data measured at the peak of the punch versus displacement curve has been analysed. In this section the analysis of an asymptotic punch data is examined.

Figure 5.3 presents the plot of the punch resistance versus the time. As pointed out in Section 5.4, the resistance to the punch penetration beyond the peak decreases to a certain value called the asymptotic resistance. The drop in resistance of the punch is due to changes occurring within the ice crystals stressed beyond the peak resistance. Plate 5.1 shows the disturbance of the ice structure directly below the punch after loading. This thin section was taken within 10 minutes of unloading the punch, hence recrystallization associated with stress relief was probably small. Plate 5.2 shows a thin section taken at the same time, but from a low stressed zone within the same sample. Note that the ice crystals are not disturbed away from the highly stressed zone beneath the punch.

In order to analyse the asymptotic punch resistance

using the expansion of a spherical cavity, the appropriate flow law for the material must be used. Equation 5.11 compared to Equation 5.10 shows that the punch settlement rate increases for a given applied punching pressure once the peak of the resistance curve is passed. This suggests that ice within the loaded zone beneath the punch becomes softer beyond the peak resistance. The softening of the ice within this zone can be compared to the decrease in resistance of the ice during a constant strain rate uniaxial compression tests shown in Figure 4.18. In this experiment the stress increases to the peak value, then it decreases to a constant stress associated with large strains. Equation 4.31 is the flow law established for the polycrystalline ice which has softened after being subjected to large strains. This flow law must be used to establish the theoretical punching resistance of the softened ice at the asymptotic resistance.

In order to calculate the theoretical punching resistance, the flow law must also be corrected to the proper grain size ratio and temperature. Equation 4.31 is the flow law for a material which initially had a grain size ratio of 0.015 before recrystallization. Recrystallization occurs beyond a failure strain of about 1% in the constant strain rate experiments therefore, grain size ratio after recrystallization cannot be determined. The punch experiments began with a grain size ratio of 0.018. During the punching experiment the crystal size beneath the punch

decreased, and as a consequence, the grain size ratio within this region also decreased. The actual amount of the change in grain size ratio was not determined as this would have required stopping the experiment before the asymptotic resistance was achieved.

It is therefore difficult to compare the measured asymptotic punch resistance and the theoretical circular punch relationship based on Equation 4.31. In the test samples, as soon as the peak resistance was reached, the grain size ratio within the sample began to change. The region beneath the punch will have one grain size ratio and the region beyond the stressed zone will have another ratio. The grain size ratio of the two experiments began at about the same value, but changed once the peak loading condition was reached. In the punch experiment, the ratio decreased while in the constant strain rate experiment it increased. The exact change in each grain size ratio was not determined. Figure 5.9 shows the comparison of the actual punch test results with the theoretical results. The theoretical punch resistance as determined using Equation 4.31 is:

$$[(ds/dt)/(ds/dt)c] = [q / 1171.]^{3.18} \qquad (5.18)$$

The lack of agreement between the actual experimental data and the theoretically predicted relationship occurs because of the size effect influence on the data and was not

accounted for in the above comparison.

Lack of agreement in the results of the asymptotic punching and theoretical expansion of a spherical cavity will not influence the use of punch penetration as a method for determining the short-term flow law for ice. It will, however, cause problems in establishing the flow law associated with the long-term loading condition. Chapter 4 demonstrated that the flow law of interest in Engineering design occurs before the inflection point, or is that associated with the peak stress. The agreement in Figure 5.8 between the actual experimental punch data and the theoretical relationship of the before-peak results is good. Therefore, the flow law of the material could be back-calculated given the punch data coupled with use of the expansion of a spherical cavity model.

5.5.3 Influence of depth of embedment on punch resistance

In previous analysis of the punch experiment results, the expansion of the spherical cavity predicted the punch data closely. Inherent in the assumption of the expansion of a spherical cavity is the fact that the cavity is expanding in a infinite medium. The use of this model to analyse the circular punch data is only appropriate if the punch is located at a sufficient distance from the surface so that the free surface will have no influence on the punch (Ladanyi and Johnston (1974)).

In this research program, the punching experiments were

conducted with the punch initially embedded less than one punch diameter below the surface. It was anticipated that as the punch penetrated into the ice sample, the punch resistance would increase in value as its penetration increased. The anticipated behaviour is illustrated in Figure 5.6. The actual punch resistance, however, did not continue to increase as it penetrated into the ice. The actual punch resistance behaviour is presented in Figure 5.3 which shows that, beyond the peak, the resistance decreased to the asymptotic value then remained constant with increased penetration. In the analysis of the data it was found that the spherical cavity model predicted the actual laboratory punch data. This suggested that the requirement that the punch be located at a certain depth beneath the surface could be relaxed in ice.

In thawed soil, Meyerhof (1963) suggests that the free surface had no influence below a depth of 4 punch diameters in clay and 7 to 8 punch diameters in sand. In frozen material this research suggests these requirements can be reduced based on laboratory studies.

Figure 5.10 is a plot of the results of the punch experiments reported in this research. In this Figure the punch resistance versus the ratio of the depth to punch diameter (D/B) is plotted. For the limited number of experiments and the shallow depths, it is observed that no influence of burial depth on the punch resistance exists. Figure 5.11 is a plot of results of experiments conducted on

frozen sand (Ladanyi and Paquin (1978)). It illustrates that the parameters which define the laboratory punch resistance versus punch settlement rate are not influenced by depth of burial from the surface. In Figure 5.11 the punch was buried at depth to diameter ratio of between 4 and 15 and in Figure 5.10 the depth to diameter ratio was between 0.5 and 3.3. The lack of influence on these results suggests the capacity of a circular punch near the surface can be evaluated using the expansion of a spherical cavity in an infinite medium as a model to obtain the relationship between the punch settlement rate and the resistance.

Vialov et al. (1973) presented results of the load deformation behaviour of circular footings on ice. He varied the depth of footing below the surface between D/B = 0 and D/B = 1.25. For this condition it was found that an increase in the burial depth decreased the deformation rate under a constant applied pressure. His results at a D/B = 1.25 are compared with the results of this research work in Figure 5.12. Both sets of experimental data of settlement rate versus punch resistance are approximately parallel. This would suggest that the same method can be used to analyse the two sets of data.

In our previous analysis of the data from this research program, it has been shown that the expansion of the spherical cavity will model the punching data. The data presented by Vialov et al. (1973) cannot be checked to see if it can be predicted using the cavity model, since the

flow law of the ice used in the experiments was not given in the report. Due to this lack of data, the difference in the two sets of results contained in Figure 5.11 cannot be accounted for.

The influence of depth of footing shown by Vialov et al. and the absence of this influence found in this research and by Ladanyi and Paquin (1978) is most important. Possible reasons for this difference must be considered. Vialov observed the depth influence at applied pressures of between 200 and 600 kPa. In this research the data was obtained at applied pressure of between 2200 and 5000 kPa. It is possible that the higher applied pressures used during this program might have obscured any depth influence that existed.

The lack of influence of the footing depth on the punch result may be influenced by the magnitude of footing displacement at which the data are compared. In this experimental program the punch penetrated an average of between 1.0 and 2.0 mm at the peak punch resistance and 10.0 mm at the asymptotic resistance. In Vialov's experiments the total settlement of the footing was 1.6 mm with an average displacement during each loading increment of 0.3 mm. Also, Vialov performed his experiments with a 160 mm diameter punch, compared to a 19.05 mm diameter punch used in this research.

The combined difference of the punch displacement and diameter will result in different strains in the ice beneath

each footing. This difference in strain results because the ratio of the settlement to the footing diameter governs the strain within the material (Ladanyi (1976)). Thus the resistance within each set of experiments are being compared at vastly different strains within the ice. In order to identify the influence of footing depth below the surface, experimental results would have to be compared at a constant ratio of footing displacement to diameter of each set of data. This would compare data at approximately the same strain in each experiment. In Vialov's experiments, because of the small ratio (strain), the ice beneath the footing was still in the primary region of a typical creep curve. In the experiments reported in this thesis the ice beneath the footings was strained beyond the inflection point. Thus these two sets of results can not be compared directly.

The significance of the above results are two-fold as far as geotechnical engineering is concerned. First, if there is no influence of punch depth on the bearing resistance of a circular footing, it suggests that, a higher bearing capacity could be used in designing footings at shallow depth in frozen soil. A bearing capacity factor of approximately 10.0 instead of 6.2 at the surface for a circular footing in ice rich frozen soil would be justified in calculating the ultimate capacity. The use of the expansion of a spherical cavity relation also allows the footing settlement rate to be calculated along with the capacity.

In the previous paragraphs the depth of embedment of a punch has been shown to have no influence on the bearing capacity in frozen soil and ice. It should be noted that the depth influence in the bearing capacity formula is obtained using Prandtl's theoretical plasticity solution and accounting for the material above the level of the footing's base. The theoretical capacity was obtained for a material whose stress-strain behaviour was rigid plastic. Mulhearn (1959) and Hirst and Howes (1969) have shown that at the free surface the resistance to a punch penetrating into a material is dependent on the material's stress-strain behaviour.

Frozen soil and ice do not behave as rigid plastic materials a low rates of loading, therefore, Prandtl's relationships should not govern the capacity of these materials. The capacity of the footing must be evaluated using a model which is capable of accounting for the actual material behaviour. The model of an expansion of the spherical cavity is capable of accounting for the material behaviour, thus should be used to obtain the capacity. This model does not predict an influence of depth.

The second important result is that, by using the data of punching experiments, the flow law of the material into which the punch is penetrating can be evaluated. Under field conditions Ladanyi (1976) has presented two techniques to measure the relevant punch data. The static penetration apparatus applies a constant load to the punch and the

time-dependent penetration of the punch is recorded. This recorded data is used to establish the flow law of the material under a first time loading condition(Section 2.4.2). This would be the flow law required for the design of foundations within frozen material since the material will not yet have reached the teritary region of the creep curve.

In the constant penetration apparatus, the load and displacement of the punch are recorded during a constant advance of the punch into the frozen material. This could be used to determine the exponent of the flow law by performing experiments at different rates. The proof resistance required in Equation 5.12 could be determined using the peak resistance measured under different first time penetration conditions. Combining these results, Equation 5.12 could be established which is valid for field data. Then, using the relationship between Equation 5.12 and the cavity expansion model, one could calculate the flow law of the frozen material.

5.6 Analysis of multiaxial state of stress in creep studies

In this Section a limited number of results on the influence of changing the stress state within creep experiments will be examined. The triaxial compression experiment was used to examined the influence of applying a low confining pressure to a sample being deformed at a constant rate. The second experiment examined the influence

of a multiaxial state of stress using a simple shear experiment. The experimental apparatus and test procedure used in each type of experiment has been discussed in Sections 3.3 and 3.6.

5.7 Multiaxial state of stress

To this point, in discussing the experimental results, only data from uniaxial compression have been examined and the flow law has been presented in terms of this stress state. The stress state surrounding the expanding spherical cavity could be examined using the results of the uniaxial experiments because of symmetery. The use of the flow law based on the uniaxial stress was justified because Ladanyi and Johnston (1974) used the following definition for the flow law during their formulation. This defintion is for a multiaxial state of stress.

$$[dE/dt]e = [dE/dt]ec \cdot (\delta e/\delta ec)^{n} \qquad (5.19a)$$

where

$$[dE/dt]e = \{2/3([de/dt]ij \cdot [de/dt]ij\}^{0.5} \qquad (5.19b)$$

$$\delta e = \{3/2(\delta ij \cdot \delta ij\}^{0.5} \qquad (5.19c)$$

$[dE/dt]e$ = effective strain rate

$[dE/dt]ec$ = proof effective strain rate

δe = effective stress

δec = proof effective stress

$[de/dt]_{ij}$ = deviatoric strain rate tensor

δ_{ij} = deviatoric stress tensor

Equation 5.19b and Equation 5.19c were presented by Odqvist and Hult (1962) to establish a flow law using the second deviatoric stress and strain invariant. These two equations reduce to the simple uniaxial stress and strain state. Therefore, the flow law defined by Equation 5.19a reduces to Equation 2.22 which gives the flow law for the uniaxial stress state.

The reader should note that Equation 5.19b and Equation 5.19c relate the effective stress and strain rate to the second stress and strain invariants, but the results will not be the same as given by Equation 2.17a and 2.17b presented by Nye (1951). Nye's equations do not reduce to the uniaxial stress state, but they reduce to the pure shear stress state. Thus two definitions exists in the creep literature for the effective stress and the effective strain rate. These two definitions must be distinguished and used only to correlate comparable data.

As mentioned in Chapter 2, Nye's definition has been used extensively in the glaciological literature to relate field and laboratory data of various authors. In the review in Chapter 2 it was shown that the flow law of ice has been established primarily using the results of uniaxial compression experiments. In this research, the ice was subjected to a uniaxial state of stress. It is therefore

recommended that Equation 5.19a and 5.19b be used since they reduce to the uniaxial state of stress.

In geotechnical engineering Ladanyi (1972) recommends using Equation 5.19a, 5.19b and 5.19c to relate the flow law of frozen soil and ice for this reason. In Chapter 6 the results of a computer analysis will be presented. These results are influenced by the stress invariant used to define the flow law during the analysis. Emery (1979) outlined these influences and called for the use of Equation 5.19a for the flow law of ice.

5.7.1 Influence of hydrostatic stress state on flow law

The influence of applying a hydrostatic pressure to a creep experiment was studied by conducting a uniaxial creep experiment on Sample UC44 under a condition of constant displacement rate. The sample was deformed until a total axial strain of 6.0 % had been reached. At this point a confining pressure of 400 kPa. was applied to the sample. The experiment was continued at the same displacement rate until an accumulated strain of 8.4 % was attained. Throughout the experiment the temperature, the load, and the deformation of the sample were continuously recorded.

Figure 5.13 presents the stress-time and the temperature curves for the experiment. In the initial portion of the experiment, technical problems with the loading equipment resulted in establishing an incorrect peak of the stress time curve. The peak was not defined because

the load readings were in error for a period of time. These problems were corrected and the post peak behaviour recorded. It is this post-peak behaviour under a zero confining pressure which is shown in the Figure between a time of 800 hours and 3000 hours that will be compared. When the confining pressure of 400 kPa was applied to the sample the recorded deviatoric axial stress did not change. The application of a small confining pressure therefore had no influence on the creep behaviour of polycrystalline ice.

This lack of influence of the confining pressure on the creep characteristics of polycrystalline ice confirms the findings of Steinemann (1958) and Rigsby (1960). This implies that the flow law of ice is independent of the hydrostatic stress state or the first stress invariant provided that the temperature of the ice is not altered significantly during the pressure application.

5.7.2 Influence of simple shear stress state on creep deformation.

Simple shear experiments were conducted to establish whether or not Equation 5.19a is an appropriate relationship for predicting the flow law of polycrystalline ice under a multiaxial stress condition. These experiments were conducted at a temperature close to that used during the uniaxial compression experiments to ensure that the data were comparable. The results of three long-term experiments conducted under a simple shear loading condition will be

presented.

In Section 3.6 the loading system and the equipment used to perform the simple shear experiments was outlined. Figure 3.9 illustrates the loading applied to the ice sample during the experiment and demonstrates that the loading apparatus is not capable of applying a uniform shearing stress to the vertical face of the sample. It will apply a shear stress only to the horizontal sample face thus a true pure shear state of stress is not achieved within the sample under the experimental loading condition. Are the deformations within the ice uniform and do they reproduce a uniform shear behaviour?

The following experiment was conducted to examine the deformation pattern within the simple shear sample. Three holes located on a diameter of the sample were drilled vertically through the sample using the milling machine shown in Plate 3.6 to ensure that each hole was perpendicular to the face along which the shear stress was applied. A circular piece of rubber was placed in the hole and the sample was mounted in the simple shear apparatus as outline Section 3.6.3. The load was applied to the sample and the deformations of the sample were recorded with time under a constant effective shear stress. Upon completion of the experiment, the sample was removed from the test apparatus, and cut in half to expose the pieces of rubber. The deformed shape of the rubber resulting from the loading condition could be viewed. Since the rubber is softer than

the ice it deforms in response to the deformation of the ice. Thus the deformed shape of the rubber gives the deformation pattern within the ice sample.

Plate 5.3 shows a photograph taken immediately after the experiment was completed. In this Plate the ice's deformation is illustrated by the deformed shape of the embedded rubber. The uniform shear deformation within the sample is illustrated by comparing the deformed shape of the rubber with the initial position shown by the solid line sketched on the photograph. This illustrates that the simple shear device imparts a uniform shear deformation to the sample even though pure shear stresses are not applied to the sample.

Duncan and Dunlop (1969) compared the stress-strain curve of a clay sample from a simple shear loading condition with the stress-strain curve predicted using a pure shear analysis for this loading condition. They showed that the pure shear analysis closely predicted the actual material behaviour resulting from the simple shear loading. The authors recommend the use of a pure shear analysis to analyse the data of a simple shear experiment. This method was used in reducing the simple shear experimental results.

In the analysis of the simple shear experiments the uniform pure shear state of stress was used and to it was added the vertical normal stress applied to the sample. The shear stress was the shear force divided by the sample area. The normal stress applied to the sample was the normal load

divided by the sample area. The loading condition applied to the simple shear sample is illustrated in Figure 3.9. Figure 5.14 shows the idealized stress distribution used to analyse the material behaviour. The effective stress and the effective strain rate resulting from this loading condition are given by:

$$\delta^2 e = \delta^2 ii + 3 \cdot \delta^2 ij \qquad (5.20a)$$

and

$$[dE/dt]^2 e = 2/3[de/dt]^2 ii + 1/3\,[de/dt]^2 ij \qquad (5.20b)$$

where

δij = deviatoric stress

δc = effective stress

$[de/dt]$ = strain rate

$[dE/dt]$ = effective strain rate

$i = 1$

$j = 2$

The applied stress direction resulting from the loading condition are shown in Figure 5.14.

A summary of the simple shear experimental results are contained in Table 5.2 Figure 3.10 shows a typical simple shear effective strain-time plot. The constant effective stress applied during this experiment is given on the plot. This strain-time curve has the same shape as the constant uniaxial compression experiments. The data contained in Table 5.2 has been plotted in Figure 5.15 along with

Equation 4.19. This equation gives the flow law of the uniaxial compression experiments as established in Chapter 4. The simple shear data points cluster near to the line defining the flow law for the uniaxial compression results.

This would suggest that Equation 5.19 is an appropriate flow law for a multiaxial state of stress. The flow law determined for the uniaxial state of stress can be extended to include the results of a multiaxial state of stress provided Equation 5.19b and 5.19c are used to obtain the effective shear stress. This also requires that the third stress invariant not have an influence on the flow law of ice which Byers (1973) showed to be the case.

5.8 Conclusion

The punching experiments can be used to derive the flow law of ice which suggests that the penetration method of field testing can be used to establish the long-term strength and the creep properties of ice and frozen soils. Confining pressure has no influence on the flow law of ice. The flow law for a multiaxial state of stress can be predicted by using Equation 5.19a.

Table 5.1

Summary of punch test data

Sample Number	Test Temperature C	Peak Punch Resistance (kPa)	Asymptotic Punch Resistance (kPa)	Normalized Settlement Rate
16	-1.0	3080	2350	2.3
25	-0.9	2780	2000	2.3
32	-1.0	3280	2573	2.3
29	-1.0	----	3667	11.0
36	---	4935	3500	11.0
41	-0.9	4960	4000	11.0
48	-0.8	4805	4050	11.0

Table 5.2

Summary of simple shear experiments

Sample Number	Effective Shear Stress (kPa)	Normalized Effective Shear Strain Rate
SS30	285	3.1
SS32	167	0.43
SS44	308	3.2

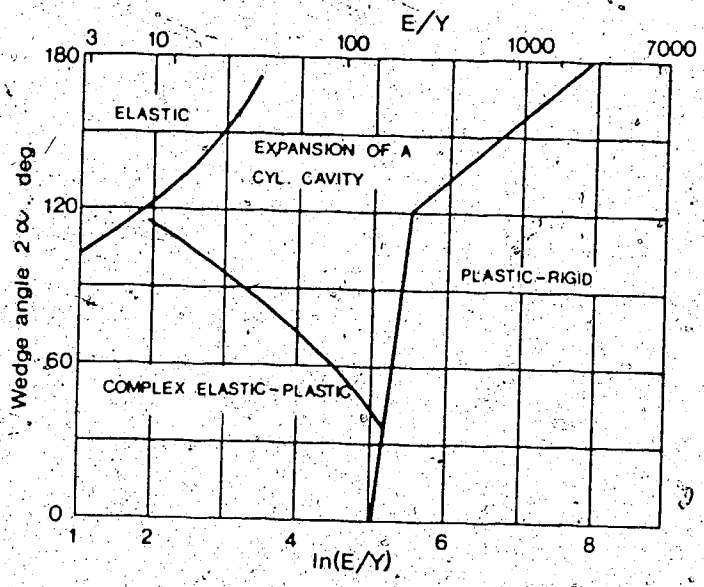

Figure 5.1: Regions of operation of different wedge indentation mechanism from Ladanyi and Johnston (1974).

B = Diameter Footing
q = Applied Pressure
$\alpha = 45°$
p_i = Pressure which causes cavity to expand

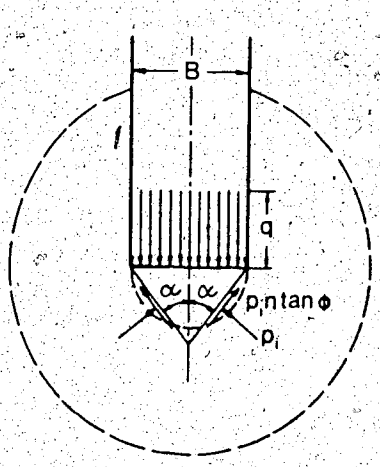

Figure 5.2: Schema for transformation of a cavity expansion to a deep circular punch problem from Ladanyi and Johnston (1974).

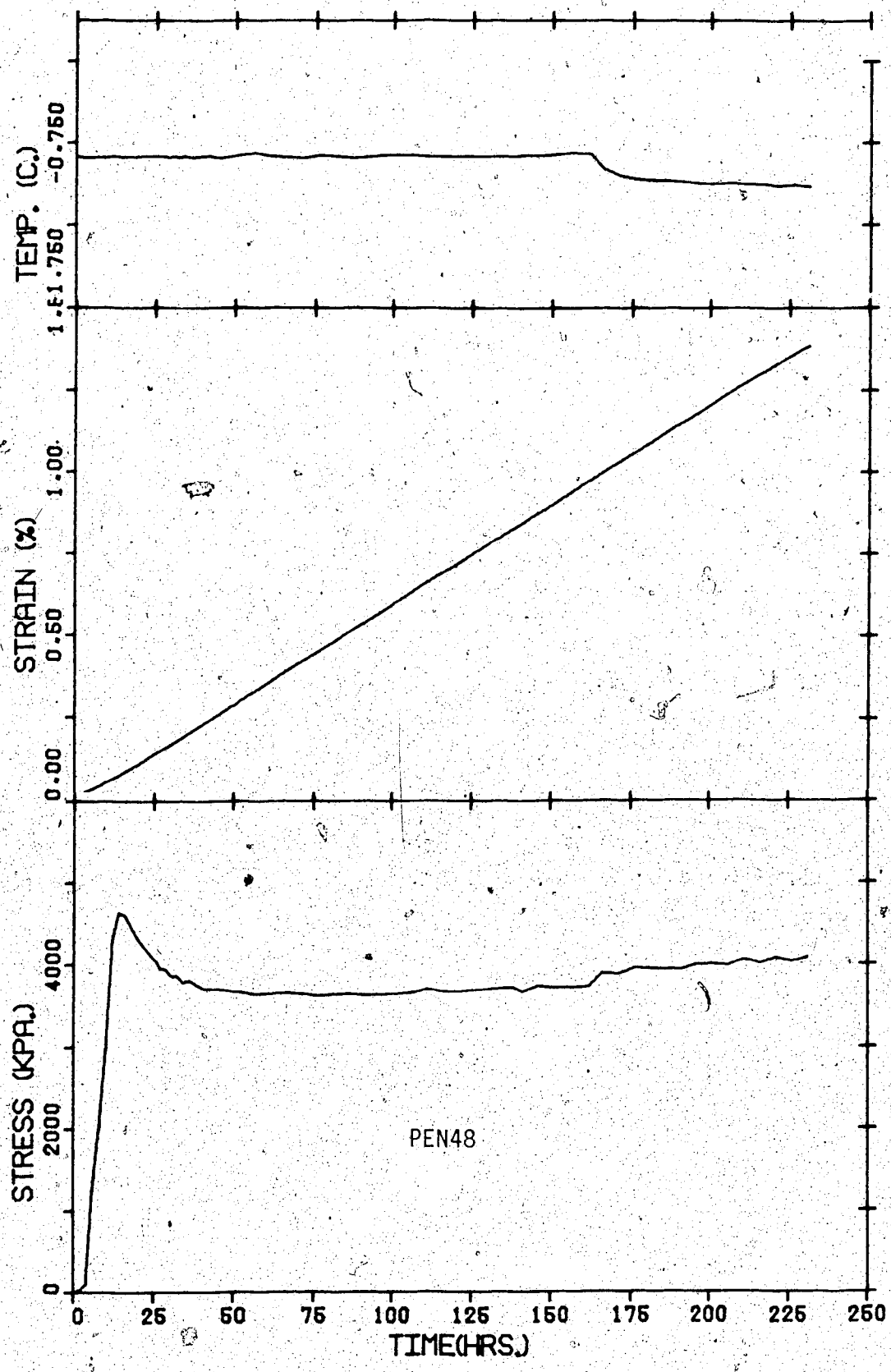

Figure 5.3: Typical plot of punch resistance versus time during constant displacement rate experiment.

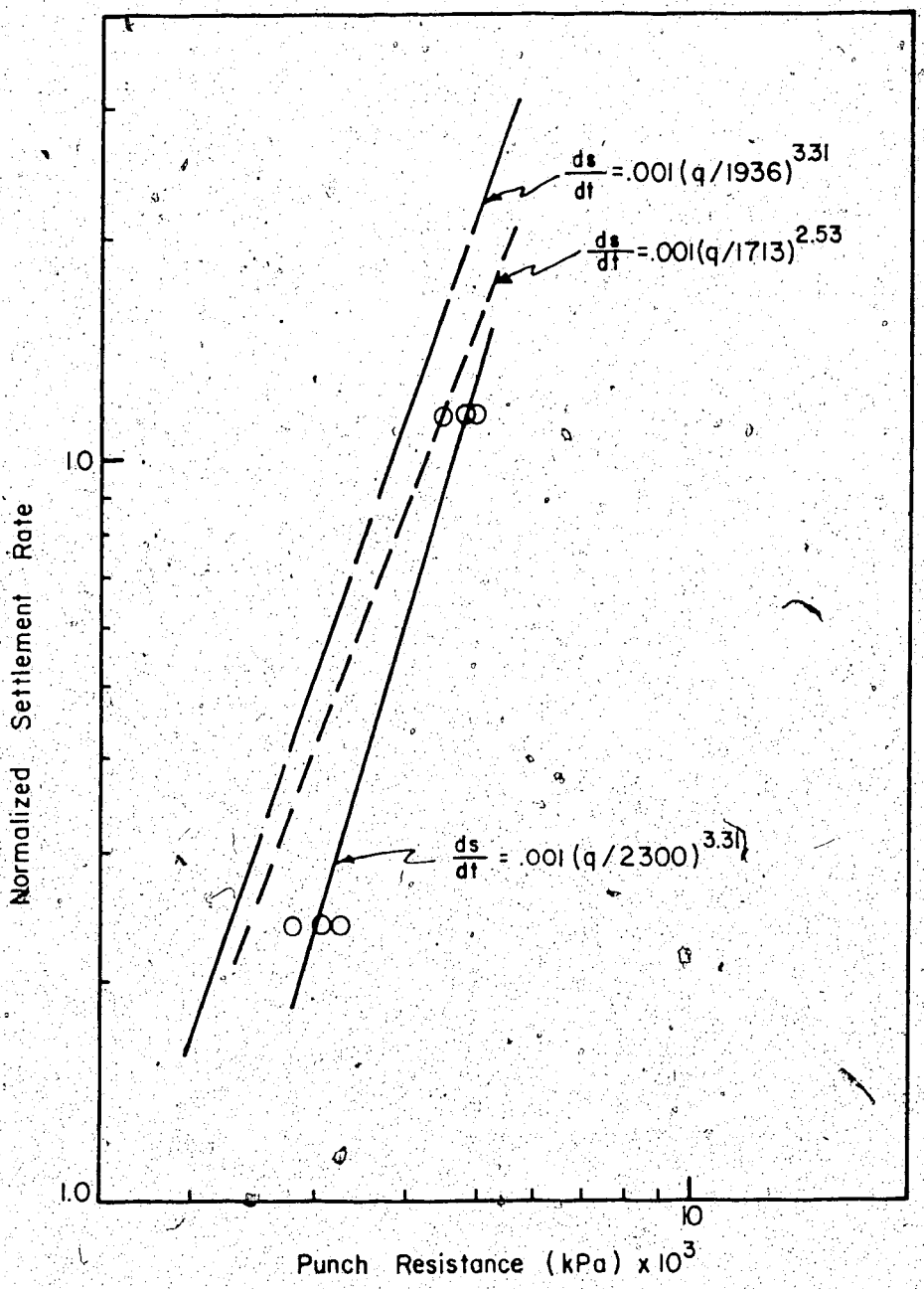

Figure 5.4 Normalized settlement rate versus punch resistance.

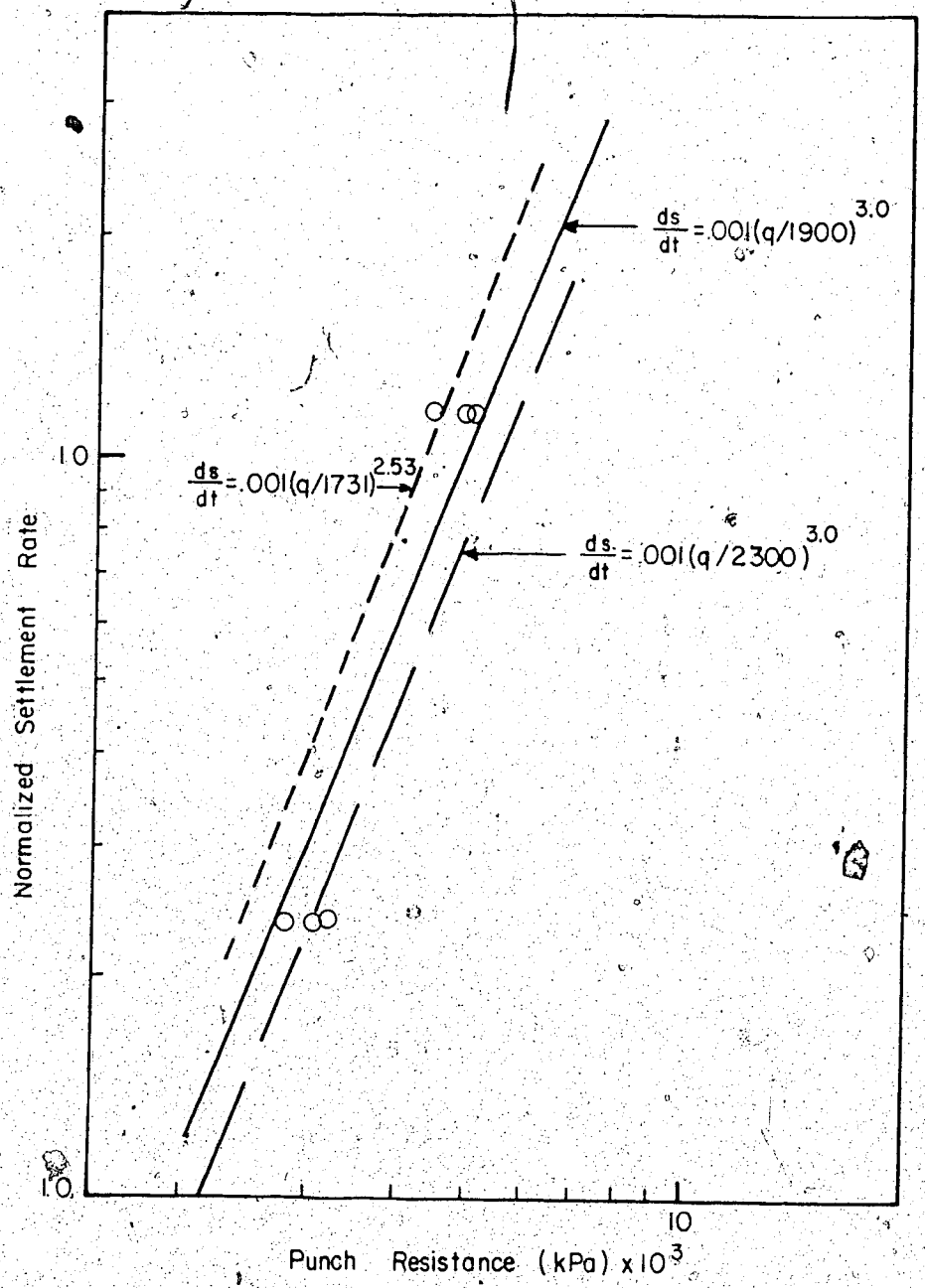

Figure 5.5 Normalized settlement rate versus punch resistance using an exponent equal to 3.0

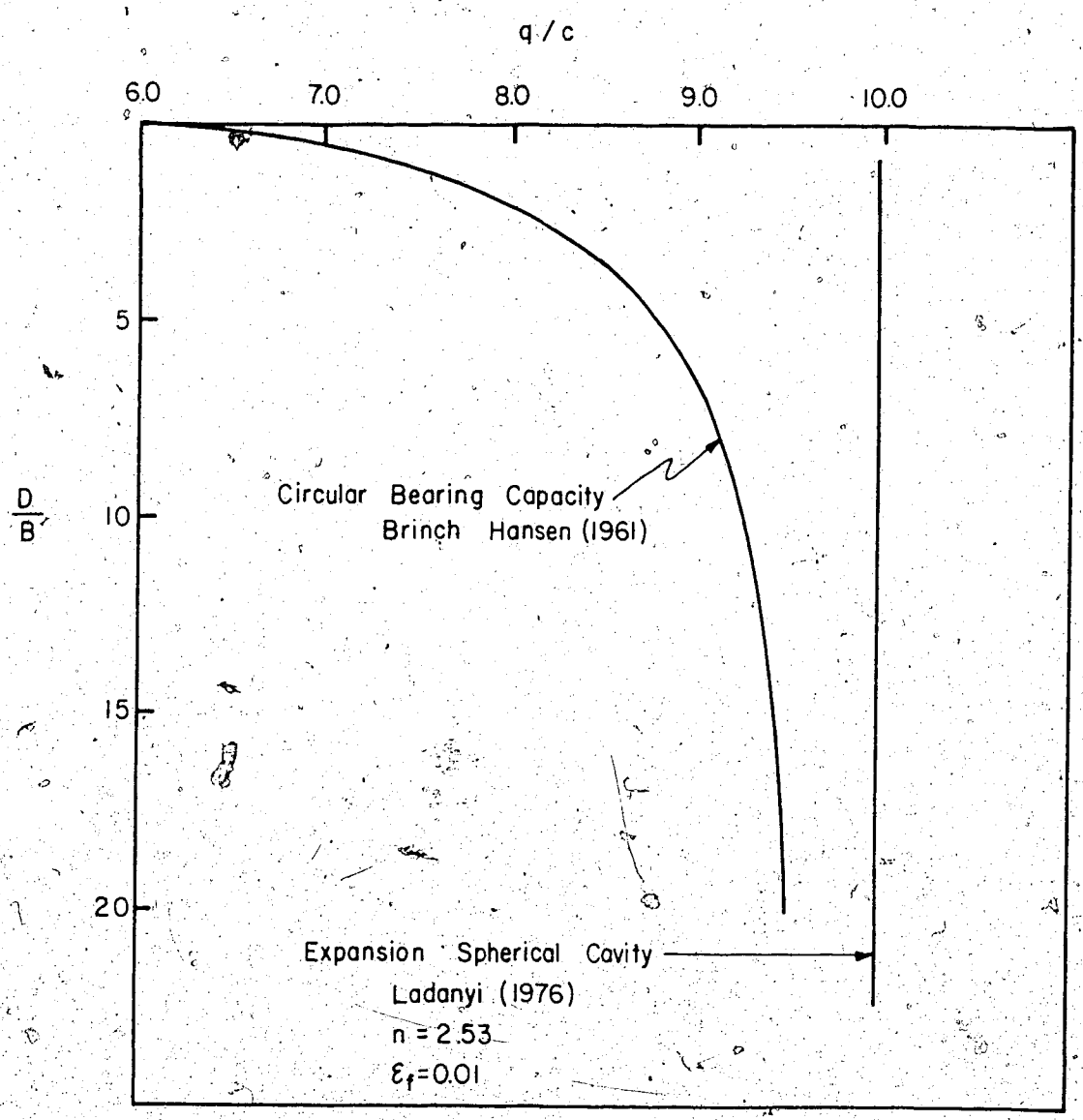

Figure 5.6 Bearing capacity versus depth of embeddement in a cohesive material.

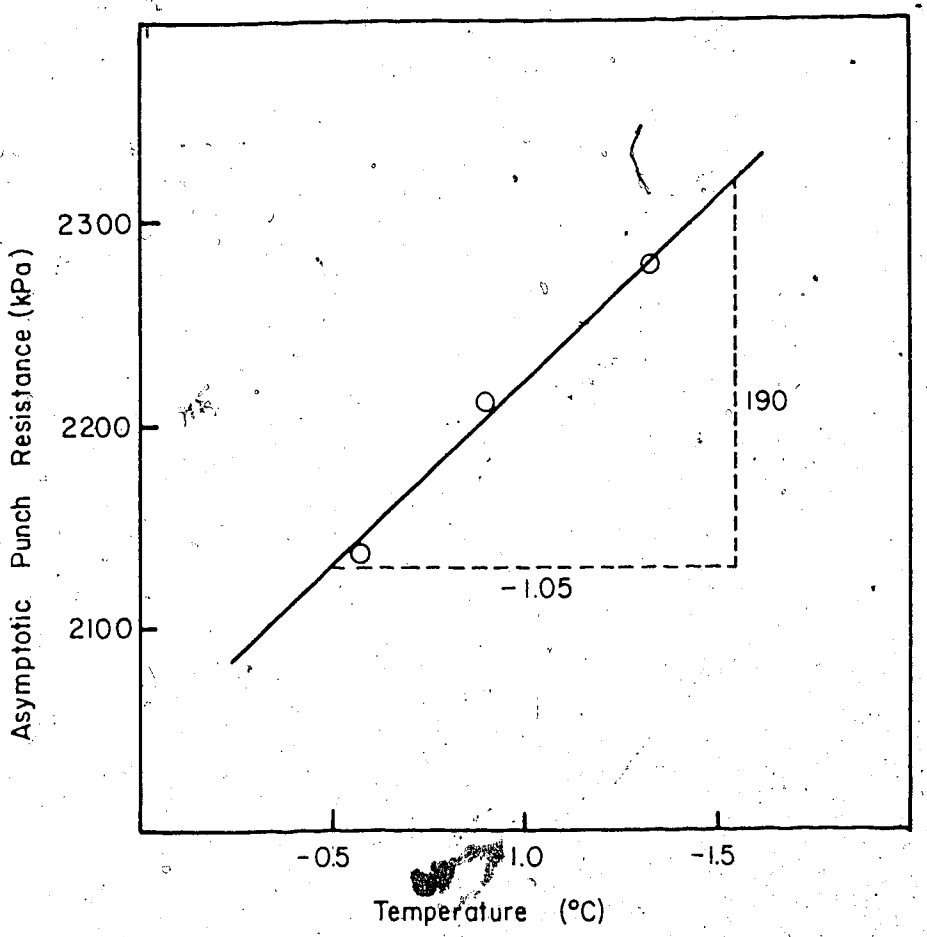

Figure 5.7 Temperature versus asymptotic resistance.

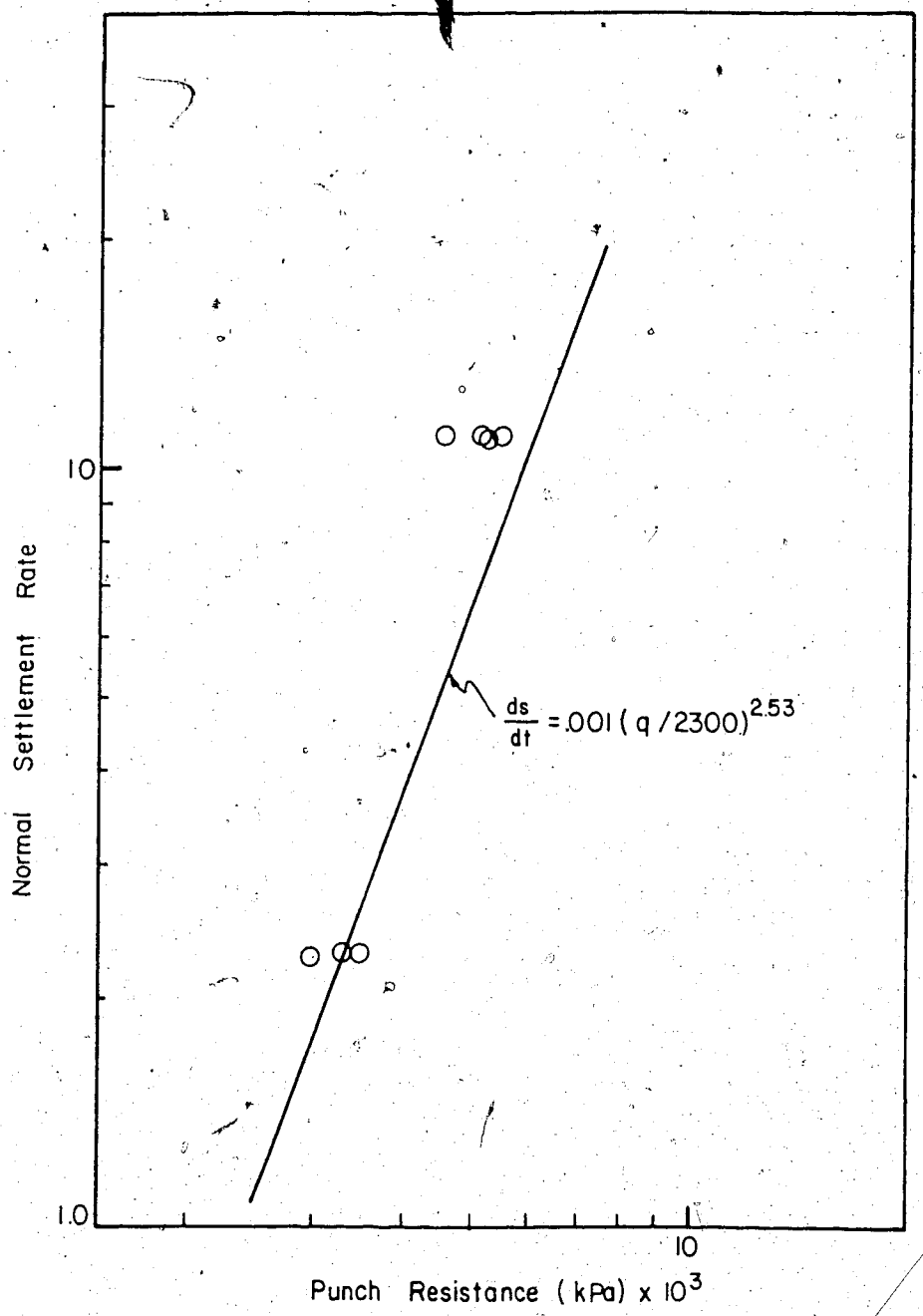

Figure 5.8 Normalized settlement rate versus peak punch resistance corrected to -2.0°C.

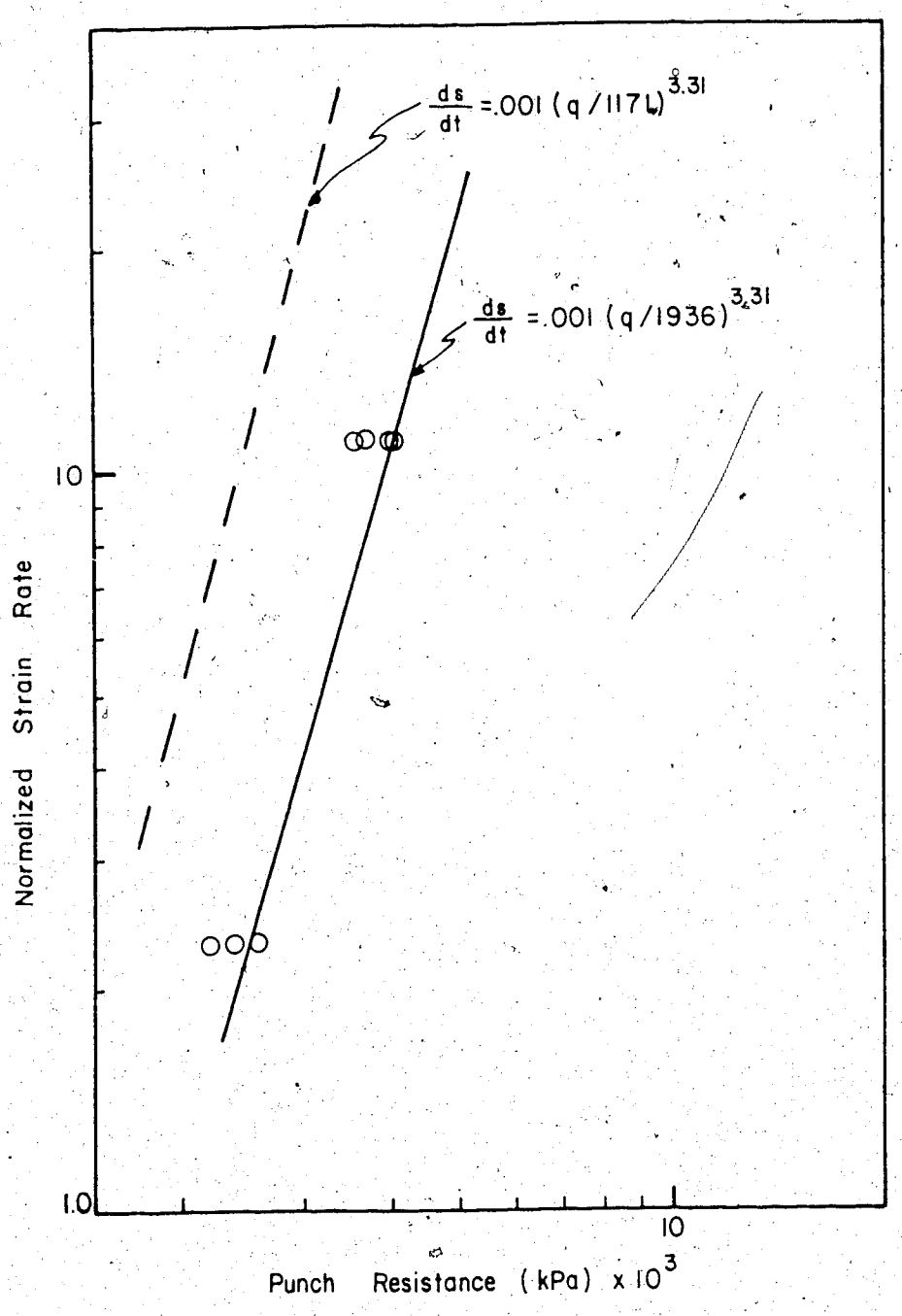

Figure 5.9 Normalized settlement rate versus asymptotic punch resistance corrected to -2.0°C.

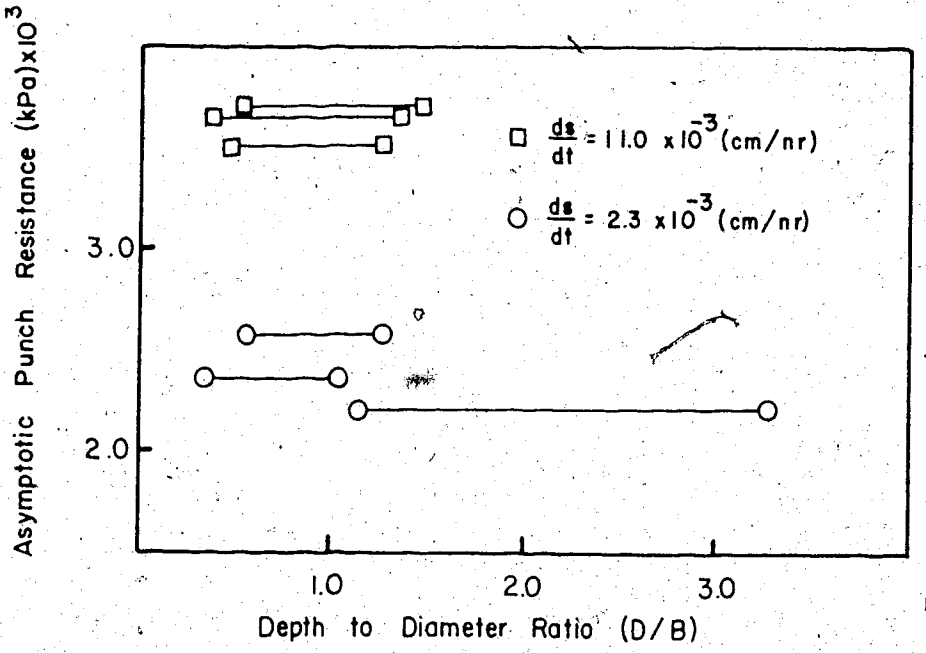

Figure 5.10 Asymptotic punch resistance versus the depth to the diameter ratio (D/B).

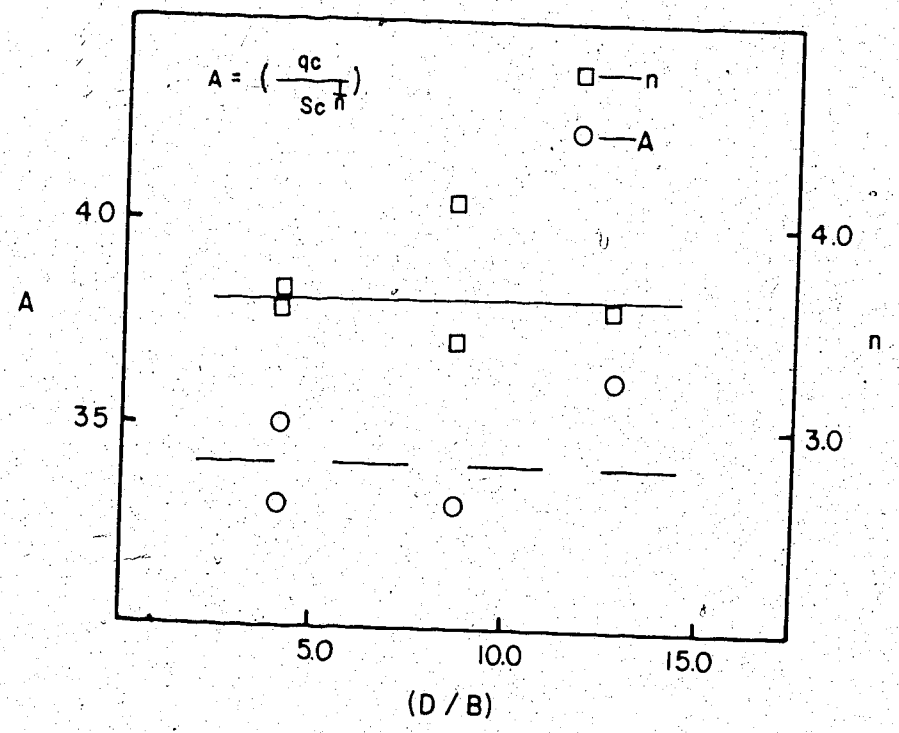

Figure 5.11 Parameters governing punch resistance versus depth to diameter ratio (D/B) for frozen sand.

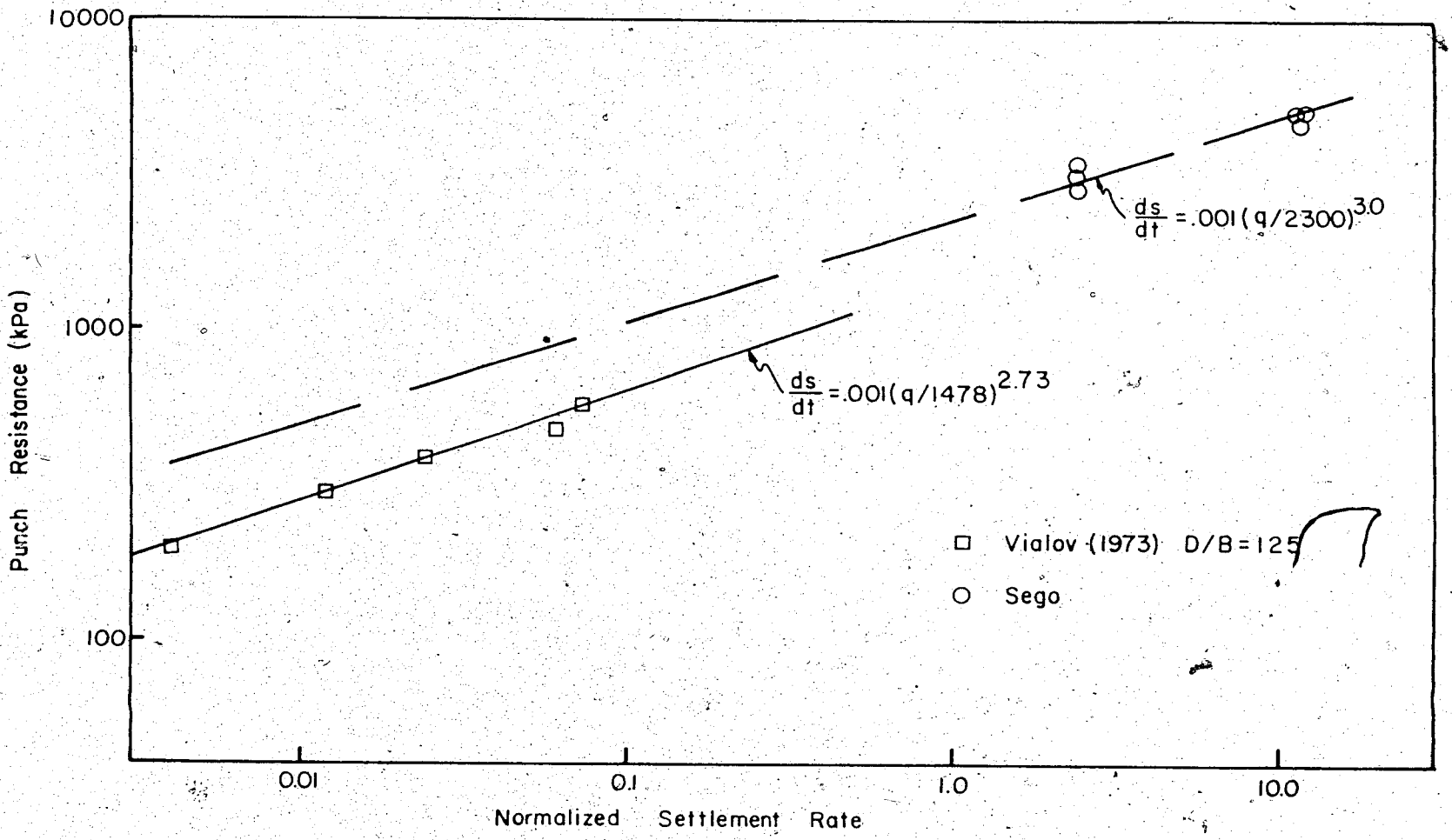

Figure 5.12 Punch resistance versus normalized settlement rate of punch experiments on polycrystalline ice.

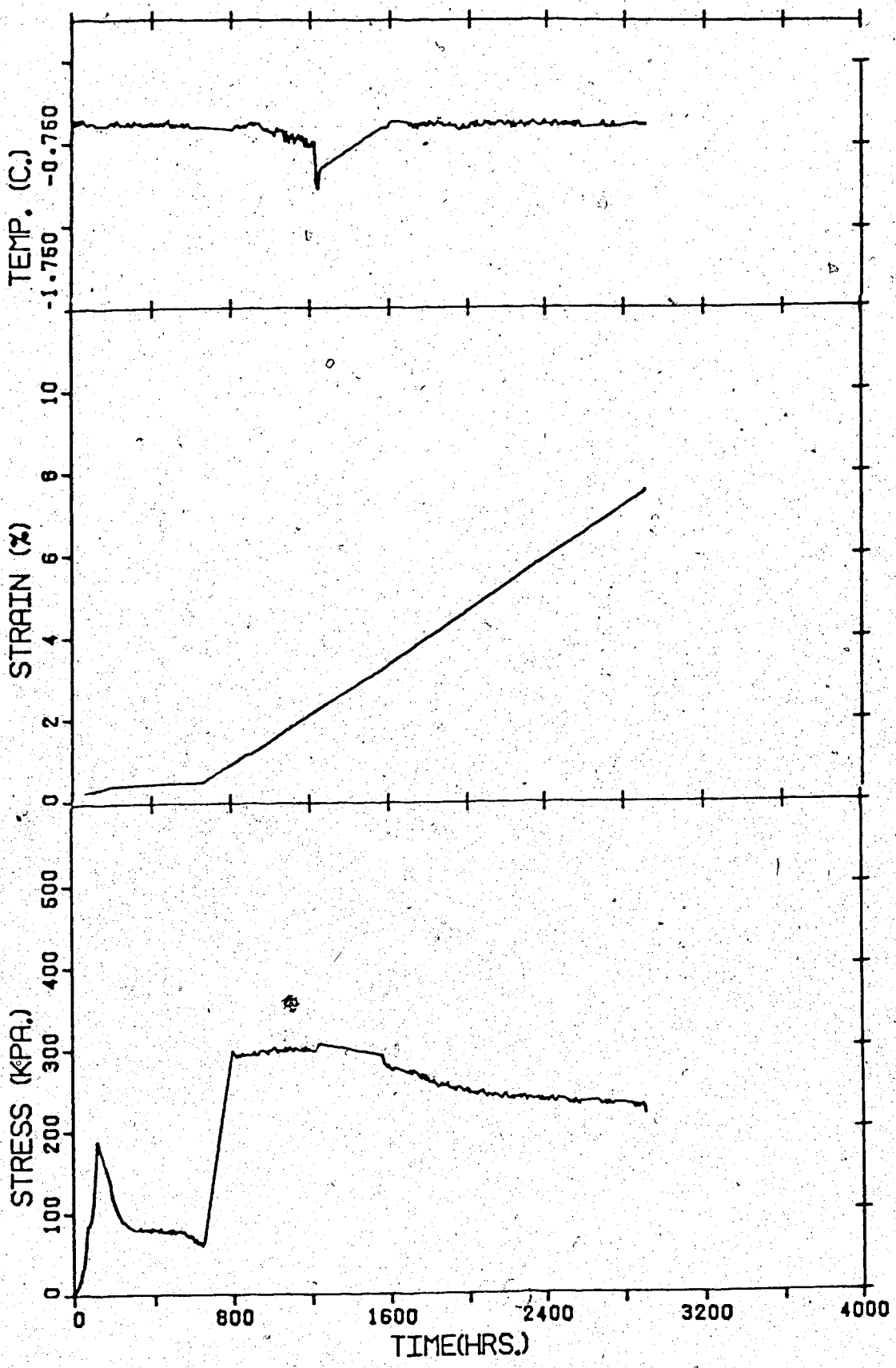

Figure 5.13 Plot of stress versus time of Sample UC44 which illustrates influence of confining pressure on experiment.

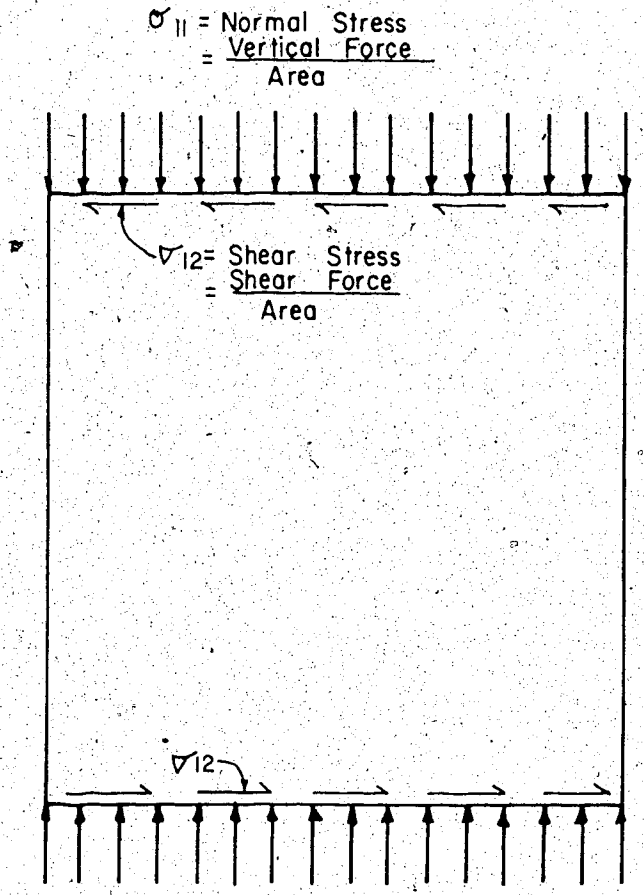

Figure 5.14 Idealized stress distribution in simple shear experiment.

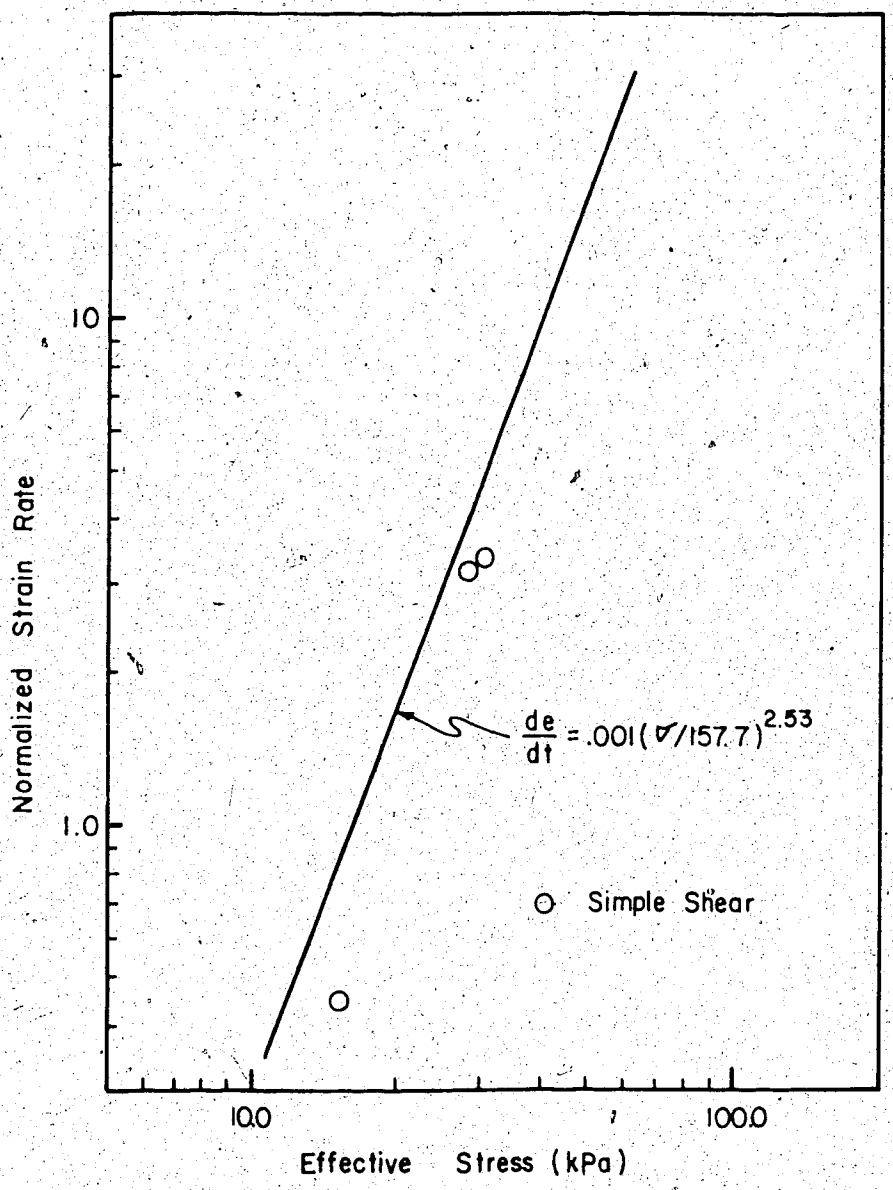

Figure 5.15 Normalized strain rate versus effective shear stress comparison between simple shear data and Equation 4.19

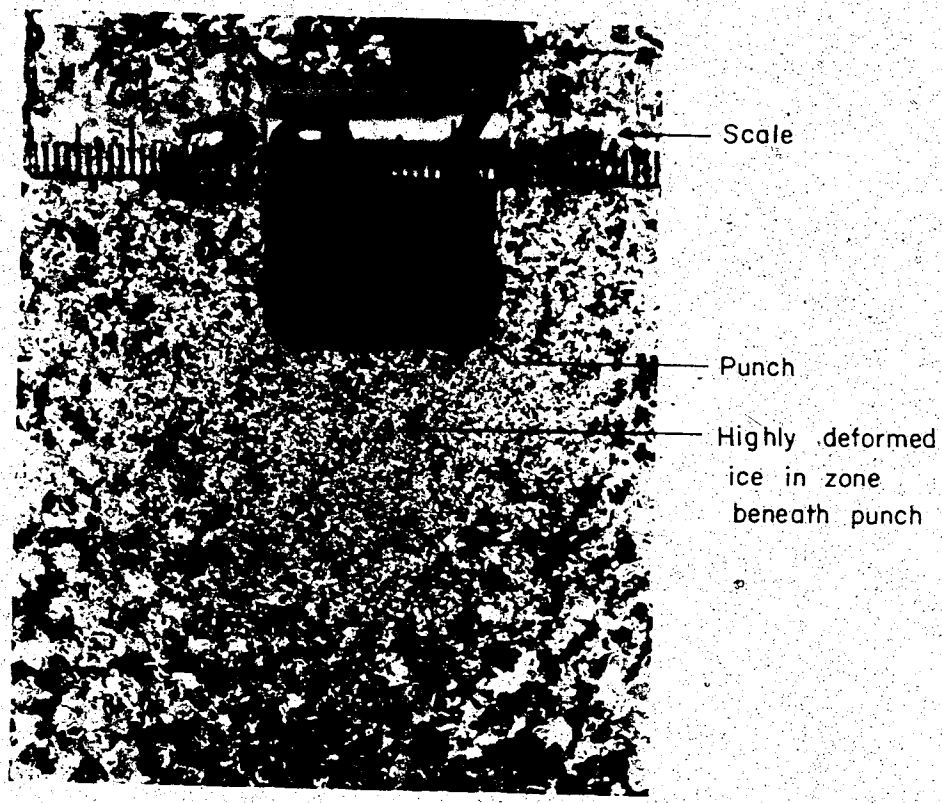

Plate 5.1: Thin section showing highly disturbed zone of ice crystals beneath punch.

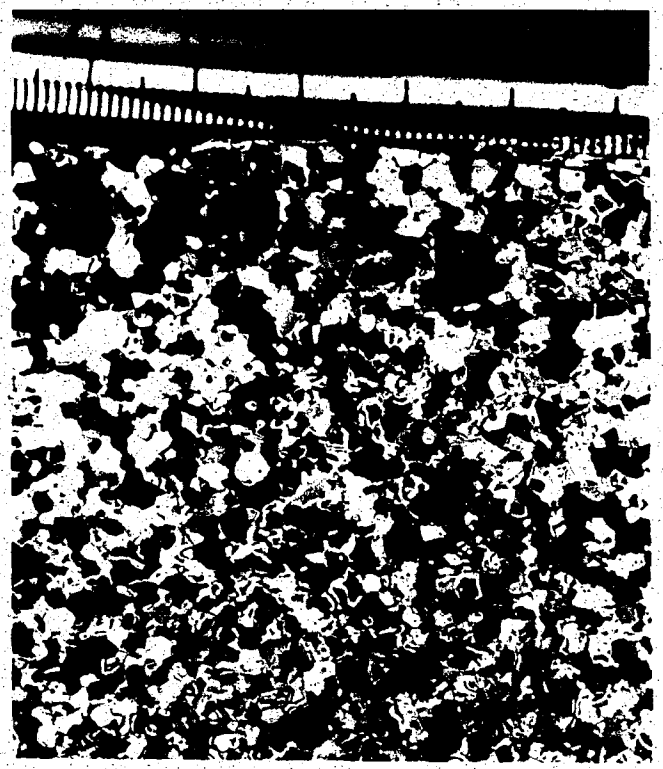

Plate 5.2: Thin section showing undisturbed ice crystals at distance from punch

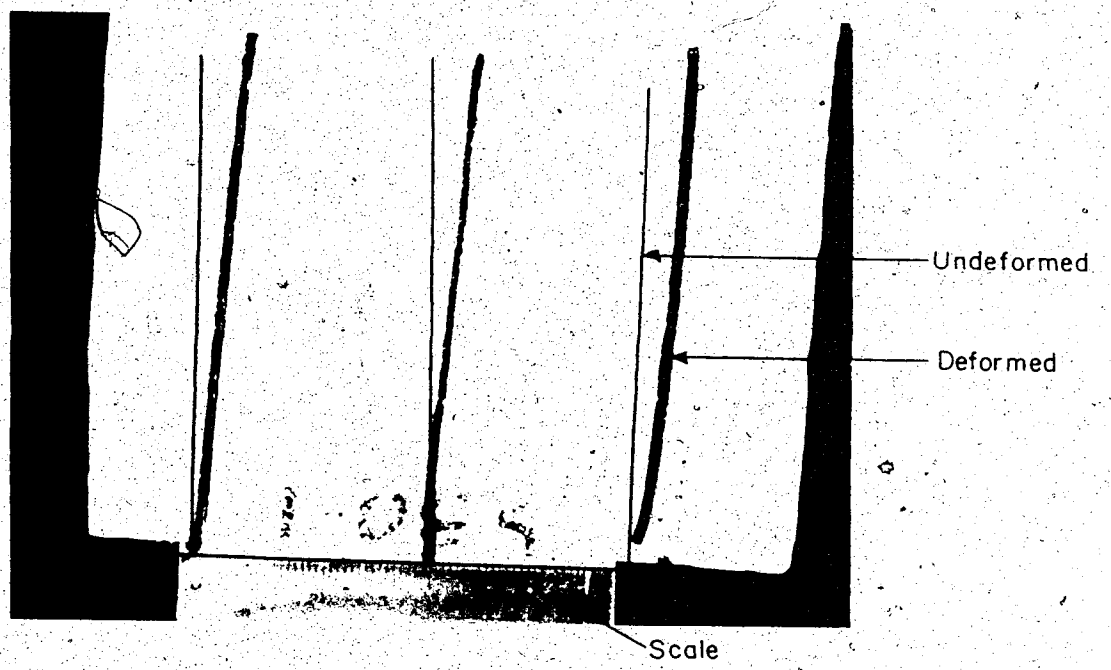

Plate 5.3: Photo of simple shear experiment illustrating uniform deformation of ice sample.

Chapter 6

Finite Element Analysis of Laboratory Data

6.1 Introduction

In this chapter the modification of and use of two finite element programs will be discussed. These two programs were used during this research to model the steady-state creep behaviour which is known to exist in frozen soil and ice (Glen (1955), Vialov (1965b), and Thompson and Sayles (1972)). The programs were adapted to study the deformation of frozen material when subjected to uniform loading conditions.

The first program is capable of analysing the plane strain loading condition for a material in which the strain-rate is related to stress using the simple power law given by Equation 5.19a. The second program analyses the axi-symmetric loading and deformation condition for materials in which Equation 5.19a governs the relationship between strain-rate and stress. Both programs are unable to account for the primary or time dependent strain-rates within the material illustrated in Figure 2.4. All calculations of the programs are performed for isothermal conditions.

The two programs were only developed to this stage because in the early part of this research it was recognized from the ice and frozen ground literature that the deformations associated with the steady state or secondary

creep of frozen material dominated the deformations of the material (Glen (1955), Steinemann (1958), Vialov (1965b), Sayles (1968), and Sayles (1973)). The isothermal temperature condition was used since foundations are located at a certain depth and designed using the warmest yearly temperature at this depth. The design method suggested that an isothermal program was adequate for the scope of work associated with this thesis.

The two programs were developed by modifying the basic constant strain triangle program obtained from Professor D. W. Murray of the Department of Civil Engineering. The strain triangle was considered to be the proper from which to develop a capability for handling the a types of loadings.

In the following sections a brief review of the theory use to guide the modification made to the program will be outlined. The comparison of the results of these two programs with the closed-form solution of the expansion of a thick-walled cylinder will be presented. Then a comparison between the laboratory results of the uniaxial compression and the punch experiments, and the calculated results given by the finite element program, will be made.

6.2 Finite element method

Zienkiewicz (1971) and Desai and Abel (1972) discuss the basic concepts and techniques used to solve boundary value problems within engineering. They present the basic

concept of discretization of the continuum and the methods used to obtain the stresses and strains within the continuum. Initially the stresses and strains are related within a discrete element by analysing the loading and deformation of this element. The continuum is formed by linking the discrete element together. This linking process allows the solution of the displacements within the continuum for the total loads applied.

The equations used to formulate the finite element method for the constant strain triangle used during this research are contained in Chapter II and Chapter IV of Zienkiewicz (1971). The finite element method as presented in these two chapters relates the stresses and strains within the element for linear elastic behaviour of the material.

It has been established that geotechnical engineering materials are not linearly elastic but behave as non-linear materials. These materials also creep when subjected to load. This is the class of problems to which this thesis was directed. In Chapter XVIII of Zienkiewicz (1971) the equations for analysing a nonlinear material behaviour and three methods of solving this class of problem are presented. The methods of solution are:

1. the variable stiffness method.
2. the initial stress method.
3. the initial strain method.

Each of the above methods uses an incremental approach to

arrive at the solution. Zienkiewicz (1971) and Chang et al. (1974), both recommend the initial strain method to solve creep problems.

Zienkiewicz (1971) presents a detailed discussion of the initial strain method and Chang et al. (1974) give a concise but complete listing of the stress/strain-rate relationships which govern the plane strain creep problem. Chang and his colleagues extend the uniaxial creep relationship to the multiaxial condition using Equations 5.19b and 5.19c. They also give a concise explanation of the method used to solve creep problems.

The steps in solving the incremental initial strain method are given as:

1. A solution to the elastic analysis provides the stresses at time equal to zero for the applied loads and boundary conditions.
2. The increment of equivalent creep strains during a short time interval from t=0 to t=t1 are established using the creep law. During this increment of time the stresses are assumed constant.
3. The creep strains are treated as initial strains. These initial strains are then converted into equivalent fictitious nodal loads. The fictitious loads are added to the applied loads and for this loading condition the displacements are evaluated.
4. The stress is calculated from the strains for this increment and then the process is repeated.

These steps are illustrated in the flow chart given in Figure 6.2.

In the program presented by Chang et al. (1974) a failure criterion was incorporated to establish which elements would reach failure. This criterion is not required in order to carry out the creep analysis provided the applied loads are maintained at such a level that all elements would not reach failure. In the programs developed in this thesis a failure criterion was not included because the loads applied to the sample problems were usually maintained below a failure load.

The incremental initial strain method described above has been used by many authors in solving problems related to creep in geotechnical materials (Emery (1971), Nair and Boresi (1970), Emery and Finn (1972), Van Winkel et al. (1972), and Chang et al. (1974)). It has been used to analyse the creep behaviour of tunnels, excavations and slopes in frozen soil and ice (Thompson and Sayles (1972), Emery and Nguyen (1974), Emery (1978), and Emery (1979)). The reasons for the wide use of the incremental initial strain method are (Weerdenburg 1979):

1. it is independent of the type of creep law used.
2. it provides a description of intermediate stages of creep.
3. it is simple to extend the basic elastic finite element program coding to include the non-linear effects arising from creep.

When the material undergoes creep, the stresses (σ_{ij}) within the material change with time as is illustrated in Figure 6.1 by the solid line. In the incremental procedure the smooth stress-time curve is replaced by a series of incremental steps. Each step consists of a constant stress period during a time increment [dt] followed by an instantaneous increment in stress [$d\sigma_{ij}$].

During this procedure it is assumed that the time can be subdivided into sufficiently small intervals [dt] such that the stress [σ_{ij}] can be considered constant. This allows the nonlinear creep problem to be solved using a linear elastic solution for each time interval. The creep strains from the previous time intervals are used as the initial strains for the current time interval. These initial strains establish a set of fictitious boundary loads, for which the displacements are solved.

To solve for the creep deformations using the finite element method, the stress/strain-rate relationship for the material must be known. In order that this relationship be as general as possible the effective shear stress and effective shear strain-rate as defined in Equation 5.19b and 5.29c are used along with the following assumptions (Chang et al. (1974)):

1. No volume change occurs due to creep strains; i.e. material is incompressible after creep begins.
2. The principal shear strain-rates are directly proportional to the corresponding principal shear

stresses.

3. The principal strain axes do not rotate under deformation; i.e. the direction of principal normal strains are in the same direction as the corresponding principal normal stresses.

4. The strains are small.

These assumptions allow the effective strain rate and the effective shear stress to be related by:

$$[de/dt]_{ijc} = (3/2)[dE/dt]_{ec}(1/\delta e)\bullet\delta'_{ij} \qquad (6.1)$$

where

$[de/dt]_{ij}$ = strain-rate tensor

$[dE/dt]_e$ = defined by Equation 5.19b

δe = defined by Equation 5.19c

δ'_{ij} = deviatoric stress tensor

c = refers to component due to creep.

These steps are followed in both the plane strain and axi-symmetric programs.

6.3 Finite element programs

In this section the two finite element programs which resulted from modifications to the constant strain triangle program are described.

6.3.1 Modifications to constant strain triangle

The major modification to the constant strain triangle program consisted of adding a subroutine to calculate the increment of creep strains for the constant stresses during a given time interval. The increment of creep strains were evaluated by first calculating the effective strain-rate which resulted from the assumed constant stresses within each element. The creep strain was obtained by multiplying this effective strain-rate by the constant time increment. The component of the increment of creep strain in each direction was evaluated using:

$$[de]ij\underline{c} = [de/dt]ij\underline{c} \bullet [dt] \qquad (6.2)$$

where

$[de]ij\underline{c}$ = component of increment of creep strain

$[de/dt]ij\underline{c}$ = component of creep strain rate defined by Equation 6.1

dt = increment of time.

For each element the components of creep strain were stored and used later as the initial strains of the next time increment.

The second modification consisted of evaluating the fictitious loads resulting from the calculated initial strains. The fictitious loads were then added to the existing loads of the problem. These accumulated loads were

used with the boundary conditions of the problem to evaluate the displacements within the material. The total displacements for the loading condition were calculated using the Gaussian elimination technique.

The third modification was required to calculate the stresses for this time increment. To accomplish this the strains calculated for all previous time increments were accumulated so they could be subtracted from the total strain resulting from the previously calculated displacements. At this point the stresses for the next time increment were evaluated.

To facilitate a reduction in computing costs, a number of minor alterations to the constant strain triangle program were also implemented. The stiffness matrix was formed and saved during each run to reduce computation times. The method of storing the various matrices in the computer was altered to reduce storage and computation time.

The actual alterations made to the constant strain triangle program listing are contained in Appendix B. It contains the original constant strain triangle program listing and an inventory of the variable names used. The second program listed is the creep program used to solve plane strain steady-state creep problems. It also has a listing of the variable names and contains the alterations made to the original program. These alterations are indicated with an (*). The third program listed in Appendix B is the axi-symmetric program. This program listing

contains the alterations to the original constant strain triangle program in order to solve both axi-symmetric elastic and axi-symmetric steady-state creep problems. In this listing the alteration necessary to accomplish the creep solution are designated with an (*) and those to accomplish the axi-symmetric solution by a (/).

6.3.2 Check on solutions of programs

A comparision of the results of the finite element programs with the results of the closed-form solution of the expansion of a thick-walled cylinder is presented and demonstrates that the approximations and the techniques used give a correct solution. The comparison will be made for a thick-walled cylinder consisting of a material which behaves linearly elastically and then fully plastic. During the fully plastic behaviour the strain-rates are related to the stresses by a simple power law. Each comparison will be made using both the results of the plane strain and axi-symmetric program. The comparison of each program will be discussed separately.

To facilitate the comparison between the theoretical and the finite element method, the problem and the material properties used is presented in Figure 6.3. The boundary conditions for which the solution is required appear in the Figure. The equations for the closed-form solution appear in Hult (1966) and Odqvist (1966). Table 6.1 contains the pertinent values for the elastic solution. Table 6.2

contains values of the solution to the above problem when the material behaviour is governed by the following steady state creep flow law:

$$[de/dt] = 0.001[\ 5/157.7]^{2.53} \qquad (6.3)$$

Initially the comparison of the axi-symmetric finite element solution will be presented. In order to evaluate the results of the finite element program the grid given in Figure 6.4 was used. The material property assigned to each element is given in Figure 6.3 and an internal applied pressure of 700 kPa was used. The elastic response of the grid to the applied loads calculated using the finite element axi-symmetric program are presented in Figure 6.5 and Figure 6.6.

In Figure 6.5 the variation of both the elastic radial and tangential stress versus the normalized radial distance (r/B) are plotted. B is the value of the external radius of the cylinder. In this plot the value of each stress is plotted from the internal to the external radius of the thick-walled cylinder. The results of the axi-symmetric finite element program are plotted as open circles in the Figure. The comparison between the closed form solution and the finite element solution show that this program will calculate the elastic stress correctly for an axi-symmetric loading condition.

Figure 6.6 compares the theoretical value of the

elastic displacements with those calculated using the finite element method. Again, the solid line represents the displacements which result from the closed-form solutions. The open circles are the results obtained from the axi-symmetric finite element solution. This comparison also illustrates that the axi-symmetric finite element program recovers the elastic displacements at the internal radius and throughout the cylinder.

The comparison of the results of the axi-symmetric finite element program and the closed-form solution under conditions of steady-state creep are contained in Figure 6.7 and Figure 6.8. The stresses resulting from a condition of steady-state creep of the thick-walled cylinder are given in Figure 6.7. The results of the closed-form solution are again presented by the solid line. The tangential, radial, and the axial stress which results are plotted in the Figure. The stresses which result from the constant applied internal pressure using the axi-symmetric program are plotted as open circles.

It is immediately apparent that this program does not reproduce the stresses within the material near the internal radius of the cylinder. The tangential stress is overestimated close to the internal radius while the radial stress is underpredicted. As the radius increases the comparison between the closed-form solution and the stresses from the finite element method improve.

The displacements of the inner radius of the

thick-walled cylinder are compared in Figure 6.8. This shows that the calculated displacement using the axi-symmetric finite element program and the displacement calculated using the closed-form solution are comparable. These displacements result in displacement rates of the inner radius of the thick-walled cylinder which differ by 2.3%. This analysis illustrates that the displacement rate resulting from the axi-symmetric program compare closely with the results of the closed-form solution, whereas, the stresses are not as comparable.

This lack of comparison of the stresses is partly due to the fact that the axi-symmetric program uses an approximate procedure to establish the elemental stiffness and nodal loads. The approximation is given by Zienkiewicz (1971). The lack of agreement between the stresses is also due to the fact that the constant strain triangle is used while it is well known that the strain varies with the radial distance in an axi-symmetric problem. This element is not capable of accounting for this variation in strain with radial distance .

The differences in the stresses as noted occurs near the internal boundary. At this boundary the applied pressure was simulated by applying a concentrated force at each node. The concentrated forces were evaluated as equivalent to the load resulting from the uniform pressure applied over the area of each element. This equivalent force was then applied at the nodes of each element. The concentrated forces had a

major influence on the stresses within the elements at the internal boundary.

The inaccuracy in calculating the stresses at the internal boundary was not considered detrimental since the displacement and displacement rate are the output of interest in this work. These, it will be noted, are reproduced quite well by this program.

A similar comparison between the results of the plane strain program and the closed-form solution will be examined. To facilitate this comparison, the grid plotted in Figure 6.9 was used. The displacement and stress distribution for this grid was determined for both the elastic and the steady-state condition.

The elastic stress distribution compared to the theoretical distribution for the thick-walled cylinder is presented in Figure 6.5. The results of the plane strain program are plotted as open squares. This Figure shows that the elastic stresses throughout the thick-walled cylinder are reproduced by the plane strain program. The elastic displacements also are compared with the theoretical values in Figure 6.6. Again, the plane strain program compares closely with the results of the closed-form solution. The comparison in Figure 6.5 and Figure 6.6 shows that program will solve the elastic problems accurately.

Figure 6.8 and Figure 6.10 show the comparison between the displacement rate and the stress distribution under a condition of a steady-state creep. Again, in each of these

Figures the comparison is made with the theoretical displacement rate and stress distribution. The displacement rate from the plane strain program compares within 2.0 % of the theoretical value given in Figure 6.8. The stress distribution within the thick-walled cylinder presented in Figure 6.10 is not as close as is the displacement rate.

The lack of agreement between the stresses is due to the fact that during the analysis of the plane strain program the internal pressure was again applied by using an equivalent concentrated force at the internal boundary nodes. These concentrated forces cause stress concentrations within the boundary elements. It is these boundary elements within which the stress distribution deviates from the results of the closed-form solution as shown in Figure 6.10. The problem could be solved by establishing a constant pressure boundary loading condition, but it was not felt that this was justified. Again, the displacements and especially the displacement rates are of most interest and these compare well.

The comparison of the results from these two programs with the theoretical results for the thick-walled cylinder problem show that each program will reproduce the thick-walled cylinder results. The loading conditions for which it is used must be specified and if concentrated loads are applied the stress distribution close to the load will be questionable but the displacement rates will not be influenced by the concentrated forces. If the stress

distribution is important the method of applying the equivalent loading to simulate the uniformly distributed loads should be modified.

6.4 Use of finite element to predict behaviour of experiments

To this point in this thesis, the flow law of ice has been measured and it has been shown to be valid under various complex stress conditions. The penetration behaviour of a punch into this ice has also been studied and the results analysed in Chapter 5. In the previous section of Chapter 6 two finite element programs developed to study the deformation behaviour of ice under load have been outlined. Now these three separate aspects of the thesis will be used to analyse the behaviour of an unconfined compression test and a punch test.

The purpose of the study of the unconfined compression test is to show that, given the following:

1. a grid which represents an unconfined compression sample;
2. a steady-state flow law for the material behaviour; and,
3. a finite element program which is capable of solving an axi-symmetric loading condition;

the actual experimental data can be predicted using the finite element program.

Figure 6.11 gives the finite element grid used to model the compression experiment. The flow law of the ice used to

specify the material behaviour in the calculations is given in Equation 4.19. Note that the grid allows for a length to diameter ratio of greater than two. The uniform stress was applied by giving the top row of elements a unit weight which applies a uniform stress to the material below.

The axi-symmetric finite element program was used to solve for the axial displacement of the top row of elements. This information was then used to establish the magnitude of the strain-rate associated with the constant displacement rate of the nodes of these elements.

The results of the analysis of the unconfined compression experiment are presented in Figure 6.12 which shows that the finite element program with the flow law of Equation 4.19 predicts the actual laboratory data and reproduces the flow law used. The agreement between the finite element determinations and laboratory measured results is extremely good.

This agreement is as expected because the flow law used in the analysis was that evaluated using the laboratory data. The important conclusion to be drawn is the support it gives to the previous finding that the finite element program will predict the displacement rate accurately and can be used to analyse different types of boundary value problems.

The second portion of this study was to examine how well the finite element solution would predict the punch penetration behaviour. Again the input data was

1. a grid which represents a punch experiment;
2. a steady-state flow law for the material behaviour; and,
3. a finite element program capable of solving an axi-symmetric loading condition.

This analysis had two objectives. One was to predict the laboratory punch data, and the second was to study the influence of changing the embedment depth of the punch beneath the surface.

Figure 6.13 shows the grid used in the first analysis. The ratio of the depth of the punch embedment to the diameter of the punch (D/B) was zero. This was used because during the laboratory testing program the majority of the experiments had a D/B ratio of less than 1.0. Various constant pressures were applied to the circular punch and the displacement rate of the punch evaluated from the output of the finite element method. Figure 6.14 is a plot of the actual laboratory data and the results of this finite element study. The results of the first study are plotted as open squares with a dashed line drawn through the points.

The finite element analysis reproduces the measured punch data. In Figure 6.14 the results of the theoretical cavity model prediction from Chapter 5 are also included. This relationship also was obtained by using Equation 4.19 as the flow law of ice. The comparison of the data illustrates that the cavity model and the finite element analysis bracket the actual laboratory punch data. The finite element results agree more closely with the measured

data than the results of the cavity expansion theory at low punch resistance. At a given displacment rate of the punch, the finite element method predicts that the resistance of the punch is about 37 % higher than that calculated using the cavity expansion model.

Figure 6.14 also includes the data from a finite element analysis in which the influence of increasing the depth of the circular punch beneath the surface was studied. The finite element grid used during this study is contained in Figure 6.15. The D/B ratio was equal to 5. The results indicate that the depth of the punch beneath the surface has little or no influence on the pressure required to cause the punch to penetrate at a constant rate. This finding supports the laboratory data presented in Section 5.4.3 that the depth of the punch beneath the surface had little influence on the pressure required to penetrate at a constant rate.

The displacement field resulting from the punch analysis using the finite element program for D/B equal to 5 is given in Figure 6.16. This is the displacement field during the time increment at which the displacement rate for the applied pressure of 5000 Kpa was calculated. The solid lines with an arrow at the tip are drawn to scale and equal the displacement at the point from which the arrow starts and gives its direction. The dashed lines give the outline of a quarter of a spherical cavity and the radial lines are drawn outward from the center of the cavity at an arc interval of 15°.

At radial distances from the center of the punch of less than B the displacements are directed vertically downward with a slight rotation near the outer edge of the punch. This deformation is associated with the disturbed zone of ice illustrated in Plate 5.1. At radial distances greater than B, the displacement field parallels the radial lines which conforms with the displacement field of an expanding spherical cavity. The comparsion between these two displacement fields supports the agreement between the finite element and cavity expansion results presented in Figure 6.14.

To facilitate comparison between the data of each method given in Figure 6.14 the data is summarized in Table 6.3. The tabulated results show that the finite element method predicts the punch experimental results at a pressure of 3000 kPa, but underpredicts the data at 5000 kPa. The cavity expansion model closely predicts the data at 5000 kPa and overpredicts the 3000 kPa results. The difference in the predicted rate and the measured value of each method varies with the applied pressure.

The difference in the results may be due to the definition and use of a failure strain of the ice during the analysis of the cavity expansion model. This was used to predict an average strain-rate for constant rate of penetration (Ladanyi (1976)). The finite element program does not incorporate a failure criterion. Thus, it is incapable of accounting for failure and this shortcoming may

cause the difference between the calculated results and the measured values. A failure criterion would cause the displacement rate at each given applied pressure to increase since stresses within the failed elements would be redistributed to the surrounding elements thus increasing the stresses in these elements. This increase in stress would cause the nodal displacement to increase. This behaviour however was not evaluated during this project.

6.5 Conclusion

The finite element method has been briefly described and it has been shown to be valid in solving two simple boundary value problems. The method gives good results when the displacement rates of a boundary value problem are compared. The stresses for this problem are very sensitive to the method of applying the load and this must be studied. As a result of analysing the punch experiment using this method, the lack of influence of the punch embedment is supported.

Table 6.1

Summary of elastic solution to thick walled cylinder problem presented in Figure 6.3

r	(r/B)	?σr/pi?	?σθ/pi?	ui mm
1.4	0.42	-1.00	1.43	8.45
1.65	0.50	-0.65	1.09	7.16
1.90	0.58	-0.44	0.87	6.22
2.15	0.65	-0.29	0.73	5.59
2.41	0.73	-0.19	0.63	4.93
2.67	0.81	-0.12	0.55	4.47
2.92	0.88	-0.07	0.50	4.09
3.30	1.00	-0.00	0.44	3.63

Table 6.2

Summary of the steady state creep solution to the thick walled cylinder problem presented in Figure 6.3

r	(r/B)	[δr/pi]	[δθ/pi]	[du/dt]i (m/hr.)
1.40	0.42	-1.00	0.43	0.42
1.52	0.46	-0.88	0.49	0.40
1.90	0.58	-0.59	0.64	0.32
2.15	0.65	-0.44	0.71	0.27
2.41	0.73	-0.32	0.78	0.24
2.67	0.81	-0.22	0.83	0.23
3.00	0.92	-0.10	0.89	0.20
3.30	1.00	-0.00	0.93	0.18

Table 6.3

Summary of punch data and predicted results using cavity expansion model and finite element program.

Punch Resistance (kPa)	Normalized Settlement Rate (Experiment)	Normalized Settlement Rate (Finite Element)	Normalized Settlement Rate (Cavity)
3000	2.3	2.3	4.6
3100	2.3	2.3	4.7
3300	2.3	2.4	5.4
4600	11.0	6.0	11.0
4675	11.0	6.2	14.0
5000	11.0	7.0	16.0

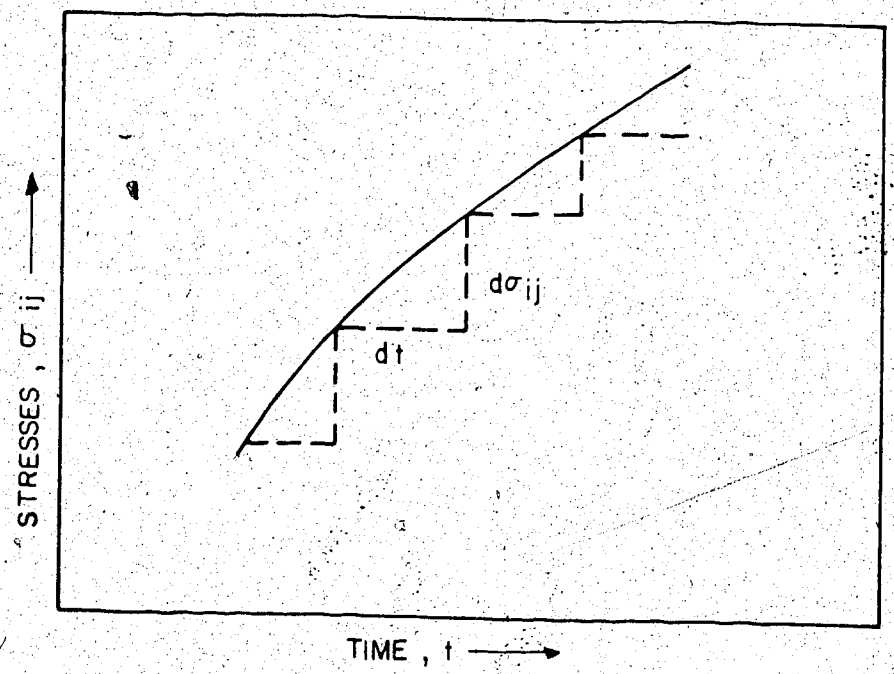

Figure 6.1 Approximation of smooth stress time curve.

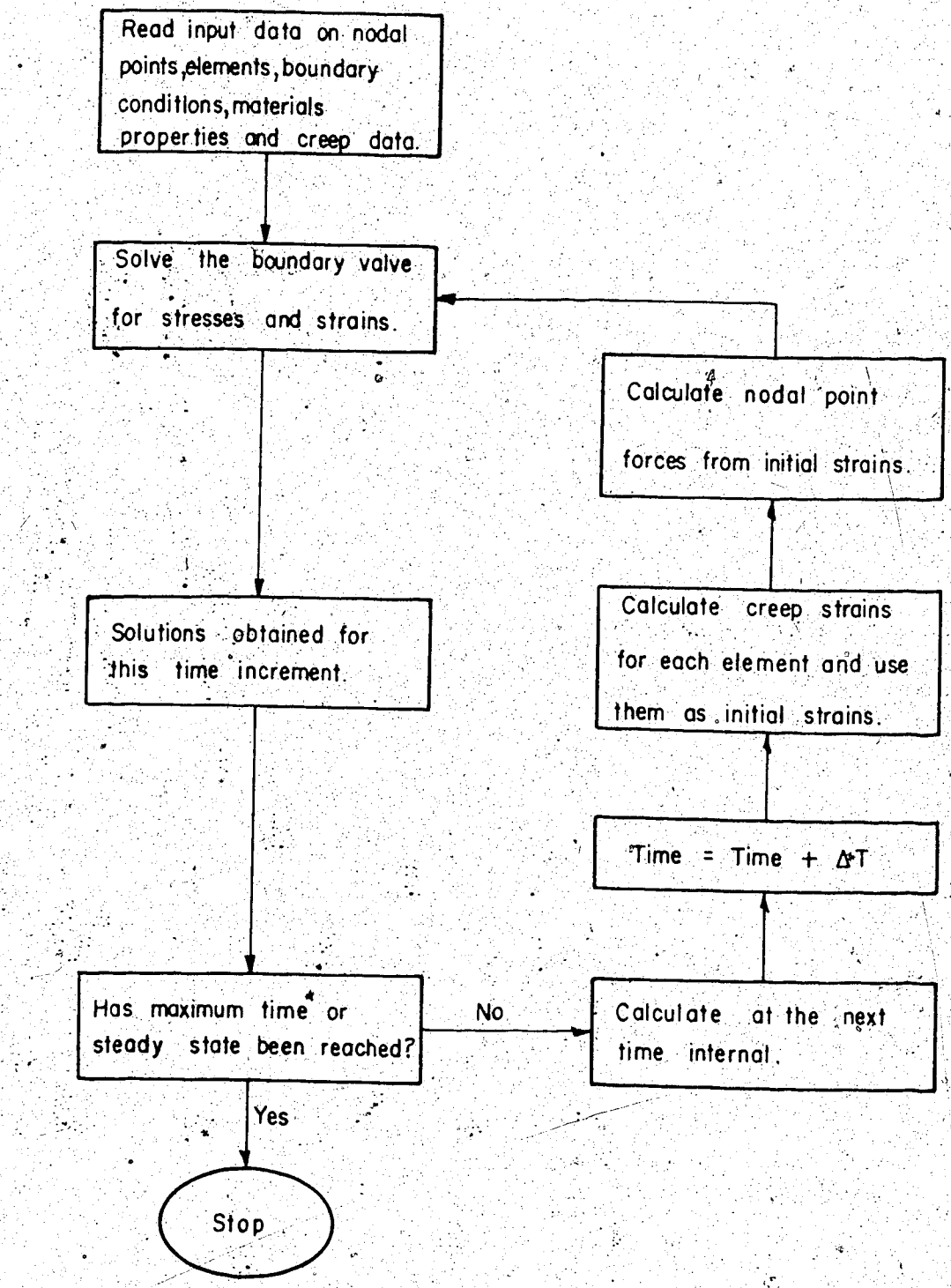

Figure 6.2 Simplified flow chart for incremental analysis of creep.

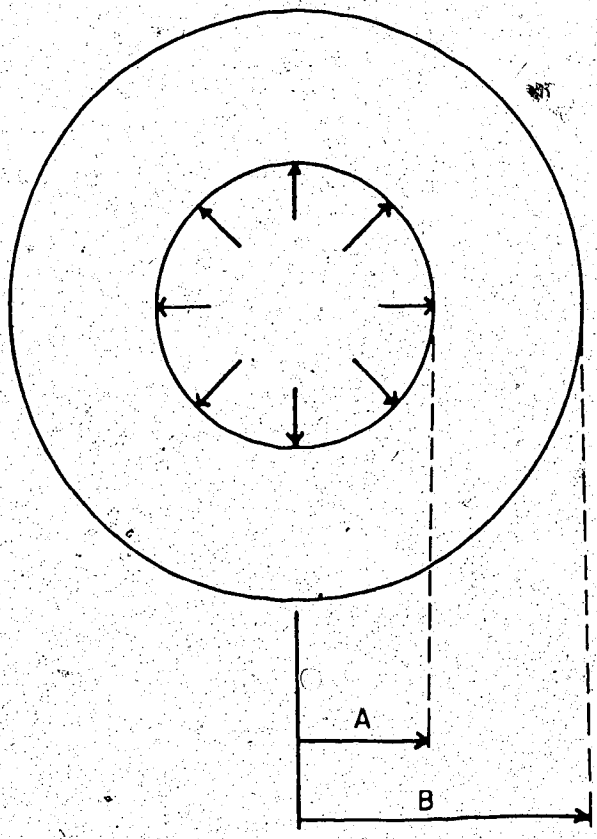

Dimension

A = 1.4 m.

B = 3.3 m.

Material Properties

Elastic

E = 21000 kPa.

ν = 0.495

Creep

$$\frac{de}{dt} = .001 \left(\frac{\sigma}{157.7}\right)^{2.53}$$

Internal Pressure = 700 kPa.

External Pressure = 0 kPa.

Figure 6.3 Boundary conditions and material properties of thick-walled cylinder problem.

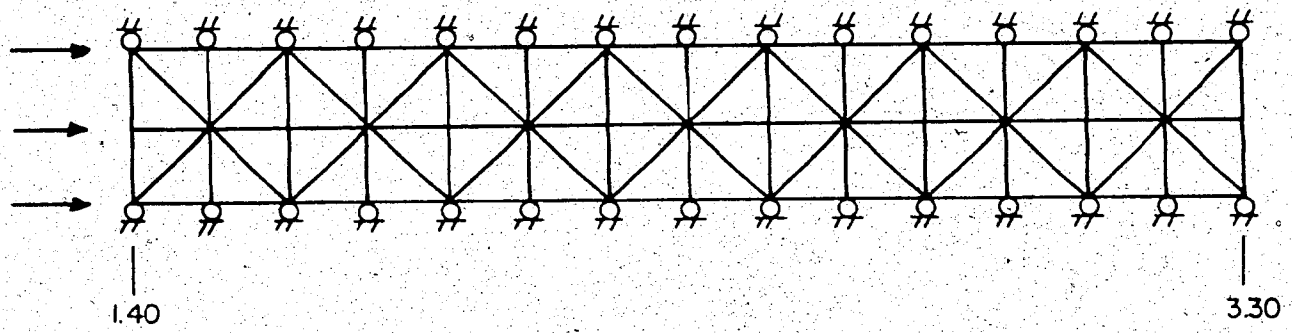

Figure 6.4 Finite element grid used to evaluate axi-symmetric program.

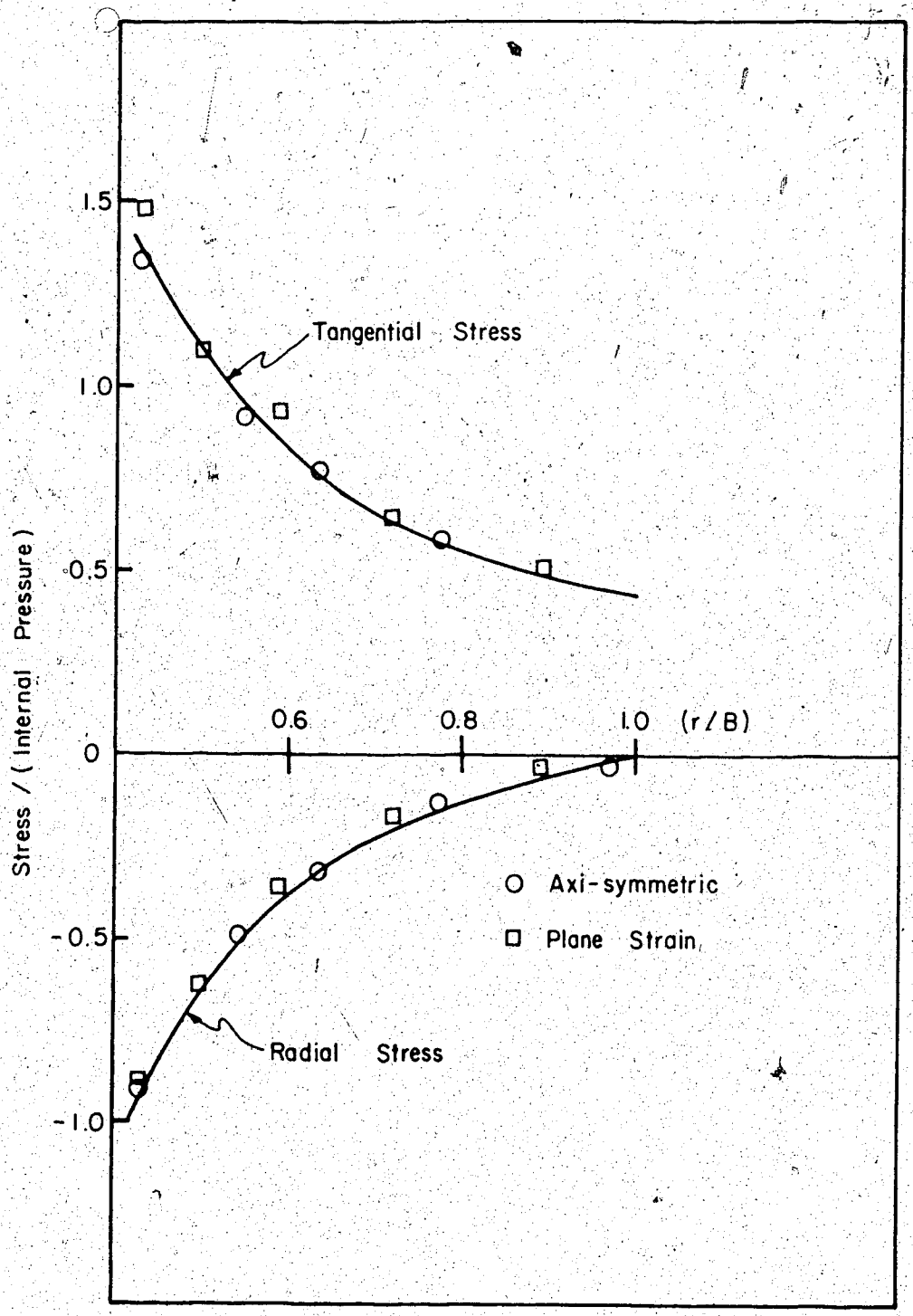

Figure 6.5 Elastic stress distribution versus r/B for thick -walled cylinder problem.

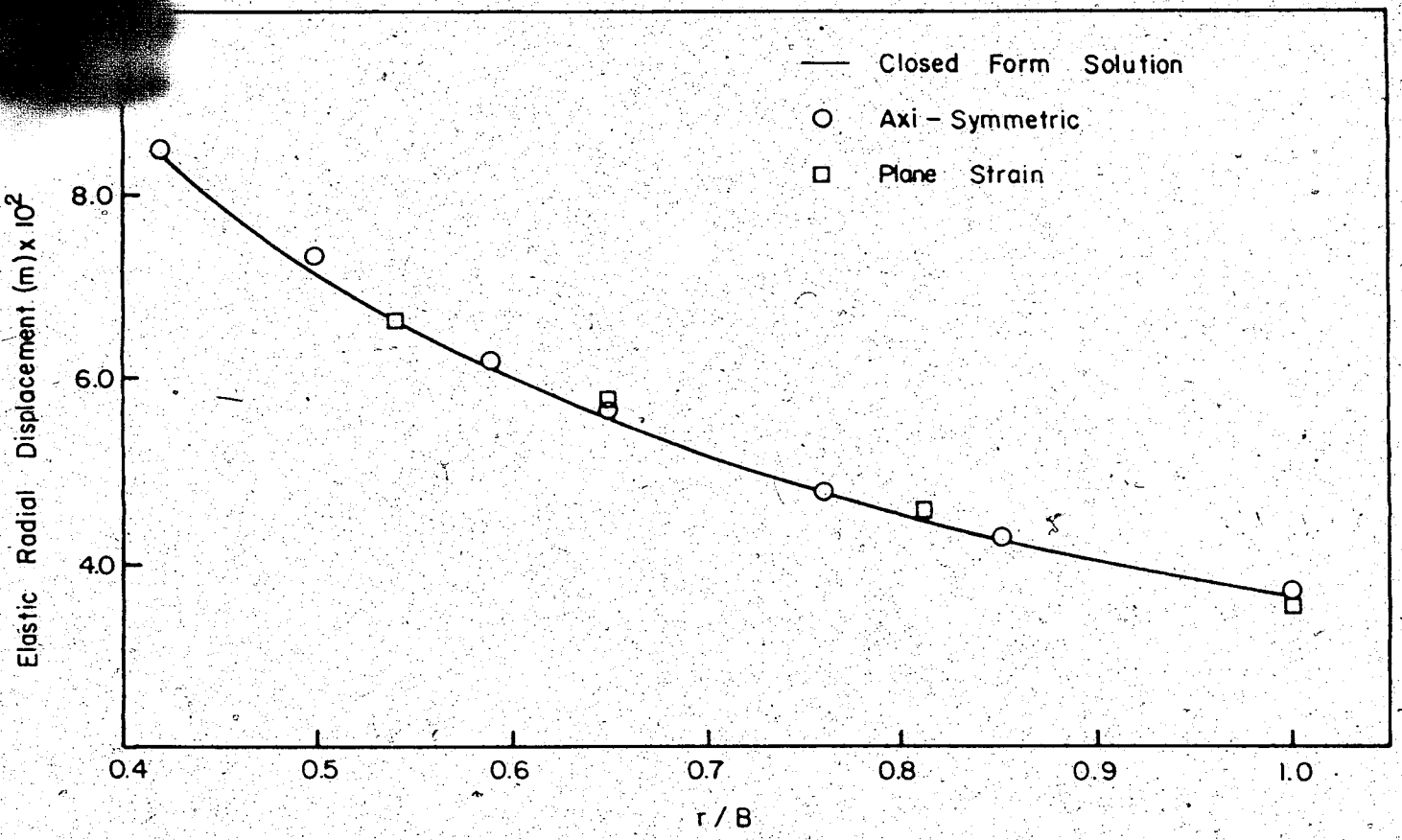

Figure 6.6 Elastic radial displacement versus r/B for thick -walled cylinder problem.

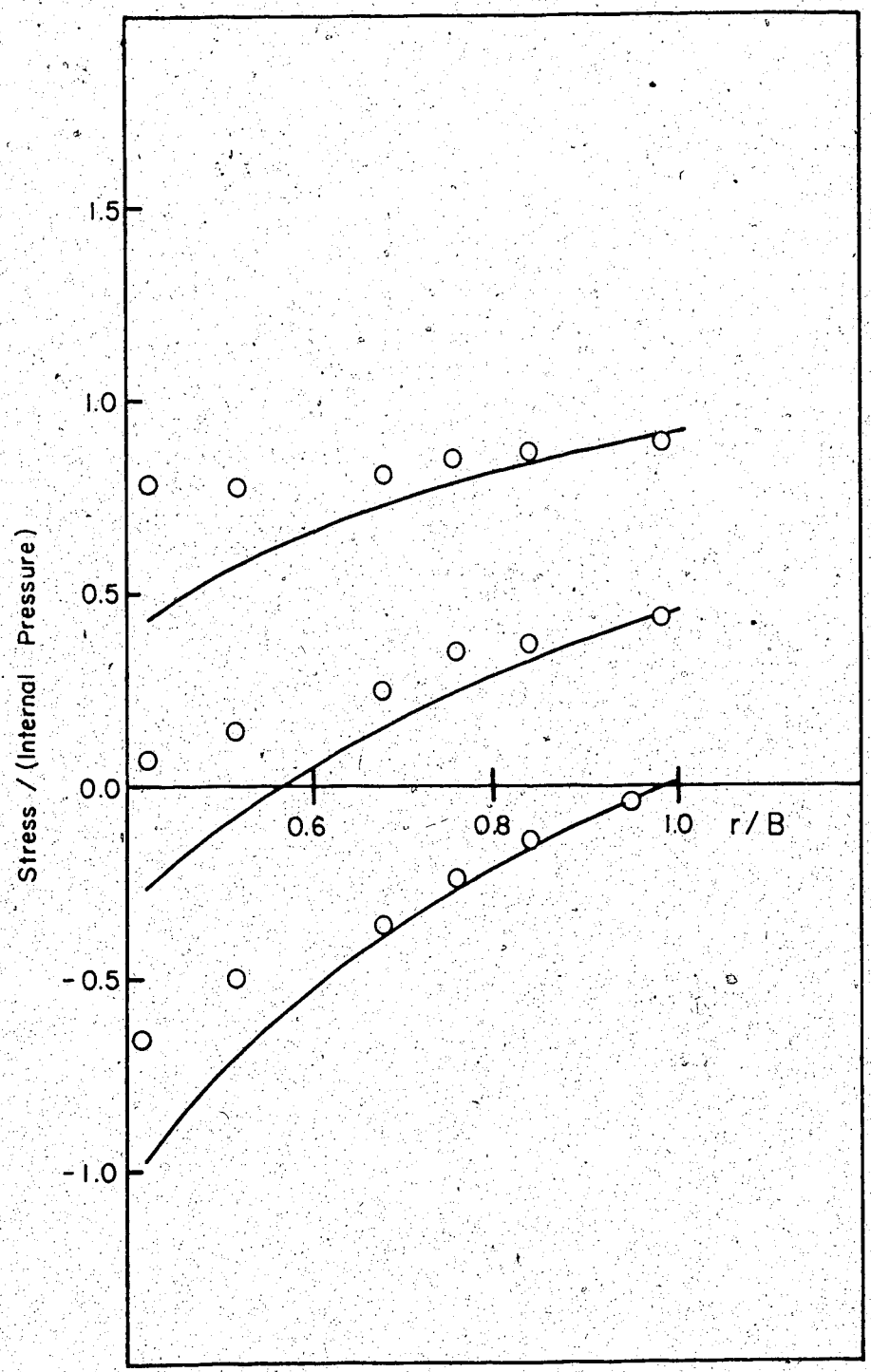

Figure 6.7 Comparison of stress distribution of axisymmetric finite element results to closed form solution during steady state creep

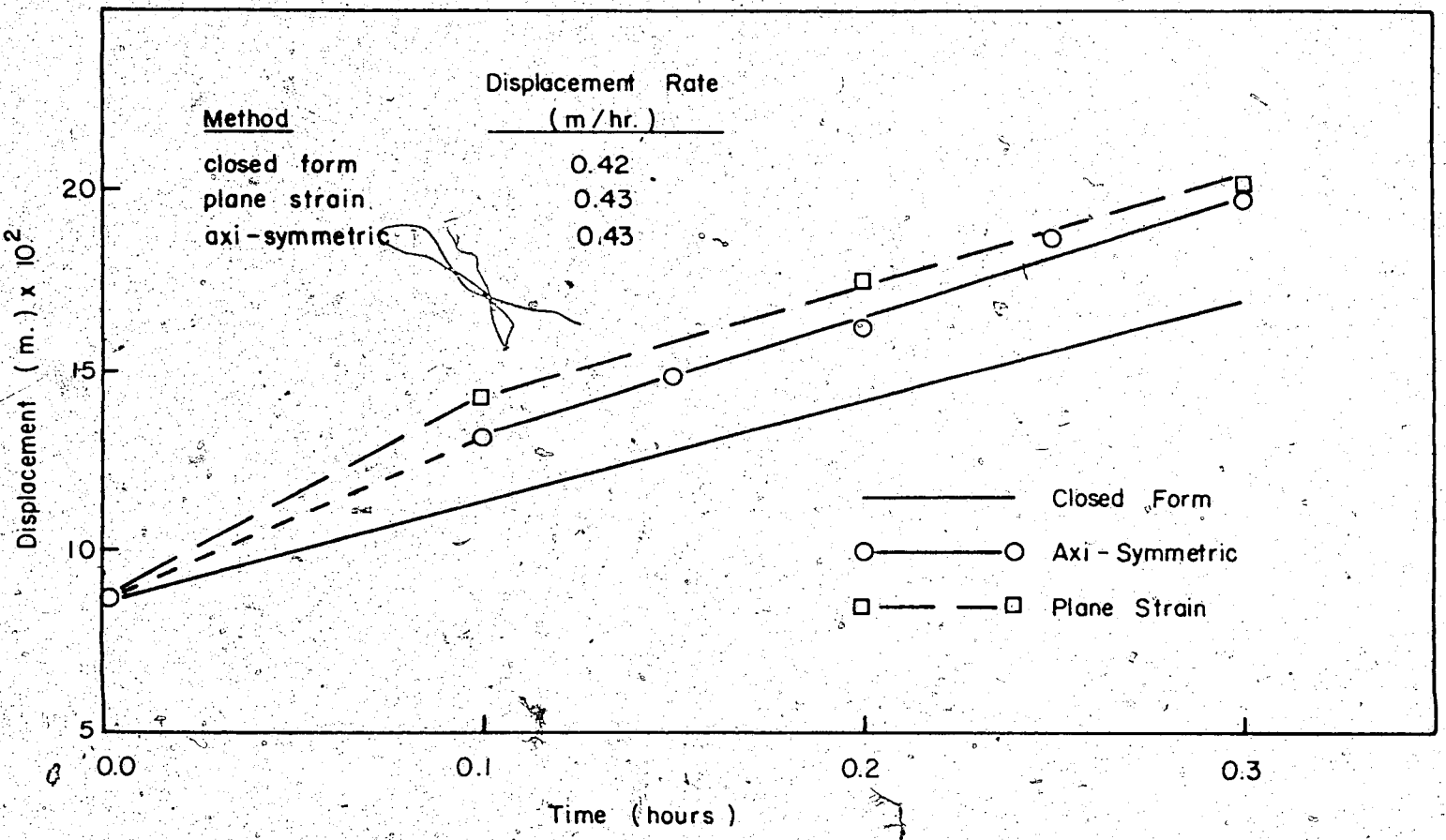

Figure 6.8 Comparison of displacement and displacement rateof the internal radius of thick-walled cylinder problem during steady state creep

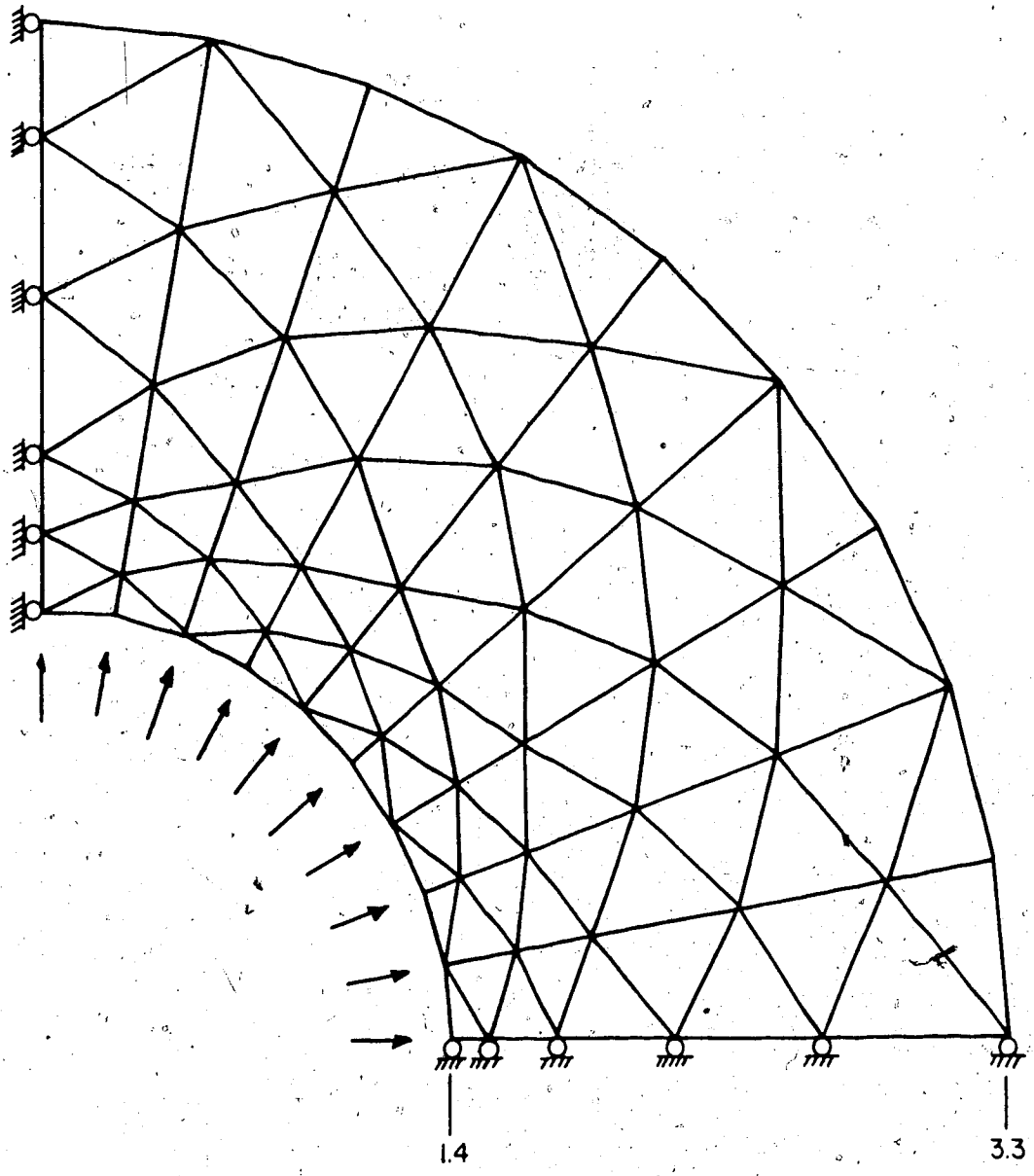

Figure 6.9 Finite element grid used to evaluate the plane strain program.

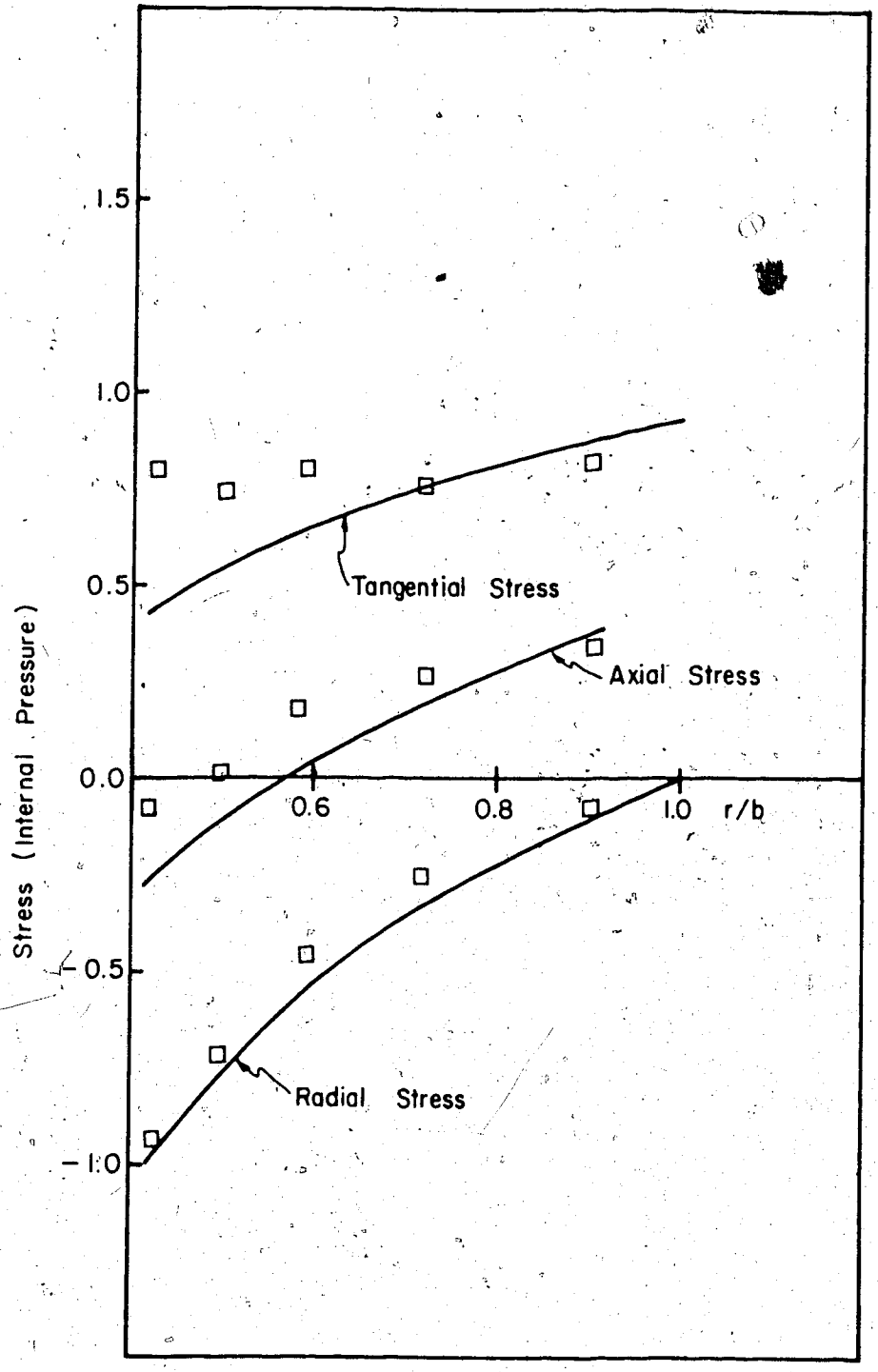

Figure 6.10 Comparison of stress distribution of plane strain finite element results to closed form solution during steady-state creep.

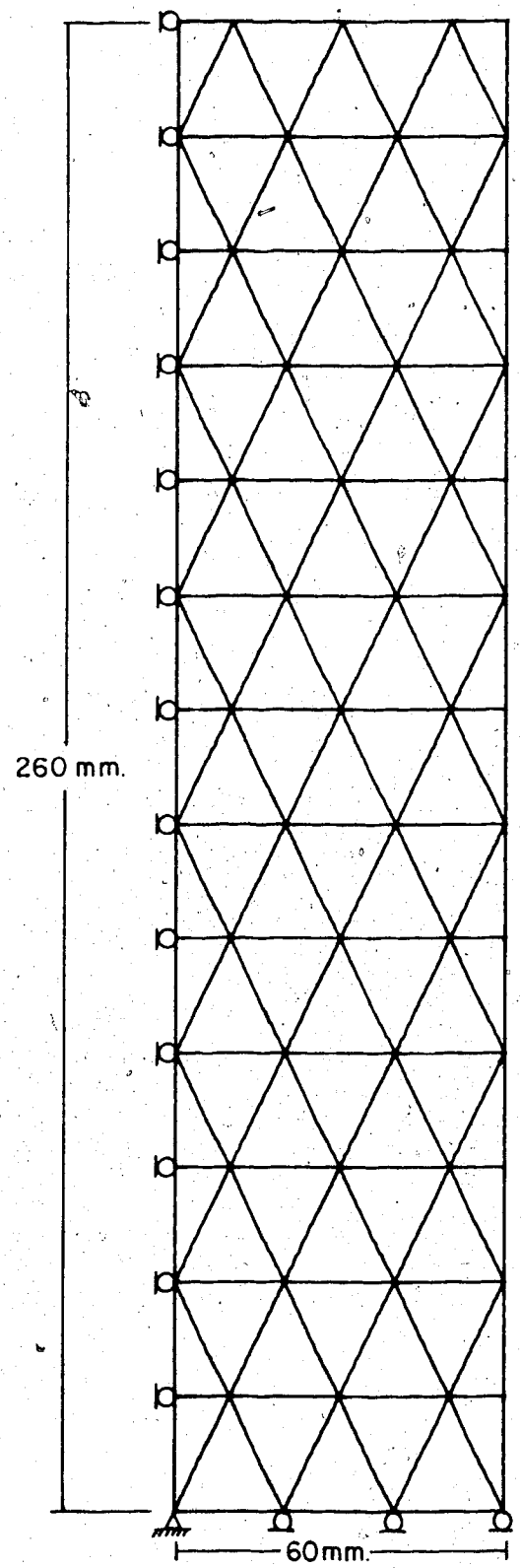

Figure 6.11 Finite element grid used to study unconfined compression test.

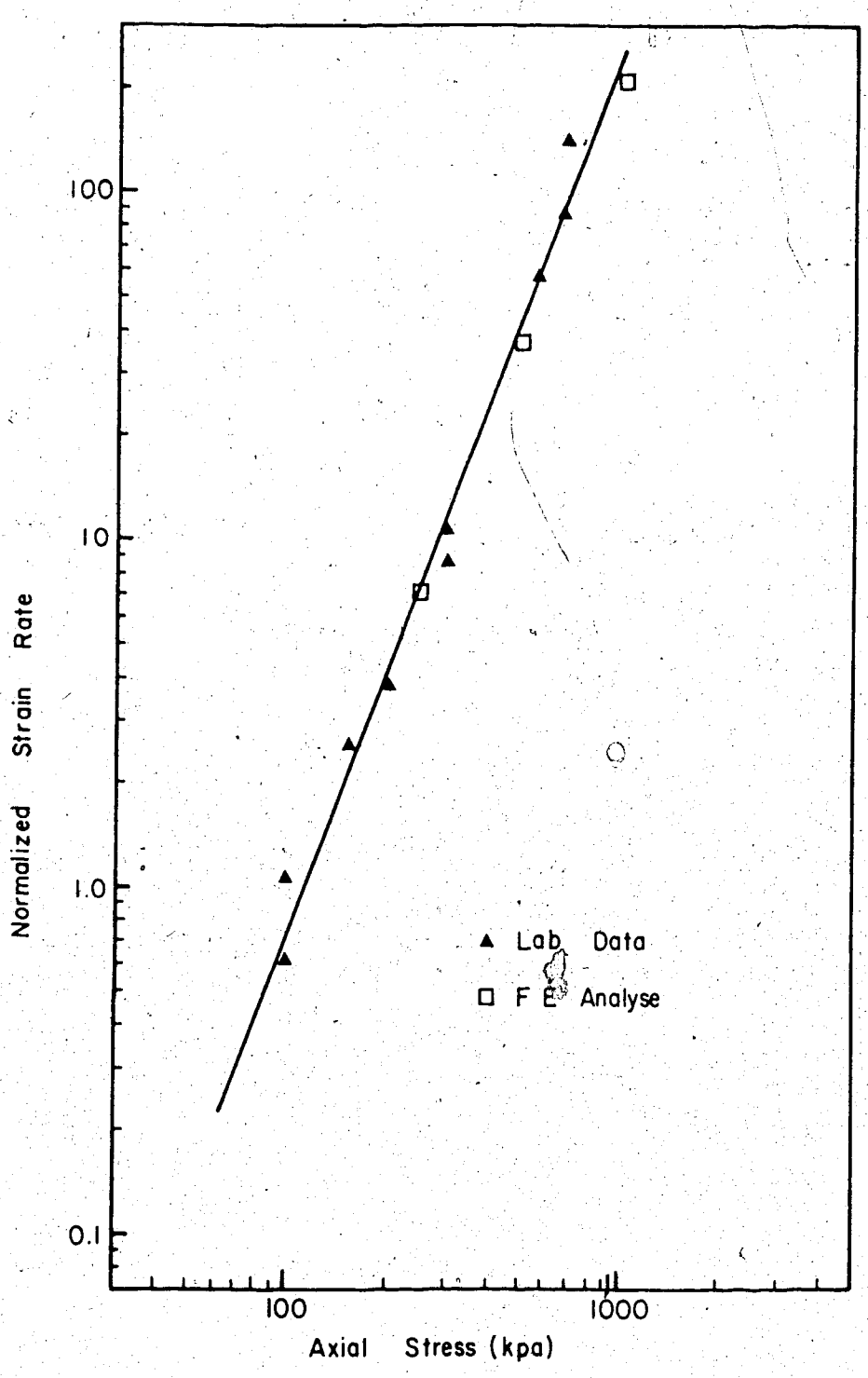

Figure 6.12 Normalized strain rate versus axial stress comparsion of finite element results and laboratory measured data.

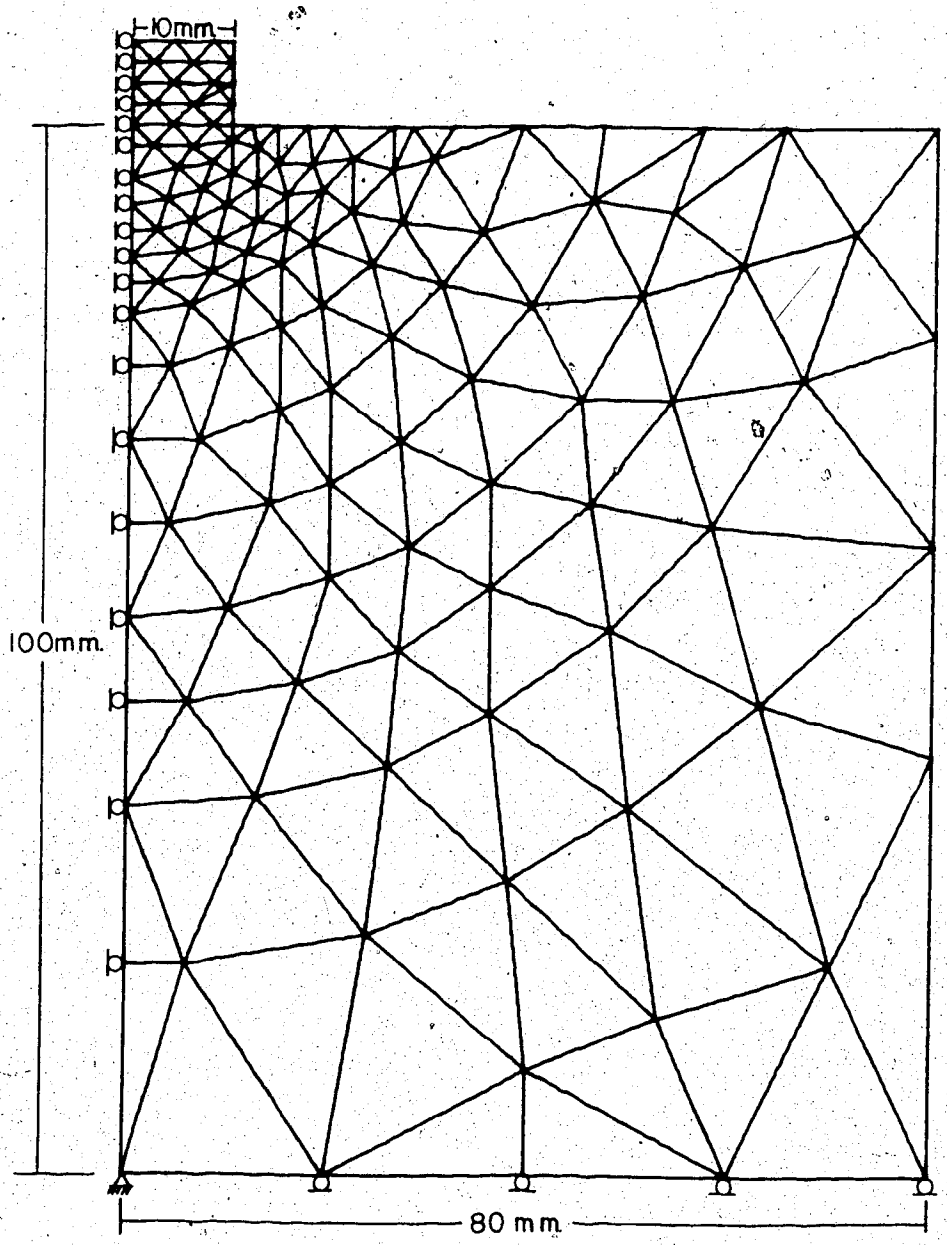

Figure 6.13 Finite element grid used to study penetration test.

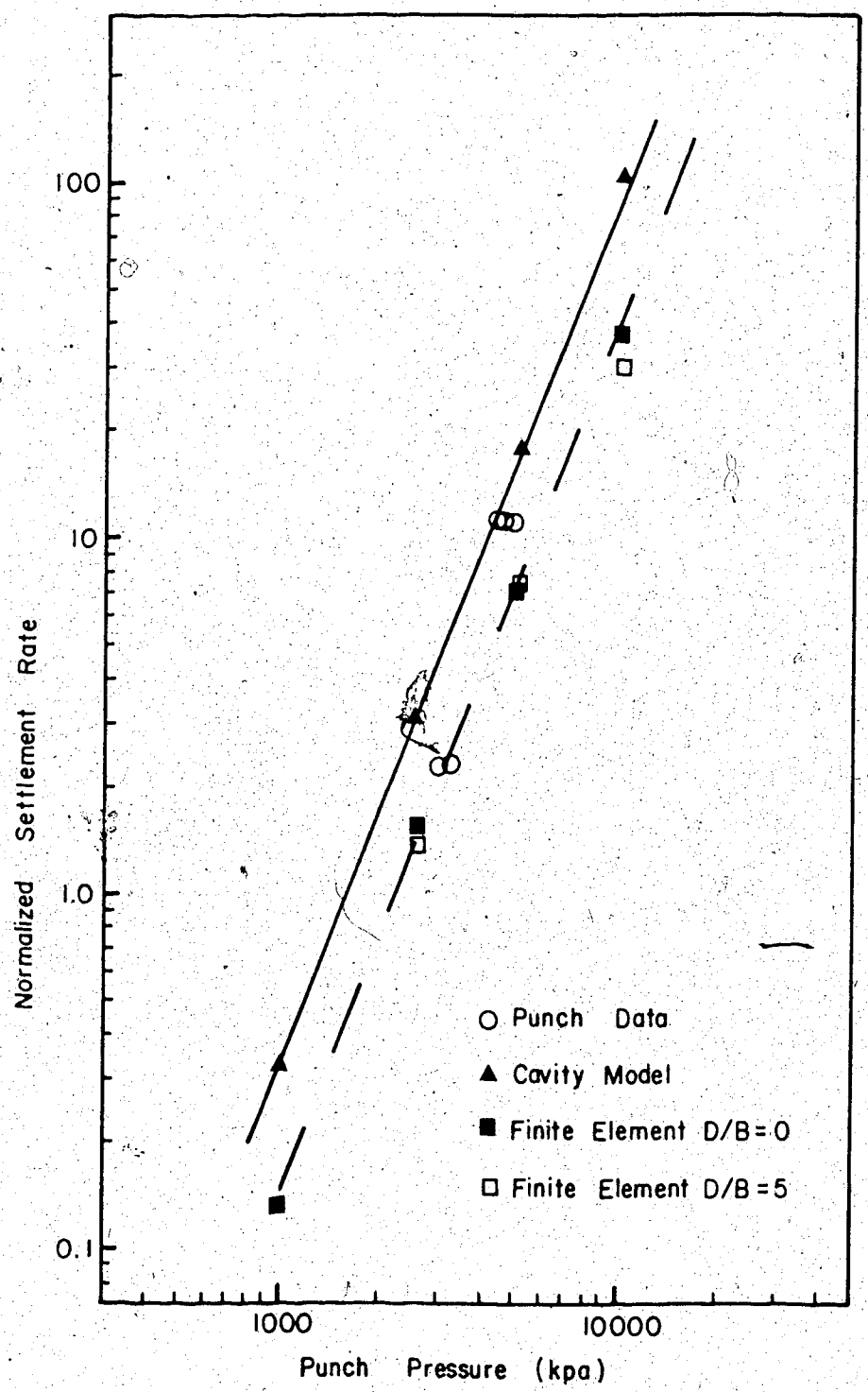

Figure 6.14 Normalized settlement rate versus punch resistance comparison of finite element and laboratory measured data.

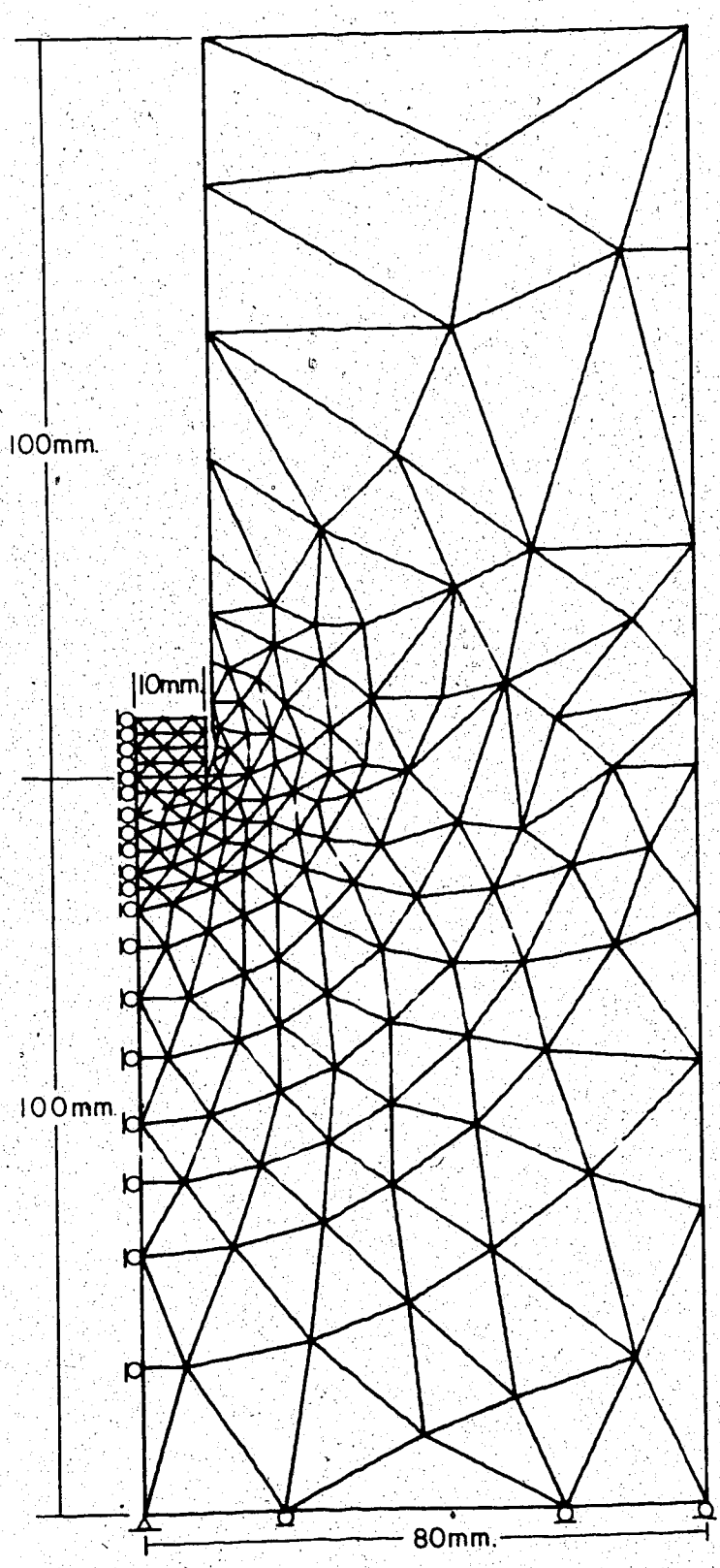

Figure 6.15 Finite element grid used to study influence of depth of embeddment of punch penetration results.

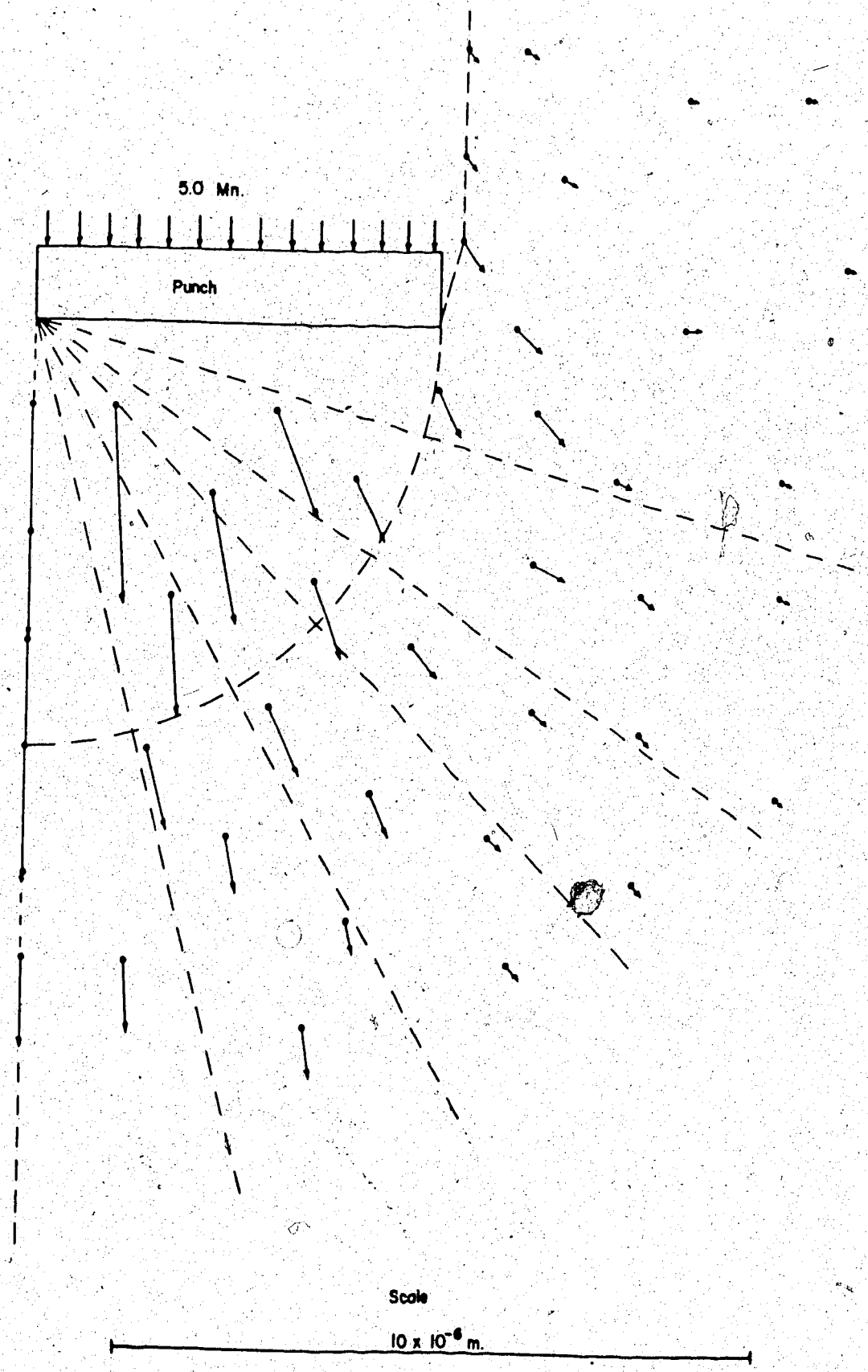

Figure 6.16 Plot of displacement field surrounding the punch for D/B=5

CHAPTER 7

Concluding Remarks

7.1 Strain time behaviour

A review of published relationships for predicting the strain time curve of a creep experiment suggests that the Andrade one-third law would predict the data. In this thesis this method as well as three others were evaluated and all failed to reproduce the experimental strain-time data. The analysis of this data showed that an equation which related the influence of time using a power law and to this adding the strain associated with the minimum strain-rate predicts the strain-time behaviour. The applied stress during the experiments influenced the parameters which establish the power law function of time. The influence of the stress on the exponent of the power law was such that Andrade one-third law would not predict the behaviour of the data. These results suggest that further work should be devoted to establishing the influence of the temperature on the strain-time data.

The importance attached to the strain-time relationship results from the finding during this research of a lack of prolonged steady-state creep behaviour under uniaxial stress conditions. The strain-rate during the experiments decreased to a minimum value, maintained this value for a short period, then accelerated. This acceleration in the strain-rate occurred at a total accumulated strain of about

1.0%. This suggests that the method of analysing the deformation within ice as a steady-state creep process is a convenient simplification, but one with serious limitations. The limitations are associated with the fact that up to 1% strain the majority of the deformation of the material is associated with primary creep behaviour, not steady-state behaviour.

7.2 Flow law of polycrystalline ice

The review of published creep results established that the flow law of polycrystalline ice is best expressed using a simple power law relation with an exponent equal to 3.0. The separation of the data between ice which has undergone strains of less than 1% and ice which has undergone large strains was emphasised. These two separate flow laws of ice were evaluated from the laboratory measurements. Both flow laws were found to be parallel.

Creep within natural ice bodies has been measured under low stresses, and when compared with laboratory creep the flow laws are also parallel. This allows the short-term flow law to be extended into the low stress region using an exponent of 3.0.

The need for extending the laboratory determined flow law in this manner results from the time required to conduct experiments at stresses of less than 100 kPa. The time to establish a minimum strain-rate has been studied, and it shows that creep experiments at stresses less than 100 kPa

require loading times in excess of 2000 hours.

The published literature also presents limited information on the influence of the crystal size. In this research the influence of a size effect within ice samples loaded for the first time was established. It was found that all data used to establish the flow law of ice must be compared at a common grain size ratio. The data from various authors have been compared at a constant grain size ratio and the flow law of ice for the combined results presented. This finding suggests that the size effect ratio must be accounted for before the flow law is used to analyse a field loading condition or alternatively the properties used in the analysis must be measured in the field.

During the research program the strain at which the ice fails under various loading conditions was measured. This data suggests the flow law of polycrystalline ice under a short-term loading condition is only valid provided less than about 1% strain has accumulated within the ice.

7.3 Complex loading conditions

The literature suggests that varying the stress state within an ice body will only influence the deformation of the ice if the second stress invariant is changed. This has been supported by experiments conducted as part of this program.

Work associated with the frozen soil studies suggested that experiments in which a punch was penetrated into frozen

soil could be used to evaluate the creep properties of the frozen soil. The use of this technique to establish the flow law of ice has been justified by this research. Experiments conducted confirm the use of the theory of an expanding spherical cavity to analyse the results.

The experimental data established that the influence of the size effect must be accounted for during the analysis of the punch experiments. The depth of embedment of a punch below the surface had no influence on the resistance required to penetrate it into the ice. This was also supported by results from a finite element analysis.

The flow law of the ice under both the simple uniaxial and the punch loading condition was confirmed using a finite element analysis of these experiments.

7.4 Further research

This discussion will be limited to aspects of creep behaviour of ice which have direct influence on the design of foundations in permafrost regions. The flow law of ice to be used for the design of foundations is influenced by a size effect which is reflected in the grain size ratio. The extent of this size effect influence must be ascertained to allow for proper scaling of ice properties during the design to reflect the field condition. The influence of this ratio should be studied to establish its changes during a creep experiment conducted to large strains. This would achieve a detailed understanding of the creep curve of ice and allow

the designer to understand the foundation behaviour during its design life. The implications of under design on deformations of the foundation could also be evaluated.

The influence of temperatures warmer than about -5°C on the strain-time behaviour and on the flow law of ice need clarification. This would allow the complete strain-time behaviour of the material to be evaluated and allow the time deformation curve of the foundation to be calculated for all possible field conditions. Better prediction of the deformation behaviour of the foundation would result.

The validity of using the punch experiment to determine the creep properties of ice has been established. The influence of the punch size relative to the ice crystal size must be studied to allow scaling of this influence to field behaviour. The influence of a change of the footing shape should also be studied. Shape factors for each geometry of footing would result and could be used in future designs. The lack of influence of an embedment depth on the punch resistance should be checked using field experiments in ice. Punch experiments should also be conducted in the field to measure the flow law of ice and compare this flow law to other flow laws measured for the ice using different loading conditions.

The finite element program should be extended to account for the strain time relationship in addtion to the constant strain-rate behaviour. This would enhance its use in predicting the total time versus deformation data for a

loading condition. The ability of the program to account for temperature variation should also be added.

References

Andrade, E.N.Da C., 1910. "On the viscous flow in metals and allied phenomena.", Proceedings of the Royal Society of London, Vol. A134, pp. 1-12.,

Baker, R.W., 1978. "The influence of ice crystal size on creep.", Journal of Glaciology, Vol.21, pp. 485-500.,

Barnes, P. and Tabor, D., 1966. "Plastic flow and pressure melting in the deformation of ice I." Nature London, Vol. 210, p 878-882.,

Barnes, P.,Tabor, D. and Walker, J.C.F., 1971. "The friction and creep of polycrystalline ice.", Proceedings of the Royal Society, London, Vol.324A, pp. 127-155.,

Bartlett, J.T. and Readings, C.J., 1968. "Some optical effects in deformed single crystals of ice. International Association of Scientific Hydrology Publication 79, pp. 316-325.,

Bass, R.,Rossberg, D. and Ziegler, G., 1957. "Die elastichen Konstanten des Eises.", Z. Phys. Vol.149, pp. 199-203.,

Bennett, H.B., 1972. "Meaurements of ultrasonic wave velocities in ice cores from Greenland and Antarctica.", U.S. Army Cold Regions Research and Engineering Laboratory., Hanover, N.H. Research Report 237.,

Bishop, J.F.W., Green, A.P. and Hill, R., 1956. "A note on the deformable region in a rigid-plastic body.", Journal of the Mechanics and Physics of Solids, Vol. 4, pp. 256-258.,

Bishop, R.F., Hill, R., and Mott, N.F., 1945. "The theory of indentation and hardness tests.", Proceeding of the Physical Society of London, Vol. 57, pp. 147-159.,

Boyle, R.W., and Sproule, D.O., 1931. "Velocity of longitudinal vibration in solid rods (ultrasonic method) with special reference to the elasticity of ice.", Canadian Journal of Research, Vol. 5, pp. 601-618.,

Brinch Hansen, J., 1961. "A general formula for bearing capacity.", Danish Geotechnical Institute, Copenhagen, Denmark. Bulletin No. 11.,

Brown, R.J.E. and Kupsch, W.O., 1974. "Permafrost Terminlogy", National Research Council of Canada, Technical Memorandum No. 111. 62 p.,

Brown, R.J.E., 1970. Permafrost in Canada., University of Toronto Press, Toronto. 234 p.,

Budd, W.F., 1969. "The dynamics of ice masses."Australian National Antarctic Research Expedition, Scientific Reports, Series A(IV), Glaciology Publication No.108. 216 p.,

Butkovich, T.R. and Landauer, J.K., 1958. "The flow law for ice."International Association of Scientific Hydrology., Publication No. 47, pp. 318-327.,

Butkovich, T.R. and Landauer, J.K., 1959. "The flow law for ice.", U.S. Army Snow, Ice and Permafrost Research Establishment., Wilmette, Illinois. Research Report 56, p. 7.,

Butkovich, T.R. and Landauer, J.K., 1960. "Creep of ice at low stresses.", U.S. Army Snow, Ice and Permafrost Research Establishment., Wilmette, Illinois. Research Report 72, p. 6.,

Byers, B., 1973. "Secondary creep of polycrstalline ice under biaxial stress.", Unpublished Ph.D Thesis, University of Washington, 136 p.,

Chang, C.Y., Nair, K., and Sing, R.D., 1974. "Finite element methods for the nonlinear and time-dependent analysis of Geotechnical Engineering Problems.", Proceeding, Analysis and Design in Geotechnical Engineering pp 269-302,

Colbeck, S.C., and Evans, R.J., 1973. "A flow law for a temperate glacier ice.", Journal of Glaciology, Vol. 12, pp. 71-86.,

Colbeck, S.C., 1970. "The flow law for temperate glacier ice." Unpublished Ph.D. University of Washington, Seattle,Washington. 149p.,

Conway, J.B., 1967. Numerical Methods for Creep and Rupture Analysis., Gordon and Breach, Science Publishers, New York. 204 p.,

Dantl, G., 1968. "Elastic Moduli of ice." In Physics of Ice, Riehl,N.,Bullemer,B.,and Englehandt,H. (eds), Plenum Press, New York. pp. 223-230.,

Desai, C.S. and Abel, J.F., 1972. Introduction to the Finite Element Method: A Numerical Method for Engineering Analysis., Van Nostrand Reinhold Co., New York, 477p.,

Dillon, H.B. and Andersland, O.B., 1967. "Deformation rates of polycrystalline ice.", In:Physics of Snow and Ice., H. Oura (editor), Institute of low Temperature Science, Hokkaido University, Sapporo, Japan. pp. 313-328.,

Duncan, J.M., and Dunlop, P., 1969. "Behaviour of soils in simple shear test.", Proceedings 7th. International Conference on Soil Mechanics and Foundation Engineering, Vol.1, pp. 101-109.,

Emery, J.J. and Nguyen, J.J., 1974. "Simulation of ice flow problems.", In, Applications of Solid Mechanics, Second Symposium (CSME-CSCE-ASME), McMaster University, Vol.1, pp. 30-45.,

Emery, J.J., and Finn, W.D.L., 1972. "Creep problems in soil mechanics." Proceeding Symposium on Solid Mechanics, University of Waterloo, Waterloo, Ontario, pp. 417-437.,

Emery, J.J., 1971."Finite Element Analysis of Creep Problems in Soil Mechanics." Unpublished Ph.D. thesis, University of British Columbia, Vancouver,

B.C. 155 p.,

Emery, J.J., 1978. "Simulation of Slope Creep. Rockslides and Avalances." Volume 1. Natural Phenomena, Edited by B. Voight, Recent Developments in Geotechnical Engineering, pp.669-691.,

Ewing, M., Crary, A.P., and Thorne, A.M., 1934. "Propagation of elastic waves in ice.", Physics, Vol. 5, pp. 165-168.,

Frankenstein, G.F., and Garner, R., 1970. "Dynamic Young's Modulus and flexural strength of sea ice.", U.S. Army Cold Regions Research and Engineering Laboratory., Hanover, N.H. Technical Report 222.,

Gibson, R.E., 1950. Discussion. Journal of the Institute of Civil Engineers, Vol. 34, 382 p.,

Glen, J.W. and Jones, S.J., 1967. "The deformation of ice single crystals at low temperatures. "In:Physics of Snow and Ice., H. Oura (editor), Institute of low Temperature Science, HokKaido University, Sapporo, Japan. pp. 267-275.,

Glen, J.W. and Perutz, M.F., 1954. "The growth and deformation of ice crystals.", Journal of Glaciology, Vol. 2, pp. 397-403.,

Glen, J.W., 1952. "Experiments on the deformation of ice.", Journal of Glaciology, Vol. 2, pp. 111-114.,

Glen, J.W., 1953. "Rate of flow of polycrystalline ice.", Nature, Lond., Vol. 172, pp. 721-723.,

Glen, J.W., 1955. "The flow law of polycrystalline ice", Proceedings of the Royal Society, London, Vol. 228A, pp. 519-538.,

Glen, J.W., 1958. "The flow law of ice.", International Association of Scientific Hydrology Publication 47, pp. 171-183.,

Glen, J.W., 1968. "The effect of hydrogen disorder on dislocation movement and plastic deformation of ice.", Phys. Condens. Mater., Vol. 7, pp. 43-51.,

Glen, J.W., 1974. "The Physics of ice."U.S. Army Cold Regions Research and Engineering Laboratory., Hanover, N.H.,Monograph II-C2a. 86p.,

Glen, J.W., 1975. "The mechanics of ice.", U.S.Army Cold Regions Research and Engineering Laboratory., Hanover, N.H., Monograph II-2cb, 47 p.,

Gold, L.W., and Sinha, N.K., 1979. "The rheological behaviour of ice at small strains.", International Union of Theoretical and Applied Mechanics, Symposium on the Physics and Mechanics of Ice. August 6-10, Copenhagen, Denmark.,

Gold, L.W., and Traetteberg, A., 1975. "Young's Modulus of ice and ice engineering problem.", In: Proceeding. Second Symposium Application of Solid Mechanics., McMaster University, Vol. 1, pp. 1-16.,

Gold, L.W., 1958. "Some observations on the dependence of strain on stress for ice."Canadian Journal of Physic., Vol.36, pp.1265-1275.,

Gold, L.W., 1960. "The cracking activity in ice during creep." Canadian Journal of Physic., Vol. 38, pp.1137-1148.,

Gold, L.W., 1965. "The initial creep of columnar-grained ice.", Canadian Journal of Physic, Vol. 43, pp. 1414-1434.,

Gold, L.W., 1972. "The failure process in columnar-grained ice.", National Research Council Division of Building Research, Technical Paper 369, 108p.,

Gold, L.W., 1973. "Activation energy of creep of columnar-ground ice.", In: Physics and Chemistry of Ice: Symposium on the Physics and Chemistry of Ice, Ottawa, Canada, August 1972. Royal Society of Canada. pp. 362-364.,

Gow, A.J., and Williamson, T. "Rheological implications of the internal structure and crystal fabric of the west antartic ice sheet as revealed by deep core drilling at Byrd Station", U.S. Army CRREL, CRREL Report 76-35.,

Green, R.J. Jr. and McKinnon, L., 1956. "Determination of the elastic constants of ice single crystals by an ultrasonic pulse method." Journal Accoust. Society of America, Vol. 28, p.1292.,

Griggs, D.T. and Coles, N.E., 1954. "Creep of single crystals of ice." U.S. Army Snow, Ice and Permafrost Research Establishment., Wilmette, Illinois. Technical Report No. 11, 24 p.,

Hansen, B.L., and Landauer, J.K., 1958. "Some results of ice cap drill hole measurements." International Association of Scientific Hydrology., Publication No. 47, pp. 313-317.,

Hawkes, I. and Mellor, H., 1972. "Deformation and fracture of ice under uniaxial stress.", Journal of Glaciology, Vol.11, pp. 103-131.,

Higashi, A., Koinuma, S. and Mae, S., 1964. "Plastic yielding in ice single crystals.", Japanese Journal Applied Physic, Vol. 3, pp. 610-616.,

Higashi, A., Koinuma, S. and Mae, S., 1965. "Bending creep of ice single crystals.", Japanese Journal of Applied Physic. Vol. 4, pp. 575-582.,

Hill, R., 1950. The Mathematical Theory of Plasticity, Clarendon Press, Oxford, England.,

Hirst, W. and Howse, M.G.J.W., 1969. "The indentation of material by wedges.", Proceedings of the Physical Society of London, Vol. A311, pp. 429-444.,

Hobbs, P.V., 1974. Ice Physics., Clarendon Press, Oxford, 837pp.,

Hoff, N.J., 1954. "Approximate analysis of structures in

the presence of moderately large creep deformations.", Quarterly Journal of Applied Mathematic, Vol. 12, pp. 49-55.,

Hooke, R.L.,Dahlin, B.B. and Kauper, M.T., 1972. "Creep of ice containing fine dispersed sand.", Journal of Glaciology, Vol.11, pp.327-336.,

Hudleston, P.J., 1977. "Progressive deformation in development of fabric across zones of shear in glacial ice" . IN: Energetics of Geological Processes, Saxena, S.K. and Bhattacharji, S. (eds.) Springer-Verlag, New York., pp. 121-150.,

Hult, J.A.H., 1966. Creep in Engineering Structures., Blaisdell Publishing Company, Massachusets, 115 p.,

Iverson, K., and Moum, J., 1974. "The paraffin method-triaxial testing without a rubber membrane."Ge'otechnique, Vol. 24. pp.665-670.,

Jellinek, H.H.G., and Brill, R., 1956. "Viscoelastic properties of ice.", Journal of Applied Physic., Vol. 27, pp. 1198-1209.,

Johnston, G.H. and Ladanyi, B., 1972. "Field tests of grouted rod anchors in permafrost", Canadian Geotechnical Journal, Vol.9, pp.63-80,

Jona, F. and Scherrer, P., 1952. "Die elastischen Konstanten von Eis-Einkristallen.", Helv. phys. Acta. Vol. 25, pp. 35-54.,

Jones, S.F. and Glen, J.S., 1969. "The mechanical properties of single crystals of pure ice.", Journal of Glaciology,, Vol. 8, pp. 463-473.,

Jones, S.F. and Glen, J.W., 1968. "The mechanical properties of single crystals of pure ice at low temperatures.", International Association of Scientific Hydrology, Publication 79, pp. 326-340.,

Jones, S.J. and Burnet, J., 1978. "Deformation of ice single crystals close to the melting point.",

Journal of Glaciology, Vol. 21, pp. 445-456.,

Jones, S.J., 1967. "Softening of ice crystals by dissolved fluoride ions.", Physics Letters, Vol. 25A, pp. 366-367.,

Kaiser, P.K., 1979. "Time-dependent behaviour of tunnels in jointed rock masses.", Unpublished Ph.D. thesis, University of Alberta, Edmonton, Alberta.,

Kamb, B., 1961. "The glide direction in ice.", Journal of Glaciology, Vol. 3, pp. 1097-1106.,

Kamb, B., 1972. "Experimental recrystallization of ice under stress.", In: Flow and Fracture of Rocks, Heard, H.C., Borg, I.Y., Carter, N.L., Raleigh, C.B. (eds.) American Geophysical Union, Geophysic Monograph No. 16 pp. 211-241.,

Kamb, W.F., 1959. "Ice petrofabric observation from Blue Glacier, Washington in relation to theory and experiment.", Journal of Physical Research, Vol. 64, pp. 1891-1910.,

Kaplar, C.W., 1969. "Laboratory determination of dynamic Moduli of frozen soils and ice.", U.S. Army Cold Regions Research and Engineering Laboratory., Hanover, N.H. Research Report 163.,

Kauzmann, W., 1941. "Flow of solid metals from the stand-point of the chemical-rate theory.", Transactions American Institute Mineral and Metall. Engineers, Vol. 143, pp. 57-83.,

Kohnen, H. and Bentley, C.R., 1973. "Seismic refraction and reflection measurements at Byrd Station, Antarctica.", Journal of Glaciology, Vol. 12, pp. 101-111.,

Kohnen, H., 1974. "The temperature dependence of seismic waves in ice.", Journal of Glaciology, Vol. 13, pp. 144-147.,

Kuo, S.S., 1972. "Stress and time effect on the creep

rate of polycrystalline ice." Unpublished Ph.D Thesis, Michigan State University, 176 p.,

Ladanyi, B. and Johnston, G.H., 1974. "Behaviour of circular footings and plate anchors embedded in permafrost.", Canadian Geotechnical Journal, Vol.11, pp. 531-553,

Ladanyi, B., and Paquin, J.,1978. "Creep behaviour of frozen sand under a deep circular load.", Proceedings Third International Conference on Permafrost, Vol.1, Edmonton, Canada, pp. 679-686.,

Ladanyi, B., 1959. "Etude theorique et experiment ale du probleme de l'expansion dans un sol poulverulent d'une cavite presentant une symetrie spherique ou cylindrique.", Unpublished Ph.D. thesis, University of Louvain, Louvaine, Belgium.,

Ladanyi, B., 1966. "Failure mechanism of rock under plate load.", Proceeding First Congress of the International Society of Rock Mechanic, Lisbon, Portugal, Vol. 1, pp. 415-420.,

Ladanyi, B., 1972. "An engineering theory of creep of frozen soils.", Canadian Geotechnical Journal, Vol.9, pp. 33-80,

Ladanyi, B., 1972a. "Design of laterally loaded piles in permafrost.", Report for Mackenzie Valley Pipeline Research Limited, Calgary, Alberta, 27pp.,

Ladanyi, B., 1976. "Use of the static penetration test in frozen soils.", Canadian Geotechnical Journal., Vol. 13, pp. 95-111.,

Langdon T.G., 1973. "Creep mechanisms in ice.", In, Proceedings Symposium Physics and Chemistry of Ice, Royal Society of Canada, Ottawa, pp. 356-364.,

Langway, C.C., 1958. "Ice Fabrics and the universal stage.", U.S. Army Snow, Ice and Permafrost Research Establishment., Wilmette, Illinois.Technical Report. 62.,

Lavrov, V.V., 1947. "Vyagkostl'da v zavisimostic ot temperatury.", Zh. tekh. Fiz. 17, pp. 1027-1034.,

Mackay, J.R., 1972. "The world of underground ice.", Annals of the Association of American Geographers, Vol. 62, pp. 1- 22.,

Masterson, D.M., Anderson, K.G., and Strandberg, A.G., 1979. "Strain measurements in floating ice platforms and their application to platform design.", Canadian Journal of Civil Engineering, Vol. 6, pp. 394-412.,

McConnel, J.C., and Kidd, D.A., 1888. "On the plasticity of glacier and other ice.", Proceedings of the Royal Society of London, Vol. 44 pp. 331-367.,

McConnel, J.C., 1891. "On the plasticity of an ice crystal.", Proceeding of Royal Society, Vol. 49, pp. 323-343.,

McRoberts, E.C., Law, T.C. and Murray, T.K., 1978. "Creep tests on undisturbed ice-rich silt.", Proceeding, Third International Conference on Permafrost, Vol.1, Edmonton, Canada, pp.539-545,

McRoberts, E.C., 1973."Stability of slopes in permafrost." Unpublished Ph.D. thesis, University of Alberta, Edmonton, Alberta. 370 p.,

McRoberts, E.C., 1975. "Some aspects of a simple secondary creep model for determining deformations in permafrost slopes.", Canadian Geotechnical Journal, Vol.12, pp. 98-105,

Meier, M.F., 1960. "Mode of flow of the Saskatchewan Glacier, Alberta, Canada.", United States Geologic Survey, Paper 351. p70.,

Mellor, M. and Smith, J.H., 1967. "Creep of snow and ice.", In:Physics of Snow and Ice., H. Oura (editor), Institute of low Temperature Science, Hokkaido University, Sapporo, Japan. pp. 843-855.,

Mellor, M., and Testa, R., 1969a. "Effect of temperature on the creep of ice.", Journal of Glaciology, Vol. 8, pp. 131-145.,

Mellor, M., and Testa, R., 1969b. "Creep of ice under low stress.", Journal of Glaciology, Vol. 8, pp. 147-152.,

Mellor, M., 1979. "Mechanical properties of polycrystalline ice.", International Union of Theoretical and Applied Mechanics, Symposium on the Physics and Mechanics of Ice. August 6-10, Copenhagen, Denmark.,

Meyerhof, G.G., 1963. "Some recent research on the bearing capacity of foundations.", Canadian Geotechnical Journal., Vol. 1, pp. 15-26.,

Michel, B. and Ramseier, R.O., 1971. "Classification of river and lake ice.", Canadian Geotechnical Journal., Vol. 8, pp. 36-45.,

Michel, B., 1978. "A mechanical model of creep of polycrystalline ice.", Canadian Geotechnical Journal., Vol. 15, pp.,

Michel, B., 1979. Ice Mechanics, Les Presses de l'Universite Laval. 500 pp.,

Michel, B., 1979b. "Mechanical model of creep of polycrystalline ice with cracking activity.", International Union of Theoretical and Applied Mechanics, Symposium on the Physics and Mechanics of Ice. August 6-10, Copenhagen, Denmark.,

Morgenstern, N.R., and Tchalenko, J.S., 1967. "Microscopic observations in shear zones from slips in natural clays.", Proceedings of Geotechnical Conference, Olso, Vol. 1, pp. 147-152.,

Morgenstern, N.R., Roggensack, W.D. and Weaver, J.S., 1979. "Behaviour of friction piles in ice and ice rich frozen soils.", (in press).,

Mugge, O., 1895. "Ueber die Plasticitat der Esikrystalle.", Neves Jb. Miner Geol. Palaont Ref. Vol. 2, pp. 211-228.,

Muguruma, J., 1969. "Effects of surface condition on the mechanical properties of ice crystals.", British Journal of Applied Physics (Journal of Physics D), Ser. 2, Vol. 2, pp. 1517-1525.,

Mulhearn, T.O., 1959, "The deformation of metals by Vickers-type pyramidal indenters.", Journal of the Mechanics and Physics ofsolids, Vol. 7, pp. 85-91.,

Nair, K., and Boresi, A.P., 1970. "Stress analysis for time-dependent problems in rock mechanics." Proceeding, Second Congressof International Society for Rock Mechanics, Belgrade, Vol. 2 pp.531-536.,

Nakamura, T. and Jones, S.J., 1970. "Softening effect of dissolved hydrogen chloride in ice crystals.", Scr. Met., Vol. 4, pp. 123-126.,

Nakaya, V., 1958. "Mechanical properties of single crystals of ice.", U.S. Army Snow, Ice and Permafrost Research Establishment., Wilmette, Illinois. Research Report 28, 46 p.,

Nakaya, V., 1959. "Visco-elastic properties of snow and ice in the Greenland ice cap.", U.S. Army Snow, Ice and Permafrost Research Establishment., Wilmette, Illinois. Research Report 46, 46 p.,

Nixon, J.F., and McRoberts, E.C., 1976. "A design approach for pile foundations in permafrost.", Canadian Geotechnical Journal, Vol.13, pp. 40-57,

Nixon, J.F., 1978. "Foundation design approaches in permafrost areas.", Canadian Geotechnical Journal, Vol.15, pp. 96-112,

Northwood, T.D., 1947. "Sonic determination of the elastic properties of ice.", Canadian Journal of Research, Section A, Vol. 25, pp. 88-95.,

Nuttal, J., 1974. "Personal communication.",

Nye, J.F., 1951. "The flow of glaciers and ice-sheets a problem in plasticity.", Proceedings of the Royal Society of London, Vol. A213, pp. 546-548.,

Nye, J.F., 1952. "The mechanics of glacier flow.", Journal of Glaciology, Vol. 2, pp. 182-193.,

Nye, J.F., 1953. "The flow law of ice from measurements in glacier tunnels, laboratory experiments and the Jungfraufim experiment.", Proceeding of the Royal Society, Vol. A219, pp. 477-489.,

Odqvist,F.K.G., 1966. Mathematical Theory of Creep and Creep Rupture., Oxford Mathematical Monograph, Clarendon Press, Oxford, 168 p.,

Orowan, E., 1947. "Discussion meeting.", Journal of Glaciology,Vol. 1, pp. 231-240.,

Paterson, W.S.B., and Savage, J.C., 1963. "Measurements on Athabasca Glacier relating to the flow law of ice.", Journal of Geophysics Research, Vol. 68, pp. 4537-4543.,

Paterson, W.S.B., 1969. The physics of glaciers., Pergamon Press, Oxford, 250. p,

Paterson, W.S.B., 1976. "Vertical strain-rate measurements in an Arctic ice cap and deductions from them. Journal of Glaciology, No. 75.,

Penny, A.H., 1948. "A theoretical determination of the elastic constants of ice.", Proc. Camb. phil. Soc. Math. Phys. Sci., Vol. 44, pp. 423-439. ,

Pounder, E.R., 1965. "The Physics of Ice.", Pergamon, New York.,

Raymond, C.F., 1973. "Inversion of flow measurements for stress and reheological parameters in a valley glacier.", Journal of Glaciology, Vol. 12, pp.

19-44.,

Raymond, C.F., 1978. "Mechanics of Glacier Movement." Volume 1. Natural Phenomena, Edited by B. Voight, Recent Developments in Geotechnical Engineering, pp.794-826.,

Readey, D.W. and Kingery, W.D., 1964. "Plastic deformation of single crystals of ice.", Acta m etall., Vol. 12, pp. 171-178.,

Readings, C.J. and Bartlett, J.T., 1968. "Slip in single crystals of ice.", Journal of Glaciology, Vol. 7, pp. 479-491.,

Reusch, E., 1864. "Beitrage zur Lehre vom Eis." Annln Phys. Chem. Vol. 121, pp. 573-578.,

Rigsby, G.P., 1955. "Study of ice fabrics, Thule area, Greenland.", U.S. Army Snow, Ice and Permafrost Research Establishment., Wilmette, Illinois. Report 26.,

Rigsby, G.P., 1957. "Effect of hydrostatic pressure on velocity of shear deformation of single crystals of ice.", U.S. Army Snow, Ice and Permafrost Research Establishment., Wilmette, Illinois. Research Report 32, 7 p.,

Rigsby, G.P., 1960. "Crystal orientation in glacier and in experimentally deformed ice.", Journal of Glaciology, Vol. 3, pp. 589-606.,

Robin, G. de Q., 1958. "Seismic shooting and related investigations, Glaciology III.", Norwegian, British, Swedish Antarctica Expedition 1949-1952., Science Research Vol. 5, No. 3, pp. 48-80.,

Roethlisberger, H., 1972. "Seismic exploration in cold regions.", U.S. Army Cold Regions Research and Engineering Laboratory., Hanover, N.H. Technical Monograph II-A2a.,

Roggensack, W.D., 1977. "Geotechnical Properties of

Fine-grained Soils.", Unpublished Ph.D Thesis, University of Alberta, 449 p.,

Savigny, K.W., 1980."Insitu analysis of naturally occurring creep in ice-rich permafrost soil." Unpublished Ph.D. thesis, University of Alberta, Edmonton, Alberta. 500p.,

Sayles, F.H., 1968. "Creep of frozen sands."U.S. Army Cold Regions and Engineering Laboratory, Hanover, N.H., Technical Report No. 190.,

Sayles, F.H., 1973. "Traixial and creep tests on frozen sand.", Permafrost: North American contribution to the Second International Conference, N.A.S., Washington D.C. pp. 384-391.,

Sego, D.C. and Morgenstern, N.R., 1977. "Preliminary results on deformation behaviour of polycrystalline ice.", National Research Council, Technical Memorandum No. 121, pp. 124-130.,

Shahinian, P. and Lane, J.R., 1953. "Influence of grain size on high temperature properties of Monel.", Transactions of the American Society of Metals. Vol. 45, pp. 177-199.,

Shreve, R.L., and Sharp, R.P., 1970. "Internal deformation and thermal anomalies in lower Blue Glacier, Mount Olympus, Washington, U.S.A.", Journal of Glaciology, Vol. 9, pp 65-86.,

Sinha, N.K., 1978. "Short-term rheology of polycrystalline ice.", Journal of Glaciology, Vol. 85, pp. 457-474.,

Skempton, A.W., Yassin, A.A. and Gibson, R.E., 1953. "Theorie de la force portante des pieux dans le sable.", Vol. 63/64, pp. 285-289.,

Skempton, A.W., 1964. "Long-term stability of clay slopes.", Geotechnique, Vol. 14, pp. 77-101.,

Smith, N., 1969. "Determining the dynamic properties of

.snow and ice by forced vibration.", U.S. Army Cold Regions Research and Engineering Laboratory., Hanover, N.H. Technical Report 216.,

Somigliana, C., 1921. "Sulla profondita dei ghiacciai.", Atti. Accad. naz. Lincei Rc., (Classe di scienze fisiche matermatiche e naturali) 30, pp. 291-296.,

Steinemann, S., 1954. "Results of preliminary experiments on the plasticity of ice crystals.", Journal of Glaciology, Vol. 2, pp. 404-412.,

Steinemann, S., 1958. "Experimental investigation of the plasticity of ice.", U.S. Airforce, Cambridge Research Laboratory, Research Translation AMST-G-166.,

Stevens, H.W., 1975. "The responses of frozen soils to vibratory loads.", U.S. Army Cold Regions Research and Engineering Laboratory., Hanover, N.H. Technical Report 265.,

Taylor, G.I., 1938. "Analysis of Plastic Strain in Cubic Crystal.", Stephen Timoshenko 60th Anniversary Volume, Macmillan Company, New York.,

Terzaghi, K., and Peck, R.B., 1967. Soil Mechanics in Engineering Practise., John Wiley and Sons. 673 pp.,

Thomas, R.H., 1971. "Flow law for Antarctic ice shelves.", Nature (Physical Science), Vol. 232, pp. 85-89.,

Thomas, R.H., 1973a. "The creep of ice shelves: theory.", Journal of Glaciology, Vol. 12, pp. 45-53.,

Thomas, R.H., 1973b. "The creep of ice shelves: interpretation of observed behaviour.", Journal of Glaciology, Vol. 12, pp. 55-70.,

Van Winkel, B., Gerstle, K.H., and Ko, H.Y., 1972. "Analysis of time-dependent deformation of openings in salt media.", International Journal of Rock

Mechanics and Mining Science, Vol. 9, pp. 249-260.,

Vesic, A.S., 1972. "Expansion of cavities in infinite soil mass."; Journal Soil Mechanics and Foundation Division. American Society of Civil Engineers, Vol. 98, No. SM3, pp. 265-290.,

Vialov, S.S., Dokuchayev, V.V., Sheynkmen, D.A., Gaydayenko, Y.I., and Goncharov, Y.M., 1973. "Ground ice as the bearing surface for construction.", U.S.Army CRREL, Hanover, N.H. Translation TL 438.,

Vialov, S.S., 1965a. "Rheological Properties and Bearing Capacity of Frozen Soils.", U.S.Army Cold Regions Engineering and Research Laboratory, Hanover, N.H. Translation No.74, 219 pp.,

Vialov, S.S., 1965b. "The strength and creep of frozen soils and calculations for ice-soil retaining structures.", U.S.Army Cold Regions Engineering and Research Laboratory, Hanover, N.H. Translation No.76. 301 pp.,

Vialov, S.S., 1958. "Regularities of ice deformation.", International Association of Scientific Hydrology., Publication No. 47, pp. 383-391.,

Vinson, T.S. and Chaichanavong, T., 1976. "Dynamic properties of ice and frozen clay under cyclic triaxial loading conditions.", Michigan State University Division Engineering Research ReportMSU-CE-77-1.,

Vinson, T.S., 1978. "Response of frozen ground to dynamic loading."; In: Geotechnical Engineering for Cold Regions, Andersland, O.B. and Anderson, D.M. (eds), McGraw-Hill, New York, pp. 405-458.,

Voitkovskii, K.F., 1960. "Mekhanicheskiye svoystva lda The mechanical properties of ice," Moscow, Izd. Akademii Nauk, English Translation AFCRL-62-838, AMS-T-R#391+, 92pp.,

Wakahama, G., 1962. "On the plastic deformation of ice.", Low Temperature Science, Vol. A20, pp.

57-130.,

Walker, J.C.F., 1970. Unpublished Ph.D. University of Cambridge.,

Weaver, J., 1979. "Pile foundations in permafrost.", Unpublished Ph.D. Thesis, University of Alberta, Edmonton, Alberta.,

Weerdenburg, P., 1979. "Utilization of underground space in frozen ground.", Unpublished report to Department of National Defence, Ralston, Alberta 27 p.,

Weertman, J., 1963. "The Eshelby-Schoeck viscous dislocation damping mechanism applied to the steady-state creep of ice.", In Ice and snow:Properties, processes and applications (W.D. Kingery, ed.). Cambridge, Mass., MIT Press, pp.28-33.,

Weertman, J., 1973. "Creep of Ice.", In Proceedings Symposium Physics and Chemistry of Ice, Royal Society of Canada, Ottawa, pp. 320-337.,

Weinberg, B., 1905. "Uber die innere Reibung des Eises.", Annln Phys. 8, pp. 405-431.,

Weinberg, B., 1907. "Uber die innere Reibung des Eises.", Annln Phys. Vol. 22, pp. 321-332.,

Yamaji, K., and Kuroiwa, D., 1956. "Viscoelasticity of ice in the temperature 0 to -100°C. I", Teion-kagaku:Low TemperatureScience. Series a, No. 15, pp. 171-183. D.R.B Translation T633 (1958).

Zarembovitch, A. and Kahane, A., 1964. "Determination des vitesses de propagation d'ondes ultrasonores longitudinales dans la glace.", C.r. hebd. Seance, Acad., Sci., Paris, Vol. 258, pp. 2529-2532.,

Zienkiewicz, O.C., 1971. The Finite Element Method in Engineering Science., McGraw Hill Book Company, London, 521 p.,

APPENDIX A
Laboratory Experiment Data

A.1 Constant Stress Data

A.2 Constant Strain Rate Data

A.3 Constant Displacement Rate Punch Experiments

A.4 Constant Stress Simple Shear Experiments

A.5 Logarith strain rate versus logarith (t+1)

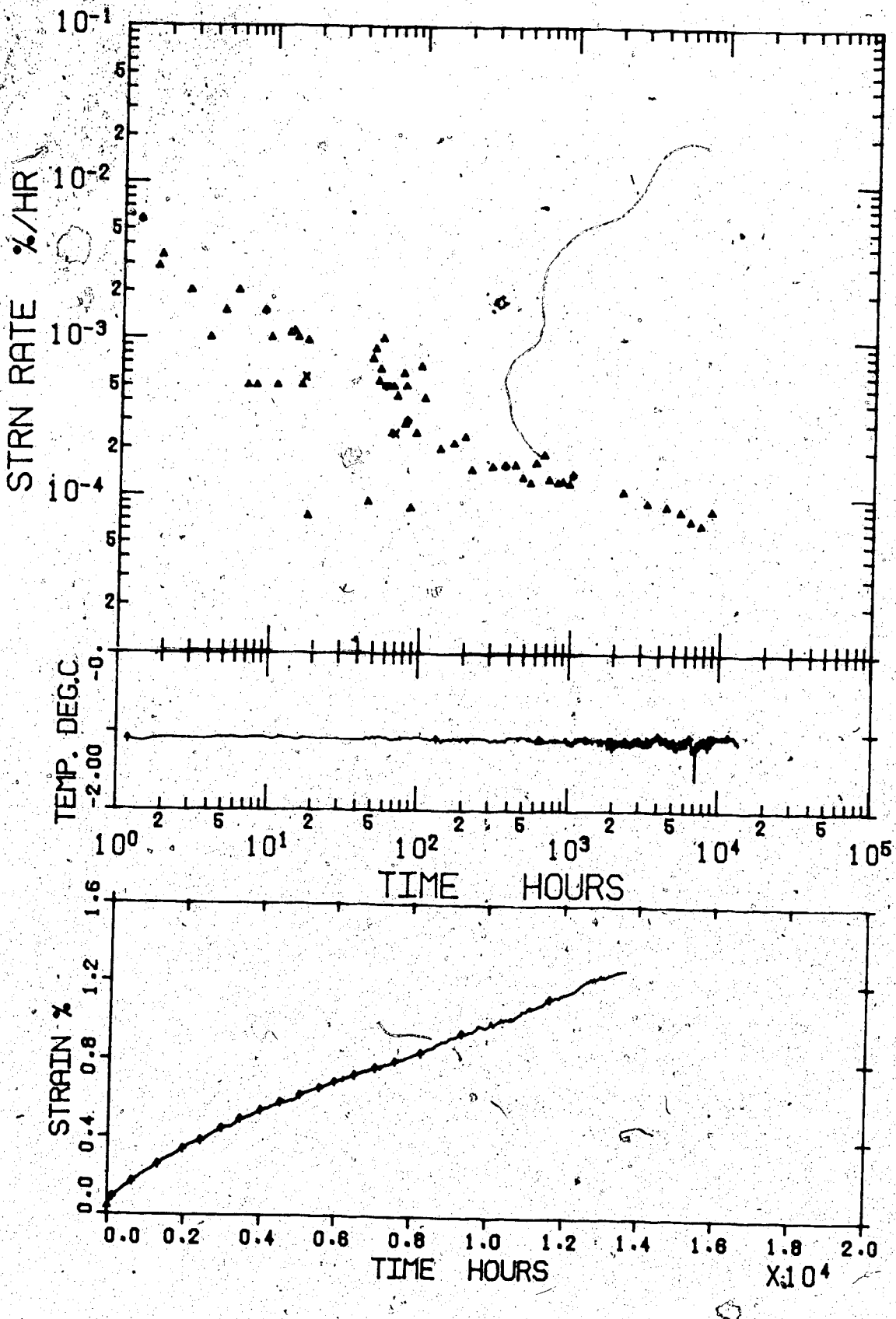

Figure A.1 Data plot of constant stress sample CSA34.

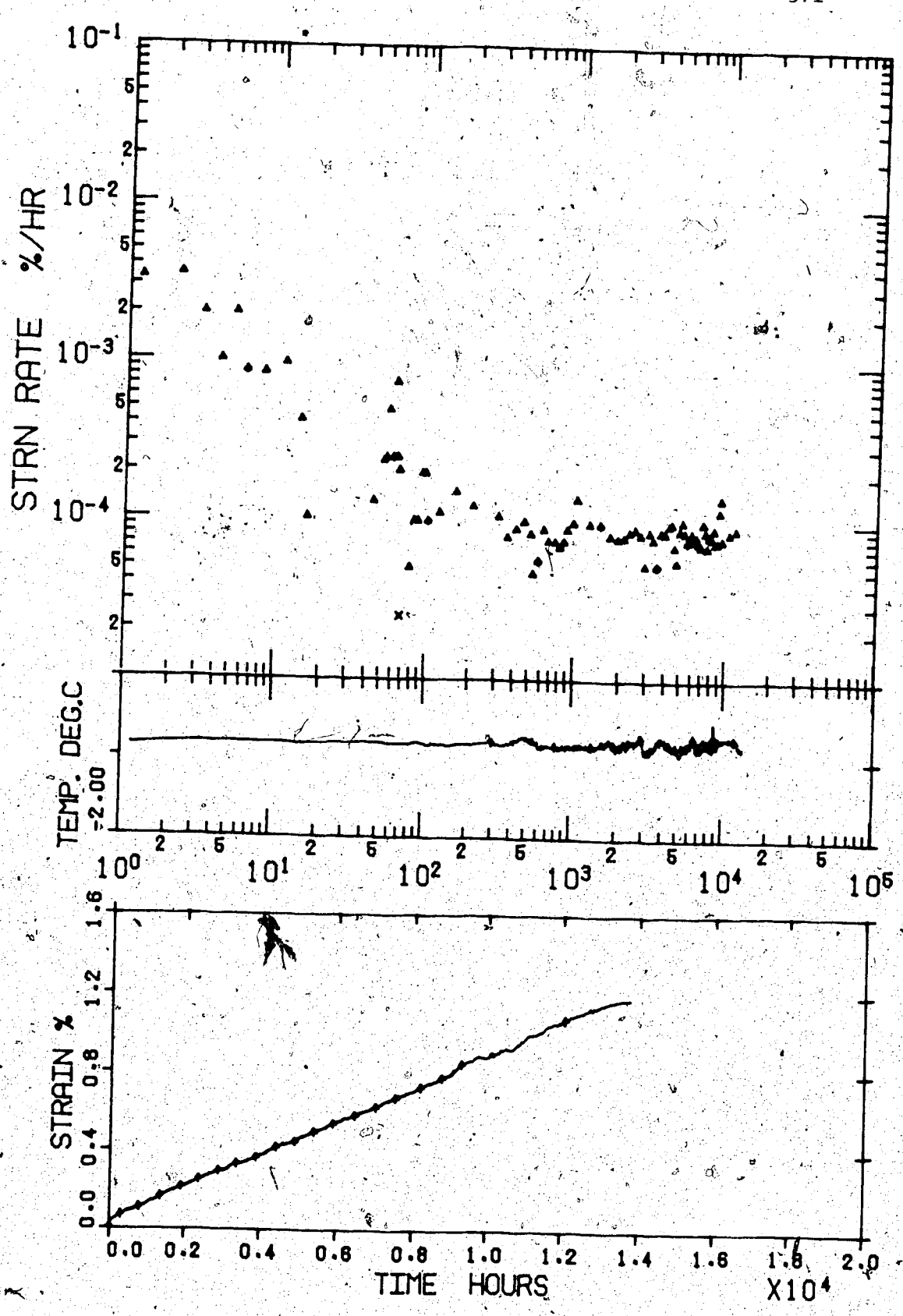

Figure A.2 Data plot of constant stress sample CSB35.

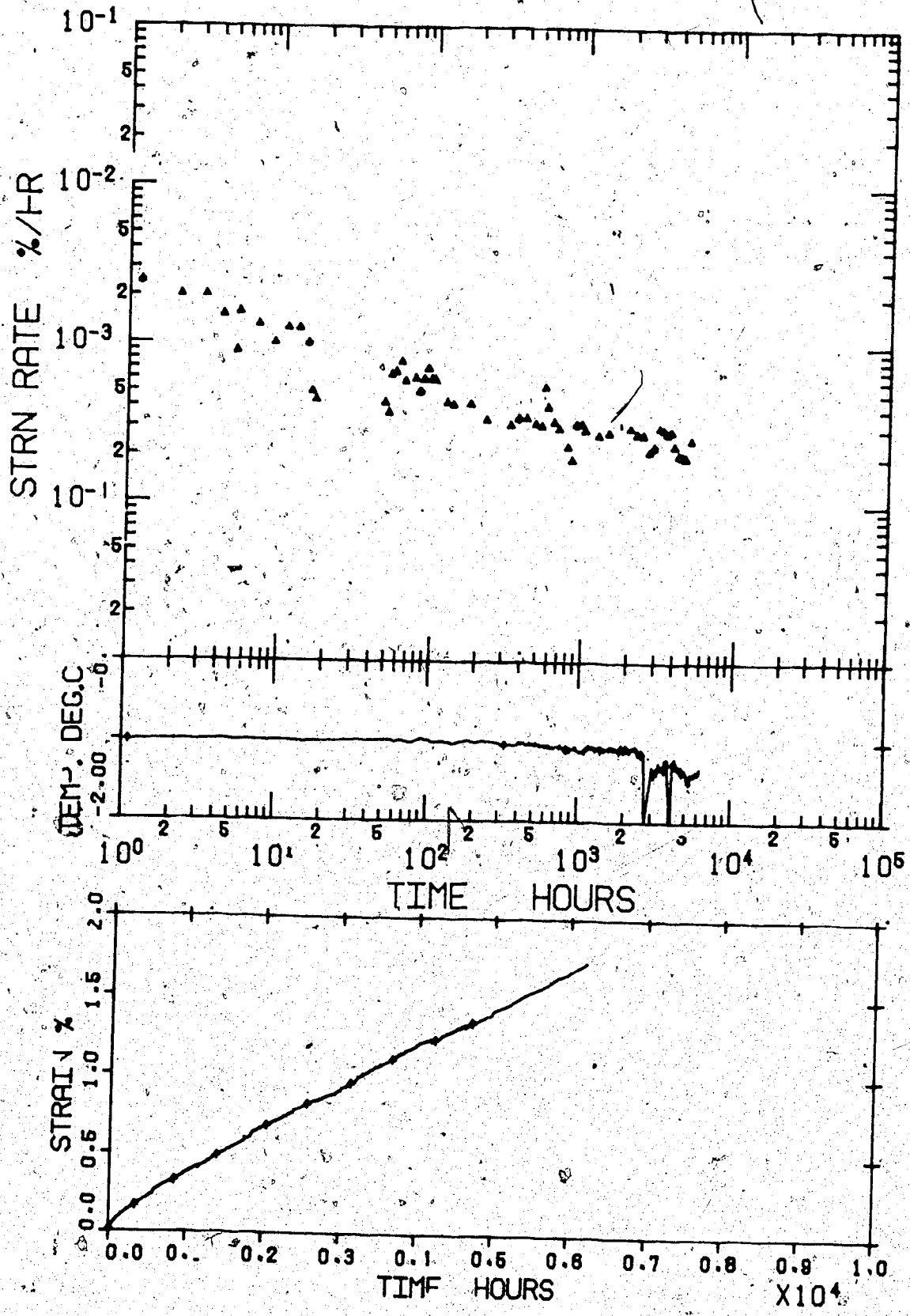

Figure A.3 Data plot of constant stress sample CSGR38.

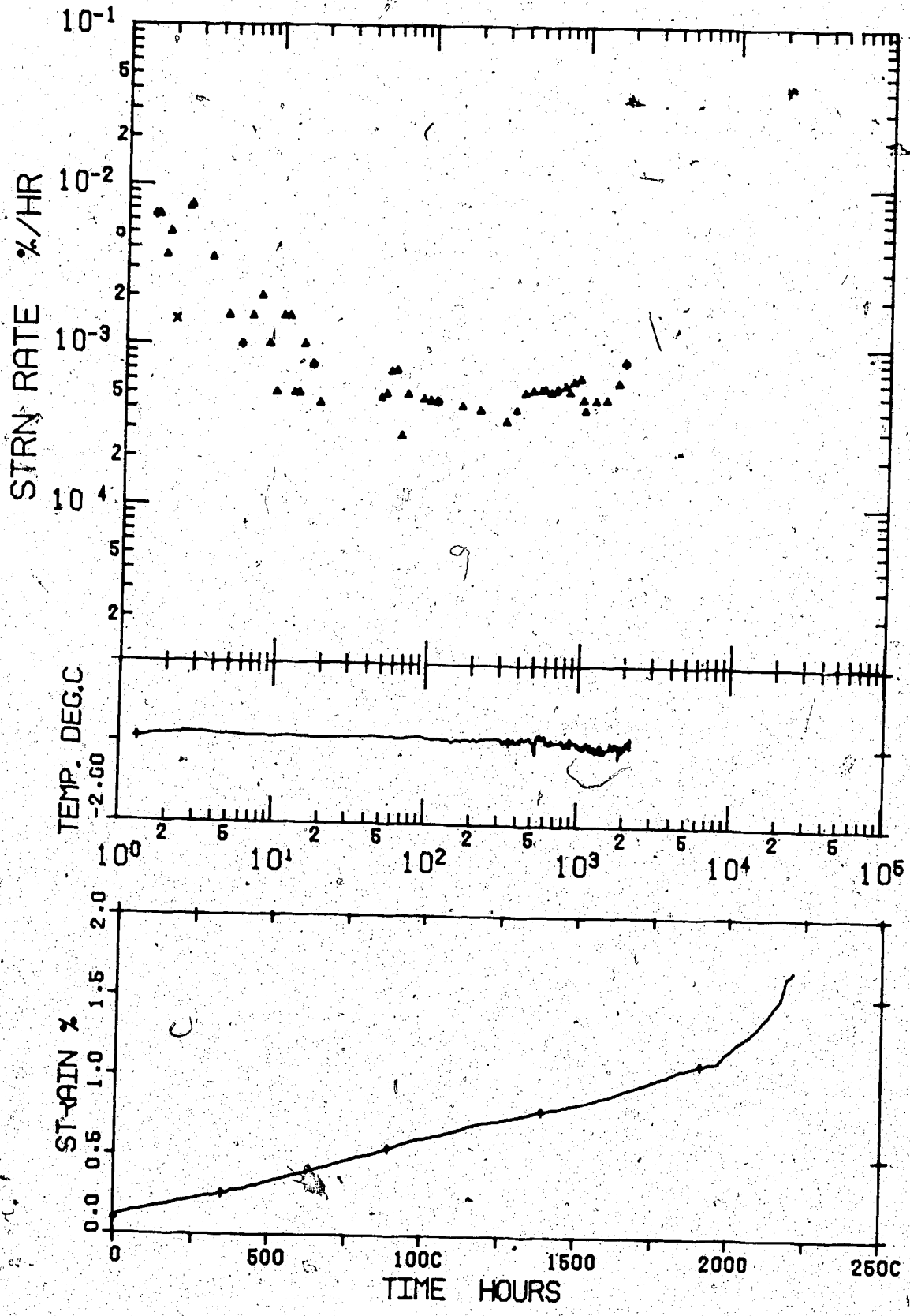

Figure A.4 Data plot of constant stress sample CSC37.

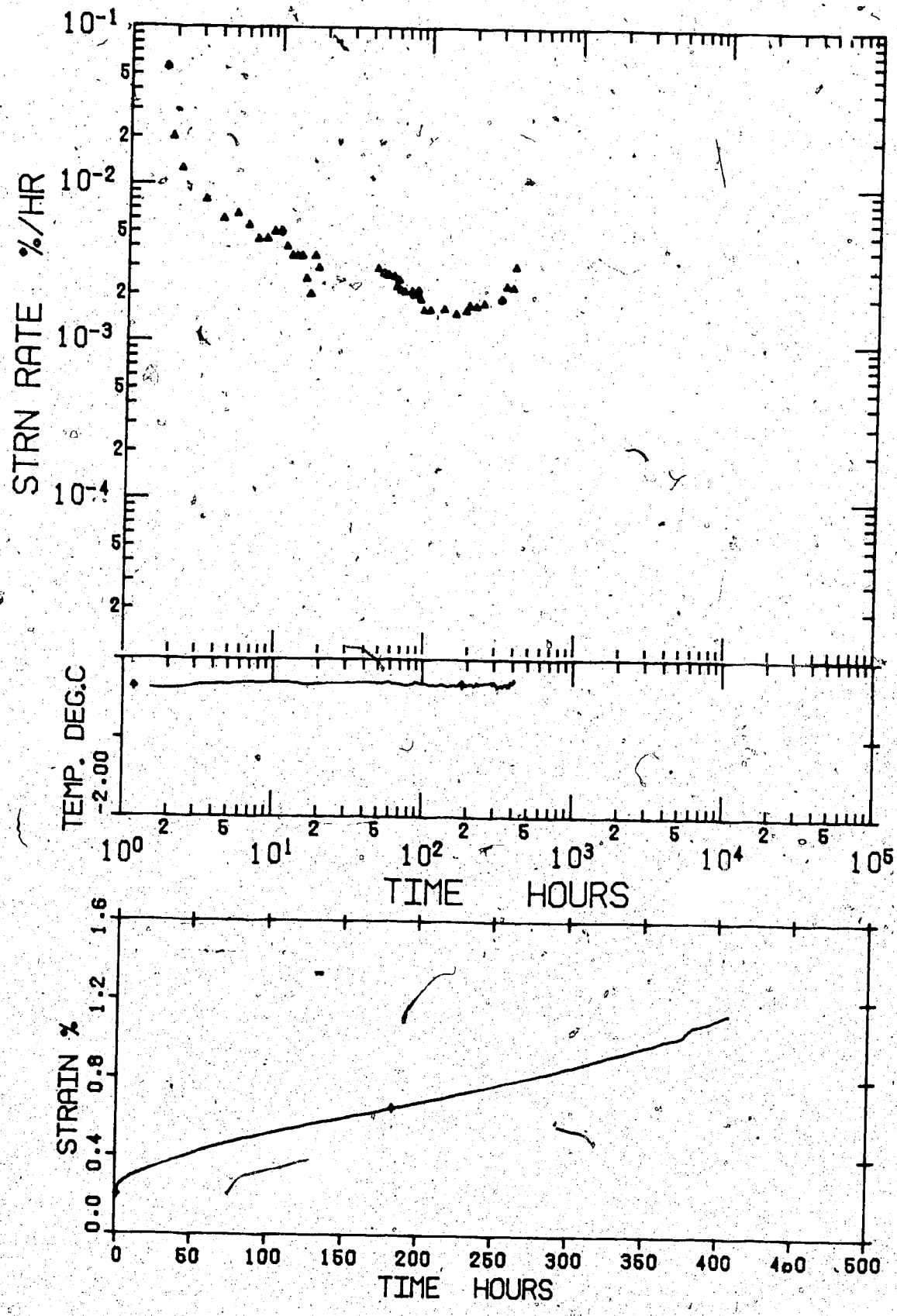

Figure A.5 Data plot of constant stress sample CSD39.

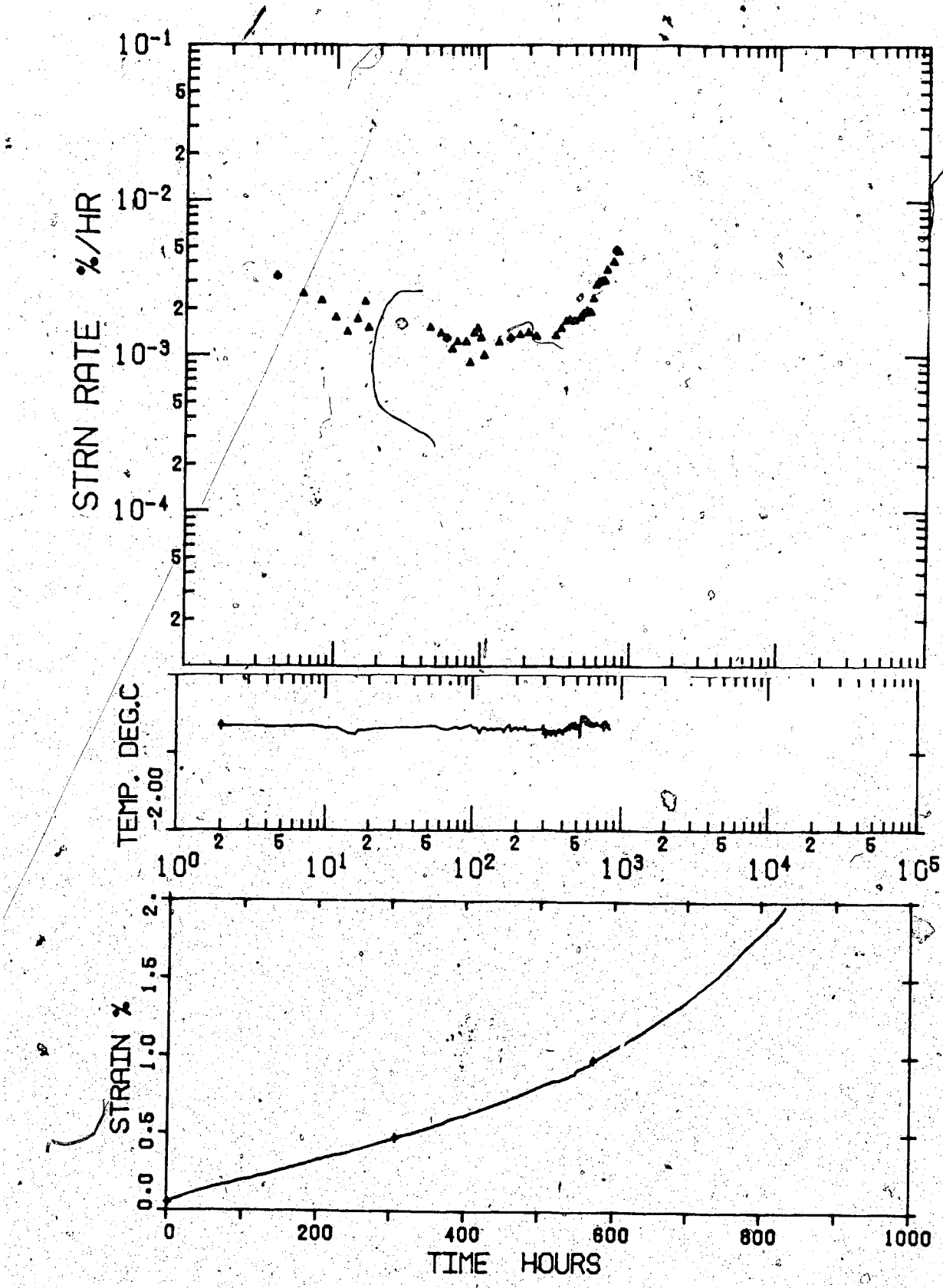

Figure A.6 Data plot of constant stress sample CSE42.

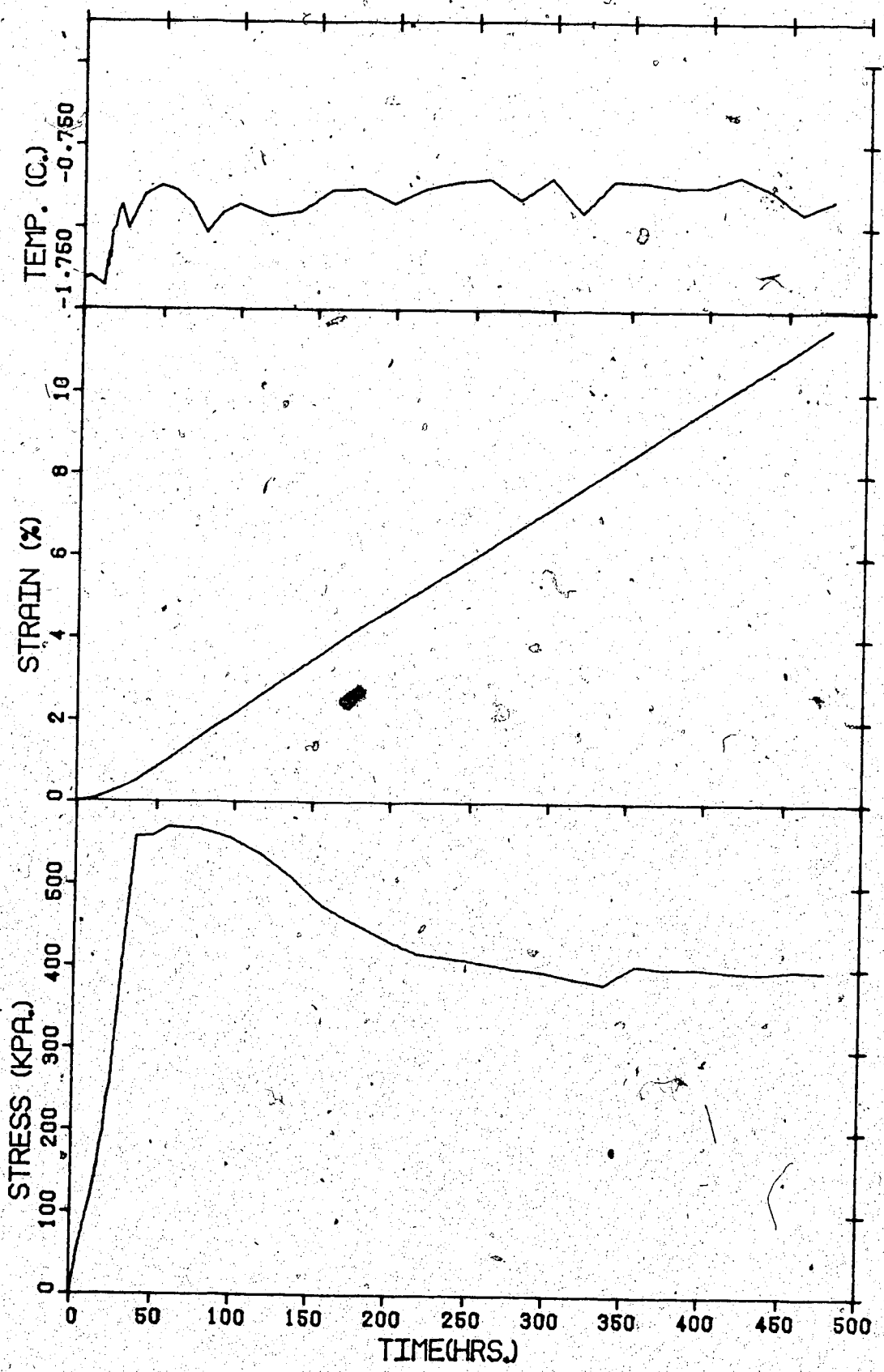

Figure A.7 Data plot of constant strain rate sample UC15.

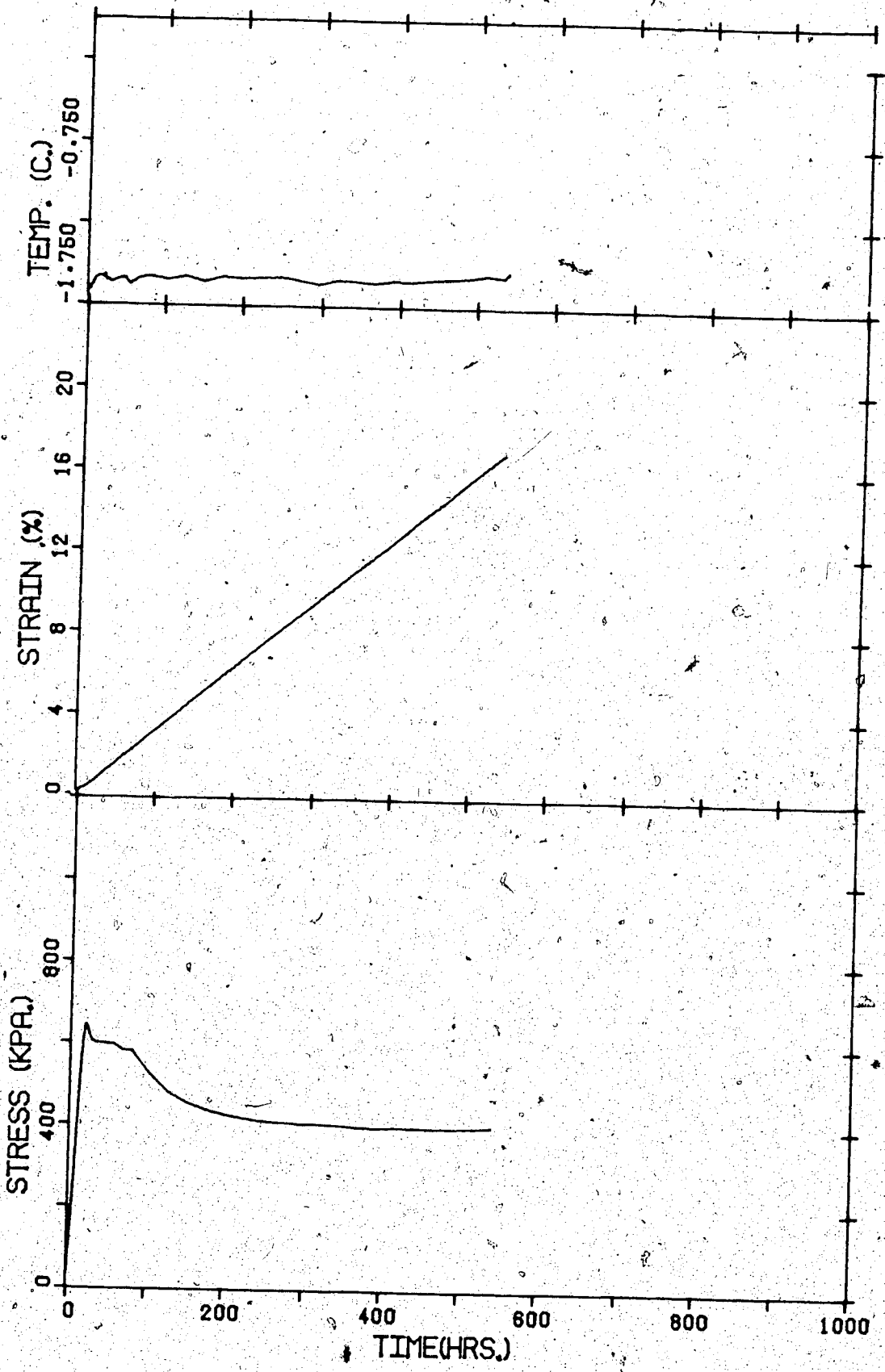

Figure A.8 Data plot of constant strain rate sample UC19.

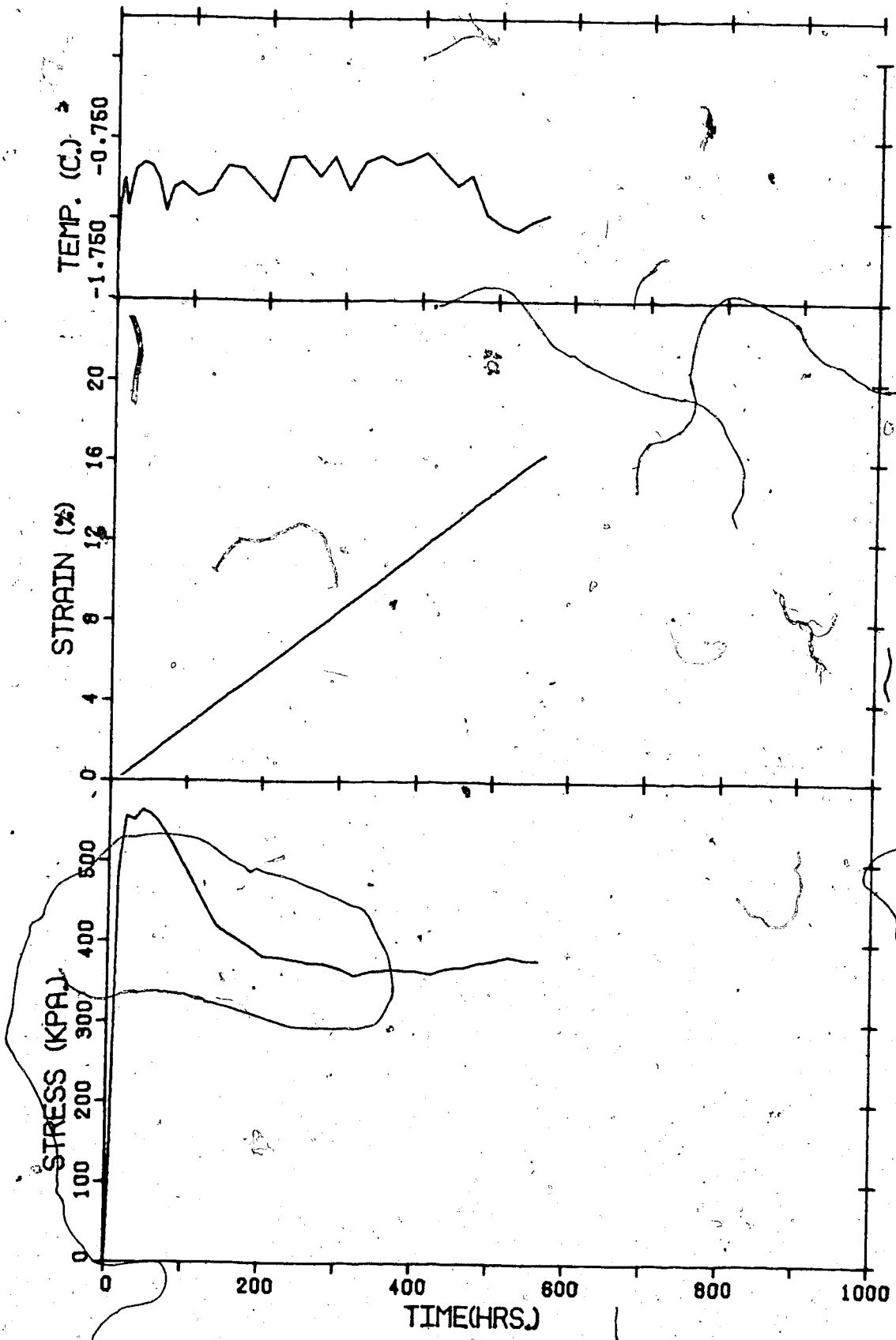

Figure A.9 Data plot of constant strain rate sample UC20.

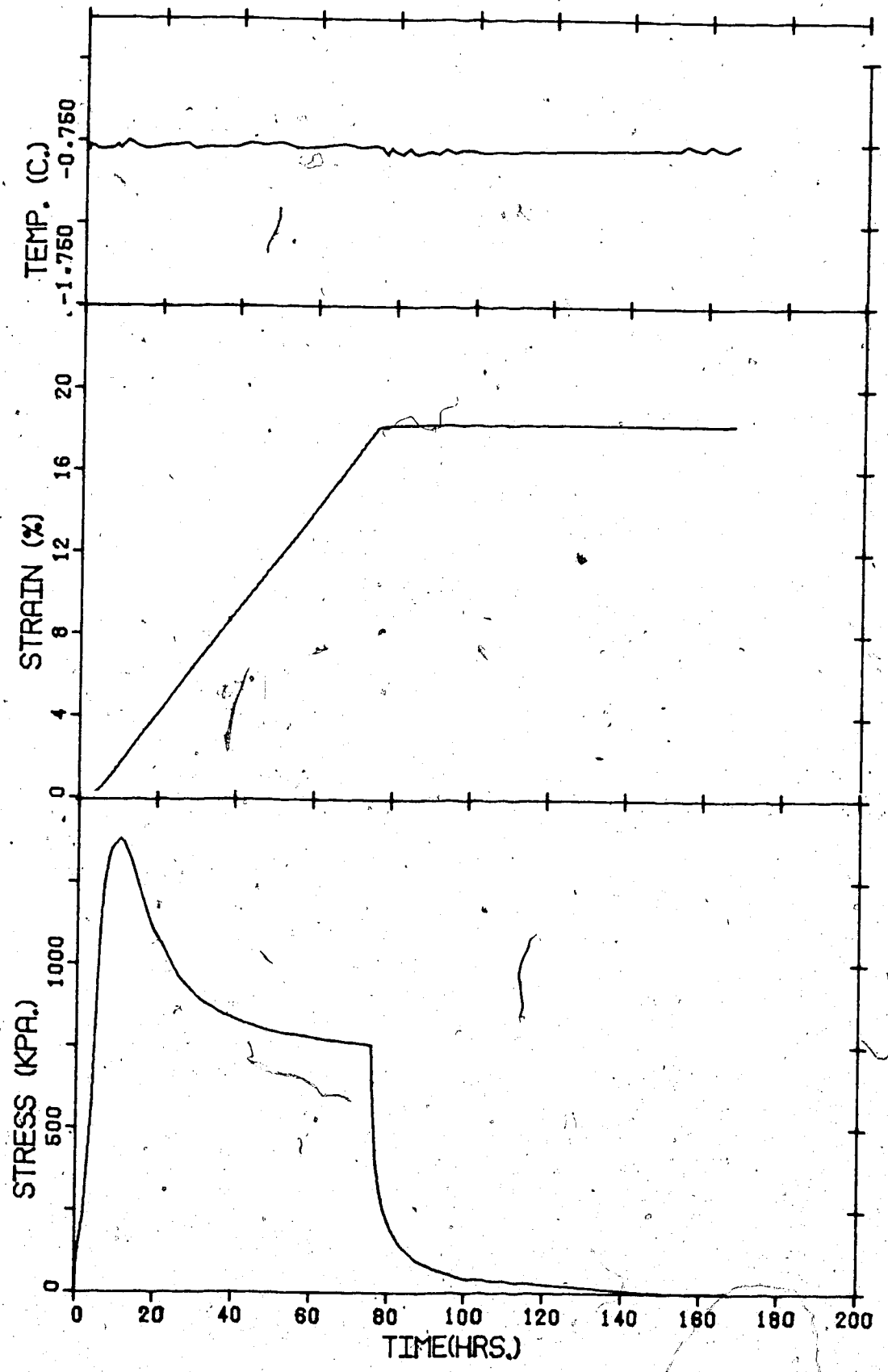

Figure A.10 Data plot of constant strain rate sample UC29.

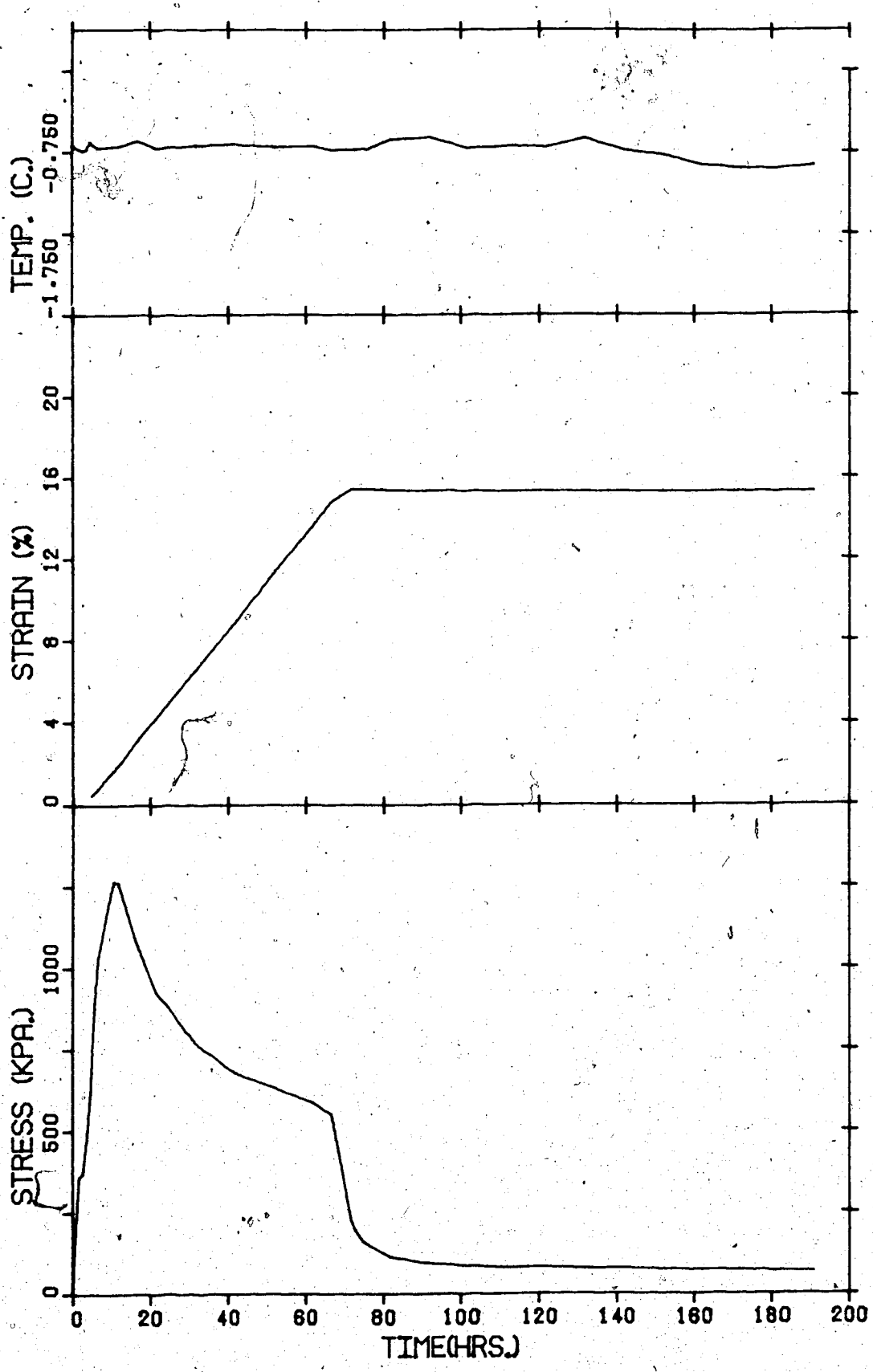

Figure A.11 Data plot of constant strain rate sample UC33.

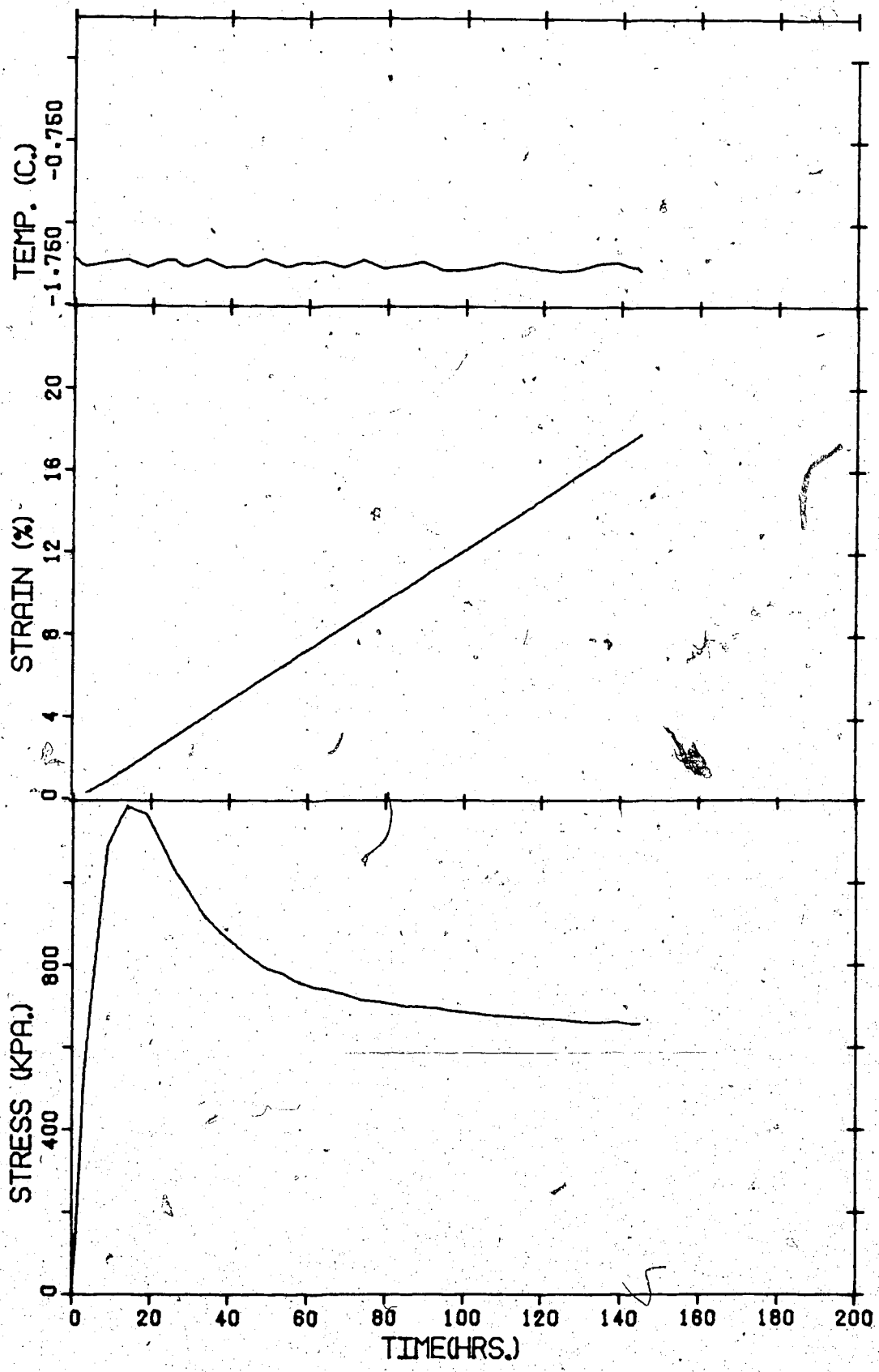

Figure A.12 Data plot of constant strain rate sample UC43.

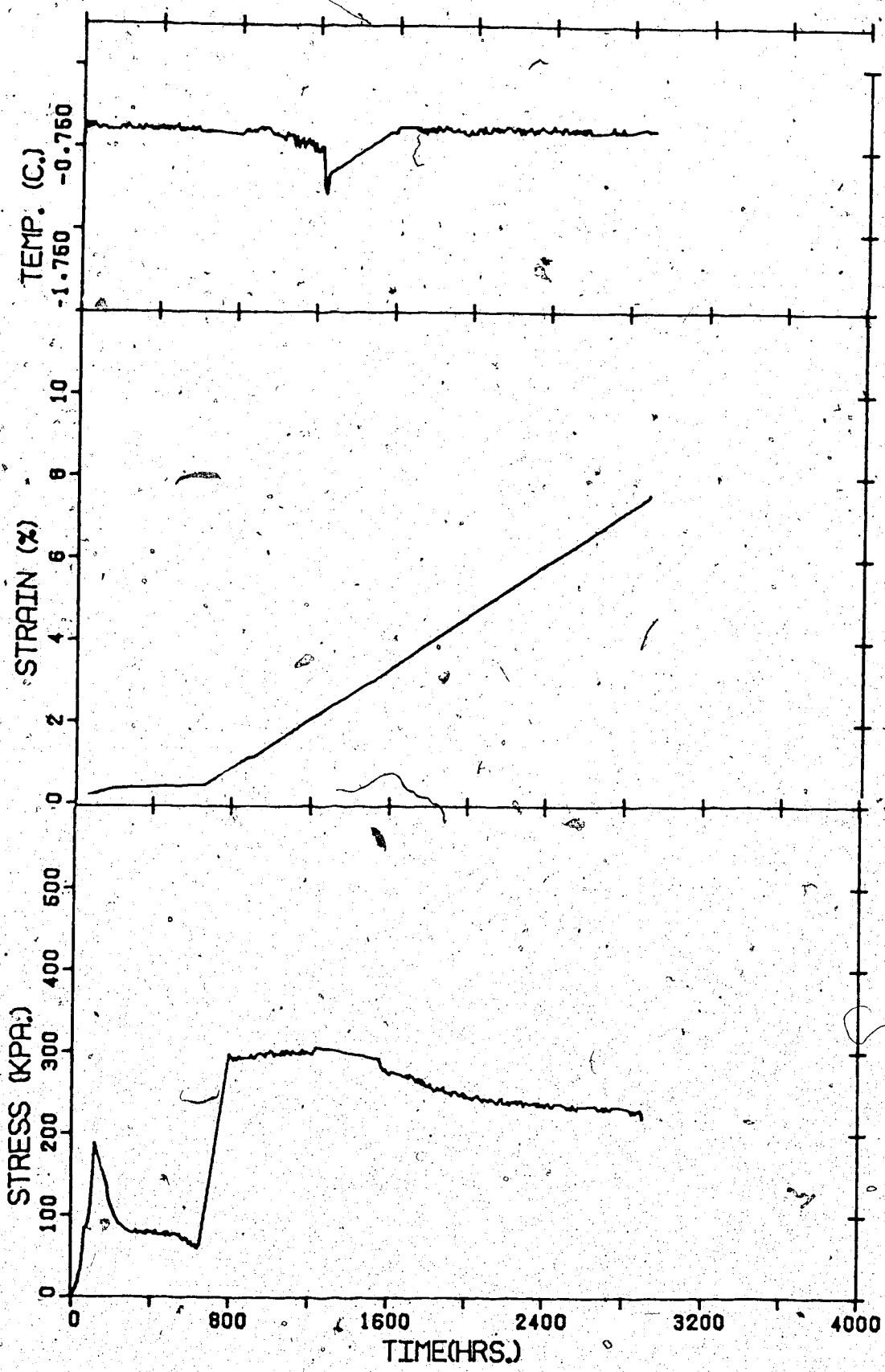

Figure A.13 Data plot of constant strain rate sample UC44.

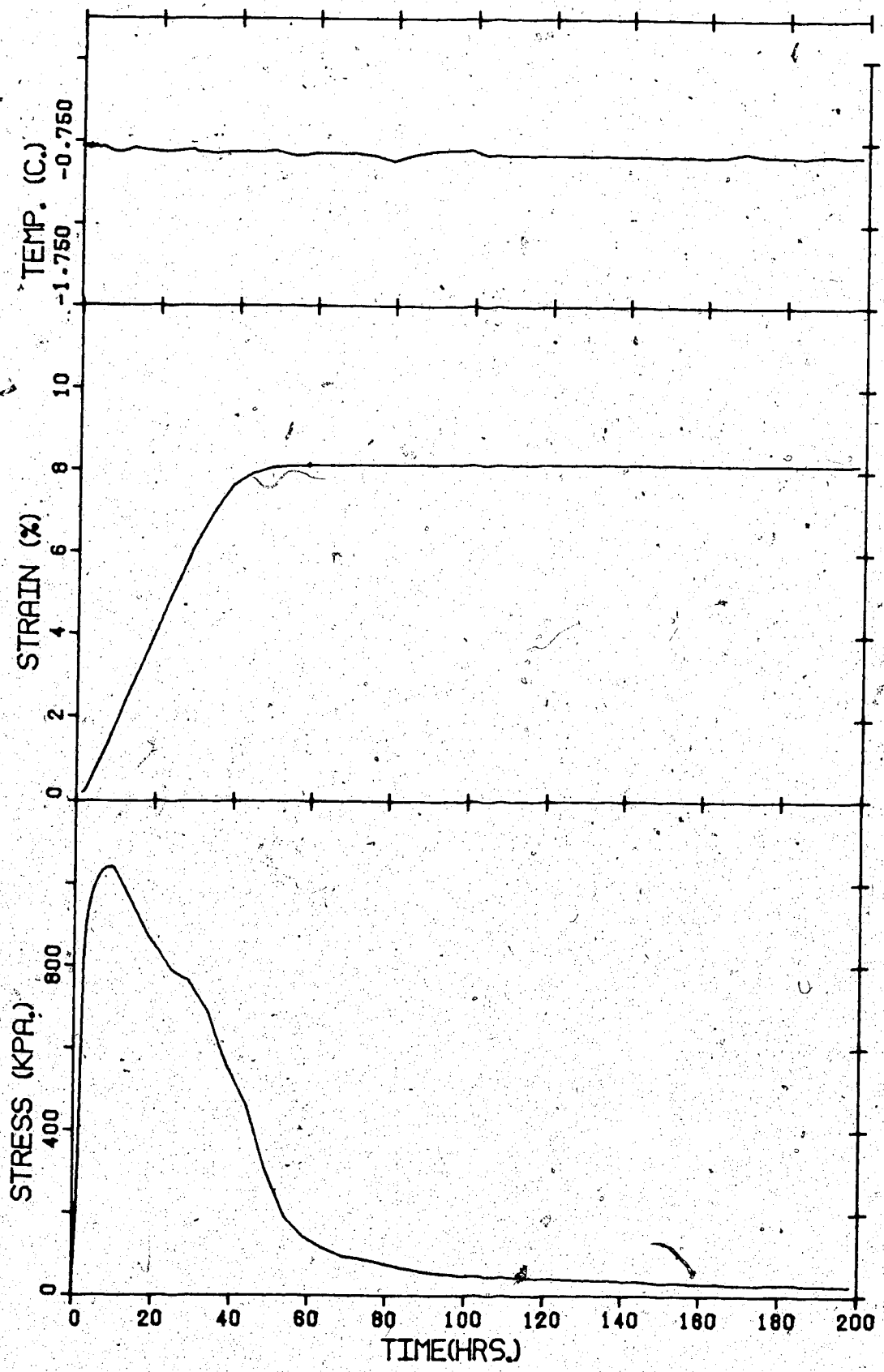

Figure A.14 Data plot of constant strain rate sample UC46.

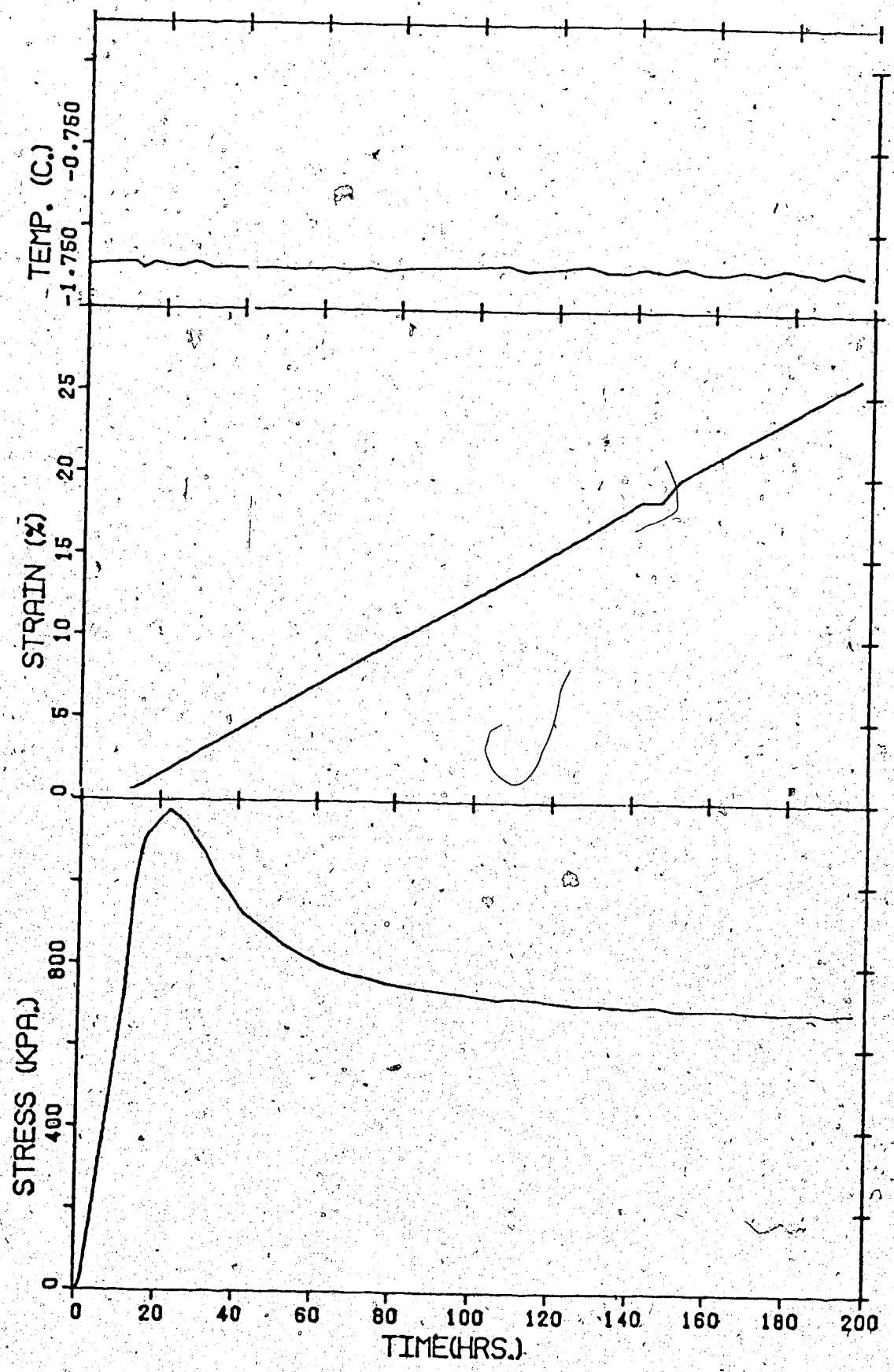

Figure A.15 Data plot of constant strain rate sample UC48.

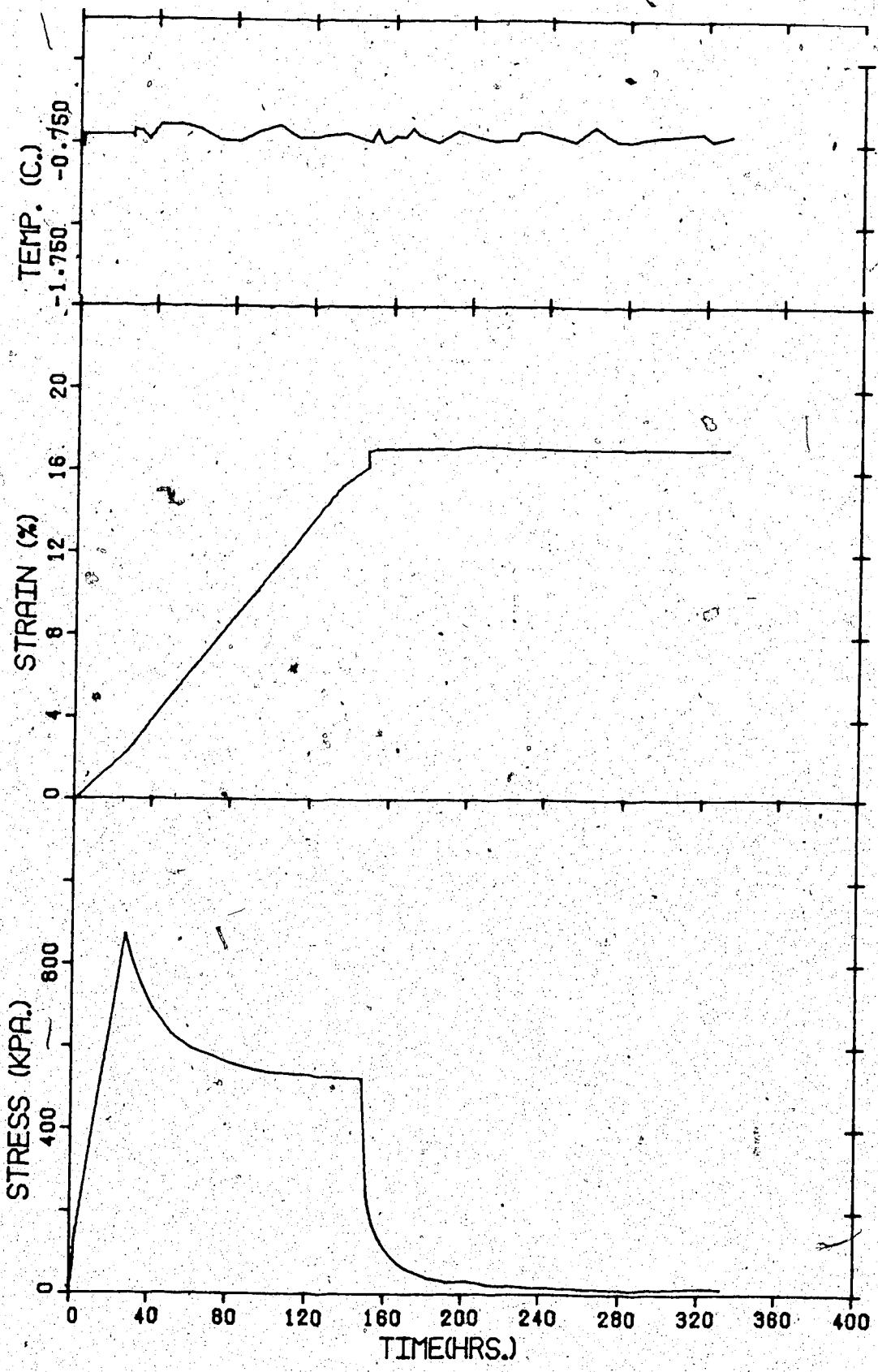

Figure A.16 Data plot of constant strain rate sample UC50

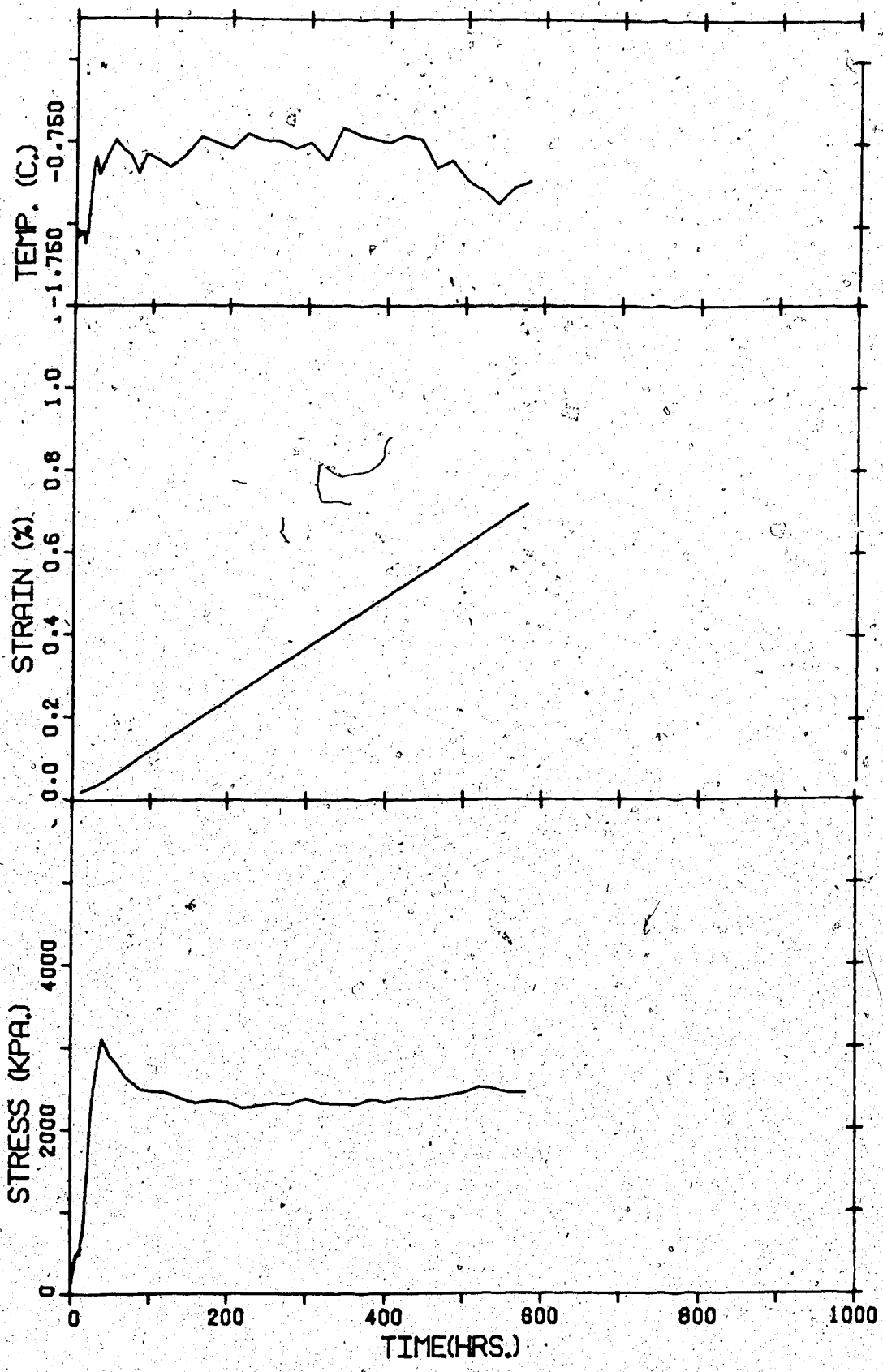

Figure A.17 Data plot of constant displacement rate punch sample Pen16.

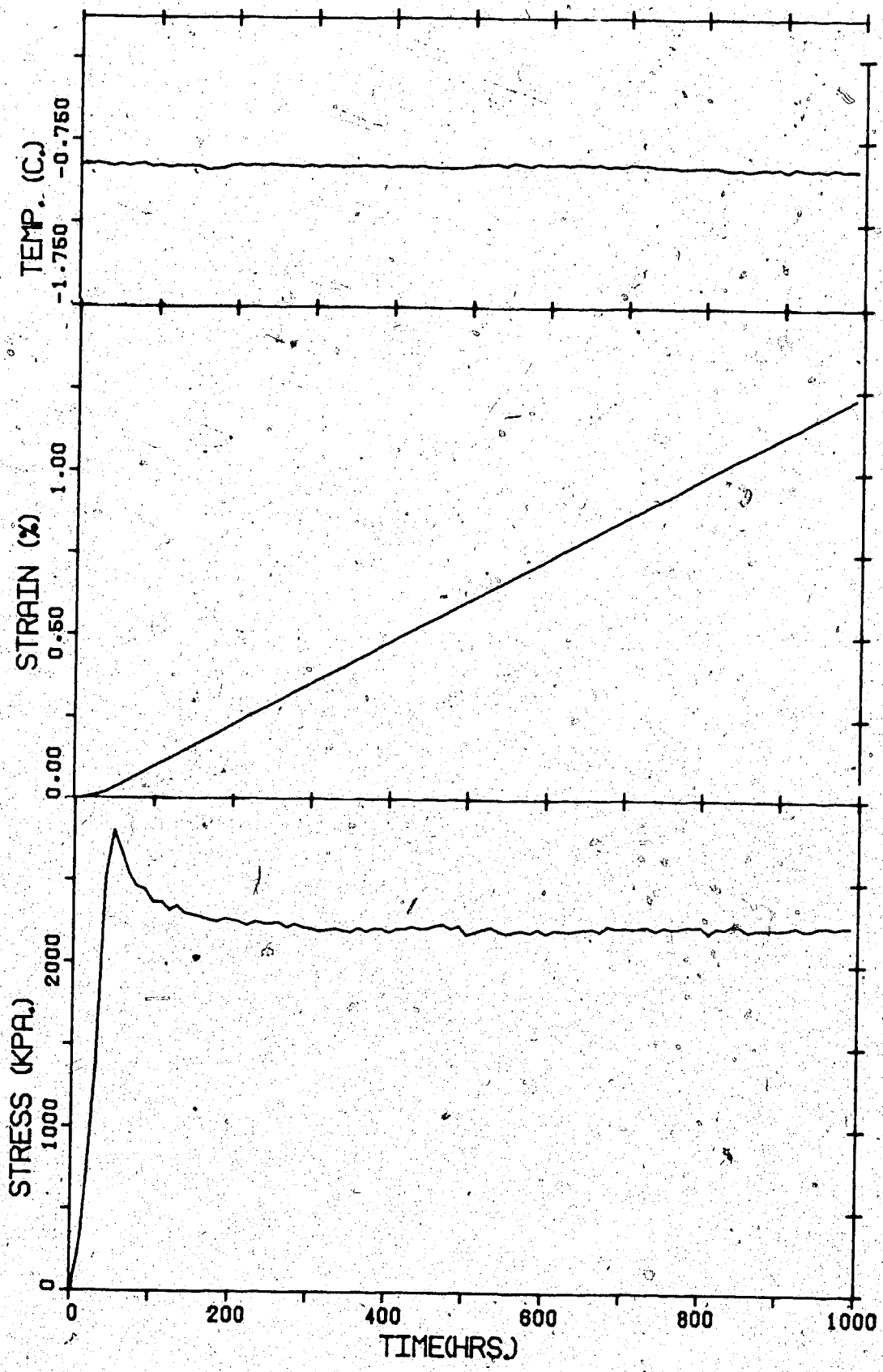

Figure A.18 Data plot of constant displacement rate punch sample Pen25.

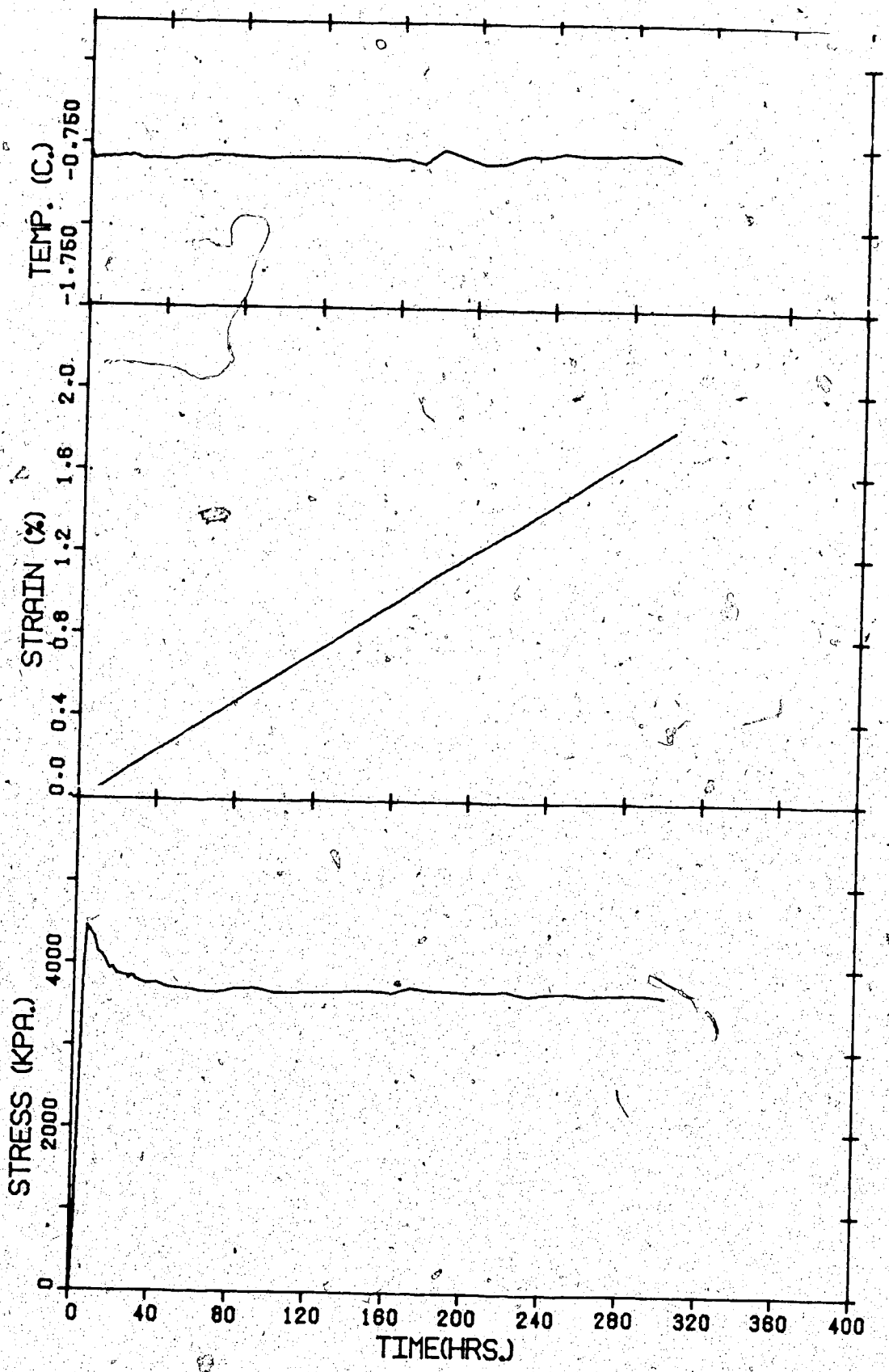

Figure A.19 Data plot of constant displacement rate punch sample Pen29.

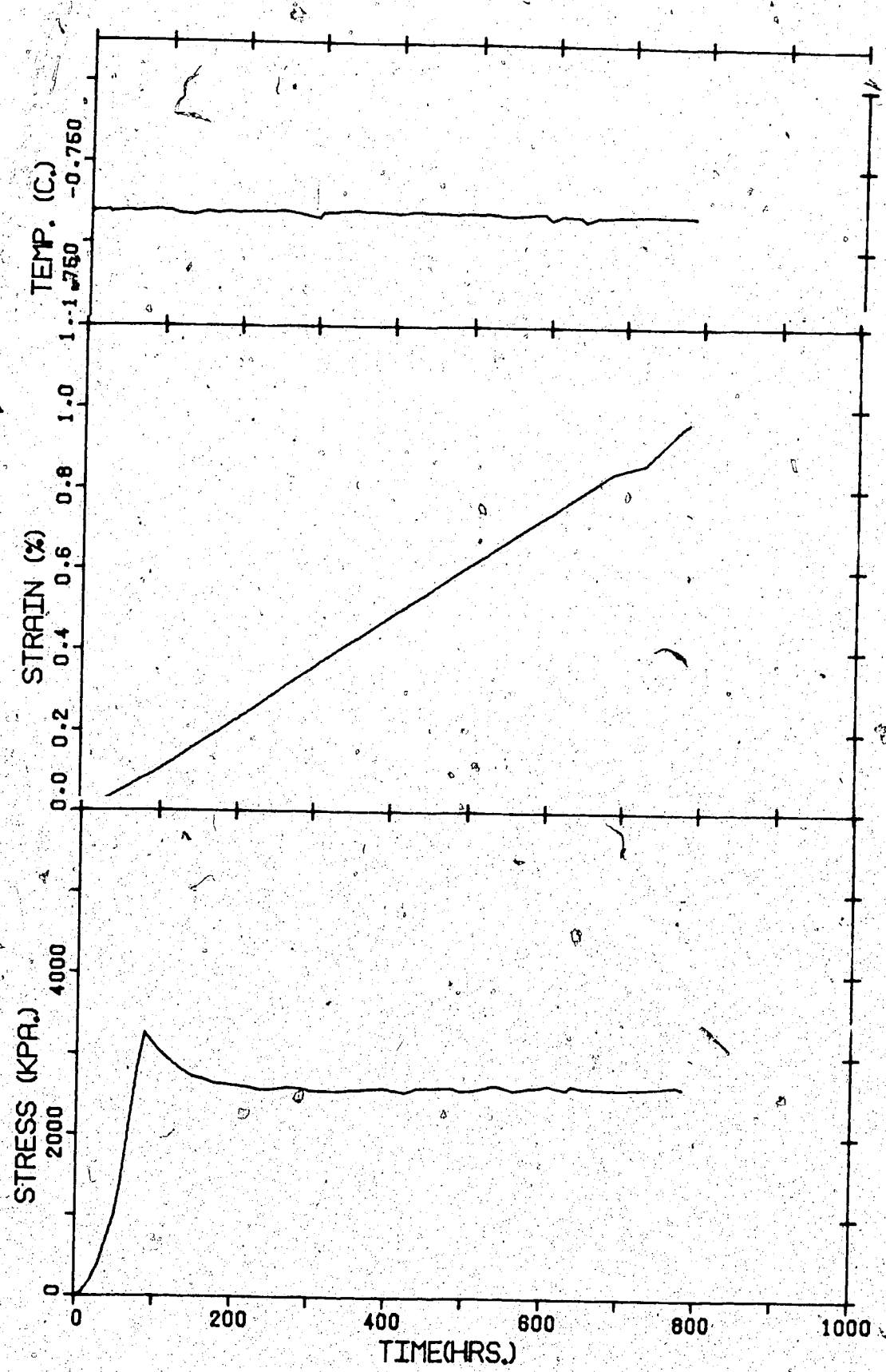

Figure A.20 Data plot of constant displacement rate punch sample Pen32.

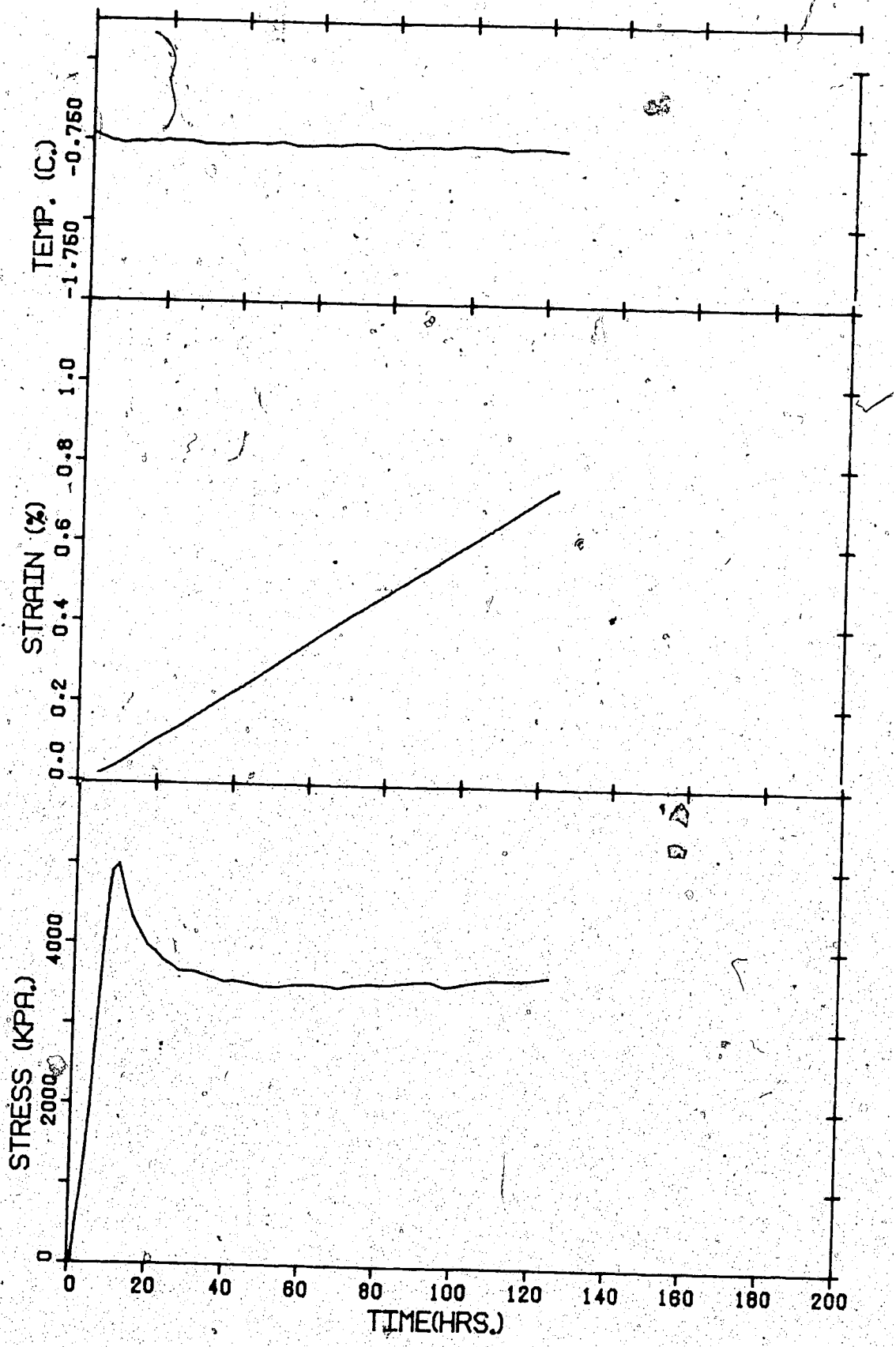

Figure A.21 Data plot of constant displacement rate punch sample Pen36.

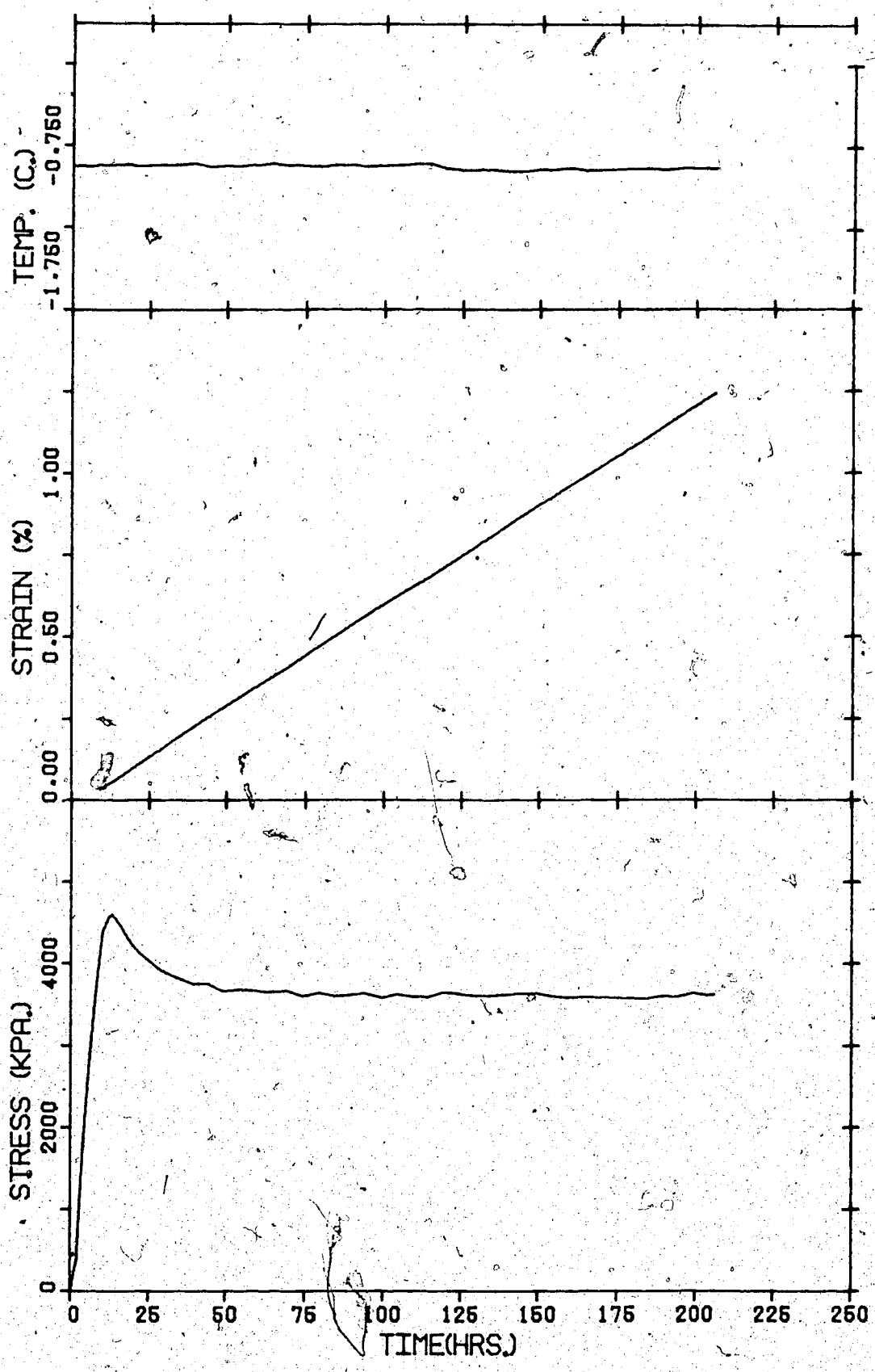

Figure A.22 Data plot of constant displacement rate punch sample Pen41.

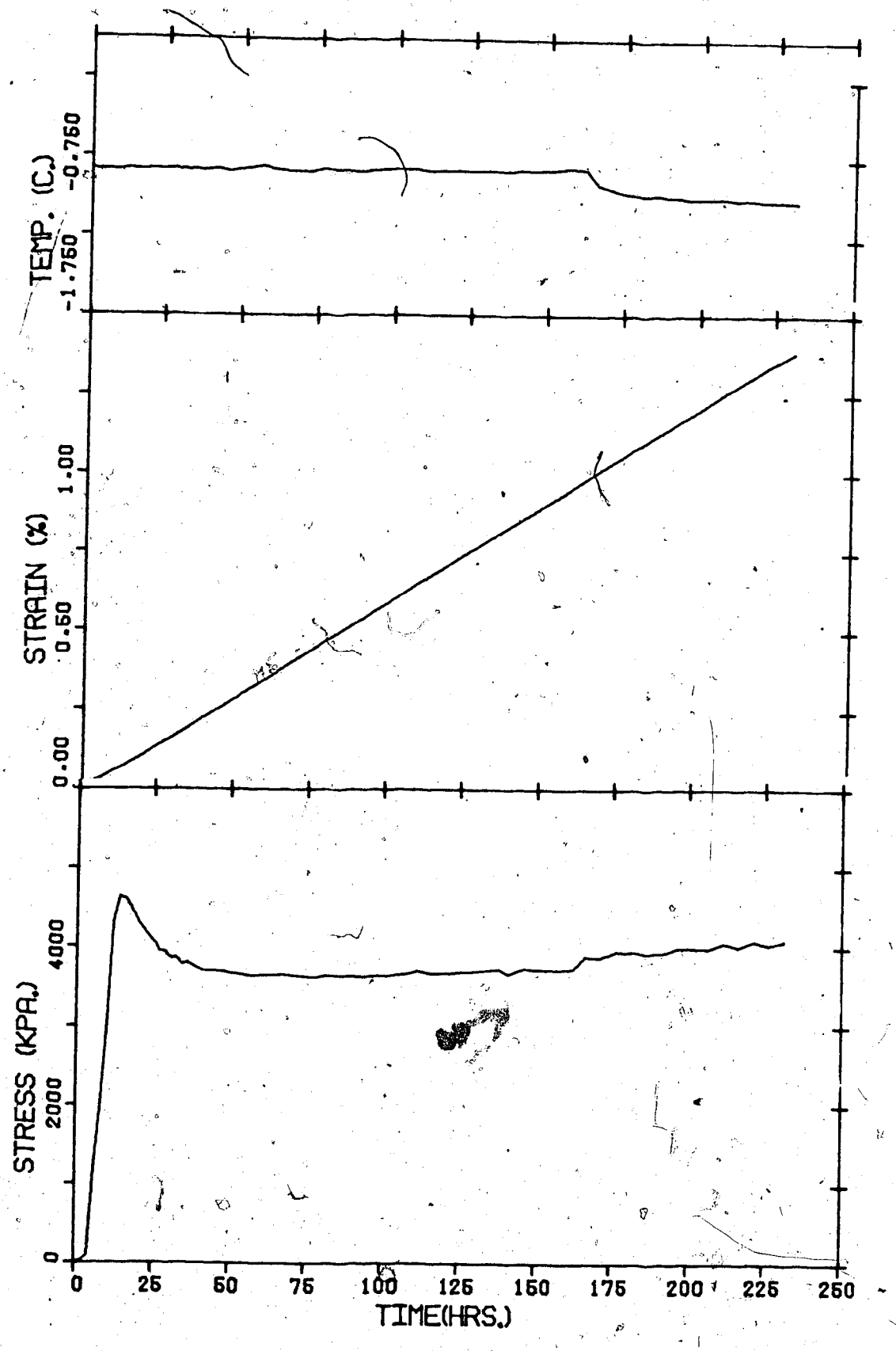

Figure A.23 Data plot of constant displacement rate punch sample Pen48.

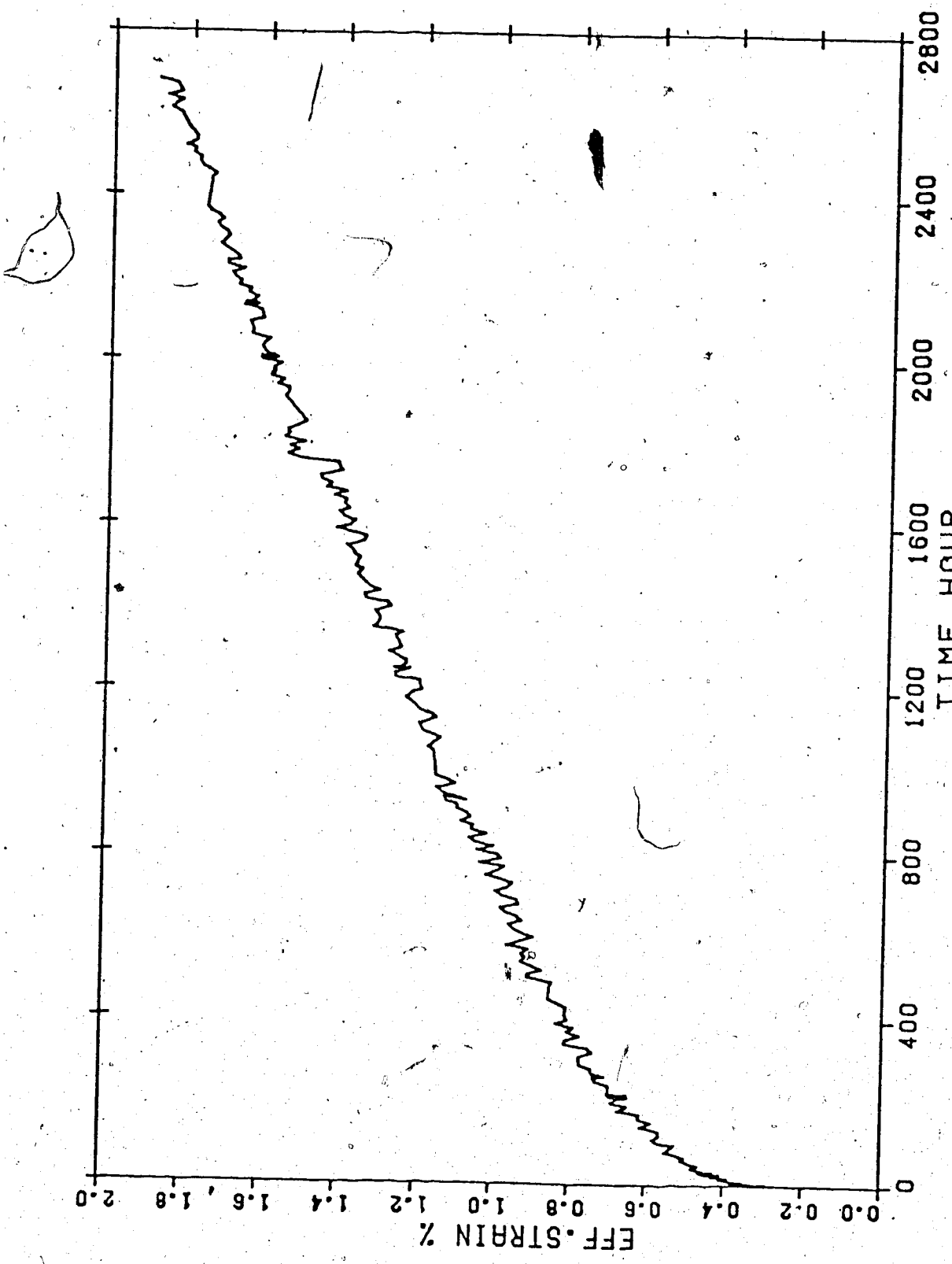

Figure A.24 Data plot of constant stress simple shear sample SS32.

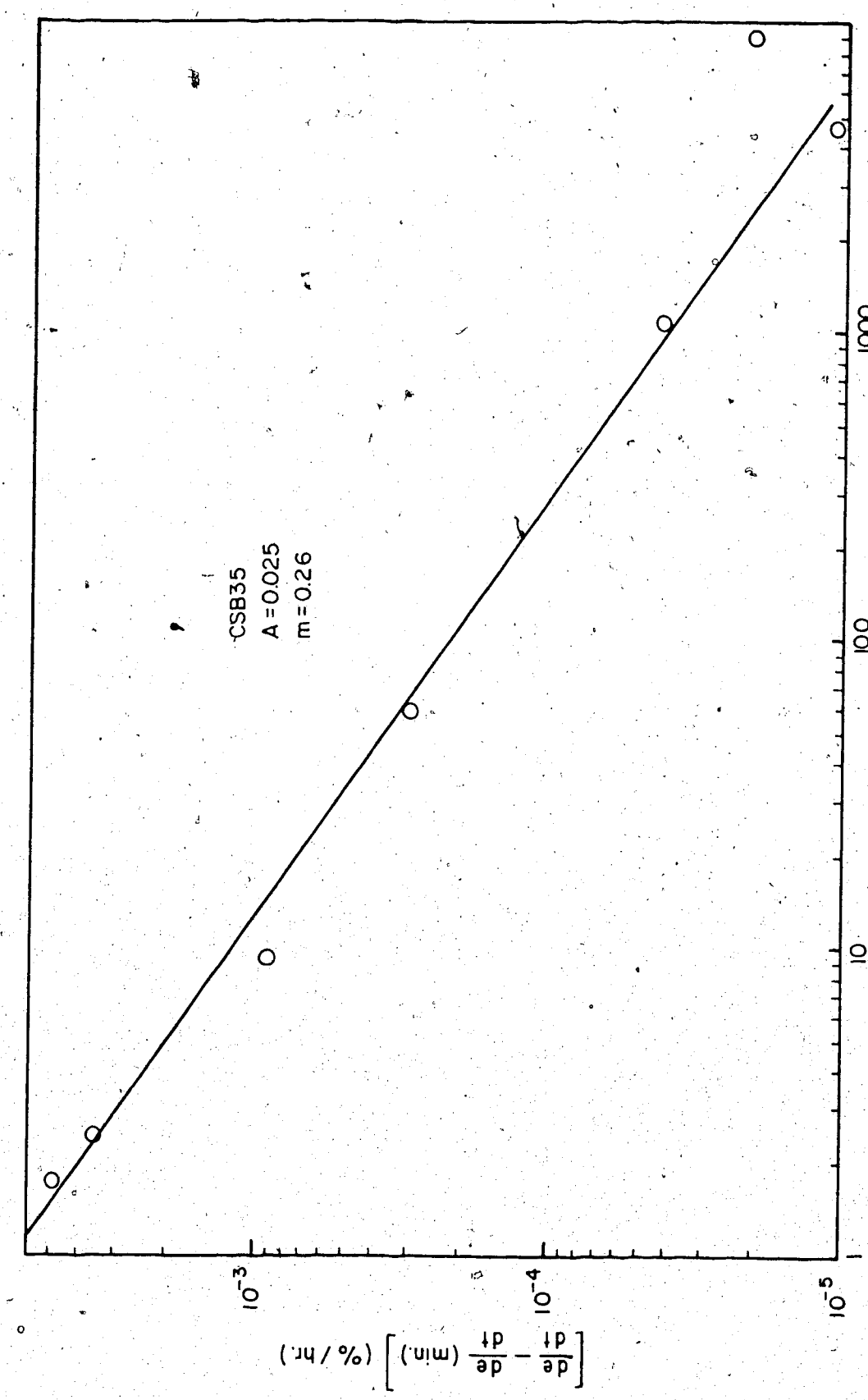

Figure A.25 Logarithm strain rate versus logarithm (t+1) of sample CSB35.

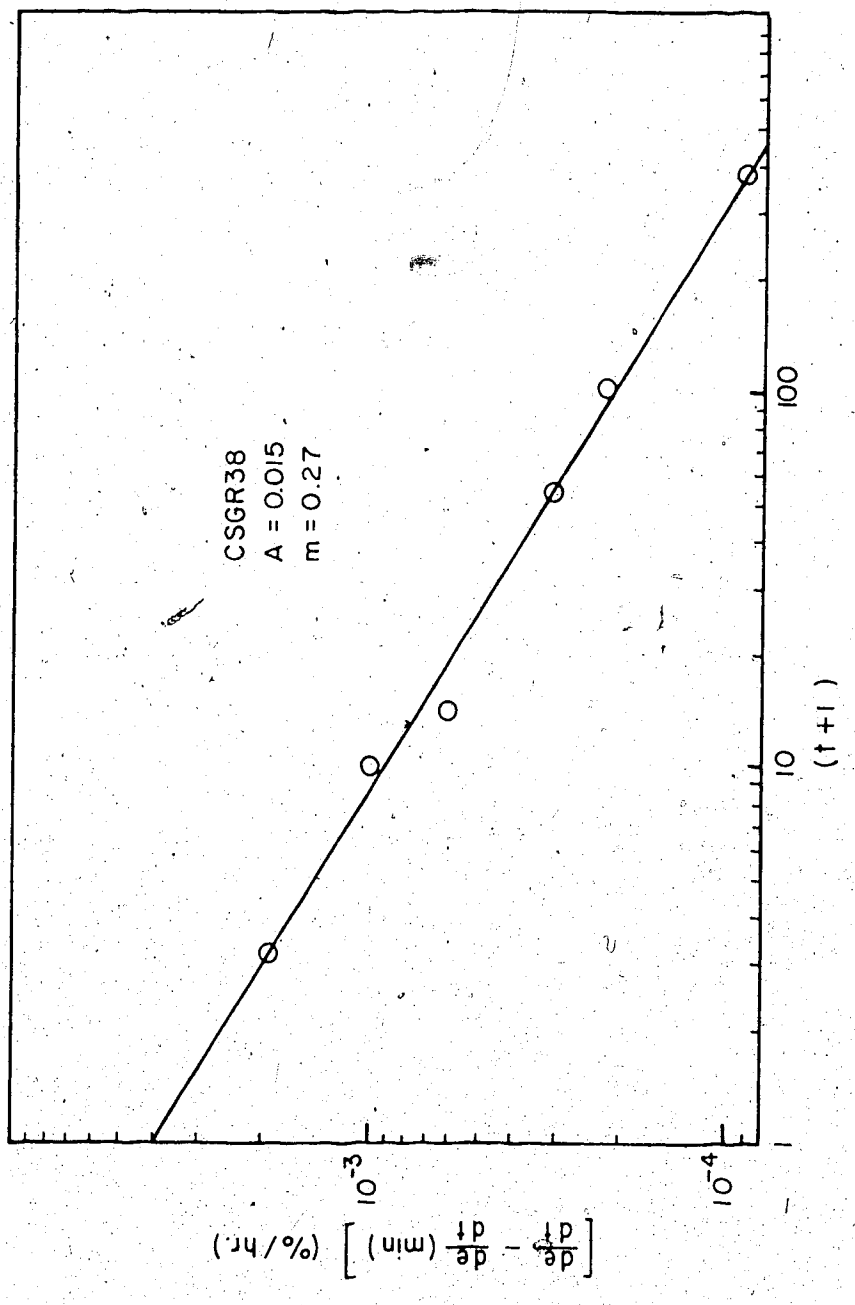

Figure A.26 Logarithm strain rate versus logarithm (t+1) of sample CSGR38.

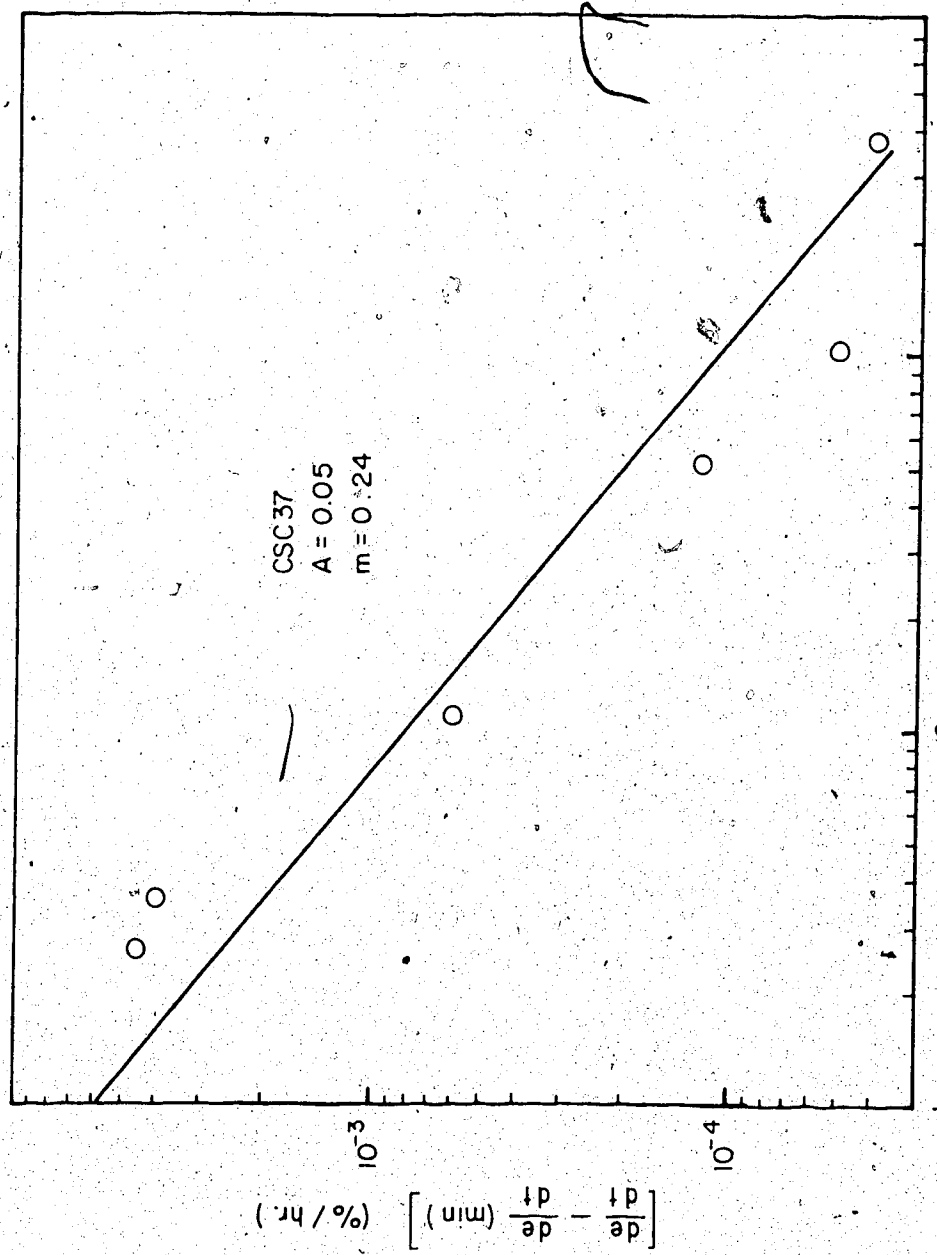

Figure A.27 Logarithm strain rate versus logarithm (t+1) of sample CSC37.

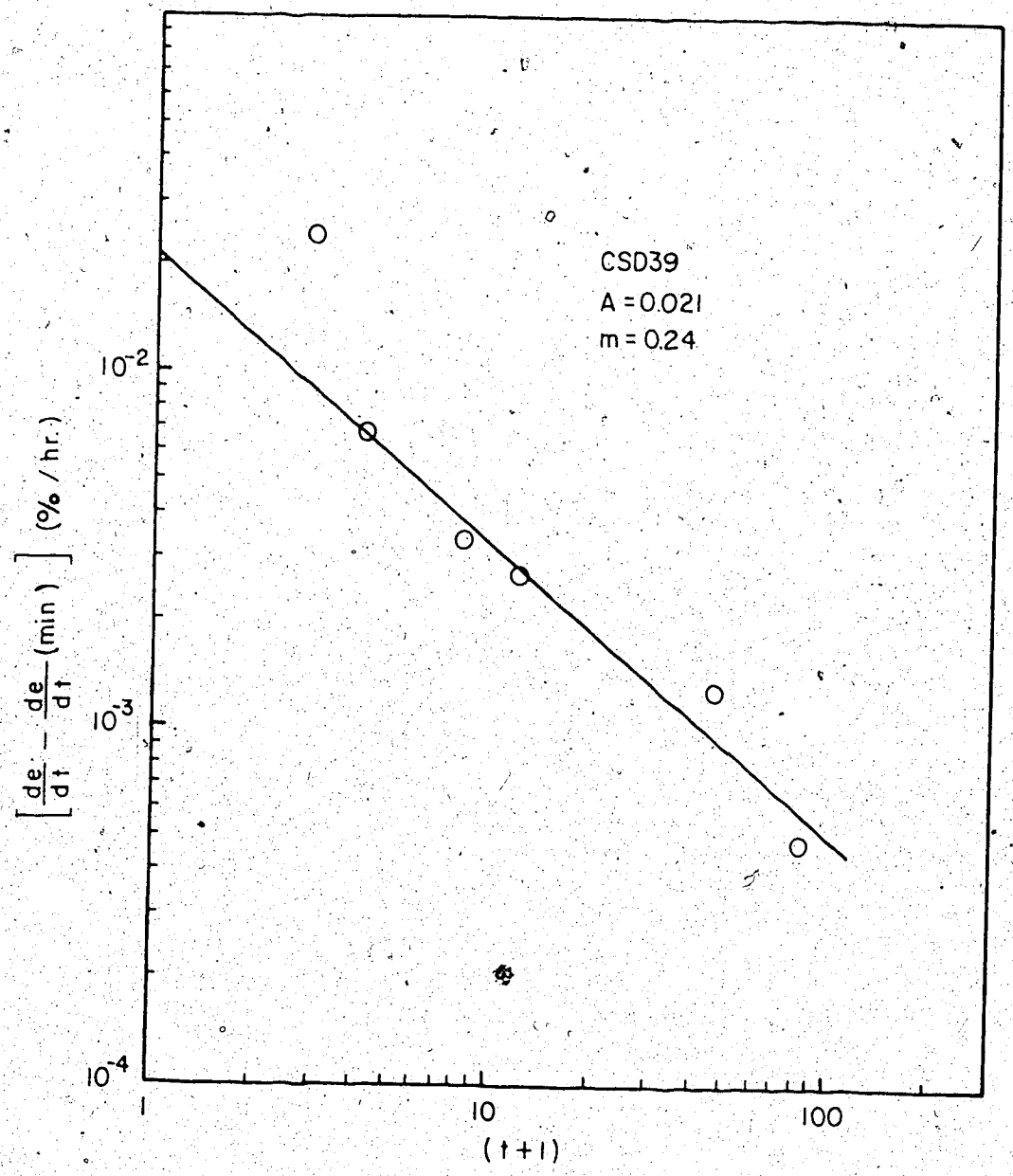

Figure A.28 Logarithm strain rate versus logarithm (t+1) of sample CSD39.

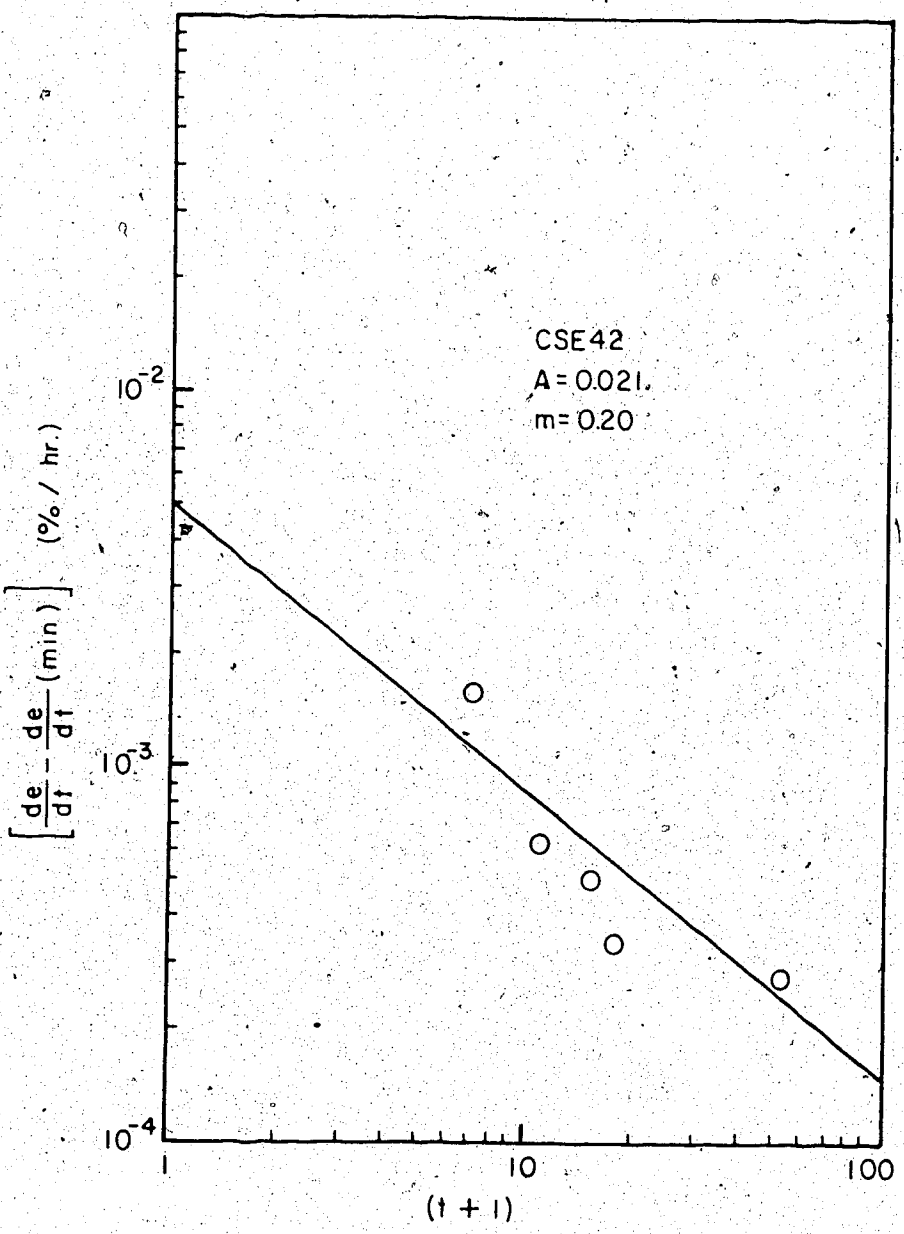

Figure A.29 Logarithm strain rate versus logarithm (t+1) of sample CSE42.

APPENDIX B
Finte Element Programs and Modification to model steady state creep

B.1 Introduction

ORIGINAL CONSTANT STRAIN TRIANGLE PROGRAM

Directory of variable names:

I. Material properties input

e(m)	Young's Modulus
pr(m)	Poisson' Ratio
ro(m)	Unit Weight
Acof(m)	Parameter of flow law
En(m)	Exponent of flow law

II. Nodal data input

Kode(n)	Boundary code
x(n)	x coordinate of node
y(n)	y coordinate of node
u(n)	x displacement or load at node
v(n)	y displacement or load at node

III. Element data input

m	Element number
np(i,m)	Nodal point at the three corners of of the element in counterclockwise order.
mat(m)	Element material number
th(m)	Thickness of element

IV. Varaibles used in ASTIF subroutine

ap(n)	Applied load vector
stif(mband,neq)	Structure stiffness matrix
neq	Number of equations
mband	Band width of problem

V. Varibles used in ELSTIF subroutine

ecm(3,3)	Element constitutive matrix
ebm(3,6)	Element B matrix
esm(3,6)	Element stress matrix
estif(6,6)	Element stiffness matrix

VI. Varibles used in STRESS subroutine

sigel(m,3)	Element stresses
sigp(m,4)	Element principal stress
siga(m,3)	Average element stress

```
C
CCCCC   THIS PROGRAM SOLVES PLANE STRAIN BOUNDARY
CCCCC   VALUE PROBLEMS
C
      COMMON E(8),PR(8),RO(8),X(200),Y(200),U(200),V(200)
     1  STIF(40,400),AP(400),ECM(3,3),
     1TH(200),EBM(3,6),ESM(3,6),WT,MBAND
      COMMON NUMNP,NUMEL,NUMAT,KODE(200),NP(3,200),
     1 NEQ,EN(8),M,LM(6)
      COMMON ESTIF(6,6),
     1SIGP(200,4),SIGEL(200,3),MAT(200)

C
1     CALL READIN
C
2     CALL ASTIF
C
      CALL BAND1
C
      CALL STRESS
C
C
3     STOP
      END
C
      SUBROUTINE READIN
C
C  THIS SUBROUTINE READS AND PRINTS MATERIAL DATA,
C  NODAL DATA, ELEMENT DATA.
C  IT GENERATES COORDINATES OF INTERMEDIATE NODAL
C  POINTS AND CALCULATES THE BAND WIDTH AND
C  NUMBER OF EQUATIONS
C
      COMMON E(8),PR(8),RO(8),X(200),Y(200),U(200),V(200),
     1  STIF(40,400),AP(400),ECM(3,3),
     1TH(200),EBM(3,6),ESM(3,6),WT,MBAND
      COMMON NUMNP,NUMEL,NUMAT,KODE(200),NP(3,200),
     1 NEQ,EN(8),M,LM(6)
      COMMON ESTIF(6,6),
     1SIGP(200,4),SIGEL(200,3),MAT(200)
C
      DIMENSION HED(18)
C  READ PRELIMINARY INFORMATION
      READ(5,1000) HED
      READ(5,1001) NUMNP,NUMEL,NUMAT
      WRITE(6,2000) HED,NUMNP,NUMEL,NUMAT
C
C  READ IN MATERIAL PROPERTIES FOR
C  ELASTIC AND INELASTIC STRAIN COMPUTATION
C
      WRITE(6,2005)
      DO 10 M=1,NUMAT
      READ(5,1010)  E(M),PR(M),RO(M)
10    WRITE(6,2010)  M,E(M),PR(M),RO(M)
C
C  READ AND WRITE NODAL DATA AND GENERATE INTERMEDIATE NODAL DATA
C
      WRITE(6,2014)
      WRITE(6,2015)
      L=1
      READ(5,1020) N,KODE(N),X(N),Y(N),U(N),V(N)
      GO TO 40
C
20    READ(5,1020) N,KODE(N),X(N),Y(N),U(N),V(N)
      DN = N-L
      DX =(X(N)-X(L))/DN
      DY =(Y(N)-Y(L))/DN
25    L=L+1
C
      IF(N-L) 50,40,30
30    X(L) = X(L-1)+DX
      Y(L) = Y(L-1)+DY
      KODE(L)= 0
      U(L)=0
      V(L)=0
      GO TO 25
C
40    CONTINUE
C     WRITE(6,2020)N,KODE(N),X(N),Y(N),U(N),V(N)
      IF(NUMNP-N) 50,60,20
C
50    WRITE (6,2025) N
      CALL EXIT
C
60    CONTINUE
C     WRITE(6,2016)
C     WRITE(6,2015)
C     WRITE (6,2020)  (N,KODE(N),X(N),Y(N),U(N),V(N),N=1,NUMNP)
C
C  READ AND WRITE ELEMENT DATA
C
C     WRITE(6,2031)
C     WRITE(6,2030)
      ML=0
51    IF (ML.GE.NUMEL)  GO TO 70
      READ(5,1035)  M,NP(1,M),NP(2,M),NP(3,M),MAT(M),TH(M)
C     WRITE (6,2035)M,NP(1,M),NP(2,M),NP(3,M),MAT(M),TH(M)
      MM=ML+1
      IF (MM.EQ.M)  GO TO 65
C
```

```
      55 ML1=ML+1
         IF(ML1.EQ.M)  GO TO 65
         ML2=ML+2
         MLM1=ML-1
         IF(MLM1.LE.0) GO TO 85
         DO 62  I=1,3
         NP(I,ML2)=NP(I,ML)+1
      62 NP(I,ML1)=NP(I,MLM1)+1
         MAT(ML2)=MAT(ML)
         MAT(ML1)=MAT(MLM1)
         TH(ML2)=TH(ML)
         TH(ML1)=TH(MLM1)
         ML=ML2
         GO TO 55
C
      65 ML=M
         GO TO 51
      70 CONTINUE
C     WRITE(6,2032)
C     WRITE(6,2030)
C     WRITE (6,2035) (M,(NP(J,M),J=1,3),MAT(M),TH(M)
C
C     DETERMINE BAND WIDTH AND NUMBER OF EQUATIONS
C
         L=0
         DO 80 M=1,NUMEL
         DO 80 I=1,2
         II=I+1
         DO 80 J=II,3
         K= IABS(NP(I,M)-NP(J,M))
         IF (K.GT.L)   L=K
      80 CONTINUE
C
         MBAND = 2*(L+1)
         NEQ= 2*NUMNP
C
         WRITE(6,2040)MBAND,NEQ
         IF(MBAND.LE. 40.AND.NEQ.LE.200)  GO TO 90
         WRITE(6,2050)
         CALL EXIT
      85 WRITE(6,2060)
         CALL EXIT
C
      90 WRITE(6,3000)
    3000 FORMAT(    '  READIN COMPLETED ' ///)
         RETURN
C
C  FORMAT STATEMENTS
    1000 FORMAT(18A4)
    1001 FORMAT(3I6,2F10.6)
```

```
         1,10X,18A4,////
         25H NUMBER OF NODAL POINTS = ,I6/
         25H NUMBER OF ELEMENTS     = ,I6/
         25H NUMBER OF MATERIALS    = ,I6/)
         1H ,23X, 20H MATERIAL PROPERTIES //
         3,,2X, 9HMODULUS E,2X,12HPOISS. RATIO,2X,
        2810.6,//)
    1010 FORMAT(E11.4,2F10.6,E11.4,F10.6)
    2010 FORMAT(1H ,1X,I5,E11.4,F15.3,F9.2,E11.4,F8.2)
    2014 FORMAT( '1', 5X, 'OUTPUT OF INPUT NODAL DATA ')
    2015 FORMAT(///,10X,19H NODAL POINT OUTPUT,///
        11H ,59H NODE   KODE     X COORD      Y COORD      X FORCE
        2      Y FORCE//)
    2016 FORMAT('1', 5X, 'OUTPUT OF COMPLETE NODAL DATA ')
    1020 FORMAT(2I6,4F12.0)
    2020 FORMAT(I4,I6,F13.3,3F12.3)
    2025 FORMAT(1HO,28H ERROR IN NODAL DATA,NODE = ,I4)
    2030 FORMAT(///,10X, 13H ELEMENT DATA ///
        1 40H ELEM     I     J     K     MAT  THICKNESS //)
    2031 FORMAT('1',5X, 'OUTPUT OF INPUT ELEMENT DATA' )
    2032 FORMAT( '1', 5X, 'OUTPUT OF COMPLETE ELEMENT DATA ' )
    1035 FORMAT (5I6,F6.0)
    2035 FORMAT ( I4, 4I6,F11.4)
    2040 FORMAT (///10X, 22H BAND WIDTH           = ,I6/
        1        10X, 22H NUMBER OF EQUATIONS = ,I6)
    2050 FORMAT(///10X, 33H PROBLEM EXCEEDS SPECIFIED LIMITS )
    2060 FORMAT(  'MLM1 IS LESS THAN OR EQUAL TO ZERO ')
C
         END
C
         SUBROUTINE ASTIF
C
C     THIS SUBROUTINE TAKES EACH ELEMENT IN TURN AND
C     FORMS THE ELEMENT STIFFNESS MATRIX (BY CALLING
C      ELSTIF). IT ASSEMBLES THE ELEMENT STIFFNESSES
C     INTO  KSTIF.  THEN ADDS THIS INTO THE TOTAL
C     STIFFNESS TSITF.  ASSEMBLES THE APPLIED LOAD
C     VECTOR (AP) AND FICTIOUS LOAD VECTOR(FICLD).
C     MODIFIES THE  ASSEMBLAGES FOR DISPLACEMENT
C     BOUNDARY CONDITIONS (BY CALLING MODIFY)>
C
         COMMON E(8),PR(8),RO(8),X(200),Y(200),U(200),V(200),
        1  STIF(40,400),AP(400),ECM(3,3),
        1TH(200),EBM(3,6),ESM(3,6),WT,MBAND
         COMMON NUMNP,NUMEL,NUMAT,KODE(200),NP(3,200),
        1 NEQ,EN(8),M,LM(6)
         COMMON ESTIF(6,6),
        1SIGP(200,4),SIGEL(200,3),MAT(200)
C
C   INITIALIZE APPLIED LOAD VECTOR AND MASTER STIFFNESS
```

```
C   MATRIX AND ECM
C
      DO 10 I=1,NEQ
      AP(I)=0.0
      DO 10 J=1,MBAND
      STIF(J,I)=0.0
10    CONTINUE
      DO 20 I=1,3
      DO 20 J=1,3
20    ECM(I,J)=0.0
C
C   FORM ELEMENT CONSTITUTIVE MATRIX (ECM) IF NUMAT=1
C
      IF(NUMAT.NE.1) GO TO 30
      EPR=PR(1)
      COM=E(1)/((1.+EPR)*(1.-2.*EPR))
      COM1=COM*(1.-EPR)
      COM2=COM*EPR
      ECM(1,1)=COM1
      ECM(2,2)=COM1
      ECM(1,2)=COM2
      ECM(2,1)=COM2
      ECM(3,3)=E(1)/(2.*(1.+EPR))
C
30    DO 45 M=1,NUMEL
C
      CALL ELSTIF(1)
C
C   ASSEMBLE ELSTIF INTO MASTER STIFFNESS MATRIX
C
      IF(TIME.GT.0.0) GO TO 91
      DO 35 I=1,3
      I2=2*I
      LM(I2)=2*NP(I,M)
35    LM(I2-1)=LM(I2)-1
C
      DO 40 I=1,6
      II=LM(I)
      DO 40 J=1,6
      JJ=LM(J)-II+1
      STIF(JJ,II)= STIF(JJ,II)+ESTIF(J,I)
40    CONTINUE
C
C   ADD GRAVITY LOADS INTO AP VECTOR
C
      DO 31 I=2,6,2
      II=LM(I)
      AP(II)=AP(II)-WT
31    CONTINUE
C
45    CONTINUE
C
C   ADD NODAL LOADS INTO AP VECTOR
C
      DO 50 N=1,NUMNP
      N2=2*N
      V(N)=0.0
      AP(N2)=AP(N2)+V(N)
      AP(N2-1)=AP(N2-1)+U(N)
50    CONTINUE
C
C   MODIFY STIFFNESS AND LOAD VECTOR FOR
C   DISPLACEMENT BOUNDARY CONDITIONS.
C
      DO 100 N=1,NUMNP
      N2=2*N
      IF (KODE(N)-10) 80,70,60
80    II=N2-1
      CALL MODIFY(II,N)
      CALL MODIFY(N2,N)
      GO TO 100
70    II=N2-1
      CALL MODIFY(II,N)
      GO TO 100
80    IF(KODE(N).EQ.0)  GO TO 100
      CALL MODIFY(N2,N)
100   CONTINUE
C
919   RETURN
1921  FORMAT(' ','SUM HORT. FOR.=',E15.8,5X,
     1'SUM VET. FOR=',E15.8,
     15X,'FIC H LOAD',E15.8,'FIC V LOAD',E15.8)
1117  FORMAT(' ',2X,I6,F10.2,2X,I6,4X,F10.2,3X,F10.2,3X,5F10.2)
1118  FORMAT(1H1,10X,'FORCES AT THE NODES', ///,
     1'NO.',10X,'FORCE R',5X,'NO.',10X,'FORCE Z',
     2'AP(II)=',E13.6,3X,'FL(II)=',E13.6)
1116  FORMAT(/,10X,'ELEM=',I4,5X,'IJ=',I4,5X,'II=',I4,/,
     15X,'AP(IJ)=',E13.6,3X,'FL(IJ)=',E13.6,3X,
     2'AP(II)=',E13.6,3X,'FL(II)=',E13.6)
      END
C
      SUBROUTINE MODIFY (I,N)
C
C  THIS SUBROUTINE MODIFIES KSTIF AND AP IF A
C  DISPLACEMENT BOUNDARY CONDITION IS IMPOSED
C  IN EQUATION I ASSOCIATED WITH NODAL POINT N
C
      COMMON E(8),PR(8),RO(8),X(200),Y(200),U(200),V(200),
     1  STIF(40,400),AP(400),ECM(3,3),
     1TH(200),EBM(3,6),ESM(3,6),WT,MBAND
```

```
      COMMON NUMNP,NUMEL,NUMAT,KODE(200),NP(3,200),
     1 NEQ,EN(8),M,LM(6)
      COMMON ESTIF(6,6),
     1SIGP(200,4),SIGEL(200,3),MAT(200)
C
      DISP=U(N)
      IF((I-2*N).EQ.0)  DISP=V(N)
C
      DO 50 J=2,MBAND
      IL=I+J-1
      IU=I-J+1
      IF(IU.LE.0)GO TO 10
      AP(IU)=AP(IU) - STIF(J,IU)*DISP
      STIF(J,IU)=0.0
10    IF(IL.GT.NEQ) GO TO 50
      AP(IL)= AP(IL)- STIF(J,I)*DISP
      STIF(J,I)=0.0
50    CONTINUE
      AP(I)=DISP
      STIF(1,I)=1.0
      RETURN
      END

      SUBROUTINE BAND1
C
C  THIS SUBROUTINE SOLVES FOR DISPLACEMENTS USING A
C  GAUSSIAN ELIMINATION  TECHNIQUE FOR SYMMETRIC
C  BANDED MATRICES STORED IN CORE
C
      COMMON E(8),PR(8),RO(8),X(200),Y(200),U(200),V(200),
     1  STIF(40,400),AP(400),ECM(3,3),
     1TH(200),EBM(3,6),ESM(3,6),WT,MBAND
      COMMON NUMNP,NUMEL,NUMAT,KODE(200),NP(3,200),
     1 NEQ,EN(8),M,LM(6)
      COMMON ESTIF(6,6),
     1SIGP(200,4),SIGEL(200,3),MAT(200)
C
C TRIANGULARIZE AND REDUCE RIGHT HAND SIDE
      NL=NN-MM+1
      NM=NN-1
      MR=MM
C
      DO 100 N=1,NM
      IF (A(1,N).LE.0.) GO TO 700
      BN=B(N)
      B(N)=BN/A(1,N)
      IF (N.GT.NL) MR=NN-N+1
C
      DO 100 L=2,MR
      IF (A(L,N).EQ.0.)GO TO 100
      C= A(L,N)/A(1,N)
      I= N+L-1
      J= 0
      DO 50 K=L,MR
      J=J+1
50    A(J,I)= A(J,I)-C*A(K,N)
      B(I)=B(I)-C*BN
      A(L,N)=C
100   CONTINUE
C
C   BACK SUBSTITUTE
C
      I=NN
C
      B(NN)=B(NN)/A(1,NN)
      DO 600 N=1,NM
      I=I-1
      IF (N.LT.MM)      MR= N+1
      DO 600 J=2,MR
      K=I+J-1
600   B(I) =B(I)- A(J,I)*B(K)
      WRITE(6,2001)
      DO 901 II=1,NUMNP
      I2=2*II
      I2M=I2-1
      WRITE(6,1799) II,B(I2M),II,B(I2),X(II),Y(II)
901   CONTINUE
      RETURN
700   WRITE (6,1999) N
      STOP
1999  FORMAT(1HO, 81H ZERO OR NEGATIVE ELEMENT ON  MAIN DIAGONAL
     1 OF TRIANGULARIZED MATRIX FOR EQUATION  ,I5)
C
2001 FORMAT('1',  '  NODAL DISPLACEMENTS  ' ,//,    NO.',11X,
     1'U',6X,'NO.',11X, 'V',11X,'X(I)',11X'Y(I)'// )
1799  FORMAT(' ',I6,E15.5,I6,E15.5,5X,F7.2,8X,F7.2)
      END
      SUBROUTINE ELSTIF(KOP)
C
C  THIS SUBROUTINE FORMS THE ELEMENT STIFFNESS MATRIX (ESTIF) OR
C  ELEMENT STRESS MATRIX (ESM) FOR THE CONSTANT STRAIN TRIANGLE
C  THE FICTIOUS LOAD MATRIX IS FORMED USING THE INELASTIC STRAIN
C
      COMMON E(8),PR(8),RO(8),X(200),Y(200),U(200),V(200),
     1  STIF(40,400),AP(400),ECM(3,3),
     1TH(200),EBM(3,6),ESM(3,6),WT,MBAND
      COMMON NUMNP,NUMEL,NUMAT,KODE(200),NP(3,200),
     1 NEQ,EN(8),M,LM(6)
      COMMON ESTIF(6,6),
     1SIGP(200,4),SIGEL(200,3),MAT(200)
```

```
C
      DIMENSION STR(3),AV(3),BV(3)
C
      DO 10 I=1,3
      DO 10 J=1,6
10    EBM(I,J)=0.0
      I=NP(1,M)
      J=NP(2,M)
      K=NP(3,M)
C
C     FORM ELEMENT DIMENSIONS
C
      AV(1)=X(K)-X(J)
      AV(2)=X(I)-X(K)
      AV(3)=X(J)-X(I)
      BV(1)=Y(J)-Y(K)
      BV(2)=Y(K)-Y(I)
      BV(3)=Y(I)-Y(J)
      AREA2=(AV(3)*BV(2))-(AV(2)*BV(3))
C
C
21    IF (TH(M).LE.0.001) TH(M)=1.
      VOL=TH(M)*AREA2/2.
      IF (VOL.LE.0.0001) GO TO 75
C
C     FORM CONSTITUTIVE MATRIX
C
      IF (NUMAT.EQ.1) GO TO 30
      NM=MAT(M)
      EPR=PR(NM)
      COM=E(NM)/((1.+EPR)*(1.-2.*EPR))
      COM1=COM*(1.-EPR)
      COM2=COM*EPR
      ECM(1,1)=COM1
      ECM(2,2)=COM1
      ECM(1,2)=COM2
      ECM(2,1)=COM2
      ECM(3,3)=E(NM)/(2.*(1.+EPR))
C
30    IF(KOP.EQ.2) GO TO 22
C
C
C     FORM ELEMENT B MATRIX (EBM)
C
22    DO 40 I=1,3
      I2=2*I
      I2M=2*I-1
      EBM(1,I2M)=BV(I)/AREA2
      EBM(2,I2)=AV(I)/AREA2
      EBM(3,I2M)=EBM(2,I2)
40    EBM(3,I2)=EBM(1,I2M)
C
C     FORM ELEMENT STRESS MATRIX (ESM)
C
      DO 50 I=1,3
      DO 50 J=1,6
      ESM(I,J)=0.0
      DO 50 K=1,3
50    ESM(I,J)=ESM(I,J)+ECM(I,K)*EBM(K,J)
C
      IF(KOP.EQ.2) GO TO 80
C
      IF(NUMAT.EQ.1)  NM=1
      WT=VOL*RO(NM)/3.
C
C     FORM ELEMENT STIFFNESS MATRIX (ESTIF)
C
      DO 70 I=1,6
      DO 70 J=1,6
      ESTIF(I,J)=0.0
      DO 60 K=1,3
60    ESTIF(I,J)=ESTIF(I,J)+EBM(K,I)*ESM(K,J)
70    ESTIF(I,J)=ESTIF(I,J)*VOL
C
      GO TO 80
75    WRITE(6,1000) M
      CALL EXIT
80    RETURN
C
1000  FORMAT (1H1, 18H VOLUME OF ELEMENT ,I4, 18H IS
     1 LESS THAN ZERO)
C
      END
C
      SUBROUTINE STRESS
C
C     THIS SUBROUTINE FORMS THE ELEMENT STRESS MATRIX (ESM),
C     MULITIPLIES BY  THE ELEMENT DISPLACEMENT VECTOR (ELDISP)
C     SUBTRACTS THE ACCUMULATED STRAIN
C      AND RECORDS THE STRESSES IN SIGEL.
C
      COMMON E(8),PR(8),RO(8),X(200),Y(200),U(200),V(200),
     1  STIF(40,400),AP(400),ECM(3,3),
     1TH(200),EBM(3,6),ESM(3,6),WT,MBAND
      COMMON NUMNP,NUMEL,NUMAT,KODE(200),NP(3,200),
     1 NEQ,EN(8),M,LM(6)
      COMMON ESTIF(6,6),
     1SIGP(200,4),SIGEL(200,3),MAT(200)
C
      DIMENSION SIG(200,3),KOUNT(200),ELDISP(6),
```

```
      1SIGA(200,3)
C
      DO 5 N=1,NUMNP
      KOUNT(N)=0
      DO 5 J=1,3
5     SIGA(N,J)=0.0
C
      DO 100 M=1,NUMEL
C
C   COMPUTE ELEMENT DISPLACEMENTS
C
      DO 10 I=1,3
      I2=2*I
      LMI2  =2*NP(I,M)
      ELDISP(I2)=AP(LMI2)
10    ELDISP(I2-1)=AP(LMI2-1)
C  COMPUTE  ELEMENT STRESSES
C
      CALL ELSTIF(2)
C
C CALCULATES THE STRESS
      DO 21 I=1,3
       SIGEL(M,I)=0.0
      DO 20 J=1,3
      SIGEL(M,I)=SIGEL(M,I)+ECM(I,J)*ELDISP(J)
20    CONTINUE
21    CONTINUE
C
C  ACCUMULATE FOR NODAL STRESSES
C
      DO 30 K=1,3
      N=NP(K,M)
      KOUNT(N)=KOUNT(N)+1
      DO 30 I=1,3
30    SIGA(N,I)=SIGA(N,I) + SIGEL(M,I)
C
C  COMPUTE ELEMENT PRINCIPAL STRESSES  AND DIRECTIONS
C
      SIGM=(SIGEL(M,1)+SIGEL(M,2))/2.
      SIGD2=(SIGEL(M,1)-SIGEL(M,2))/2.
      RAD =SQRT(SIGD2**2 +SIGEL(M,3)**2)
      SIGP(M,1)=SIGM+RAD
      SIGP(M,2)= SIGM-RAD
      SIGP(M,3)= RAD
      SIGP(M,4)= 0.5*57.29578*ATAN2(SIGEL(M,3),SIGD2)
100   CONTINUE
C
C  FIND AVERAGE NODAL STRESSES
C
      DO 110 N=1,NUMNP
      RK=KOUNT(N)
      DO 110 I=1,3
110   SIGA(N,I)= SIGA(N,I)/RK
C
C   FIND  MAXIMUM  ELEMENT STRESSES
C
      SIG1=0.0
      SIG2=0.0
      SIG3=0.0
      M1=0
      M2=0
      M3=0
      DO 130 M=1,NUMEL
      IF (SIGP(M,1).LT.SIG1) GO TO 115
      SIG1=SIGP(M,1)
      M1=M
115   IF (SIGP(M,2).GT.SIG2) GO TO 120
      SIG2=SIGP(M,2)
      M2=M
120   IF (SIGP(M,3).LT.SIG3) GO TO 130
      SIG3=SIGP(M,3)
      M3=M
130   CONTINUE
      WRITE(6,2000)
      WRITE(6,2010) (M,(SIGEL(M,I) ,I=1,3),CX(M),CY(M),M=1,NUMEL)
C     WRITE(6,2020)
C     WRITE(6,2030) (M,(SIGP(M,I) ,I=1,4),M=1,NUMEL)
C     WRITE(6,2040) SIG1,M1,SIG2,M2,SIG3,M3
C     WRITE(6,2050)
C     WRITE(6,2010)  (N,(SIGA(N,I),I=1,3),X(N),Y(N),N=1,NUMNP)
      RETURN
2000  FORMAT(1H1,10X, 21H X-Y ELEMENT STRESSES /// 4OH ELEM
     1   SIGMA X
     1  SIGMA Y      SIGMA XY //)
2010  FORMAT(I4,1X,E12.5,1X,E12.5,1X,E12.5,5X,'X=',F10.3,5X,
     *'Y=',F10.3)
2020  FORMAT(1H1,10X,27H ELEMENT PRINCIPAL STRESSES ///
     1 55H ELEM   SIGMA I      SIGMA II     MAX TAU
     1     SIGMA I DEG //)
2030  FORMAT(I4,F11.1,2F12.1, F14.8)
2040  FORMAT(' ',
     1 27H MAXIMUM PRINCIPAL STRESS = ,F11.1,19H
     1 AND OCCURS IN ELEM,I6//
     2 27H MINIMUM PRINCIPAL STRESS = ,F11.1,19H
     2  AND OCCURS IN ELEM, I6//
     3 27H MAXIMUM SHEAR  STRESS    = ,F11.1,19H
     3 AND OCCURS IN ELEM,I6)
2050  FORMAT(1H1, ' AVERAGE NODAL STRESSES '///
     1           ' NODE   SIGMA X     SIGMA Y     SIGMA XY '//)
      END
```

PLANE STRAIN CREEP PROGRAM

Directory of variable names:

I. Material properties input

e(m)	Young's Modulus
pr(m)	Poisson' Ratio
ro(m)	Unit Weight
Acof(m)	Parameter of flow law
En(m)	Exponent of flow law

II. Nodal data input

Kode(n)	Boundary code
x(n)	x coordinate of node
y(n)	y coordinate of node
u(n)	x displacement or load at node
v(n)	y displacement or load at node

III. Element data input

m	Element number
np(i,m)	Nodal point at the three corners of of the element in counterclockwise order.
mat(m)	Element material number
th(m)	Thickness of element

IV Variables used in Main

time	Total accumulated time
tme	Increment of time
q	Time terminator

V. Varaibles used in ASTIF subroutine.

ap(n)	Applied load vector
tap(n)	Total load vector which is incremented each time
stif(mband,neq)	Structure stiffness matrix
neq	Number of equations
mband	Band width of problem calculated in READIN
tstif(mband,neq)	Total structure stiffness matrix which is saved
ficld(m,6)	Fictitous load matrix calulated in ELSTIF
tfldv	Accumulated load in vertical
tfldh	Accumulated load in horizontal

VI. Varibles used in ELSTIF subroutine

ecm(3,3)	Element constitutive matrix
ebm(3,6)	Element B matrix
esm(3,6)	Element stress matrix
estif(6,6)	Element stiffness matrix
srmt(3,m)	Inelastic strain matrix calculated in NOELAS

VII. Varibles used in STRESS subroutine

eldisp(n)	Nodal displacement vector calculated in BANDI
tstr(m,3)	Accumulated total strain
trmt(m,3)	Accumulated total strain of previous increment
sigel(m,3)	Element stresses
sigp(m,4)	Element principal stress
siga(m,3)	Average element stress

VIII. Varibles used in NOELAS subroutine

estres	Effective shear stress
estrnr	Effective shear strain rate
estrn	Effective shear strain increment
srmt(3,m)	Inelastic strain matrix

```
      CCCCC     THIS PROGRAM SOLVES PLANE STRAIN BOUNDARY
      CCCCC     VALUE PROBLEMS
C
      COMMON E(8),PR(8),RO(8),X(200),Y(200),U(200),V(200),
     1  STIF(40,400),AP(400),TSTIF(40,400),ECM(3,3),
     1TH(200),EBM(3,6),ESM(3,6),WT,MBAND
      COMMON NUMNP,NUMEL,NUMAT,KODE(200),NP(3,200),
     1 NEQ,ACOF(8),EN(8),M,LM(6),TAP(400),TRMT(3,200),
      COMMON SRMT(3,200),FICLD(200,6),APFL(200),ESTIF(6,6)
     1SIGP(200,4),SIGEL(200,3),TSTR(200,3),MAT(200)
      COMMON /TIM1/ TME,Q,TIME
C
    1 CALL READIN
C
    2 CALL ASTIF
C
      CALL BAND1
C
      CALL STRESS
C
      WRITE(6,1101) TIME,Q,TME
C
 1101 FORMAT(////,20X,9H TIME    = ,3E15.7)
      IF(TIME.GE.Q) GO TO 3
      TIME=TIME+TME
C
      CALL NOELAS
C
      GO TO 2
    3 STOP
      END
C
      SUBROUTINE READIN
C
C  THIS SUBROUTINE READS AND PRINTS MATERIAL DATA,
C  NODAL DATA, ELEMENT DATA.
C  IT GENERATES COORDINATES OF INTERMEDIATE NODAL
C  POINTS AND CALCULATES THE BAND WIDTH AND
C  NUMBER OF EQUATIONS
C
      COMMON E(8),PR(8),RO(8),X(200),Y(200),U(200),V(200),
     1  STIF(40,400),AP(400),TSTIF(40,400),ECM(3,3),
     1TH(200),EBM(3,6),ESM(3,6),WT,MBAND
      COMMON NUMNP,NUMEL,NUMAT,KODE(200),NP(3,200),
     1 NEQ,ACOF(8),EN(8),M,LM(6),TAP(400),TRMT(3,200),
      COMMON SRMT(3,200),FICLD(200,6),APFL(200),ESTIF(6,6)
     1SIGP(200,4),SIGEL(200,3),TSTR(200,3),MAT(200)
      COMMON /TIM1/ TME,Q,TIME
C
      DIMENSION HED(18)
C  READ PRELIMINARY INFORMATION
      READ(5,1000) HED
      READ(5,1001) NUMNP,NUMEL,NUMAT,TME,Q
      WRITE(6,2000) HED,NUMNP,NUMEL,NUMAT,TME,Q
C
C  READ IN MATERIAL PROPERTIES FOR
C  ELASTIC AND INELASTIC STRAIN COMPUTATION
C
      WRITE(6,2005)
      DO 10 M=1,NUMAT
      READ(5,1010)  E(M),PR(M),RO(M),ACOF(M),EN(M)
   10 WRITE(6,2010)  M,E(M),PR(M),RO(M),ACOF(M),EN(M)
C
C  INITIALIZE TIME COUNTER
C
      TIME=0.
C
C
C  READ AND WRITE NODAL DATA AND GENERATE INTERMEDIATE NODAL DATA
C
      WRITE(6,2014)
      WRITE(6,2015)
      L=1
      READ(5,1020) N,KODE(N),X(N),Y(N),U(N),V(N)
      GO TO 40
C
   20 READ(5,1020) N,KODE(N),X(N),Y(N),U(N),V(N)
      DN = N-L
      DX =(X(N)-X(L))/DN
      DY =(Y(N)-Y(L))/DN
   25 L=L+1
C
      IF(N-L) 50,40,30
   30 X(L) = X(L-1)+DX
      Y(L) = Y(L-1)+DY
      KODE(L)= 0
      U(L)=0
      V(L)=0
      GO TO 25
C
   40 CONTINUE
C    WRITE(6,2020)N,KODE(N),X(N),Y(N),U(N),V(N)
      IF(NUMNP-N) 50,60,20
C
   50 WRITE (6,2025) N
      CALL EXIT
C
   60 CONTINUE
C     WRITE(6,2016)
C     WRITE(6,2015)
```

```
C      WRITE (6,2020) (N,KODE(N),X(N),Y(N),U(N),V(N),N=1,NUMNP)
C
C  READ AND WRITE ELEMENT DATA
C
C      WRITE(6,2031)
C      WRITE(6,2030)
       ML=0
51     IF (ML.GE.NUMEL)  GO TO 70
       READ(5,1035)  M,NP(1,M),NP(2,M),NP(3,M),MAT(M),TH(M)
C      WRITE (6,2035)M,NP(1,M),NP(2,M),NP(3,M),MAT(M),TH(M)
       MM=ML+1
       IF (MM.EQ.M)  GO TO 65
C
   55  ML1=ML+1
       IF(ML1.EQ.M)  GO TO 65
       ML2=ML+2
       MLM1=ML-1
       IF(MLM1.LE.0) GO TO 85
       DO 62  I=1,3
       NP(I,ML2)=NP(I,ML)+1
   62  NP(I,ML1)=NP(I,MLM1)+1
       MAT(ML2)=MAT(ML)
       MAT(ML1)=MAT(MLM1)
       TH(ML2)=TH(ML)
       TH(ML1)=TH(MLM1)
       ML=ML2
       GO TO 55
C
65     ML=M
       GO TO 51
70     CONTINUE
C      WRITE(6,2032)
C      WRITE(6,2030)
C      WRITE (6,2035) (M,(NP(J,M),J=1,3),MAT(M),TH(M),M=1,NUMEL)
C
C      DETERMINE BAND WIDTH AND NUMBER OF EQUATIONS
C
       L=0
       DO 80 M=1,NUMEL
       DO 80 I=1,2
       II=I+1
       DO 80 J=II,3
       K= IABS(NP(I,M)-NP(J,M))
       IF (K.GT.L)   L=K
80     CONTINUE
C
       MBAND = 2*(L+1)
       NEQ= 2*NUMNP
C
       WRITE(6,2040)MBAND,NEQ
       IF(MBAND.LE. 40.AND.NEQ.LE.200)  GO TO 90
       WRITE(6,2050)
       CALL EXIT
85     WRITE(6,2060)
       CALL EXIT
C
90     WRITE(6,3000)
3000   FORMAT(    '   READIN COMPLETED ' ///)
       RETURN
C
C  FORMAT STATEMENTS
1000   FORMAT(18A4)
1001   FORMAT(3I6,2F10.6)
2000   FORMAT(1H1,10X,18A4,////
      1 1H ,     26H NUMBER OF NODAL POINTS      = ,I6/
      2 1H ,     26H NUMBER OF ELEMENTS          = ,I6/
      3 1H ,     26H NUMBER OF MATERIALS         = ,I6/
      4 1H ,     26H TIME INTERVAL               = ,F6.1/
      5 1H ,     26H TOTAL LENGTH OF RUN         = , F6.1)
2005   FORMAT(///,1H ,23X, 20H MATERIAL PROPERTIES //
      15X, 7HMAT NO.,2X, 9HMODULUS E,2X,12HPOISS. RATIO,2X,
      28HUNIT WT.,3X,7HA.COEFF.,2X,' 5HPOWER,//)
1010   FORMAT(E11.4,2F10.6,E11.4,F10.6)
2010   FORMAT(1H ,1X,I5,E11.4,F15.3,F9.2,E11.4,F8.2)
2014   FORMAT( '1',  5X, 'OUTPUT OF INPUT NODAL DATA ')
2015   FORMAT(///,10X,19H NODAL POINT OUTPUT.///
      11H ,59H NODE  KODE    X COORD      Y COORD      X FORCE
      2      Y FORCE//)
2016   FORMAT('1',  5X,  'OUTPUT OF COMPLETE NODAL DATA  ')
1020   FORMAT(2I6,4F12.0)
2020   FORMAT(I4,I6,F13.3,3F12.3)
2025   FORMAT(1HO,28H ERROR IN NODAL DATA,NODE = ,I4)
2030   FORMAT(///,10X, 13H ELEMENT DATA ///,
      1 40H ELEM    I     J     K    MAT  THICKNESS //)
2031   FORMAT('1',5X, 'OUTPUT OF INPUT ELEMENT DATA' )
2032   FORMAT( '1', 5X, 'OUTPUT OF COMPLETE ELEMENT DATA  ' )
1035   FORMAT (5I6,F6.0)
2035   FORMAT ( I4, 4I6,F11.4)
2040   FORMAT (///10X, 22H BAND WIDTH                = ,I6/
     '1           10X, 22H NUMBER OF EQUATIONS = ,I6)
2050   FORMAT(///10X, 33H PROBLEM EXCEEDS SPECIFIED LIMITS )
2060   FORMAT(   'MLM1 IS LESS THAN OR EQUAL TO ZERO ')
C
       END
C
       SUBROUTINE ASTIF
C
C      THIS SUBROUTINE TAKES EACH ELEMENT IN TURN AND
C      FORMS THE ELEMENT STIFFNESS MATRIX (BY CALLING
C       ELSTIF). IT ASSEMBLES THE ELEMENT STIFFNESSES
```

```
C      INTO *KSTIF.  THEN ADDS THIS INTO THE TOTAL
C      STIFFNESS TSITF.  ASSEMBLES THE APPLIED LOAD
C      VECTOR (AP) AND FICTIOUS LOAD VECTOR(FICLD).
C      MODIFIES THE  ASSEMBLAGES FOR DISPLACEMENT
C      BOUNDARY CONDITIONS (BY CALLING MODIFY)>
C
       COMMON E(8),PR(8),RO(8),X(200),Y(200),U(200),V(200),
      1, STIF(40,400),AP(400),TSTIF(40,400),ECM(3,3),
      1TH(200),EBM(3,6),ESM(3,6),WT,MBAND
       COMMON NUMNP,NUMEL,NUMAT,KODE(200),NP(3,200),
      1 NEQ,ACOF(8),EN(8),M,LM(6),TAP(400),TRMT(3,200),
       COMMON SRMT(3,200),FICLD(200,6),APFL(200),ESTIF(6,6)
      1SIGP(200,4),SIGEL(200,3),TSTR(200,3),MAT(200)
       COMMON /TIM1/ TME,Q,TIME
C
C   INITIALIZE APPLIED LOAD VECTOR AND MASTER STIFFNESS
C   MATRIX AND ECM
C
       DO 10 I=1,NEQ
       AP(I)=0.0
       DO 10 J=1,MBAND
       IF(TIME.GT.0.0) GO TO 11
       TAP(I)=0.0
       TSTIF(J,I)=0.0
11      STIF(J,I)=0.0
       IF(TIME.LT.0.0002) GO TO 10
       STIF(J,I)=STIF(J,I) + TSTIF(J,I)
10     CONTINUE
       DO 20 I=1,3
       DO 20 J=1,3
20     ECM(I,J)=0.0
C
C   FORM ELEMENT CONSTITUTIVE MATRIX (ECM) IF NUMAT=1)
C
       IF(NUMAT.NE.1) GO TO 30
       EPR=PR(1)
       COM=E(1)/((1.+EPR)*(1.-2.*EPR))
       COM1=COM*(1.-EPR)
       COM2=COM*EPR
       ECM(1,1)=COM1
       ECM(2,2)=COM1
       ECM(1,2)=COM2
       ECM(2,1)=COM2
       ECM(3,3)=E(1)/(2.*(1.+EPR))
C
30     DO 45 M=1,NUMEL
C
       CALL ELSTIF(1)
C
C   ASSEMBLE ELSTIF INTO MASTER STIFFNESS MATRIX
C
       IF(TIME.GT.0.0) GO TO 91
       DO 35 I=1,3
       I2=2*I
       LM(I2)=2*NP(I,M)
35     LM(I2-1)=LM(I2)-1
C
       DO 40 I=1,6
       II=LM(I)
       DO 40 J=1,6
       JJ=LM(J)-II+1
       IF (JJ.LE.0) GO TO 40
       STIF(JJ,II)= STIF(JJ,II)+ESTIF(J,I)
       TSTIF(JJ,II)=TSTIF(JJ,II)+ESTIF(J,I)
40     CONTINUE
C
C   ADD GRAVITY LOADS INTO AP VECTOR
C
91     IF(TIME.GT.0.0) GO TO 999
       DO 31 I=2,6,2
       II=LM(I)
       AP(II)=AP(II)-WT
31     CONTINUE
C
C
C FORMS ELEMENT FICTIOUS LOAD MATRIX
C
C  (II) ADDS VERTICAL LOADS
C  (IJ) ADDS HORIZONTAL LOADS
C
999    IF(TIME.EQ.0.) GO TO 45
       DO 44 I=1,3
       I2=2*I
       LM(I2)=2*NP(I,M)
       LM(I2-1)=LM(I2)-1
       II=LM(I2)
       IJ=LM(I2-1)
       APFL(IJ)=0.
       APFL(II)=0.
       APFL(II)=APFL(II)+FICLD(M,I2)
       APFL(IJ)=APFL(IJ)+FICLD(M,I2-1)
C
C
C ADD FICTIOUS LOADS TO AP MATRIX
C
       AP(II)=AP(II)+APFL(II)
       AP(IJ)=AP(IJ)+APFL(IJ)
C
44     CONTINUE
45     CONTINUE
```

```
C
C   ADD NODAL LOADS INTO AP VECTOR
C
      TFLDH=0.0
      TFLDV=0.0
      TOFV=0.0
      TOFH=0.0
      DO 50 N=1,NUMNP
      N2=2*N
      IF(TIME.EQ.0.0) GO TO 99
      TFLDH=TFLDH+AP(N2-1)
      TFLDV=TFLDV+AP(N2)
      U(N)=0.0
      V(N)=0.0
      U(N)=U(N)+TAP(N2-1)
      V(N)=V(N)+TAP(N2)
99    AP(N2)=AP(N2)+V(N)
      AP(N2-1)=AP(N2-1)+U(N)
      TAP(N2-1)=0.0
      TAP(N2)=0.0
      TAP(N2)=TAP(N2)+AP(N2)
      TAP(N2-1)=TAP(N2-1)+AP(N2-1)
      TOFV=TOFV+AP(N2)
      TOFH=TOFH+AP(N2-1)
50    CONTINUE
C
C FORCE (AP) INCLUDES ALL COMPONENTS;NOT MODIFIED
C
      WRITE(7,1118)
      DO 902 II=1,NUMNP
      I2=II*2
      I2M=I2-1
      V(II)=0.0
      U(II)=0.0
902   CONTINUE
96    WRITE(6,1921) TOFH,TOFV,TFLDH,TFLDV
C
C   MODIFY STIFFNESS AND LOAD VECTOR FOR
C   DISPLACEMENT BOUNDARY CONDITIONS.
C
      DO 100 N=1,NUMNP
      N2=2*N
      IF (KODE(N)-10) 80,70,60
60    II=N2-1
      CALL MODIFY(II,N)
      CALL MODIFY(N2,N)
      GO TO 100
70    II=N2-1
      CALL MODIFY(II,N)
      GO TO 100
80    IF(KODE(N).EQ.0)  GO TO 100
      CALL MODIFY(N2,N)
100   CONTINUE
C
919   RETURN
1921  FORMAT(' ','SUM HORT. FOR.=',E15.8,5X,
     1'SUM VET. FOR=',E15.8,
     215X,'FIC H LOAD',E15.8,'FIC V LOAD',E15.8)
1117  FORMAT(' ',2X,I6,F10.2,2X,I6,4X,F10.2,3X,F10.2,3X,5F10.2)
1118  FORMAT(1H1,10X,'FORCES AT THE NODES',///,
     1'NO.',10X,'FORCE R',5X,'NO.',10X,'FORCE Z',
     2'AP(II)=',E13.6,3X,'FL(II)=',E13.6)
1116  FORMAT(/,10X,'ELEM=',I4,5X,'IJ=',I4,5X,'II=',I4,/,
     15X,'AP(IJ)=',E13.6,3X,'FL(IJ)=',E13.6,3X,
     2'AP(II)=',E13.6,3X,'FL(II)=',E13.6)
      END
C
      SUBROUTINE MODIFY (I,N)
C
C  THIS SUBROUTINE MODIFIES KSTIF AND AP IF A
C  DISPLACEMENT BOUNDARY CONDITION IS IMPOSED
C  IN EQUATION I ASSOCIATED WITH NODAL POINT N
C
      COMMON E(8),PR(8),RO(8),X(200),Y(200),U(200),V(200),
     1  STIF(40,400),AP(400),TSTIF(40,400),ECM(3,3),
     1TH(200),EBM(3,6),ESM(3,6),WT,MBAND
      COMMON NUMNP,NUMEL,NUMAT,KODE(200),NP(3,200),
     1 NEQ,ACOF(8),EN(8),M,LM(6),TAP(400),TRMT(3,200),
      COMMON SRMT(3,200),FICLD(200,6),APFL(200),ESTIF(6,6),
     1SIGP(200,4),SIGEL(200,3),TSTR(200,3),MAT(200)
      COMMON /TIM1/ TME,Q,TIME
C
      DISP=U(N)
      IF((I-2*N).EQ.0)  DISP=V(N)
C
      DO 50 J=2,MBAND
      IL=I+J-1
      IU=I-J+1
      IF(IU.LE.0)GO TO 10
      AP(IU)=AP(IU) - STIF(J,IU)*DISP
       STIF(J,IU)=0.0
10    IF(IL.GT.NEQ) GO TO 50
      AP(IL)= AP(IL)-STIF(J,I)*DISP
       STIF(J,I)=0.0
50    CONTINUE
      AP(I)=DISP
       STIF(1,I)=1.0
      RETURN
      END
```

```
      SUBROUTINE BAND1
C
C  THIS SUBROUTINE SOLVES FOR DISPLACEMENTS USING A
C  GAUSSIAN ELIMINATION  TECHNIQUE FOR SYMMETRIC
C  BANDED MATRICES STORED IN CORE
C
      COMMON E(8),PR(8),RO(8),X(200),Y(200),U(200),V(200),
     1 STIF(40,400),AP(400),TSTIF(40,400),ECM(3,3),
     1TH(200),EBM(3,6),ESM(3,6),WT,MBAND
      COMMON NUMNP,NUMEL,NUMAT,KODE(200),NP(3,200),
     1 NEQ,ACOF(8),EN(8),M,LM(6),TAP(400),TRMT(3,200),
      COMMON SRMT(3,200),FICLD(200,6),APFL(200),ESTIF(6,6),
     1SIGP(200,4),SIGEL(200,3),TSTR(200,3),MAT(200)
      COMMON /TIM1/ TME,Q,TIME
C
C TRIANGULARIZE AND REDUCE RIGHT HAND SIDE
      NL=NN-MM+1
      NM=NN-1
      MR=MM
C
      DO 100 N=1,NM
      IF (A(1,N).LE.0.) GO TO 700
      BN=B(N)
      B(N)=BN/A(1,N)
      IF (N.GT.NL) MR=NN-N+1
C
      DO 100 L=2,MR
      IF (A(L,N).EQ.0.)GO TO 100
      C= A(L,N)/A(1,N)
      I= N+L-1
      J= 0
      DO 50 K=L,MR
      J=J+1
50    A(J,I)= A(J,I)-C*A(K,N)
      B(I)=B(I)-C*BN
      A(L,N)=C
100   CONTINUE
C
C   BACK SUBSTITUTE
C
      I=NN
C
      B(NN)=B(NN)/A(1,NN)
      DO 600 N=1,NM
      I=I-1
      IF (N.LT.MM)      MR= N+1
      DO 600 J=2,MR
      K=I+J-1
600   B(I) =B(I)- A(J,I)*B(K)
      WRITE(6,2001)
      DO 901 II=1,NUMNP
      I2=2*II
      I2M=I2-1
      WRITE(6,1799) II,B(I2M),II,B(I2),X(II),Y(II)
901   CONTINUE
      RETURN
700   WRITE (6,1999) N
      STOP
1999  FORMAT(1HO, 81H ZERO OR NEGATIVE ELEMENT ON  MAIN DIAGONAL
     1 OF TRIANGULARIZED MATRIX FOR EQUATION  ,I5)
C
 2001 FORMAT('1',  ' NODAL DISPLACEMENTS '//'   NO.',11X,
     1'U',6X,'NO.',11X,'V',11X,'X(I)',11X'Y(I)' // )
1799  FORMAT(' ',I6,E15.5,I6,E15.5,5X,F7.2,8X,F7.2)
      END
      SUBROUTINE ELSTIF(KOP)
C
C  THIS SUBROUTINE FORMS THE ELEMENT STIFFNESS MATRIX (ESTIF) OR
C  ELEMENT STRESS MATRIX (ESM) FOR THE CONSTANT STRAIN TRIANGLE
C  THE FICTIOUS LOAD MATRIX IS FORMED USING THE INELASTIC STRAIN
C
      COMMON E(8),PR(8),RO(8),X(200),Y(200),U(200),V(200),
     1  STIF(40,400),AP(400),TSTIF(40,400),ECM(3,3),
     1TH(200),EBM(3,6),ESM(3,6),WT,MBAND
      COMMON NUMNP,NUMEL,NUMAT,KODE(200),NP(3,200),
     1 NEQ,ACOF(8),EN(8),M,LM(6),TAP(400),TRMT(3,200),
      COMMON SRMT(3,200),FICLD(200,6),APFL(200),ESTIF(6,6),
     1SIGP(200,4),SIGEL(200,3),TSTR(200,3),MAT(200)
      COMMON /TIM1/ TME,Q,TIME
C
      DIMENSION STR(3),AV(3),BV(3)
C
      DO 10 I=1,3
      DO 10 J=1,6
10    EBM(I,J)=0.0
      I=NP(1,M)
      J=NP(2,M)
      K=NP(3,M)
C
C   FORM ELEMENT DIMENSIONS
C
      AV(1)=X(K)-X(J)
      AV(2)=X(I)-X(K)
      AV(3)=X(J)-X(I)
      BV(1)=Y(J)-Y(K)
      BV(2)=Y(K)-Y(I)
      BV(3)=Y(I)-Y(J)
```

```
      AREA2=(AV(3)*BV(2))-(AV(2)*BV(3))
C
21    IF (TH(M).LE.0.001) TH(M)=1.
      VOL=TH(M)*AREA2/2.
      IF (VOL.LE.0.0001) GO TO 75
C
C  FORM CONSTITUTIVE MATRIX
C
      IF (NUMAT.EQ.1) GO TO 30
      NM=MAT(M)
      EPR=PR(NM)
      COM=E(NM)/((1.+EPR)*(1.-2.*EPR))
      COM1=COM*(1.-EPR)
      COM2=COM*EPR
      ECM(1,1)=COM1
      ECM(2,2)=COM1
      ECM(1,2)=COM2
      ECM(2,1)=COM2
      ECM(3,3)=E(NM)/(2.*(1.+EPR))
C
30    IF(KOP.EQ.2) GO TO 22
C
C   FORM ELEMENT B MATRIX (EBM)
C
22    DO 40 I=1,3
      I2=2*I
      I2M=2*I-1
      EBM(1,I2M)=BV(I)/AREA2
      EBM(2,I2)=AV(I)/AREA2
      EBM(3,I2M)=EBM(2,I2)
40    EBM(3,I2)=EBM(1,I2M)
C
C.  FORM ELEMENT STRESS MATRIX (ESM)
C
      DO 50 I=1,3
      DO 50 J=1,6
      ESM(I,J)=0.0
      DO 50 K=1,3
50  ESM(I,J)=ESM(I,J)+ECM(I,K)*EBM(K,J)
C
      IF(KOP.EQ.2) GO TO 80
C
      IF(NUMAT.EQ.1)  NM=1
      WT=VOL*RO(NM)/3.
C
C     FORM ELEMENT STIFFNESS MATRIX (ESTIF)
C
      DO 70 I=1,6
      DO 70 J=1,6
      ESTIF(I,J)=0.0
      DO 60 K=1,3
60    ESTIF(I,J)=ESTIF(I,J)+EBM(K,I)*ESM(K,J)
70    ESTIF(I,J)=ESTIF(I,J)*VOL
C
      IF(TIME.EQ.0.) GO TO 80
C
C FORM FICTIOUS LOAD MATRIC (FICLD)
C
      DO 45 J=1,6
      DO 90 I=1,3
      STR(I)=0.
      FICLD(M,J)=0.
      DO 49 K=1,3
      STR(I)=STR(I)+ECM(I,K)*SRMT(K,M)
49    CONTINUE
90    CONTINUE
      DO 44 K=1,3
      FICLD(M,J)=FICLD(M,J)+EBM(K,J)*STR(K)
44    CONTINUE
      FICLD(M,J)=FICLD(M,J)*VOL
45    CONTINUE
      GO TO 80
75    WRITE(6,1000) M
      CALL EXIT
80    RETURN
C
1000  FORMAT (1H1, 18H VOLUME OF ELEMENT ,I4, 18H IS
     1 LESS THAN ZERO)
C
     7'B(3,5)=',E13.6,'B(3,6)=',E13.6)
1115  FORMAT(/,20X,'ELEM=',I3,/,10X,'STR(1)=',E13.6,5X,'STR(2)=',
     1E13.6,5X,'STR(3)=',E13.6)
1114  FORMAT(//,20X,'ELEM=',I3,/,5X,'F(M,1)=',E13.6,3X,
      END
C
      SUBROUTINE STRESS
C
C   THIS SUBROUTINE FORMS THE ELEMENT STRESS MATRIX (ESM),
C   MULITIPLIES BY  THE ELEMENT DISPLACEMENT VECTOR (ELDISP)
C   SUBTRACTS THE ACCUMULATED STRAIN
C    AND RECORDS THE STRESSES IN SIGEL
C
      COMMON E(8),PR(8),RO(8),X(200),Y(200),U(200),V(200),
     1  STIF(40,400),AP(400),TSTIF(40,400),ECM(3,3),
     1TH(200),EBM(3,6),ESM(3,6),WT,MBAND
      COMMON NUMNP,NUMEL,NUMAT,KODE(200),NP(3,200),
     1 NEQ,ACOF(8),EN(8),M,LM(6),TAP(400),TRMT(3,200),
      COMMON SRMT(3,200),FICLD(200,6),APFL(200),ESTIF(6,6),
     1SIGP(200,4),SIGEL(200,3),TSTR(200,3),MAT(200)
      COMMON /TIM1/ TME,Q,TIME
      DIMENSION STRN(3),SIG(200,3),KOUNT(200),ELDISP(6),
     1SIGA(200,3),CX(200),CY(200)
C
```

```
      DO 100 M=1,NUMEL
C
C   COMPUTE ELEMENT DISPLACEMENTS
C
      I=NP(1,M)
      J=NP(2,M)
      K=NP(3,M)
      CX(M)=(X(I)+X(J)+X(K))/3.
      CY(M)=(Y(I)+Y(J)+Y(K))/3.
      DO 10 I=1,3
      I2=2*I
      LMI2  =2*NP(I,M)
      ELDISP(I2)=AP(LMI2)
10    ELDISP(I2-1)=AP(LMI2-1)
C  COMPUTE  ELEMENT STRESSES
C
      CALL ELSTIF(2)
C
      DO 29 I=1,3
      TSTR(M,I)=0.0
      STRN(I)=0.0
      DO 39 J=1,6
      STRN(I)=STRN(I)+EBM(I,J)*ELDISP(J)
39    CONTINUE
      TSTR(M,I)=TSTR(M,I)+STRN(I)
29    CONTINUE
C     IF(M.GT.10) GO TO 111
C     WRITE(6,1111) TSTR(M,1),TSTR(M,2),TSTR(M,3)
111   DO 89 I=1,3
      IF(TIME.GT.0.0) GO TO 89
      SRMT(I,M)=0.0
      TRMT(I,M)=0.0
89    TRMT(I,M)=TRMT(I,M)+SRMT(I,M)
15    CONTINUE
C CALCULATES THE STRESS
      DO 21 I=1,3
       SIGEL(M,I)=0.0
      DO 20 J=1,3
      TOP=(TSTR(M,J)-TRMT(J,M))
      SIGEL(M,I)=SIGEL(M,I)+ECM(I,J)*TOP
20    CONTINUE
21    CONTINUE
C
C  ACCUMULATE FOR NODAL STRESSES
C
      DO 30 K=1,3
      N=NP(K,M)
      KOUNT(N)=KOUNT(N)+1
      DO 30 I=1,3
30    SIGA(N,I)=SIGA(N,I) + SIGEL(M,I)
C
C  COMPUTE ELEMENT PRINCIPAL STRESSES  AND DIRECTIONS
C
      SIGM=(SIGEL(M,1)+SIGEL(M,2))/2.
      SIGD2=(SIGEL(M,1)-SIGEL(M,2))/2.
      RAD =SQRT(SIGD2**2 +SIGEL(M,3)**2)
      SIGP(M,1)=SIGM+RAD
      SIGP(M,2)= SIGM-RAD
      SIGP(M,3)= RAD
      SIGP(M,4)= 0.5*57.29578*ATAN2(SIGEL(M,3),SIGD2)
100   CONTINUE
C
C  FIND AVERAGE NODAL STRESSES
C
      DO 110 N=1,NUMNP
      RK=KOUNT(N)
      DO 110 I=1,3
110   SIGA(N,I)= SIGA(N,I)/RK
C
C   FIND  MAXIMUM  ELEMENT STRESSES
C
      SIG1=0.0
      SIG2=0.0
      SIG3=0.0
      M1=0
      M2=0
      M3=0
      DO 130 M=1,NUMEL
      IF (SIGP(M,1).LT.SIG1) GO TO 115
      SIG1=SIGP(M,1)
      M1=M
115   IF (SIGP(M,2).GT.SIG2) GO TO 120
      SIG2=SIGP(M,2)
      M2=M
120   IF (SIGP(M,3).LT.SIG3) GO TO 130
      SIG3=SIGP(M,3)
      M3=M
130   CONTINUE
      WRITE(6,2000)
      WRITE(6,2010) (M,(SIGEL(M,I) ,I=1,3),CX(M),CY(M),M=1,NUMEL)
C     WRITE(6,2020)
C     WRITE(6,2030) (M,(SIGP(M,I) ,I=1,4),M=1,NUMEL)
C     WRITE(6,2040) SIG1,M1,SIG2,M2,SIG3,M3
C     WRITE(6,2050)
C     WRITE(6,2010)  (N,(SIGA(N,I),I=1,3),X(N),Y(N),N=1,NUMNP)
      RETURN
2000  FORMAT(1H1,10X, 21H X-Y ELEMENT STRESSES ///,40H ELEM
     1   SIGMA X
     1  SIGMA Y      SIGMA XY //)
2010  FORMAT(I4,1X,E12.5,1X,E12.5,1X,E12.5,5X,'X=',F10.3,5X,
```

```
      *'Y=',F10.3)
 2020  FORMAT(1H1,10X,27H ELEMENT PRINCIPAL STRESSES ///
     1 55H ELEM    SIGMA I      SIGMA II     MAX TAU
     1    SIGMA I DEG //)
 2030  FORMAT(I4,F11.1,2F12.1, F14.8)
 2040  FORMAT(' ',
     1 27H MAXIMUM PRINCIPAL STRESS = ,F11.1,19H
     1 AND OCCURS IN ELEM,I6//
     2 27H MINIMUM PRINCIPAL STRESS = ,F11.1,19H
     2  AND OCCURS IN ELEM, I6//
     3 27H MAXIMUM SHEAR  STRESS    = ,F11.1,19H
     3 AND OCCURS IN ELEM,I6)
 2050  FORMAT(1H1, ' AVERAGE NODAL STRESSES '///
     1           ' NODE    SIGMA X      SIGMA Y      SIGMA XY '//)
      END
C
      SUBROUTINE NOELAS
C
C THIS SUBROUTINE COMPUTES THE INELASTIC STRAIN MATRIX (SRM)
C USING THE FLOW LAW FOR ICE  AS OUTLINED BY THOMPSON (1969)
      COMMON E(8),PR(8),RO(8),X(200),Y(200),U(200),V(200),
     1  STIF(40,400),AP(400),TSTIF(40,400),ECM(3,3),
     1TH(200),EBM(8,6),ESM(3,6),WT,MBAND
      COMMON NUMNP,NUMEL,NUMAT,KODE(200),NP(3,200),
     1 NEQ,ACOF(8),EN(8),M,LM(6),TAP(400),TRMT(3,200),
      COMMON SRMT(3,200),FICLD(200,6),APFL(200),ESTIF(6,6),
     1SIGP(200,4),SIGEL(200,3),TSTR(200,3),MAT(200)
      COMMON /TIM1/ TME,Q,TIME
C
      DIMENSION ELDISP(6)
      NM=1
      A=ACOF(NM)
      TN=EN(NM)
C
C  WRITE PRINCIPAL STRESS
      WRITE(6,928)
      DO 1000 M=1,NUMEL
      ESTRNR=0.0
      ESTRN=0.0
      ESTRES=0.0
      SMEAN=0.0
      STR=0.0
      OCSTR=0.0
      OCSRA=0.0
      SIPT=0.0
      SIPP=0.0
      SIPQ=0.0
      DO 10 I=1,3
 10   CONTINUE
      SMEAN=SMEAN+(SIGP(M,1)+SIGP(M,2))/2.
      SIPP=SIPP+(SIGP(M,1)-SIGP(M,2))/2.
      SIPT=SIPT+(SIGP(M,2)-SIGP(M,
      SIPQ=SIPQ+SQRT((
C
C  COMPUTES OCTAHEDRAL STRESS
C
      OCSTR=OCSTR+SIPQ/3.
C
      ESTRES=ESTRES +OCSTR*(3./(SQRT(2.)))
C
C COMPUTES OCTAHEDRAL STRAIN RATE USING FLOW LAW
C
      ESTRNR=ESTRNR+A*(ESTRES**TN)
C
C COMPUTES OCTAHEDRAL STRAIN FOR TIME INCREMENT
C
      ESTRN=ESTRN+ESTRNR*TME
C
C CAL. PRINCIPAL STRAIN ANGLE
C
      AN=0.
      AN=AN+2.*(SIGP(M,4)/57.29578)
      IF(AN.EQ.90.) GO TO 11
      UN=0.
      ANGLE=0.0
      ANGLE=ANGLE+ABS(SIN(AN)/COS(AN))**2.
      UN=UN+(2./3.)*SQRT(3.*(1.+ANGLE))
      DO 1010 I=1,3
      SRMT(I,M)=0.
1010  CONTINUE
      SRMT(1,M)=SRMT(1,M)+ESTRN/UN.
      IF(SIGEL(M,1)-SIGEL(M,2)) 16,11,13
 16   SRMT(2,M)=SRMT(2,M)+SRMT(1,M)
      SRMT(1,M)=-SRMT(1,M)
      GO TO 28
 13   SRMT(2,M)=SRMT(2,M)-SRMT(1,M)
      GO TO 28
C     IF(SIGEL(M,1).GT.0.0) GO TO 13
C     SRMT(1,M)=-SRMT(1,M)
C13    SRMT(2,M)=SRMT(2,M)-SRMT(1,M)
 28   UNN=0.0
      UNN=UNN+(SIN(AN)/COS(AN))
      SRMT(3,M)=SRMT(3,M)+2.*ABS(SRMT(1,M)*UNN)
      IF(SIGEL(M,3).GT.0.0) GO TO 12
      SRMT(3,M)=-SRMT(3,M)
      GO TO 12
 11   SRMT(1,M)=0.0
      SRMT(2,M)=0.0
      SRMT(3,M)=0.
C
```

```
C FORMS THE INELASTIC MATRIC FOR THE STRUCTURE (SRM)
C
 12    CONTINUE
        WRITE(6,398) M,(SRMT(I,M),I=1,3),SMEAN,ESTRES,AN
C***    1
  1000 CONTINUE
       RETURN
C
 1191  FORMAT(1H1,15X,'NODAL COORDINATES',//,
      15X,'NODE',10X,'X-COORD.',10X,'Y-COORD.',//,
      2(5X,I4,10X,E13.6,5X,E13.6))
 2020  FORMAT(1H1,25X,' ELEMENT PRINCIPAL STRESSES ',///,
      11X,'ELEM',6X,'SIGMA I',7X,'SIGMA II',8X,'MAX TAU',
      24X,'SIGMA I DEG',//)
 1121  FORMAT(1H1,10X,'INFO. FROM NONELAS')
 928   FORMAT(1H1,10X,'ELEM',6X,'SRMT(1,M)',8X,'SMRT(2,M)',
      28X,'SRMT(3,M)',8X,'SNOCT',8X,'SHOCT')
 398   FORMAT(' ',10X,I4,6X,E11.4,5X,E11.4,5X,E11.4,5X,E11.4,
      15X,E11.4,5X,'AN=',E11.4)
       END
END OF
```

AXI-SYMMERTRIC CREEP PROGRAM

Directory of variable names:

I. Material properties input

e(m)	Young's Modulus
pr(m)	Poisson' Ratio
ro(m)	Unit Weight
Acof(m)	Parameter of flow law
En(m)	Exponent of flow law

II. Nodal data input

Kode(n)	Boundary code
x(n)	x coordinate of node
y(n)	y coordinate of node
u(n)	x displacement or load at node
v(n)	y displacement or load at node

III. Element data input

m	Element number
np(i,m)	Nodal point at the three corners of of the element in counterclockwise order.
mat(m)	Element material number
th(m)	Thickness of element

IV. Variables used in Main

time	Total accumulated time
tme	Increment of time
q	Time terminator

V. Varaibles used in ASTIF subroutine

ap(n)	Applied load vector
tap(n)	Total load vector which is incremented each time
stif(mband,neq)	Structure stiffness matrix
neq	Number of equations
mband	Band width of problem calculated in READIN
tstif(mband,neq)	Total structure stiffness matrix which is saved
ficld(m,6)	Fictitous load matrix calulated in ELSTIF
tfldv	Accumulated load in vertical
tfldh	Accumulated load in horizontal

VI. Varibles used in ELSTIF subroutine

ecm(3,3)	Element constitutive matrix
ebm(3,6)	Element B matrix
esm(3,6)	Element stress matrix
estif(6,6)	Element stiffness matrix
srmt(3,m)	Inelastic strain matrix calculated in NOELAS

VII. Varibles used in STRESS subroutine

eldisp(n)	Nodal displacement vector calculated in BANDI
tstr(m,3)	Accumulated total strain
trmt(m,3)	Accumulated total strain of previous increment
sigel(m,3)	Element stresses
sigp(m,4)	Element principal stress
siga(m,3)	Average element stress

VIII. Varibles used in NOELAS subroutine

estres	Effective shear stress
estrnr	Effective shear strain rate
estrn	Effective shear strain increment
srmt(3,m)	Inelastic strain matrix

```
C   THIS SOLVES ELASTIC AND INELASTIC  AXISYMMETRIC
C   BOUNDARY VALUE PROBLEMS
C
      COMMON E(8),PR(8),RO(8),R(300),Z(300),UR(300),UZ(300),
     1  STIF(60,400),AP(600),ESTIF(6,6),ECM(4,4),EBM(4,6),
     2TAP(600),ESM(4,6),TSTIF(60,400),APFL(600),MBAND,WT
      COMMON NUMNP,NUMEL,NUMAT,KODE(300),NP(3,300),MAT(300),
     1 NEQ,ACOF(8),EN(8),M,LM(6),YM(300),TSTR(300,4),
      COMMON STR(4),SIGEL(300,4),SRMT(4,300),FICLD(300,6)
      COMMON /TIMI/ TIME,Q,TME,TRMT(4,300)
C
      NIT=0
C
      CALL READIN
C
2     CALL ASTIF
C
      CALL BAND1
C
      CALL STRESS
CCCCCCCCCCCCCCC
      WRITE(6,1101) TIME,Q,TME
1101  FORMAT(/,20X,' TIME= ',E10.3,3X,'TOTAL TIME=',E10.3,3X,
     *'TME=',E10.3,3X,'TIME INCREMENT=',I5)
      IF(TIME.GE.Q) GO TO 3
      TIME=TIME  + TME
C
      CALL NOELAS
      NIT=NIT+1
      WRITE(8,1101) TIME, Q, TME,NIT
      GO TO 2
CCCCCCCCCCCCCCC
C
3     STOP
      END
C
      SUBROUTINE READIN
C
C  THIS SUBROUTINE READS AND PRINTS MATERIAL DATA,
C  NODAL DATA, ELEMENT DATA.
C  IT GENERATES COORDINATES OF INTERMEDIATE NODAL
C   POINTS AND CALCULATES THE BAND WIDTH AND
C  NUMBER OF EQUATIONS
C
      COMMON E(8),PR(8),RO(8),R(300),Z(300),UR(300),UZ(300),
     1  STIF(60,400),AP(600),ESTIF(6,6),ECM(4,4),EBM(4,6),
     2TAP(600),ESM(4,6),TSTIF(60,400),APFL(600),MBAND,WT
      COMMON NUMNP,NUMEL,NUMAT,KODE(300),NP(3,300),MAT(300),
     1 NEQ,ACOF(8),EN(8),M,LM(6),YM(300),TSTR(300,4),
      COMMON STR(4),SIGEL(300,4),SRMT(4,300),FICLD(300,6)
      COMMON /TIMI/ TIME,Q,TME,TRMT(4,300)
C
      DIMENSION HED(18)
C  READ PRELIMINARY INFORMATION
      READ(5,1000) HED
      READ(5,1001) NUMNP,NUMEL,NUMAT,TME,Q
      WRITE(6,2000) HED,NUMNP,NUMEL,NUMAT,TME,Q
C
C  READ AND WRITE MATERIAL PROPERTIES
C
CCCCCCCCCCCCC
C     READ IN MATERIAL PROPERTIES
C      FOR INELASTIC AND ELASTIC COMPUTATIONS
      WRITE(6,2005)
      DO 10 M=1,NUMAT
      READ(5,1010)  E(M),PR(M),RO(M),ACOF(M),EN(M)
10    WRITE(6,2010)  M,E(M),PR(M),RO(M),ACOF(M),EN(M)
C
      TIME=0.0
C
CCCCCCCCCCCCC
C  READ AND WRITE NODAL DATA AND GENERATE INTERMEDIATE NODAL DATA
C
C     WRITE(6,2014)
C     WRITE(6,2015)
      L=1
      READ(5,1020) N,KODE(N),R(N),Z(N),UR(N),UZ(N)
      GO TO 40
C
20    READ(5,1020) N,KODE(N),R(N),Z(N),UR(N),UZ(N)
      DN = N-L
      DR =(R(N)-R(L))/DN
      DZ =(Z(N)-Z(L))/DN
25    L=L+1
C
      IF(N-L) 50,40,30
30    R(L) = R(L-1)+DR
      Z(L) = Z(L-1)+DZ
      KODE(L)= 0
      UR(L)=0
      UZ(L)=0
      GO TO 25
C
 40   CONTINUE
      IF(NUMNP-N) 50,60,20
C
50    WRITE (6,2025) N
      CALL EXIT
C
60    CONTINUE
```

```
C
C  READ AND WRITE ELEMENT DATA
C
      ML=0
51    IF (ML.GE.NUMEL)  GO TO 70
      READ(5,1035)  M,NP(1,M),NP(2,M),NP(3,M),MAT(M)
      MM=ML+1
      IF (MM.EQ.M)  GO TO 65
C
55    ML1=ML+1
      IF(ML1.EQ.M)  GO TO 65
      ML2=ML+2
      MLM1=ML-1
      IF(MLM1.LE.0) GO TO 85
      DO 62  I=1,3
      NP(I,ML2)=NP(I,ML)+1
62    NP(I,ML1)=NP(I,MLM1)+1
      MAT(ML2)=MAT(ML)
      MAT(ML1)=MAT(MLM1)
      ML=ML2
      GO TO 55
C
65    ML=M
      GO TO 51
70    CONTINUE
C
C     DETERMINE BAND WIDTH AND NUMBER OF EQUATIONS
C
      L=0
      DO 80 M=1,NUMEL
      DO 80 I=1,2
      II=I+1
      DO 80 J=II,3
      K= IABS(NP(I,M)-NP(J,M))
      IF (K.GT.L)   L=K
80    CONTINUE
C
      MBAND = 2*(L+1)
      NEQ= 2*NUMNP
C
      WRITE(6,2040)MBAND,NEQ
       IF(MBAND.LE. 60.AND.NEQ.LE.400)  GO TO 90
      WRITE(6,2050)
      CALL EXIT
85    WRITE(6,2060)
      CALL EXIT
C
90    WRITE(6,3000)
3000  FORMAT(   '  READIN COMPLETED ' ///)
      RETURN
C
C  FORMAT STATEMENTS
1000  FORMAT(18A4)
1001  FORMAT(3I6,2F12.8)
2000  FORMAT(1H1,10X,18A4,////
     1 1H ,     26H NUMBER OF NODAL POINTS = ,I6/
     2 1H ,     26H NUMBER OF ELEMENTS     = ,I6/
     3 1H ,     26H NUMBER OF MATERIALS    = ,I6/
     4 1H ,     26H TIME INTERVAL          = ,F12.8/
     5 1H ,     26H TOTAL LENGTH OF RUN    = ,F12.8)
2005  FORMAT(///,1H ,23X, 20H MATERIAL PROPERTIES //
     15X, 7HMAT NO.,2X, 9HMODULUS E,2X,12HPOISS. RATIO,
     22X,8HUNIT WT.,3X, 7HA.COEF.,2X, 5HPOWER,//)
1010  FORMAT(F13.2,2F15.2,E11.4,F10.6)
2010  FORMAT(1H ,5X,I5,F14.0,F15.3,F9.2,E11.4,F8.2)
2014  FORMAT( '1',  5X, 'OUTPUT OF INPUT NODAL DATA ')
2015  FORMAT(///,10X,19H NODAL POINT OUTPUT.///
     11H ,59H NODE  KODE     R COORD      Z COORD      R FORCE
     2      Z FORCE//)
2016  FORMAT('1',  5X,  'OUTPUT OF COMPLETE NODAL DATA  ')
1020  FORMAT(I4,I6,4F13.3)
2020  FORMAT(I4,I6,F13.3,3F12.3)
2025  FORMAT(1HO,28H ERROR IN NODAL DATA,NODE = ,I4)
2030  FORMAT(///,10X, 13H ELEMENT DATA ///,
     1 40H ELEM     I     J     K    MAT  THICKNESS //)
2031  FORMAT( 1',5X, 'OUTPUT OF INPUT ELEMENT DATA' )
2032  FORMAT( '1', 5X, 'OUTPUT OF COMPLETE ELEMENT DATA  ' )
1035  FORMAT (5I6,F6.0)
2035  FORMAT (I4,4I6)
2040  FORMAT (///10X, 22H BAND WIDTH          = ,I6/
     1        10X, 22H NUMBER OF EQUATIONS = ,I6)
2050  FORMAT(///10X, 33H PROBLEM EXCEEDS SPECIFIED LIMITS )
2060  FORMAT(  'MLM1 IS LESS THAN OR EQUAL TO ZERO ')
C
      END
C
      SUBROUTINE ASTIF
C
C     THIS SUBROUTINE TAKES EACH ELEMENT IN TURN AND
C     FORMS THE ELEMENT STIFFNESS MATRIX (BY CALLING
C      ELSTIF).  IT ASSEMBLES THE ELEMENT STIFFNESSES
C     INTO  KSTIF.  THEN ADDS THIS INTO THE TOTAL .
C     STIFFNESS TSITF.  ASSEMBLES THE APPLIED LOAD
C     VECTOR (AP) AND FICTIOUS LOAD VECTOR(FICLD).
C     MODIFIES THE ASSEMBLAGES FOR DISPLACEMENT
C     BOUNDARY CONDITIONS (BY CALLING MODIFY)
C
      COMMON E(8),PR(8),RO(8),R(300),Z(300),UR(300),UZ(300),
     1  STIF(60,400),AP(600),ESTIF(6,6),ECM(4,4),EBM(4,6),
     2TAP(600),ESM(4,6),TSTIF(60,400),APFL(600),MBAND,WT
```

```
      COMMON NUMNP,NUMEL,NUMAT,KODE(300),NP(3,300),MAT(300),
     1 NEQ,ACOF(8),EN(8),M,LM(6),YM(300),TSTR(300,4),
      COMMON STR(4),SIGEL(300,4),SRMT(4,300),FICLD(300,6)
      COMMON /TIMI/ TIME,Q,TME,TRMT(4,300)
C
C   INITIALIZE APPLIED LOAD VECTOR AND MASTER
C    STIFNESS MATRIX AND ECM
C
      DO 10 I=1,NEQ
      AP(I)=0.0
      DO 10 J=1,MBAND
      IF(TIME.GT.0.0) GO TO 11
      TAP(I)=0.0
      TSTIF(J,I)=0.0
11     STIF(J,I)=0.0
      IF(TIME.LT.0.000000002) GO TO 10
      STIF(J,I)=STIF(J,I)+TSTIF(J,I)
10    CONTINUE
      DO 20 I=1,4
      DO 20 J=1,4
20    ECM(I,J)=0.0
C
C   FORM ELEMENT CONSTITUTIVE MATRIX (ECM) IF NUMAT=1)
C
C2    IF(TIME.GT.0.0) GO TO 30
      IF(NUMAT.NE.1) GO TO 30
      EPR=PR(1)
      COM=E(1)*(1.-EPR)/((1.+EPR)*(1.-2.*EPR))
      ECM(1,1)=COM
      COM1=COM*EPR/(1.-EPR)
      ECM(2,2)=COM
      ECM(3,3)=COM
      ECM(1,2)=COM1
      ECM(1,3)=COM1
      ECM(2,3)=COM1
      ECM(2,1)=COM1
      ECM(3,1)=COM1
      ECM(3,2)=COM1
      ECM(4,4)=COM*(1.-2.*EPR)/(2.*(1.-EPR))
C
30    DO 45 M=1,NUMEL
C
      CALL ELSTIF(1)
C
C   ASSEMBLE ELSTIF INTO MASTER STIFFNESS MATRIX
C
      IF(TIME.GT.0.0) GO TO 19
      DO 35 I=1,3
      I2=2*I
      LM(I2)=2*NP(I,M)
35    LM(I2-1)=LM(I2)-1
C
C
      DO 40 I=1,6
      II=LM(I)
      DO 40 J=1,6
      JJ=LM(J)-II+1
      IF (JJ.LE.0) GO TO 40
       STIF(JJ,II)= STIF(JJ,II)+ESTIF(I,J)
      TSTIF(JJ,II)=TSTIF(JJ,II)+ESTIF(I,J)
40    CONTINUE
C
C WRITES STIF AND ESTIF
C
C   ADD GRAVITY LOADS INTO AP VECTOR
C MODIFIED TO ADD HORIZONTAL LOAD TO AP
C
      DO 31 I=2,6,2
      II=LM(I)
      AP(II)=AP(II)+WT
31    CONTINUE
      IF(TIME.EQ.0.0) GO TO 45
C
C     FORMS ELEMENT FICTIOUS LOAD MATRIX
C
C  (II) ADDS  VERTICAL LOADS
C  (JJ) ADDS HORIZONTAL LOADS
C
C  NO FICTITIOUS LOADS FOR ELASTIC CONDITION
C
19    DO 44 I=1,3
      I2=2*I
      LM(I2)=2*NP(I,M)
      LM(I2-1)=LM(I2)-1
      II=LM(I2)
      IJ=LM(I2-1)
      APFL(IJ)=0.0
      APFL(II)=0.0
      APFL(II)=APFL(II)+FICLD(M,I2)
      APFL(IJ)=APFL(IJ)+FICLD(M,I2-1)
      AP(II)=AP(II)+APFL(II)
      AP(IJ)=AP(IJ)+APFL(IJ)
C
44     CONTINUE
45     CONTINUE
C
C  ADD NODAL LOAD TO AP VECTOR
C
      TFLDV=0.0
      TFLDR=0.0
```

```
      TOFH=0.0
      TOFV=0.0
      DO 50 N=1,NUMNP
       N2=2*N
      TFLDR=TFLDR+AP(N2-1)
      TFLDV=TFLDV+AP(N2)
      IF(TIME.EQ.0.0) GO TO 99
      UR(N)=UR(N)+TAP(N2-1)
      UZ(N)=UZ(N)+TAP(N2)
   99  AP(N2)=AP(N2)+UZ(N)
       AP(N2-1)=AP(N2-1)+UR(N)
      TAP(N2-1)=0.0
      TAP(N2)=0.0
      TAP(N2)=TAP(N2)+AP(N2)
      TAP(N2-1)=TAP(N2-1)+AP(N2-1)
      TOFV=TOFV+AP(N2)
      TOFH=TOFH+AP(N2-1)
   50 CONTINUE
C
C SET DISPLACEMENTS EQUAL TO ZERO FOR MODIFICATION
C
      DO 9999 II=1,NUMNP
      UR(II)=0.0
      UZ(II)=0.0
 9999 CONTINUE
C
   96 WRITE(6,1921) TOFH,TOFV,TFLDR,TFLDV
 1921 FORMAT(/,'SUM HOR FOR=',E15.8,5X,'SUM VET FOR.=',E15.8,
     *2X,'FIC R LOAD=',E15.8,'FIC V LOAD=',E15.8)
C  (6,(6,(6,(6,(6,(6,(6,(6,(6,
      DO 100 N=1,NUMNP
      N2=2*N
      IF (KODE(N)-10) 80,70,60
   60 II=N2-1
      CALL MODIFY(II,N)
      CALL MODIFY(N2,N)
      GO TO 100
   70 II=N2-1
      CALL MODIFY(II,N)
      GO TO 100
   80 IF(KODE(N).EQ.0)  GO TO 100
      CALL MODIFY(N2,N)
  100 CONTINUE
      IF(TIME.GE.0.0) GO TO 929
C
      DO 901 II=1,NUMNP
      I2=2*II
      I2M=I2-1
      WRITE(6,1117) II,AP(I2M),II,AP(I2),R(II),Z(II)
  901 CONTINUE

  929 RETURN
      END
C
      SUBROUTINE ELSTIF(KOP)
C
C  THIS SUBROUTINE FORMS THE ELEMENT STIFFNESS MATRIX (ESTIF) OR
C  ELEMENT STRESS MATRIX (ESM) FOR THE CONSTANT STRAIN TRIANGLE
C  THE FICTIOUS LOAD MATRIX IS FORMED USING THE INELASTIC STRAIN
C
      COMMON E(8),PR(8),RO(8),R(300),Z(300),UR(300),UZ(300),
     1  STIF(60,400),AP(600),ESTIF(6,6),ECM(4,4),EBM(4,6),
     2TAP(600),ESM(4,6),TSTIF(60,400),APFL(600),MBAND,WT
      COMMON NUMNP,NUMEL,NUMAT,KODE(300),NP(3,300),MAT(300),
     1 NEQ,ACOF(8),EN(8),M,LM(6),YM(300),TSTR(300,4),
      COMMON STR(4),SIGEL(300,4),SRMT(4,300),FICLD(300,6)
      COMMON /TIMI/ TIME,Q,TME,TRMT(4,300)
C
      DIMENSION AV(3),BV(3),CV(3),TNI(3)
C
      DO 10 I=1,4
      DO 10 J=1,6
   10 EBM(I,J)=0.0
      I=NP(1,M)
      J=NP(2,M)
      K=NP(3,M)
C
C(/)
C
C CAL. ELEMENT DIMENISONS
C
   17.  CV(1)=R(K)-R(J)
      CV(2)=R(I)-R(K)
      CV(3)=R(J)-R(I)
      BV(1)=Z(J)-Z(K)
      BV(2)=Z(K)-Z(I)
      BV(3)=Z(I)-Z(J)
      AV(1)=R(J)*Z(K)-R(K)*Z(J)
      AV(2)=R(K)*Z(I)-R(I)*Z(K)
      AV(3)=R(I)*Z(J)-R(J)*Z(I)
      AREA2=CV(3)*BV(2)-CV(2)*BV(3)
      RM=(R(I)+R(J)+R(K))/3.
      ZM=(Z(I)+Z(J)+Z(K))/3.
C
C   VOL=MEAN RADIUS*AREA
C
      PI2=2.*3.1415926
      VOL=RM*PI2*AREA2/2.
      IF (VOL.LE.0.) GO TO 75
C
C
```

```
C(/)
21    IF(NUMAT.EQ.1) GO TO 30
      NM=MAT(M)
      EPR=PR(NM)
      COM=E(NM)*(1.-EPR)/((1.+EPR)*(1.-2.*EPR))
      ECM(1,1)=COM
      COM1=COM*EPR/(1.-EPR)
      ECM(2,2)=COM
      ECM(3,3)=COM
      ECM(1,2)=COM1
      ECM(1,3)=COM1
      ECM(2,3)=COM1
      ECM(2,1)=COM1
      ECM(3,1)=COM1
      ECM(3,2)=COM1
      ECM(4,4)=COM*(1.-2.*EPR)/(2.*(1.-EPR))
C
C(/)
30    DO 41 J=1,3
      TNI(J)=0.
41    TNI(J)=TNI(J)+(AV(J)+(BV(J)*RM)+(CV(J)*ZM))/RM
31    IF(M.GT.3) GO TO 32
C
C     FORM ELEMENT B MATRIX (EBM)
C(/)
32    DO 40 I=1,3
      I2=2*I
      I2M=2*I-1
      EBM(1,I2)=CV(I)/AREA2
      EBM(2,I2M)=BV(I)/AREA2
      EBM(3,I2M)=TNI(I)/AREA2
      EBM(4,I2M)=EBM(1,I2)
40    EBM(4,I2)=EBM(2,I2M)
C
C
C     FORM ELEMENT STRESS MATRIX (ESM)
C
      IF(TIME.EQ.0.0) GO TO 23
      IF(KOP.EQ.1) GO TO 98
23     DO 50 I=1,4
      DO 50 J=1,6
      ESM(I,J)=0.0
      DO 50 K=1,4
50    ESM(I,J)=ESM(I,J)+ECM(I,K)*EBM(K,J)
C
      IF(KOP.EQ.2) GO TO 80
      IF(M.GT.3) GO TO 99
      IF(TIME.GE.0.0) GO TO 99
C
C     CAL WIEGHT OF MATERIAL
C
99    IF(NUMAT.EQ.1)  NM=1
      NM=MAT(M)
      WT=VOL*RO(NM)/3.
C
C     FORM ELEMENT STIFFNESS MATRIX (ESTIF)
C
      DO 70 I=1,6
      DO 70 J=1,6
      ESTIF(I,J)=0.0
      DO 60 K=1,4
60    ESTIF(I,J)=ESTIF(I,J)+EBM(K,I)*ESM(K,J)
70    ESTIF(I,J)=ESTIF(I,J)*VOL
C
CCCCCCCCCCCC
C
C  INTIALIZES (APFL(I)=0.0
C
      IF(TIME.EQ.0.0) GO TO 80
C
C    FFORMS FICTIOUS LOAD MATRIX
C
98    DO 45 J=1,6
      DO 90 I=1,4
      STR(I)=0.0
      FICLD(M,J)=0.0
      DO 49 K=1,4
      STR(I)=STR(I)+ECM(I,K)*SRMT(K,M)
49    CONTINUE
C
90    CONTINUE
      DO 44 K=1,4
      FICLD(M,J)=FICLD(M,J) +EBM(K,J)*STR(K)
44    CONTINUE
      FICLD(M,J)=FICLD(M,J)*VOL
45    CONTINUE
C
C
      GO TO 80
75    WRITE(6,1000) M
C
      STOP
80    RETURN
C
C
1000  FORMAT (1H1, 18H VOLUME OF ELEMENT ,I4, 18H IS
     1LESS THAN ZERO)
C
      END
C
```

```
      SUBROUTINE MODIFY (I,N)
C
C  THIS SUBROUTINE MODIFIES KSTIF AND AP IF A
C  DISPLACEMENT BOUNDARY CONDITION IS IMPOSED
C  IN EQUATION I ASSOCIATED WITH NODAL POINT N
C
      COMMON E(8),PR(8),RO(8),R(300),Z(300),UR(300),UZ(300),
     1  STIF(60,400),AP(600),ESTIF(6,6),ECM(4,4),EBM(4,6),
     2TAP(600),ESM(4,6),TSTIF(60,400),APFL(600),MBAND,WT
      COMMON NUMNP,NUMEL,NUMAT,KODE(300),NP(3,300),MAT(300),
     1 NEQ,ACOF(8),EN(8),M,LM(6),YM(300),TSTR(300,4),
      COMMON STR(4),SIGEL(300,4),SRMT(4,300),FICLD(300,6)
      COMMON /TIMI/ TIME,Q,TME,TRMT(4,300)
C
      DISP=UR(N)
      IF((I-2*N).EQ.0)  DISP=UZ(N)
C
      DO 50 J=2,MBAND
      IL=I+J-1
      IU=I-J+1
      IF(IU.LE.0)GO TO 10
      AP(IU)=AP(IU) - STIF(J,IU)*DISP
       STIF(J,IU)=0.0
10    IF(IL.GT.NEQ) GO TO 50
      AP(IL)= AP(IL)- STIF(J,I)*DISP
       STIF(J,I)=0.0
50    CONTINUE
      AP(I)=DISP
       STIF(1,I)=1.0
      RETURN
C
      END
C
      SUBROUTINE BAND1
C
C  THIS SUBROUTINE SOLVES FOR DISPLACEMENTS USING A
C  GAUSSIAN ELIMINATION  TECHNIQUE FOR SYMMETRIC
C  BANDED MATRICES STORED IN CORE
      COMMON E(8),PR(8),RO(8),R(300),Z(300),UR(300),UZ(300),
     1  STIF(60,400),AP(600),ESTIF(6,6),ECM(4,4),EBM(4,6),
     2TAP(600),ESM(4,6),TSTIF(60,400),APFL(600),MBAND,WT
      COMMON NUMNP,NUMEL,NUMAT,KODE(300),NP(3,300),MAT(300),
     1 NEQ,ACOF(8),EN(8),M,LM(6),YM(300),TSTR(300,4),
      COMMON STR(4),SIGEL(300,4),SRMT(4,300),FICLD(300,6)
      COMMON /TIMI/ TIME,Q,TME,TRMT(4,300)
C
C TRIANGULARIZE AND REDUCE RIGHT HAND SIDE
      NL=NN-MM+1
      NM=NN-1
      MR=MM
C
      DO 100 N=1,NM
      IF (A(1,N).LE.0.) GO TO 700
      BN=B(N)
      B(N)=BN/A(1,N)
      IF (N.GT.NL) MR=NN-N+1
C
      DO 100 L=2,MR
      IF (A(L,N).EQ.0.)GO TO 100
      C= A(L,N)/A(1,N)
      I= N+L-1
      J= 0
      DO 50 K=L,MR
      J=J+1
50    A(J,I)= A(J,I)-C*A(K,N)
      B(I)=B(I)-C*BN
      A(L,N)=C
100   CONTINUE
C
C   BACK SUBSTITUTE
C
      I=NN
C
      B(NN)=B(NN)/A(1,NN)
      DO 600 N=1,NM
      I=I-1
      IF (N.LT.MM)     MR= N+1
      DO 600 J=2,MR
      K=I+J-1
600   B(I) =B(I)- A(J,I)*B(K)
      WRITE(6,2001)
2001  FORMAT('1',     '   NODAL DISPLACEMENTS   ',//'    NO.',
     111X,'UR',6X,
     1 'NO.',11X, 'UZ',11X,'R(I)',11X'Z(I)' // )
      NZ=1
      NNP=NUMNP
      DO 901 II=NZ,NNP
      I2=2*II
      I2M=I2-1
      WRITE(6,1799) II,B(I2M),II,B(I2),R(II),Z(II)
1799  FORMAT(' ',I6,E15.5,I6,E15.5,5X,F7.4,8X,F7.4)
901   CONTINUE
      RETURN
700   WRITE (6,1999) N
      STOP
1999  FORMAT(1HO, 81H ZERO OR NEGATIVE ELEMENT ON  MAIN DIAGONAL
     1 OF TRIANGULARIZED MATRIX FOR EQUATION  ,I5)
C
      END
C
```

```
      SUBROUTINE STRESS
C
C   THIS SUBROUTINE FORMS THE ELEMENT STRESS MATRIX (ESM),
C   MULITIPLIES BY  THE ELEMENT DISPLACEMENT VECTOR (ELDISP)
C   SUBTRACTS THE ACCUMULATED STRAIN
C    AND RECORDS THE STRESSES IN SIGEL.
C
      COMMON E(8),PR(8),RO(8),R(300),Z(300),UR(300),UZ(300),
     1  STIF(60,400),AP(600),ESTIF(6,6),ECM(4,4),EBM(4,6),
     2TAP(600),ESM(4,6),TSTIF(60,400),APFL(600),MBAND,WT
      COMMON NUMNP,NUMEL,NUMAT,KODE(300),NP(3,300),MAT(300),
     1 NEQ,ACOF(8),EN(8),M,LM(6),YM(300),TSTR(300,4),
      COMMON STR(4),SIGEL(300,4),SRMT(4,300),FICLD(300,6)
      COMMON /TIMI/ TIME,Q,TME,TRMT(4,300)
C
      DIMENSION KOUNT(300),SIGA(300,4),ELDISP(6),STRN(4)
C
      DO 5 N=1,NUMNP
      KOUNT(N)=0
      DO 5 J=1,4
    5 SIGA(N,J)=0.0
C
      DO 100 M=1,NUMEL
C   COMPUTE ELEMENT DISPLACEMENTS
C
      DO 10 I=1,3
      I2=2*I
      LMI2  =2*NP(I,M)
      ELDISP(I2)=AP(LMI2)
   10 ELDISP(I2-1)=AP(LMI2-1)
C
C  COMPUTE  ELEMENT STRESSES
C
      CALL ELSTIF(2)
C
C(*)   ALTER TO ADD TOTAL INELASTIC STRAIN TO SUB. FROM ELASTIC
      DO 29 I=1,4
      TSTR(M,I)=0.0
      STRN(I)=0.0
      DO 39 J=1,6
      STRN(I)=STRN(I)+EBM(I,J)*ELDISP(J)
   39 CONTINUE
      TSTR(M,I)=TSTR(M,I)+STRN(I)
   29 CONTINUE
C
      DO 89 I=1,4
      IF(TIME.GT.0.0) GO TO 89
      SRMT(I,M)=0.0
      TRMT(I,M)=0.0
   89 TRMT(I,M)=TRMT(I,M)+SRMT(I,M)
      DO 21 I=1,4
       SIGEL(M,I)=0.0
      DO 20 J=1,4
      SIGEL(M,I)=SIGEL(M,I)+ECM(I,J)*(TSTR(M,J)-TRMT(J,M))
   20 CONTINUE
   21 CONTINUE
  100 CONTINUE
       NZ=1
       DO 129 M=NZ,NUMEL
       I=NP(1,M)
       J=NP(2,M)
       K=NP(3,M)
       RM=(R(I)+R(J)+R(K))/3.
       ZM=(Z(I)+Z(J)+Z(K))/3.
C
C7     WRITE(6,2011)  M,(TRMT(I,M), I=1,4)
       WRITE(7,2011) M,RM,ZM,ZM,(SIGEL(M,I), I=1,4)
C ***
  129 CONTINUE
 2011  FORMAT(I4,F12.3,2X,F8.5,2X,F8.5,2X,E11.4,5X,E11.4,
     15X,E11.4,5X,E11.4)
       IF(TIME.GE.0.0) GO TO 99
C      WRITE(6,2050)
C      WRITE(6,2010)  (N,(SIGA(N,I),I=1,4),N=1,NUMNP)
 2001  FORMAT('1',10X,'R-Z ELEMENT' ///,'  ELEM',
     13X,'MEAN RAD',3X,'R/H',3X,'Z/H',
     26X,'SIGM Z',8X,'SIGM R',6X,'SIGMA THETA',7X,'SIGM R-Z' //)
 2010  FORMAT(I4,4X,E11.4,5X,E11.4,5X,E11.4,5X,E11.4)
 2050  FORMAT(1H1,' AVERAGE NODAL STRESSES ' ///,'  NODE',
     16X,'SIGM Z',8X,'SIGM R',6X,'SIGMA THETA',7X,'SIGM R-Z' //)
   99  RETURN
       END
C
       SUBROUTINE NOELAS
C(*)
C
C    THIS SUBROUTINE CAL INELASTIC STRAIN MATRIX (SRMT)
C    USING THE EFFECTIVE FLOW LAW ONLY ( ODQVIST LAW)
C
       COMMON E(8),PR(8),RO(8),R(300),Z(300),UR(300),UZ(300),
      1  STIF(60,400),AP(600),ESTIF(6,6),ECM(4,4),EBM(4,6),
      2TAP(600),ESM(4,6),TSTIF(60,400),APFL(600),MBAND,WT
       COMMON NUMNP,NUMEL,NUMAT,KODE(300),NP(3,300),MAT(300),
      1 NEQ,ACOF(8),EN(8),M,LM(6),YM(300),TSTR(300,4),
       COMMON STR(4),SIGEL(300,4),SRMT(4,300),FICLD(300,6)
       COMMON /TIMI/ TIME,Q,TME,TRMT(4,300)
       DIMENSION RT(300),ZT(300)
C
C    ADD CAL DISPLACEMTNTS TO EXISTING COORDINATES
C
```

```
C      DO 51 J=1,NUMNP
C      I=2*J
C      RT(J)=RT(J)+AP(I-1)
C      ZT(J)=ZT(J)+AP(I)
C51     CONTINUE
C      WRITE(6,1191) (J,RT(J),ZT(J),J=1,NUMNP)
C
1191   FORMAT(1H1,15X,'NODAL COORDINATES',//,
      15X,'NODE',10X,'R-COORD.',10X,'Z-COORD',///,
      2(5X,I4,10X,E13.6,5X,E13.6))
C      WRITE(6,1121)
1121   FORMAT(1H1,10X,'INFO FROM NOELAS')
C
       WRITE(8,928)
C
       DO 1000 M=1,NUMEL
       SNOCT=0.0
       ESTRES=0.0
       DO 11 I=1,4
       SRMT(I,M)=0.0
11     CONTINUE
       NM=MAT(M)
       IF(NM.EQ.2) GO TO 998
       A=ACOF(NM)
       ENN=ETN(NM)
       DO 10 I=1,3
       SNOCT=SNOCT+(SIGEL(M,I)/3.0)
10     CONTINUE
       SDZ=0.0
       SDR=0.0
       SDTH=0.0
       SHRZ=0.0
       SDZ=SDZ+ (SIGEL(M,1)-SNOCT)
       SDR=SDR+ (SIGEL(M,2)-SNOCT)
       SDTH=SDTH+ (SIGEL(M,3)-SNOCT)
       SHRZ=SHRZ+ (SIGEL(M,4))
       DET=0.0
       DETT=0.0
       DETTT=0.0
       DET=DET+ (SDR-SDTH)*(SDR-SDTH)
       DETT=DETT + (SDTH-SDZ)*(SDTH-SDZ)
       DETTT=DETTT+ (SDZ-SDR)*(SDZ-SDR)
       DMA=0.0
       DMA=DMA + DET +DETT +DETTT + 6.*(SHRZ)*(SHRZ)
       ESTRES=ESTRES+(SQRT(DMA/2.))
C
C
       ESTRR=0.0
       ESTRR=ESTRR + A*ESTRES**ENN
C
       ESTR=0.0
       ESTR=ESTR+ (ESTRR*TME)
C
C  FIND STRAIN FOR EACH ELEMTNT USING:
C     1.  INCOMPRESSIBILITY
C     2.  STRAIN IN TANGINTIAL DIREC.=0.0
C     3.  PRINCIPAL STRAIN DIRECTION  PARAELL  TO PRINCIPAL
C         STRESS DIRECTION
C     USES THOMPSON'S METHOD OF CAL CREEP STRAIN
       COTT=0.0
       COTT=COTT+((3./2.)*(ESTR/ESTRES))
       SRMT(1,M)=SRMT(1,M)+COTT*SDZ
       SRMT(2,M)=SRMT(2,M)+COTT* SDR
       SRMT(3,M)=SRMT(3,M)+COTT*SDTH
       SRMT(4,M)=SRMT(4,M)+COTT* SHRZ
998    WRITE(8,398) M,(SIGEL(M,J),J=1,4),(SRMT(I,M),I=1,4),
      1SNOCT,ESTR
1000   CONTINUE
928    FORMAT(1H1,'ELEM',4X,'SIGM Z',6X,'SIGM R',5X,'SIGM THETA',
      *2X,'SIGM R-Z',4X,'SRMT(1,M)',3X,'SRMT(2,M)',
      *3X,'SRMT(3,M)',3X,'SRMT(4,M)',4X,'SNOCT',6X,'ESTRES')
398    FORMAT(' ',I4,2X,E10.3,2X,E10.3,2X,E10.3,2X,E10.3,2X,E10.3,
      12X,E10.3,2X,E10.3,2X,E10.3,2X,E10.3,2X,E10.3)
C  WE HAVE ZEROED ELASTIC LOAD MATRIX (ABOVE)
       RETURN
       END
       UN=UN+(2./3.)*SQRT(3.*(1.+ANGLE))
       DO 1010 I=1,3
       SRMT(I,M)=0.
1010   CONTINUE
       SRMT(1,M)=SRMT(1,M)+ESTRN/UN
       IF(SIGEL(M,1)-SIGEL(M,2)) 16,11,13
16     SRMT(2,M)=SRMT(2,M)+SRMT(1,M)
       SRMT(1,M)=-SRMT(1,M)
       GO TO 28
13     SRMT(2,M)=SRMT(2,M)-SRMT(1,M)
       GO TO 28
C      IF(SIGEL(M,1).GT.0.0) GO TO 13
C      SRMT(1,M)=-SRMT(1,M)
C13     SRMT(2,M)=SRMT(2,M)-SRMT(1,M)
28     UNN=0.0
       UNN=UNN+(SIN(AN)/COS(AN))
       SRMT(3,M)=SRMT(3,M)+2.*ABS(SRMT(1,M)*UNN)
       IF(SIGEL(M,3).GT.0.0) GO TO 12
       SRMT(3,M)=-SRMT(3,M)
       GO TO 12
11     SRMT(1,M)=0.0
       SRMT(2,M)=0.0
       SRMT(3,M)=0.
C
```

```
C FORMS THE INELASTIC MATRIC FOR THE STRUCTURE (SRM)
C
12      CONTINUE
        WRITE(6,398) M,(SRMT(I,M),I=1,3),SMEAN,ESTRES,AN
C***
1000  CONTINUE
      RETURN
C
1121  FORMAT(1H1,15X,'NODAL COORDINATES',//,
     15X,'NODE',10X,'X-COORD.',10X,'Y-COORD.',//,
     2(5X,I4,10X,E13.6,5X,E13.6))
1220  FORMAT(1H1,25X,' ELEMENT PRINCIPAL STRESSES ',///,
     11X,'ELEM',6X,'SIGMA I',7X,'SIGMA II',8X,'MAX TAU',
     24X,'SIGMA I DEG',//)
1121  FORMAT(1H1,10X,'INFO. FROM NONELAS')
928   FORMAT(1H1,10X,'ELEM',6X,'SRMT(1,M)',8X,'SMRT(2,M)',
     28X,'SRMT(3,M)',8X,'SNOCT',8X,'SHOCT')
398   FORMAT(' ',10X,I4,6X,E11.4,5X,E11.4,5X,E11.4,5X,E11.4,
     15X,E11.4,5X,'AN=',E11.4)
      END
```